This is to certify that the

dissertation entitled

THE STUDY OF ION/MOLECULE REACTIONS
BY TRIPLE QUADRUPOLE MASS SPECTROMETRY

presented by

Gregory G. Dolnikowski

has been accepted towards fulfillment
of the requirements for

Ph. D. degree in Chemistry

J. Throckmorton Watson
Major professor

Date 15 January 1988

THE STUDY OF ION/MOLECULE REACTIONS BY TRIPLE QUADRUPOLE MASS SPECTROMETRY

By

Gregory G. Dolnikowski

A DISSERTATION

Submitted to
Michigan State University
in partial fulfillment of the requirements
for the degree of

DOCTOR OF PHILOSOPHY

Department of Chemistry

1987

ABSTRACT

THE STUDY OF ORGANIC ION/MOLECULE REACTIONS BY TRIPLE QUADRUPOLE MASS SPECTROMETRY

By

Gregory G. Dolnikowski

Ion/molecule reactions in the gas phase, some of which are analogous to those that occur in solution, are intrinsically interesting because they facilitate studies of chemical systems unobstructed by solvent effects. These same reactions also may be useful analytically as chemical probes for specific structural features in analytes of unknown structure. The triple quadrupole mass spectrometer (TQMS) is a versatile and sensitive instrument for observing ion/molecule reactions that occur in its ion source and collision chamber. Both the collision chamber and the ion source are necessary for a complete study of an ion/molecule reaction because each provides different and complementary information.

Since ion/molecule reactions in the collision chamber have usually had low yields of products due to insufficient interaction time between ions and molecules, an ion-trapping technique has been devised which greatly increases the interaction time. This technique yields results that are similar to double resonance techniques in ion cyclotron resonance spectrometry in that one can select a reagent ion, store it in the presence of reactive molecules, and detect

the product ions. However, the TQMS operates under a wider range of pressures than the ICR can, and can employ many more ionization methods. The ion-trapping technique in the TQMS enhances the observed yield of product ions, increases the signal-to-noise ratio of stable product ions, yields product ions that would otherwise not be observed, and decreases the need for high pressures of reactive gases.

The reactions studied in the TQMS included the reactions of methanol with protonated aldehydes, protonated acids, protonated esters, protonated alcohols, aromatic ions, and an anionic aromatic heterocycle. Also studied were the self-condensation and mixed condensation reactions of aldehydes, ketones, esters, and acids; the condensation reactions in aromatic systems; and ion/molecule reactions which occur in the FAB process. In addition, a computerized ion-trapped multiple reaction monitoring reaction technique was developed for selective detection of chromatographic eluents by means of ion/molecule reactions.

. . . [B]ecause the bonds between the atoms differ and matter itself is eternal, a thing remains with its body uninjured until assailed by a force whose keenness is a match for its own structure. Therefore no thing is reduced to nothing, but all things when destroyed change back into particles of matter.

De rerum natura, II, 244-49
Lucretius -1st century B. C.

ACKNOWLEDGEMENTS

I would like to thank my major professor Dr. J. Throck Watson, who helped pull me through the bad times and helped me celebrate in the good times, and who helped to make my entire graduate program a success. I would like to thank my second reader, Dr. John Allison, who read all of my manuscripts and was an invaluable resource. I would like to thank the other members of my committee, Dr. Cristie G. Enke, Dr. Jack F. Holland, and Dr. William Reusch, whose insights and help I drew upon throughout my graduate career. I would also like to thank all those persons in the Michigan State Mass Spectrometry Facility who helped with my research, especially Mike Davenport, Brad Ackermann, Tim Heath, John Stults, Linda McCarraher, Gour-Rong Her, Brian Musselman, Mike Kristo, Mark Bauer, and Pete Palmer.

I would especially like to thank Jo Dutson, who spent considerable effort fixing up my manuscripts with her high-tech toys, and mailing them to me across the Atlantic.

To my parents and my wife, Edie, I give my warmest thanks: to my parents for raising me with love and with concern for intellectual matters, and for telling me never to have children in graduate school; and to Edie for loving support, for typing, cutting and pasting, and for being generally indispensable.

TABLE OF CONTENTS

LIST OF FIGURES

LIST OF TABLES

LIST OF SCHEMES

LIST OF ABBREVIATIONS

A	Ampere
ADC	Analog-to-Digital Converter
amu	Atomic Mass Unit
API	Atmospheric Pressure Ionization
CI	Chemical Ionization
-CI	Negative Ion Chemical Ionization
CID	Collision-Induced Dissociation
2CL5NP	2-Chloro-5-Nitropyridine
DAC	Digital-to-Analog Converter
dc	Direct Current
DIP	Direct Insertion Probe
DMSO	Dimethylsulfoxide
ECNI	Electron-Capture Negative Ionization
EI	Electron Ionization
eV	Electron Volts
FA	Flowing Afterglow
FAB	Fast Atom Bombardment
+FAB	Positive Ion Fast Atom Bombardment
-FAB	Negative Ion Fast Atom Bombardment
FIB	Fast Ion Bombardment
FT	Fourier Transform
FTMS	Fourier Transform Mass Spectrometry
GC	Gas Chromatography
GCM	Gas-Phase Collision Model
GPR	Gas-Phase Radiolysis

ICR	Ion Cyclotron Resonance
i.d.	Inside Diameter
I.P.	Ionization Potential
kcal	Kilocalories
keV	Kiloelectron Volts
kV	Kilovolts
LC	Liquid Chromatography
LD	Laser Desorption
M	Molecule
$M^{+}\cdot$	Molecular Ion
mA	Milliampere
MDDB	Multi-Dimensional Data Base
MED	Method Editor
$(M+H)^{+}$	Protonated Molecule
$(M-H)^{+}$	Molecular Ion with Loss of a Hydrogen Radical
$(MH-H_2O)^{+}$	Protonated Molecule with Loss of Water
MIKES	Mass-Analyzed Ion Kinetic Energy Spectrometry
mmol	Millimoles
mol. wt.	Molecular Weight
MRM	Multiple Reaction Monitoring
MS	Mass Spectrometry
MS1	First Mass Spectrometer
MS2	Second Mass Spectrometer
MS/MS	Tandem Mass Spectrometry
msec	Milliseconds
MSU-NIH-MSF	Michigan State University National Institutes of Health Mass Spectrometry Facility

m/z	Mass-to-Charge Ratio
NCI	Negative Ion Chemical Ionization
ng	Nanogram
NMR	Nuclear Magnetic Resonance
o.d.	Outside Diameter
2OH5NP	2-Hydroxy-5-Nitropyridine
P.A.	Proton Affinity
PAC	Polycyclic Aromatic Compounds
PED	Parameter Editor
psi	Pounds Per Square Inch
PTM	Programmed Test Mixture
QUISTOR	Quadrupole Ion Store
rf	Radio Frequency
R-MRM	Ion-Trapped Multiple Reaction Monitoring
RPD/MS	Radio Frequency Plasma Discharge Mass Spectrometry
SDIR	Scan Directory
SID	Surface-Induced Dissociation
SIMS	Secondary Ion Mass Spectrometry
S/N	Signal-to-Noise Ratio
S_N(AE)	Aromatic Nucleophilic Substitution with Addition Elimination Mechanism
S_N(EA)	Aromatic Nucleophilic Substitution with Elimination Addition Mechanism
S_N(ANRORC)	Aromatic Nucleophilic Substitution with Ring Opening and Ring Closing
TA-FAB	Thermally Assisted Fast Atom Bombardment

TI/MS	Trapped-Ion Mass Spectrometry
TIC	Total Ion Chromatogram
TMS	Trimethylsilyl
TQMS	Triple Quadrupole Mass Spectrometer
TRIKES	Time-Resolved Ion Kinetic Energy Spectrometry
TRIMS	Time-Resolved Ion Momentum Spectrometry
V	Volts
ug	Microgram
ul	Microliter

CHAPTER I.

INTRODUCTION AND OBJECTIVES

A. Tandem Mass Spectrometry (MS/MS)

1. Introduction

Tandem mass spectrometry (MS/MS) is a powerful new analytical technique that has a wide variety of chemical, biomedical, and environmental applications. MS/MS consists of two or more sequential mass spectrometric steps. Most often this is accomplished with a series of two or more mass spectrometers linked with one or more collision chambers. A block diagram of a typical MS/MS is shown in Figure 1.

2. MS/MS Ion Sources

The sample to be studied by MS/MS can be introduced into the ion source of the instrument by any of several methods. These include direct insertion probe (DIP) (1), gas chromatography (GC) (2,3), and liquid chromatography (LC) (4,5). The ion source can produce ions by any of numerous methods including electron ionization (EI) (6), chemical ionization (CI) (7), laser desorption (LD) (8,9), and fast atom/fast ion bombardment (FAB/FIB) (10-18) (both FAB and FIB are also called secondary ion mass spectrometry (SIMS)).

3. The First Mass Analyzer

The ions produced in the ion source are accelerated into the first mass analyzer which is tuned to select an ion of interest. This ion is

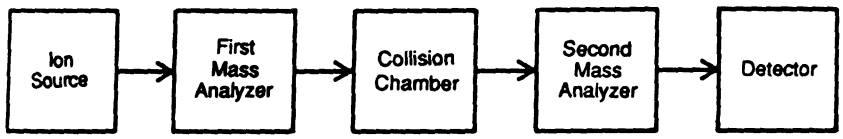

Figure 1. Block Diagram of an MS/MS Instrument

called the parent ion. The parent ion may be a molecular ion, a protonated molecule, a cluster ion, or a fragment ion depending on the ionization technique. If the first mass spectrometer (MS1) is a high resolution mass analyzer, it may be able to separate nominally isobaric ions; that is, ions that have different chemical formulas but the same nominal mass. It is never possible, however, for MS1 to separate isomeric ions (19).

4. The Collision Chamber

The parent ion is introduced by the MS1 into the collision chamber in which the ion interacts with a target of some kind, such as a gas (20), a beam of photons (21), or a metal plate (22). The reaction products that result from this interaction in the collision chamber are called daughter ions. Daughter ions are usually formed with less kinetic energy than their corresponding parents. Some MS/MS techniques use this kinetic energy difference to advantage (23), but since the mass resolution of kinetic energy analyzers is poor, modern MS/MS instruments have been designed to achieve higher resolution.

5. The Second Mass Analyzer

The daughter ions are gathered by ion optics as they emerge from the collision chamber and are introduced into the second mass analyzer, which can be scanned to produce a complete daughter spectrum of a given parent. This process is called a daughter scan. In many MS/MS instruments it is also possible to produce a parent scan that gives all of the parents of a given daughter, and to produce a neutral loss scan that gives all of the parents that lost a particular neutral fragment.

The parent and neutral loss scans are often implemented by a process of linked-scanning which involves scanning both mass analyzers simultaneously (24). Whether or not the second mass analyzer has high resolution characteristics, it is sometimes possible using the second analyzer to distinguish between isomers, since isomers may produce daughter spectra that are sufficiently different (25).

6. Data Collection Systems

Parent and daughter ions are detected in MS/MS by a variety of devices including faraday cups, electron multipliers (6), and marginal oscillators (163). Electron multipliers are used most frequently since they can detect small quantities of ions, have a large dynamic range, and are common detectors on ordinary MS instrumentation.

An MS/MS experiment, obviously, can be extremely complex. Therefore, many MS/MS systems have been extensively computerized (26) to aid the experimenter, both in the process of collecting data and in the interpreting of that data. Since a single compound frequently can generate hundreds of MS/MS spectra, the use of computerized magnetic storage of data is often essential.

B. MS/MS Instrumentation

1. Introduction

Many different types of MS/MS instruments have been constructed for research purposes. Figure 2 includes some of the designs that are prevalent in this kind of instrumentation. The instrumental arrangements in Figure 2 suggest only some of the many possibilities for developing MS/MS instruments. Presently, the development of novel MS/MS

QQQ
Triple Quadripole Mass Spectrometer (TQMS)
Triple Sector Quadrupole (TSQ)

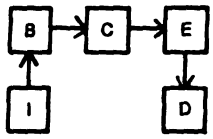

BE
Reversed Geometry Double Focussion Mass Spectrometer
Mass-Analized Ion Kinetic Energy Spectrometer (MIKES)

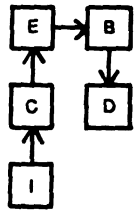

EB
Forward Geometry Double Focussing Mass Spectrometer

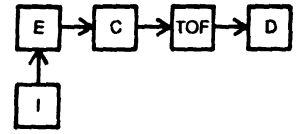

ETOF
Time- Resolved Ion Kinetic Energy Spectrometer (TRIKES)

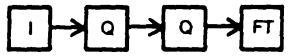

QQ FT
Tandem Quadruple Fourier Transform Mass Spectrometer

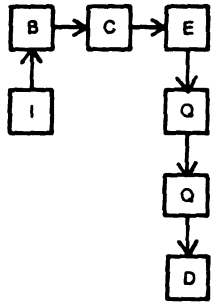

BEQQ
Hybrid Tandem Mass Spectrometer

B = Magnetic Sector
C = Collision Cell
D = Detector
E = Electrostatic Sector
FT = Fourier-Transform Sector
I = Ion Source
Q = Quadrupole Sector
TOF = Time of Flight Sector

Figure 2. MS/MS Instrumentation

instrumentation is an expanding field, and there are still many interesting combinations of mass analyzers under construction. There is another class of MS/MS instruments in which there is only one physical mass analyzer and the second dimension of MS/MS is accomplished in the time domain. Included in this class are the time-resolved ion momentum spectrometer (TRIMS) (31), the time-resolved ion kinetic energy spectrometer (TRIKES) (29), and the Fourier-transform mass spectrometer (FTMS) (32).

2. MS/MS Instrumentation at Michigan State

The MS/MS instruments currently available in the Michigan State Mass Spectrometry Facility (MSU-NIH-MSF) are the MIKES, the TQMS, the TRIKES, and the TRIMS (See Figure 2). The primary MS/MS instrument that will be used in this project will be the TQMS, but some data have been collected using the MIKES instrument and the new forward geometry double focussing instrument (JEOL HX-110).

3. The Triple Quadrupole Mass Spectrometer

A schematic diagram of the TQMS is given in Figure 3. The TQMS has a wide variety of ionization modes and sample introduction systems which allow the user to ionize virtually any sample. Samples that have been analyzed on this TQMS include volatile organics, jet fuel, peptides, vitamins, triglycerides, heavy metals, and organo-metallic compounds. In addition to the GC, EI, CI, and FAB shown in the Figure 3, atmospheric pressure ionization (API) has been acquired for the instrument but is not yet installed. The EI and CI ion sources are physically separated and have different filaments. Ion source design and

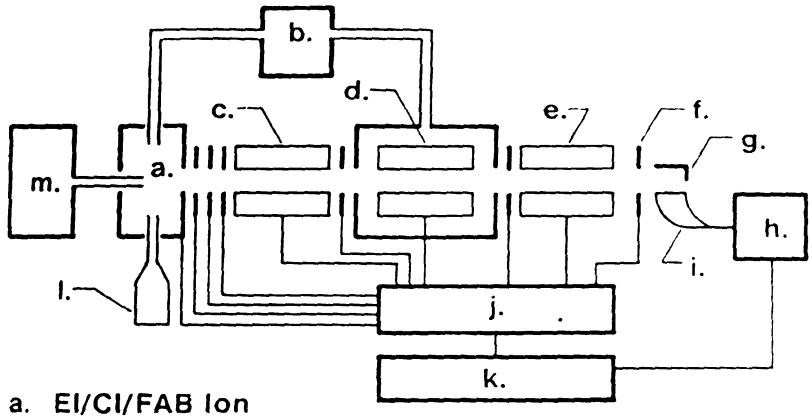

a. EI/CI/FAB Ion Source
b. Reactive Gases (or Argon)
c. First Quadrupole
d. Central Quadrupole, Collision Chamber
e. Third Quadrupole
f. Faraday Plate
g. Conversion Dynode
h. Analog-to-Digital Converter
i. Electron Multiplier
j. Multiple Digital-to-Analog Coverters
k. Microcomputer
l. Direct Insertion Probe
m. Gas Chromatograph

Figure 3. Schematic Diagram of the TQMS

computer control make it possible to acquire EI and CI spectra of the same compound on alternate scans.

The three plates after the ion source act as an Einzel lens to focus ions into the first quadrupole. The first quadrupole is used as the first mass filter. The third quadrupole is used as the second mass filter. These two quadrupoles have a mass range of 0-1000 daltons, and they are capable of unit resolution throughout the mass range. Newer instruments have extended the mass range of the quadrupole to 3000 mass units. The second quadrupole is enclosed in a stainless steel can and is used as the collision chamber.

Quadrupole analyzers can be made to act as mass filters; as such, their ability to separate ions of different masses is much less affected by changes in ion kinetic energy than is the case in other mass analyzers. Quadrupole mass filters provide dynamic separation of ions of different masses by means of radio frequency (rf) and direct current (dc) fields applied to four parallel stainless steel rods. When a quadrupole is tuned to a particular set of rf and dc voltages, only ions of one particular mass to charge ratio will have a stable trajectory through the center gap between the four rods. All other ions will collide with the rods and not be transmitted through the mass filter. It is possible to permit the quadrupoles to transmit higher mass to charge ratio ions by increasing the magnitude of both the dc and rf fields while keeping their ratio constant. The dc and rf fields can be changed very rapidly and with good reproducibility. It is therefore possible to obtain a scan over the whole mass range of the quadrupole in one to two seconds.

If the rf voltage alone is applied to a quadrupole, the device acts not as a mass filter, but rather as a focussing field which will transmit ions with a wide range of masses. The central quadrupole in the TQMS is always operated in rf-only mode. The central quadrupole is enclosed in a chamber which can be filled with gas. When a significant pressure of gas (50 microtorr or higher) is present in the chamber, central quadrupole acts as a collision chamber to produce daughter ions, and as a focussing device to direct daughter ions along the axis of the instrument toward the third quadrupole. Daughter scans on the TQMS are implemented by passing a single parent ion through first quadrupole and scanning the third quadrupole to separate the daughter ions generated by collisions in the central quadrupole. Parent scans are implemented by scanning the first quadrupole to pass all parents into the collision chamber, but only those parents that produce the specific daughter that is selected by the third quadrupole will be detected. Neutral loss scans are implemented by scanning both the first quadrupole and the third quadrupole simultaneously with a fixed mass difference (N) between them. In this way only parents (P) that produce a daughter of mass (P-N) will be detected. Daughter scans are used primarily to investigate the structure of parent ions. Parent and neutral loss scans are used primarily in mixture analysis to detect all parents that lose a fragment of the same mass, either as an ion in the case of parent scans, or as a neutral particle in the case of neutral loss scans.

An Intel 8086 micro-computer on the TQMS controls all of power supplies that produce the necessary voltages for obtaining the three types of MS/MS scans. The micro-computer also stores on magnetic disks all of the data acquired by the TQMS along with the parameters for each

scan. The micro-computer can transfer this information to a PDP 11/23 mini-computer for data analysis and hard-copy plotting of data as bar graphs, multiple-reaction monitoring experiments, or mass chromatograms. Most of the MS/MS data presented in this dissertation were generated by the TQMS and its data system.

C. Collision Processes in MS/MS

1. Introduction

MS/MS experiments are generally separated into two categories: those in which the parent ion is given a large initial kinetic energy, typically in the KeV range; and those in which the parent ion is given a lower initial kinetic energy, typically in the 1-100 eV range. The MIKES instrument, for example, is considered to be a high energy instrument since parent ions are given 3000-10000 eV of kinetic energy. On the other hand, the TQMS is considered to be a low energy instrument, since the potential drop between the ion source and the collision chamber is almost never more than 100 eV.

The three major means of performing MS/MS involve colliding parent ions with gases, with solid metal surfaces, and with photons. All three of these interactions have been performed at both high and low energies.

2. MS/MS With a Collision Gas

When a parent ion collides with a target gas, many different reactions are possible. In Scheme 1, these reactions are classified into five broad categories.

Scheme 1

Types of Collision Processes in MS/MS

High Energy Charge Stripping	$M_1^+ + N \longrightarrow M_1^{2+} + N + e^-$
High Energy Charge Inversion	$M_1^- + N \longrightarrow M_1^+ + N + 2e^-$
High or Low Energy Charge Exchange	$M_1^+ + M_2 \longrightarrow M_1 + M_2^+$
High or Low Energy Collision-Induced Dissociation	$M_1^+ + N \longrightarrow M_1^{+*} + N \longrightarrow M_3^+ + N$
Low Energy Ion/Molecule Reaction	$M_1^+ + M_2 \longrightarrow M_1M_2^{+*} \longrightarrow M_3^+ + M_4$

N = Unreactive Collision Gas
M_2 = Reactive Collision Gas
$M_1M_2^+$ = Adduct Ion
M_1^{+*} = Collisionally Activated Ion: Excess Thermal Energy

Of the reaction types shown in Figure 4, collision-induced dissociation (CID) has been used most often in analytical applications. Charge stripping and charge inversion have found limited use in magnetic sector instruments. Only very recently have ion/molecule reactions been used analytically in the collision region of an MS/MS instrument. CID and ion/molecule reactions are the two major techniques used currently for gas phase analysis of parent ions and both will be discussed under their own chapter headings.

3. MS/MS with Surface Collisions

When parent ions collide with metal surfaces, the ions may fragment if the collision energy is low (22), or release secondary

electrons or ions if the collision energy is high (78). Charge inversion has been shown to occur when ions strike quadrupole rods in the process of being mass filtered (79). The interactions of ions with metal surfaces are largely unexplored as an analytical method, but there is a recent article on surface-induced dissociation (SID) that claims high fragmentation efficiencies are possible using this method (77).

4. MS/MS with Photodissociation

When parent ions collide with photons the ions may absorb enough energy to fragment. This process is called photodissociation, and it is usually accomplished by means of lasers. Laser photodissociation has been investigated in the TQMS (80, 81). The wavelength of the photons is of critical importance in photodissociation. The compound must be able to absorb light energy of the selected wavelength. Photodissociation is generally thought to be a more selective fragmentation technique than CID or SID, but the fragment ion yields have not been competitive with either technique.

D. Collision-Induced Dissociation (CID)

1. Theory of Fragment Formation by CID

CID is a two-step process. When a parent ion collides with a target gas molecule, some of the electronic energy is transferred to vibrational energy. This first step is called collisional activation, and it produces a parent ion with excess vibrational energy. The collisionally activated parent ion (indicated in Scheme 1 with an asterisk) can undergo unimolecular decomposition into fragments when the excess vibrational energy leads to dissociation. The fragments of

unimolecular decomposition that are charged can be detected as daughter ions if the rate of unimolecular decomposition is fast on the time scale of the MS/MS experiment. Increasing the initial kinetic energy of the parent ion or increasing the pressure of the target gas tends to increase both the intensity and the number of different daughter ions produced by CID. Scattering, which decreases the observed intensity of daughter ions, also increases with increasing kinetic energy and target gas pressure. Therefore, the observed yield of daughter ions plotted against either target gas pressure or parent ion kinetic energy is described by a curve which increases to a maximum and then declines. Depending on the nature of the parent ion, the efficiency of daughter ion production by CID is 3-10% in sector instruments and can be as high as 50% in the TQMS (20).

2. Analytical Applications of CID

CID has been used for detecting and quantifying compounds in many complex mixtures, including a wide range of environmental pollutants (25), pharmacological drugs in blood serum (33), toluene degradation products in air (34), and nitro-polycyclic aromatic hydrocarbons in coal liquids (35). MS/MS of complex mixtures is a rapidly expanding field because it can provide information comparable to that from capillary GC-MS more efficiently and economically (25). CID has been used for structural analysis of many types of compounds, including peptides (10,15,18,36), transition metal complexes (13), fatty acids (37), vitamins (16), and surfactants (14). CID has also been used to study the products of ion/molecule reactions that occur in the CI ion source of an MS/MS instrument (38-44).

3. Disadvantages of CID

In spite of these successes, CID does not always give the analyst all of the necessary information for determining the structure of a compound. CID is not always specific enough to distinguish components from complex mixtures. Using CID, it is particularly difficult to separate a mixture of isomers, or to distinguish which isomeric structure is correct for a pure compound of unknown structure. In this respect CID MS/MS lags behind GC, which can readily separate structural, positional, and even optical isomers.

By varying several instrumental parameters, including collision energy, angle of daughter ion production, and collision gas pressure, the researcher can derive more information from CID MS/MS. CID, however, is not always the most effective method for solving structural problems using MS/MS. The effectiveness of CID decreases as molecular weight increases. Larger molecules have proportionally larger vibrational degrees of freedom. Thus the amount of vibrational energy deposited into the molecule by collisional activation may not be sufficient to cause fragmentation. The net result is that CID of larger molecules becomes increasingly inefficient. Furthermore, certain very stable molecules, such as the polycyclic aromatic compounds (PAC) cannot be fragmented by CID due to insufficient energy deposition by gas-phase collisions. Therefore, the MS/MS community has been searching for novel methods to determine the structures of these large and/or stable molecules.

E. Ion/Molecule Reaction in MS/MS

1. Introduction

One particularly novel and potentially powerful means of increasing the information content of MS/MS is to employ reactive gases in the collision chamber (45). Parent ions may undergo gas-phase ion/molecule reactions with the reactive collision gas. If the kinetics and thermodynamics of the interaction between the target gas and the analyte are favorable, an adduct ion may be formed. This adduct ion may be detected directly if it is stabilized by a high pressure of collision gas. At lower pressures, however, the adduct has some excess vibrational energy which it can release by decomposition to the reactants (no net reaction), or it may lose a neutral (such as H_2O) to form a new chemical species. Unlike CID daughter ions, the products of ion/molecule reactions can be of higher or lower mass than their parent ion.

2. Techniques for Studying Ion/Molecule Reactions

Ion/molecule reactions have the potential to be used in MS/MS for analytical purposes. These reactions, however, are of intrinsic interest to the scientific community, since they represent an opportunity to study chemical reactions without the influence of a solvent. Therefore, a number of techniques have been developed to study fundamental ion/molecule chemistry. Ion/molecule chemistry has been studied in the gas phase by classic vacuum-line techniques (46-52), ion cyclotron resonance spectrometry (ICR) (53-55), FTMS (150), flowing afterglow (FA) (56), and CI/MS/MS (38-44). Recently, experimenters

have also used the collision chamber of a TQMS to study ion/molecule chemistry.

3. Advantages of Using the TQMS for Ion/Molecule Reactions

The TQMS has several major advantages over a number of the other techniques which have been used to study ion/molecule reactions. First, the two materials to be reacted are physically separated, so that one does not have mixing of the reactants in the gas phase before the ion/molecule reaction. Second, the quadrupoles and the quadrupole ion source are largely insensitive to pressure, and therefore can be used with high pressure techniques such as gas chromatography, CI, API, and FAB. The third major advantage is that one can mass-select both the reactant ion and the product ions with unit resolution. Therefore, unlike, single cell instruments like the ICR, the quadrupole ion trap, and CI/MS, the TQMS can perform selected ion/molecule reactions, at a range of pressures from $1X10^{-8}$ torr up to $1X10^{-3}$ torr, and can accommodate the full range of ionization techniques that are available for mass spectrometry. The TQMS also has the advantage that it was developed as an analytical instrument and has been used to detect trace amounts (less than one ng) of certain compounds. Certain techniques for ion/molecule study, such as the vacuum line and FA, are valuable in their own right but are clearly not designed for analytical purposes. Furthermore, the TQMS is a full-fledged MS/MS instrument that can provide parent scans and neutral loss/gain scans that are either impossible or extremely difficult to achieve using other types of instrumentation. There is only one instrument that is commercially

available that is more versatile than the TQMS, and that is the newly developed BEQQ instrument. The BEQQ instrument is very similar to the TQMS but it contains a high resolution mass spectrometer instead of the first quadrupole (82)

4. Disadvantages of Using the TQMS for Ion/Molecule Reactions

The energy with which reactions occur in the collision chamber of the TQMS is not well regulated in current instrumental designs. The collision energy of ions and collision gas molecules is usually defined as the difference between the ion source potential and the central quadrupole offset voltage. This definition is, however, only an approximation, since there are two other factors that influence the kinetic energy of the parent ions. Two focussing lenses, one prior to and one following the second quadrupole, accelerate ions through the fringing fields around the central quadrupole. These lenses may be set to

-100 V relative to the ion source, and they can increase considerably the axial kinetic energy of ions as they enter and leave the central quadrupole. In addition to the axial kinetic energy boost of the inter-quadrupole lenses, the radio frequency voltage on the the central quadrupole rods can act to give ions within the central quadrupole substantial radial kinetic energy during portions of their trajectories, even though the average radial kinetic energy may be quite small.

Because ions in the central quadrupole exhibit a range of energies, daughter ions may be formed by a variety of mechanisms. The interaction of parent ions with a reactive collision gas could produce

both CID daughter ions and ion/molecule reactions at the same nominal collision energy, with CID occurring during the brief periods of higher kinetic energy and the ion/molecule reactions during the longer periods of lower kinetic energy. This process could result in a more complicated daughter spectrum than is generated by an unreactive collision gas, but one that is potentially more informative. Many ion/molecule reactions are exothermic and occur at axial kinetic energies approaching zero eV. CID reactions, on the other hand, are favored at higher axial kinetic energies because they are endothermic. Therefore, one should expect to distinguish between competitive ion/molecule and CID reactions by means of collision energy, even though some ion/molecule and CID products should be produced in the TQMS at virtually all axial kinetic energies when sufficient target gas is present.

A further disadvantage of the TQMS for ion/molecule reactions is that the residence time of ions in the central quadrupole can be controlled only very crudely by varying the the central quadrupole dc offset and the collision gas pressure. In comparison, the ion/trapping techniques, such as the quadrupole ion store (QUISTOR), the ICR and the FTMS, have precise control over the time that the parent ion may react with the collision gas, as an independent variable from the pressure of the collision gas. The major problem with the lack of residence time control in the TQMS is that, due to the short residence time of ions in a quadrupole (no longer than a few msec), the yield of ion/molecule reactions in the central quadrupole is often quite low. The low ion signal, of course, limits the analytical potential of the method.

Clearly, some of these disadvantages will have to be overcome before the TQMS can compete directly with other techniques as a truly viable means of studying ion/molecule reactions. One of the disadvantages with the TQMS for studying ion/molecule reactions has already been overcome. The TQMS cannot be used to study the structure of the ion/molecule products created in the central quadrupole by CID. Recently, therefore, a five quadrupole instrument has been developed that can perform an ion/molecule reaction in the second quadrupole followed by CID of a selected product ion in the fourth quadrupole. Thus one can obtain a daughter spectrum of an ion/molecule product ion by scanning the fifth quadrupole. Unfortunately, a five quadrupole instrument is not currently available at Michigan State University.

F. Review of Organic Ion/Molecule Reactions

1. Introduction

There is a large body of scientific literature regarding the ion/molecule reactions of inorganic and organometallic compounds (83). The literature for organic ion/molecule reactions is not nearly so extensive, and thus these reactions deserve more attention. This dissertation will concern itself chiefly with organic reactions, and, therefore, it is appropriate to review those relatively few studies that have preceded this one.

2. Fundamental Studies

The vast majority of organic ion/molecule studies have used ICR or FT-ICR techniques, and the majority of those are involved with determining relative gas-phase acidities and basicities by means of

proton transfer reactions. These studies have been compiled (84, 85). While this fundamental physical chemistry is essential to science, it is far removed from the purpose of this thesis.

3. Parallels with Solution Chemistry

Closer to the topic of this research are the studies of gas-phase ion/molecule reactions which are analogous to common bimolecular condensed phase reactions. The following organic reactions have been observed in the gas phase: the Schiff base synthesis (86), the Diekmann condensation (87), nucleophilic substitution (88), electrophilic aromatic substitution (89), and the Fisher esterification (90), and the Claisen condensation (91).

4. Gas Phase Synthesis

A number of research groups are currently publishing articles on gas-phase synthesis (92). The only methods that actually produce products that can be isolated, however, are the gas-phase radiolysis syntheses (50), matrix isolation on cold fingers, and sometimes flowing afterglow syntheses (56). Table 1 shows the various functional groups that have been studied.

Table 1

Functional Groups Used to Date
In Organic Gas Phase Synthesis

Aliphatic	Aromatic
alcohols	phenols
carboxylic acids	benzene carboxylic acids
diols	catachol
glycols	
saccharides	
amines	pyridine, aniline
iodides	
fluorides	chlorobenzenes
aldehydes	benzaldehyde
esters	phenylbenzoate
ketenes	
alkenes	
trimethylsilyl ethers	
enols	
ammonia	
	nitrobenzenes
alkanes	toluene

5. Analytical Applications

There have been very few attempts to use organic reactions for analytical purposes, but they have been used for the most part quite successfully. Suming et. al. used trimethylborate in CI as a stereoselective reagent gas for diols in a variety of compounds (93). Anderson et. al. found that methane CI reacted stereospecifically with cinnamic acids (94). Bursey et. al. proposed acetylation as a CI technique for alcohols (162). Jalonen was able to differentiate among $C_2H_3O^+$ and $C_2H_5O^+$ isomers by using butadiene and benzene as reactive collision gases in TQMS (95). Kinter and Bursey were able to differentiate among $C_2H_5O^+$ isomers by using ammonia as the collision gas in the TQMS (96). Fetterolf and Yost were able to differentiate between $C_3H_3^+$ isomers using acetylene as a reactive collision gas in the TQMs

(97). Chakel and Enke were able to distinguish among positional isomers of substituted benzenes using D_2O as a reactive collision gas in the TQMS (98).

G. Fast Atom Bombardment (FAB) in MS/MS

1. Theories of Ion Formation in FAB

One of the innovations in MS/MS that has greatly increased the scope of molecules studied by this technique is fast atom bombardment (FAB) (10,63). In FAB, an energetic (7-10 KeV) beam of atoms or ions, such as Xe^{o} or Cs^{+}, is used to bombard an aliquot of sample molecules dissolved in a viscous liquid matrix such as glycerol, thioglycerol, polyethylene glycol, or polyphenyl ether. The appearance of the spectrum remains essentially the same whether the FAB beam is charged or neutral. The bombardment produces ions that are characteristic of both the solvent and the analyte. Using appropriate ion-optics, it is possible to collect a steady, intense, and long-lived beam of secondary ions that have been generated by FAB. Analyte ions are generally thought to be created from a monolayer on the surface of the liquid. This monolayer is continually replenished by the mobility of the liquid as the surface is sputtered away by the action of the FAB beam. Recent MS/MS studies (64) have shown that the relative proton affinities of the analyte and the solvent may determine whether FAB can produce the protonated molecule of the analyte. These studies suggest that FAB produces the proton bound adduct ion, (glycerol+analyte)H^{+}. This adduct may survive intact and has been detected in many FAB spectra, or it may dissociate in the gas phase. If the analyte has a higher proton affinity than glycerol, the analyte will capture the proton and be

detected by the mass spectrometer. If sufficient analyte is present, glycerol ions may be entirely absent from the spectrum. If glycerol has the higher proton affinity, it will capture the proton and no protonated molecule of the analyte will be present in the spectrum. In this case, a solvent of lower proton affinity may be effective as a FAB matrix where glycerol was not. An extreme example of this effect has been reported (65) in which aromatic hydrocarbons of low proton affinity have for the first time been analyzed successfully by FAB by dissolving them in a viscous saturated hydrocarbon fraction of even lower proton affinity.

Another aspect of FAB that has received considerable attention is the appearance of cationized species such as $M+H^+$, $M+Na^+$, and $M+Ag^+$. It has been shown by visible spectroscopy (154) that these species are present in the solutions from which the ions are desorbed. These findings lend credence to the theory that preformed ions play a major role in the FAB process. Cationized species have already been shown to have analytical utility. $M+Ag^+$ seems to be particularly useful for determining which peaks in the complex FAB spectrum represent the analyte, and which peaks represent the ions from the liquid matrix.

2. Matrix Interferences in FAB

The matrix background is often quite large in FAB, (68) and occasionally may obscure entirely the peaks of interest in the spectrum. Numerous attempts have been made to reduce the effect of the matrix background (also called chemical noise) in FAB, including background subtraction (68), thermally-assisted FAB (99). MS/MS has been found to be especially useful in FAB for eliminating most or all of the chemical

noise that is present in the FAB spectrum due to ions produced from the liquid matrix. FAB sometimes produces more fragmentation than either CI or FD. Unfortunately, much of this useful fragmentation is usually obscured by the large number of intense glycerol fragments and clusters at low mass. Therefore, only molecular weight information is frequently obtained from FAB-MS. In FAB-MS/MS, a daughter scan of the protonated molecule yields only ions derived from the analyte and none from the liquid matrix (unless there is a matrix ion of the same nominal mass, in which case one needs to use another matrix).

3. Analytical Utility of FAB-MS and FAB-MS/MS

Many of the samples that chemists and biochemists study are thermally unstable compounds, nonvolatile materials such as salts or metal complexes, or are simply large molecules with several weak bonds. These three types of molecules are very difficult to analyze by EI or CI because either these compounds cannot be volatilized into the ion source, or they yield no molecular ions due to thermal decomposition or excessive fragmentation. FAB ionization is most efficient with these kinds of molecules. FAB provides molecular weight information in both positive and negative ion modes for a large variety of underivitized, polar molecules, including peptides, proteins, carbohydrates, lipids, and nucleic acids (66), insulins (67), acetaminophen metabolites (68), transition metal complexes (13), and vitamins (15,16). FAB in conjunction with CID-MS/MS has been used successfully with all of the types of molecules listed above to determine structural characteristics. FAB-MS/MS using CID has been particularly successful for providing sequence information for oligopeptides (10,15,18,36,66,69). In many

cases, however, FAB-MS/MS using CID does not produce complete characterization of structure, especially when one tries to determine double bond positions in fatty acids. Researchers have used this method to determine positions of individual double bonds (37), but compounds with multiple double bonds often yield ambiguous daughter spectra. In the case of unsaturated fatty acids and other difficult structural puzzles, FAB-MS/MS using ion/molecule reactions may be very informative due to the specificity of ion/molecule reactions for particular functional groups on a molecule. The TQMS provides us with the possibility of performing both FAB-MS/MS and ion/molecule reactions. This combination is particularly interesting because is enables the user to investigate the mechanisms of both FAB and ion/molecule reactions. Furthermore, ion/molecule reactions may have considerable analytical utility for the structural determination of ions desorbed by FAB.

H. Objectives of the Research Topic

The goals of this research are to establish the TQMS as an instrument with which one can perform and analyze ion/molecule reactions of all types, and to accomplish studies in organic ion/molecule chemistry. To meet these goals, six objectives have been established.

The first objective of this research project requires modification of the TQMS so that it is possible to perform FAB ionization and to permit reactive collision gases to be introduced into the collision chamber.

The second objective of this research is to use the TQMS to study a number of chemical reactions that have already been studied by other gas-phase techniques. The point of this study is to determine if

ion/molecule reactions in the TQMS produce product ions which are similar to the products of ion/molecule reactions that have been reported in the chemical literature.

The third objective of this research is to study a matrix of reactions of selected organic compounds with a set of reactive collision gases. The selected organic compounds will have a range of molecular weights and will each contain a different functional group. A similar approach has been used by McLafferty to study EI spectra (136). The reagent gases selected for this study will be those that show the greatest reactivity in the ion/molecule reaction studied in the literature. The purpose of the third objective is to determine what kinds of ion/molecule reactions occur in the central quadrupole, the CI volume, and in FAB, with the hope of finding reactions that are indicative of the presence of specific functional groups in the parent ion.

The fourth objective of this research is to do more complete studies of some of the reactions that are observed to occur as a result of completing objectives two and three. Those reactions that seem to be indicative of the presence of a functional group will be tested to see whether the same reaction can be used with a wide variety of molecules containing that functional group. The intention of this objective is to observe the effects of chain length, proton affinity, and the presence of other functional groups on the reactions being studied. The plan is to determine which of these ion/molecule reactions might be suitable for development into analytically useful methods for functional group identification and structural analysis of complex molecules.

The fifth objective of this project is to apply ion/molecule reactions in the central quadrupole to the study of the unique ions generated by FAB. Organic ion/molecule reactions may be strongly influenced by the presence of a cation. For example, a reaction that proceeds when the molecule is cationized by H^+, may or may not occur when the same molecule is cationized by Na^+.

The sixth objective of this study is to improve the probability of forming and detecting ion/molecule products in the central quadrupole. Several studies have shown that ion/molecule reactions in the central quadrupole are not very efficient when compared with CID or with ion/molecule processes that occur in the CI volume or in an ICR. The reason for this lack of efficiency is that there is no practical means of controlling the interaction time of the parent ions with the reactive target gas as in the ion-trapping techniques. Therefore, the plan is to pursue ion trapping in the central quadrupole as a means of increasing the observed yield of ion/molecule reactions in the central quadrupole region.

CHAPTER II.

SURVEY OF ION/MOLECULE REACTIONS IN THE TQMS BY GC-CI/TQMS

A. Introduction

Researchers in the past several years have described techniques for using either the CI volume or the central quadrupole region of the TQMS for studying organic ion/molecule reactions. One of the goals of this project was to begin a survey of the reactions which occur in those two zones of the TQMS. The strategy of the first part of this survey was to ionize a number of reactive gases in the CI volume region, and to react the reagent ions thus created with numerous other compounds containing a variety of functional groups. The strategy of the second part of this survey was to react ions containing various functional groups with reactive gases in the second quadrupole region. The point of this survey approach is to assess the feasibility of observing ion/molecule reactions for the presence of various combinations of functional groups. Information of this kind will help determine which ion/molecule reactions should receive further investigation. The difficulty with the survey approach is that considerable time is required to accomplish a complete survey if each compound to be studied is introduced individually by direct probe. The author sought to overcome this difficulty by using the capillary gas chromatograph (GC) which is available for use with the TQMS in the MSU-NIH-MSF. If one chooses a suitable mixture of compounds that do not react with each other in solution, one can inject that mixture into the GC and separate the components of the mixture so that they are presented sequentially to

the TQMS where they undergo ion/molecule reactions, the products of which are detected "on-the-fly" by repetitive MS or MS/MS scans.

Fortunately, such a mixture of test compounds already existed as a commercial product and did not have to be prepared by the author. K. Grob Jr., et al. (155) developed a solution of polar compounds for testing the separating power and reactivity of GC columns. This solution is marketed under the following name: Programmed Test Mixture (PTM). The PTM was clearly not designed for testing ion/molecule reactions in the TQMS, but it nevertheless is an ideal mixture for this purpose. The PTM contains 0.2-0.5 ug/ul of twelve different compounds dissolved in methylene chloride with molecular weights ranging from 90 to 214, and comprising ten different functional groups. Table 3 is a list of all the compounds in the PTM with names, structures, and molecular weights in order of their elution from an SPB-1 (bonded SE-30) capillary column.

The major advantage of the PTM for ion/molecule reactions is that all of the components of the mixture are underivatized. This means that their chemical reactivity has not been altered by the presence of trimethylsilyl groups that are often added to compounds in GC mixtures to improve their chromatographic properties. Of course, this also means that one needs an exceptionally unreactive capillary column to maintain chromatographic peak shape and resolution. A fused silica capillary column coated with DB-1 stationary phase was used for this purpose.

The author chose isobutane, methanol, benzene, and acetone as the reactive gases to be used in both the CI volume and the central quadrupole. All four of these chemicals were available in the MSU-NIH-MSF in large quantities as high purity gases or as volatile HPLC-grade

Table 3

Table of Names, Structures, and Molecular Weights of the PTM Compounds

Name	Structure	Molecular Weight
1. 2, 3-Butanediol		90
2. Decane	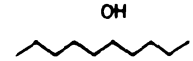	142
3. 1-Octanol		130
4. 2,6-Dimethylphenol	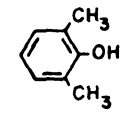	122
5. Nonanal	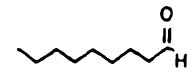	142
6. Undecane		156
7. 2-Ethylhexanoic Acid	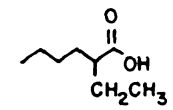	144
8. 2, 6-Dimethylaniline	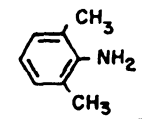	121
9. C_{10}-Acid Methyl Ester	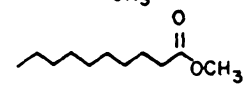	186
10. Dicyclohexylamine	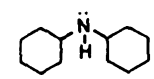	181
11. C_{11}- Acid Methyl Ester	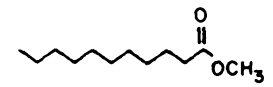	200
12. C_{12}-Acid Methyl Ester	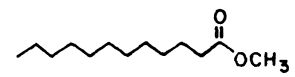	214

liquids. Isobutane CI was chosen to serve as a standard soft ionization method that produced mostly MH^+ ions. Methanol, benzene, and acetone were chosen because they have not been used extensively as CI gases and they represent the most common categories of functional groups: alcoholic (hydroxy) compounds, aromatic compounds, and carbonyl compounds. Ammonia was readily available, but was not used since another research group has already started an extensive research program into the organic ion/molecule reactions of ammonia and amines using a TQMS (92).

B. Experimental

1. Gas Chromatographic Conditions

The gas chromatograph used for separating the compounds in the PTM was an Hitachi model 663-30 that was equipped with two vaporizing injection ports, one for capillary columns, the other for packed columns. The splits for the vaporizing injectors were turned off so that all of the sample was swept onto the column. The column employed for this research was a 30 meter bonded-phase DB-5 fused-silica narrow-bore high-performance capillary column. The column was threaded through a glass heated transfer line directly into the ion source without any enrichment by a separator.

The same chromatographic conditions were used for all of the runs shown in this chapter. The injection port temperature was set a 250°C. The split was closed so that all of the vaporized sample was swept onto the column. The column oven was temperature programmed from 50°C to 250°C at a rate of 10°C per minute. This rate is five times as fast as recommended by the manufacturer of the PTM. The increase in the rate of

temperature programming was necessary to decrease the analysis time and to conserve the amount of space used for data storage on magnetic disk. The upper limit of the temperature program was set 50°C higher than that recommended by the manufacturer in order to purge any impurities with high boiling points from the column. Thus, the total analysis time for a single chromatographic run was 20 minutes rather than the 50 minutes recommended for optimum resolution of all components of the mixture. Fortunately the capillary column used for this study had sufficient resolving power that the increase in the temperature programming rate did not seriously degrade the chromatography. The transfer line from the GC oven to the TQMS ion source was heated to 200°C, and the ion source of the TQMS was heated to 150°C. The helium carrier gas pressure at the head of the column was 15 psi.

2. TQMS Conditions for CI/MS

Table 3 shows the TQMS parameters used for acquisition of the ion/molecule reaction data by chemical ionization. The first quadrupole was scanned repetitively from m/z 50 to m/z 275 to acquire the data for CI/MS. Both the second and third quadrupoles were set to the rf-only mode. The CI reagent gases were regulated by a needle valve to a pressure of $2X10^{-4}$ torr as measured by the ion source chamber pressure gauge. The total amount of sample injected onto the column in this mode was 2 ul. The total amount of each component injected onto the column ranged from 2-5 ug.

Table 3

TQMS Parameters for GC-CI/MS

Parameter	Value	Parameter	Value
Mode	+CI	M1	50-275 amu
EV	70.0 eV	M2	rf only
REP	33.3 V	M3	rf-only
CIV	33.9 V	DM1	1.8
EIV	-38.0 V	DM2	8.8
EXT	60.1 V	RM1	-
L1	-136.0 V	RM2	-
L2	-	P2	-
L3	13.4 V	THR	0
Q1	25.4 V	PWD	3
L4	5.3 V	MWD	30
Q2	24.0 V	RTE	2
L5	4.5 V	CI Volume Temp.	150°C
Q3	23.0 V	CI Gas Pressure	$2X10^{-4}$ torr
MHV	1600.0 V		

3. TQMS Conditions for CI/MS/MS

Table 4 shows the TQMS parameters used for acquisition of the ion/molecule reaction data by means of reactive collisions in the central quadrupole. Isobutane CI was chosen as the method of producing the six parent ions chosen for MS/MS analysis. A pressure of $2X10^{-4}$ torr isobutane was used as the reagent gas. Isobutane, methanol, acetone, and benzene were used as reactive collision gases in the central quadrupole. All of the reactive collision gases were regulated to a pressure of $2X10^{-3}$ torr in the collision chamber by a Granville-Phillips pressure controller.

4. Data System Programs Used for the GC/MS and GC/MS/MS

In order to take advantage of all the information generated by the PTM approach to ion/molecule reactions, the author wrote a very short method in the FORTH command language used by the TQMS microcomputer. This method enabled the TQMS to take repetitive full scanning MS and MS/MS data. All of the data in this section were converted to MSF format so that the GC/MS software called MSOUT which was available in the MSU-NIH-MSF could be used.

C. Results

1. Introduction

Separating the PTM is a difficult challenge for an ordinary chromatographic column since the compounds are all quite polar and would ordinarily be derivatized before chromatographic analysis. Figure 4

Table 4

TQMS Parameters for GC-CI/MS/MS

Parameter	Value
Mode	+CI
EV	70.0V
REP	33.3V
CIV	33.9V
EIV	-38.0V
EXT	60.1V
L1	-136.0V
L2	0.0V
L3	134V
Q1	25.5V
L4	5.8V
Q2	31.3V
L5	17.1V
Q3	26.0
MHV	1930.0V

Parameter	Value
M1	See text
M2	RF-Only
M3	70-275amu
DM1	2.0
DM3	8.8
RS1	—
RS3	—
THR	0
PWD	4
MWD	30
RTE	2
CI Volume Temp	150°C
CI Gas Pressure	2×10^{-4} torr
Central Quadrupole Pressure	2×10^{-4} torr

Programmed Test Mixture
Catalog No. 4-7304

This test mixture was formulated by K. Grob, Jr., *et. al.* (J. Chromatogr. *156*, 1-20, 1978). Their article contains operating parameters, elution orders (see example on reverse side of this form), and a theoretical description of how the test functions. Analysts must be familiar with the information in this article before using the test mixture.

The concentration of each component in this mixture is tenfold higher than that used by Grob, *et. al.* A 0.5µl injection of this mix, split at a 100:1 ratio, will deliver approximately the same amount of sample on-column (2-5ng/component) as the 20:1 split used by Grob.

This mixture contains the following components in methylene chloride:

Component	Concentration	Component	Concentration
C10 acid methyl ester	0.42µg/µl	2,6-Dimethylphenol	0.32µg/µl
C11 acid methyl ester	0.42µg/µl	2-Ethylhexanoic acid	0.38µg/µl
C12 acid methyl ester	0.41µg/µl	Nonanal	0.40µg/µl
2,3-Butanediol	0.53µg/µl	1-Octanol	0.36µg/µl
Dicyclohexylamine	0.31µg/µl	Undecane	0.29µg/µl
2,6-Dimethylaniline	0.32µg/µl	Decane	0.28µg/µl

S Methylene chloride (solvent)
I Impurity in solvent
1 2,3-Butanediol
2. Decane
3. 1-Octanol
4 2,6-Dimethylphenol
5. Nonanal
6. Undecane
7 2-Ethylhexanoic acid
8. 2,6-Dimethylaniline
9. C10 acid methyl ester
10. Dicyclohexylamine
11. C11 acid methyl ester
12. C12 acid methyl ester

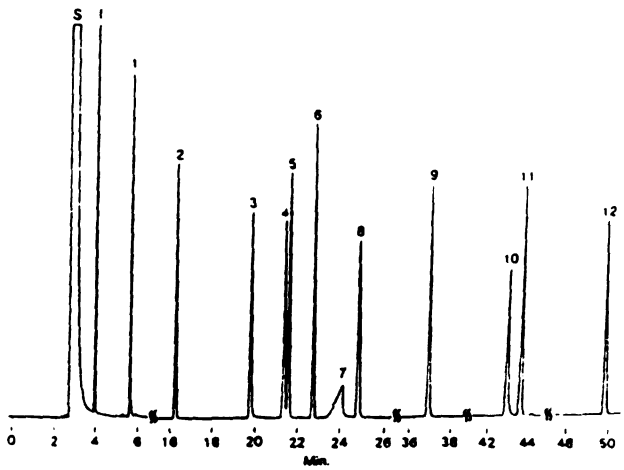

SPB-1 (bonded SE-30) capillary column, 30m x 0.25mm ID, Col. Temp.: 50°C to 200°C at 2°C/min., Inj. and Det. Temp.: 250°C, Linear Velocity: 20cm/sec. He, Det.: FID, Sens.: 4 x 10^{-11} AFS, Sample: 1µl of Cat. No. 4-7304, 100:1 Split Ratio.

NOTE - This elution pattern is specific for an SPB-1 column. Consult Grob's article for elution orders for other column polarities.

Figure 4. Chromatogram of the PTM Supplied by the Manufacturer

shows the chromatogram supplied by the manufacturer of the PTM. Figure 5 demonstrated that even a very good column has difficulty separating 2,6-dimethylphenol from nonanal (compounds 4 and 5), and dicyclohexylamine from C_{11}-acid methyl ester (compounds 10 and 11). Figure 4 also shows that the peak shape for 2-hexanoic acid (compound 7) is very poor due to its reactivity with the column.

Since CI was being employed as the ionization method in the TQMS, the author did not expect to observe either of the hydrocarbons in the mixture since the proton affinity of straight chain hydrocarbons is so low. Also, the author did not expect the column to resolve the two pairs of compounds mentioned in the preceding paragraph, since the rate of temperature programming had been set 5 times faster than in Figure 4 (see experimental section of this chapter for details). The maximum scan rate of the TQMS quadrupoles as driven by the microcomputer was such that a scan from m/z 50-275 could be completed and stored every 2 seconds. This slow scan rate means that each of the sharp capillary chromatographic peaks are represented by only 2 or 3 points in the reconstructed total ion current chromatograms shown in this chapter. Therefore, the representation of the resolution of the column was degraded. It is extremely fortunate in this regard that the compounds in the PTM, which are difficult to separate, all have $(M+H)^+$ ions with different m/z values. This fact means that those peaks which are not resolved in the total ion chromatogram can nevertheless be distinguished by means of mass chromatograms.

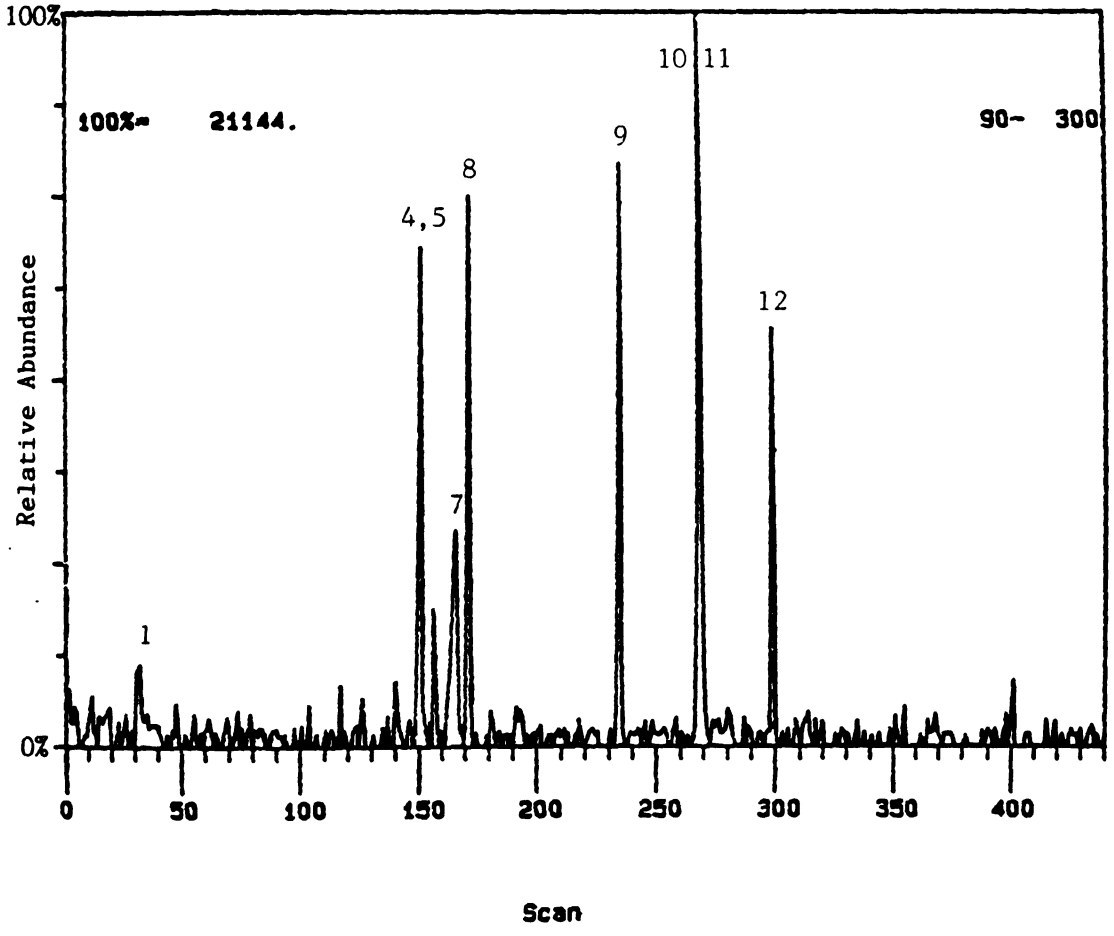

Figure 5. Reconstructed Total Ion Chromatogram of the PTM (Isobutane CI)

2. Isobutane CI/MS of the PTM

Figure 5 shows the reconstructed total ion chromatogram (TIC) of the PTM as ionized by isobutane CI. Actually ions with m/z values less than 90 have been excluded from Figure 6 so that the extremely abundant reagent ions of isobutane do not obscure the features of the chromatogram. Figure 5 shows that, as expected, there is no peak for decane (compound 2), but unexpectedly there is a peak for undecane (compound 6) and there is no peak for octanol (compound 3). There is also a peak at a very long retention time which is quite reproducible that is apparently an impurity in the PTM. Figure 5 also reveals that compounds 4 and 5 are not resolved chromatographically. Although it does not appear so in Figure 5, compounds 10 and 11 are resolved chromatographically as a close inspection of the mass chromatograms reveals in Figure 6. If the TQMS were capable of scanning more quickly, the resolution of the two compounds would be easier to observe. As in Figure 4, the peak shape of compound 7 is quite poor due to its reactivity with the column. In spite of the slow scan rate of the TQMS and the rapid temperature program of the GC oven, the mass chromatography of these difficult polar compounds is excellent.

The sensitivity of the method, as judged by the signal to noise ratios of peaks in the total ion current chromatogram is not ideal, but all of the peaks have signal to noise ratios of three or better. The signal level was, therefore, sufficient to generate reproducible mass chromatograms and mass spectra, but minor mass spectral details such as isotope peaks are sometimes missing from the figures in this chapter.

The reagent ion peaks of the four CI gases and other interfering background peaks have been subtracted from the mass spectra shown in

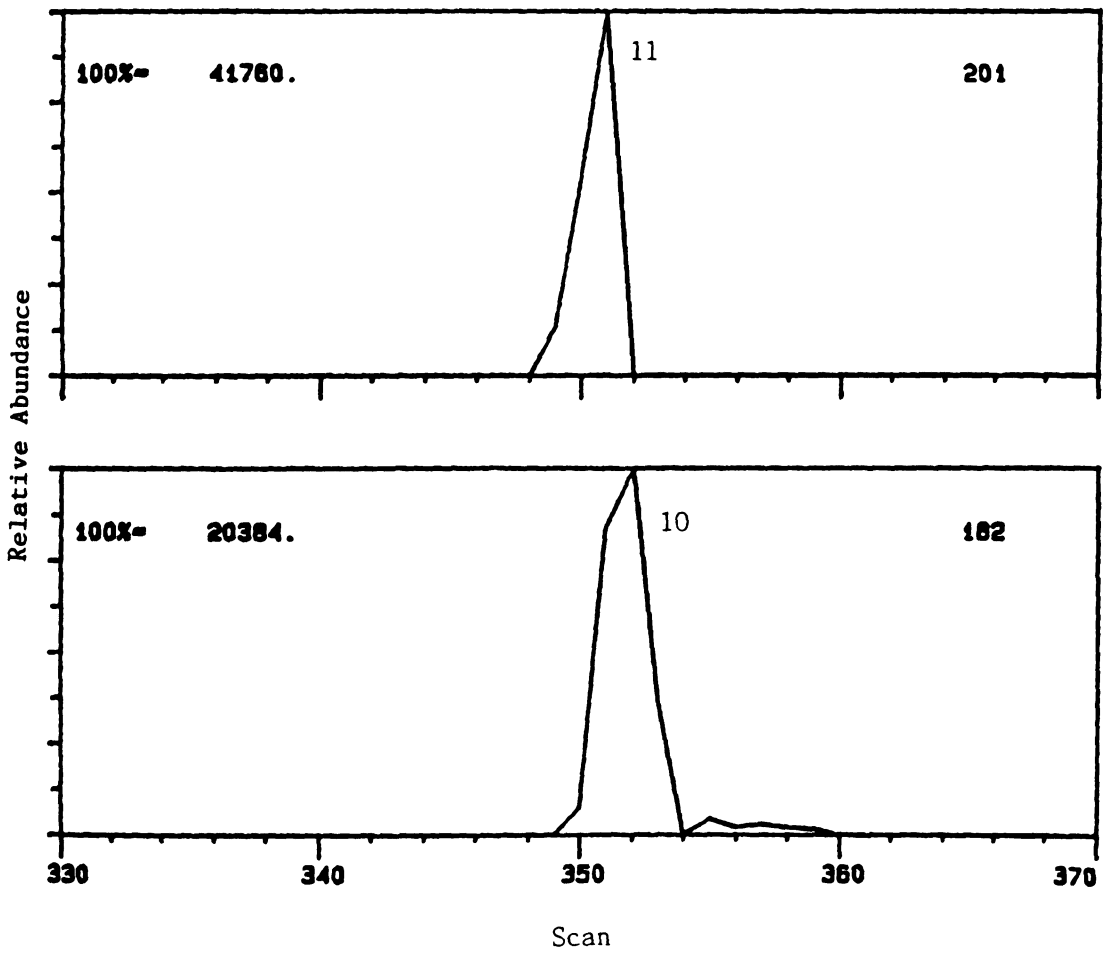

Figure 6. Partial Mass Chromatograms Showing Resolution of Dicyclohexylamine and C_{11}-Acid Methyl Ester

this chapter. Figure 7 shows the mass spectrum of 2,3-butanediol (compound 1) showing an $(M+H)^+$ ion and one major fragment ion, the $(MH-H_2O)^+$ ion. Figure 8 shows the overlapping mass spectra of 2,6-dimethylphenol and nonanal due to lack of chromatographic resolution. The spectrum of each compound consists solely of the $(M+H)^+$ ion, so there is no ambiguity in determining the identity of the mass spectral peaks. Figure 9 shows the mass spectrum of undecane which includes the $(M-H)^+$ not an $(M+H)^+$ ion. The hydride-abstracted molecule is characteristic of hydrocarbons ionized by CI. Figure 9 also shows a number of peaks that are representative of typical hydrocarbon fragment ions. Figure 10 shows the mass spectrum of 2-ethylhexanoic acid with its $(M+H)^+$ ion. Figure 11 shows the mass spectrum of 2,6-dimethylaniline with an $(M+H)^+$ ion and an $(MH-NH_2)^+$ fragment ion. Figure 12 shows the mass spectrum of C_{10}-acid methyl ester with an $(M+H)^+$ ion and an $(MH-CH_3OH)^+$ fragment ion. Figure 13 shows the mass spectrum of dicyclohexylamine with an $(M+H)^+$ ion. Figure 14 shows the mass spectra of C_{11}-acid methyl ester (14a), and C_{12}-acid methyl ester (14b) both with $(M+H)^+$ ions but without the loss of methanol seen in the spectrum of the C_{10}-acid methyl ester. Figure 15 shows the mass spectrum of an impurity in the PTM whose structure is unknown. The unknown shows an ion of m/z 246; if this is the $(M+H^+)$ ion, the even m/z value indicates the presence of an odd number of nitrogens. The fragment ion at m/z 77 is probably the phenyl cation. McLafferty (136) indicates that a fragment ion of m/z 132 (as is observed in the spectrum of the unknown) is common in the spectra of aromatic amines and aromatic amides. These factors indicate that the unknown is a aromatic nitrogen

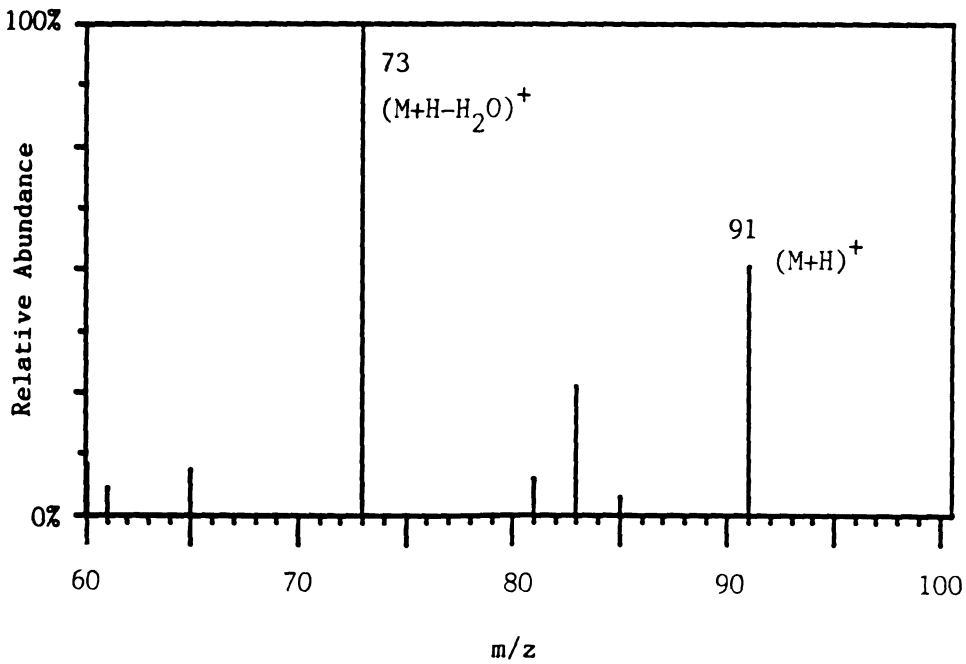

Figure 7. Isobutane CI Mass Spectrum of 2,3-Butanediol

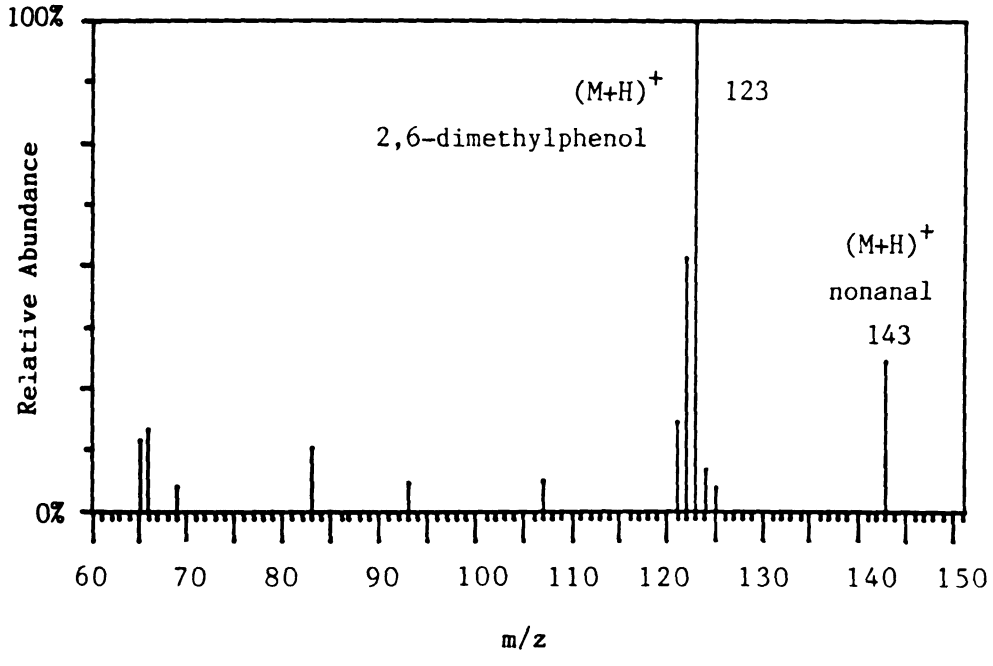

Figure 8. Isobutane CI Mass Spectrum of a Mixture of Nonanal and 2,6-Dimethylphenol

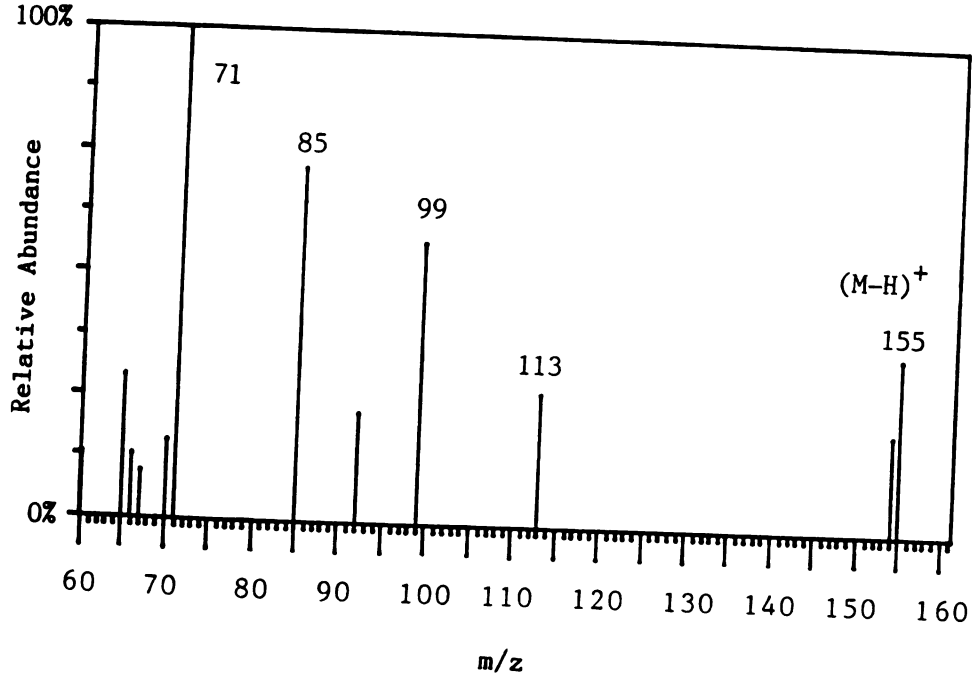

Figure 9. Isobutane CI Mass Spectrum of Undecane

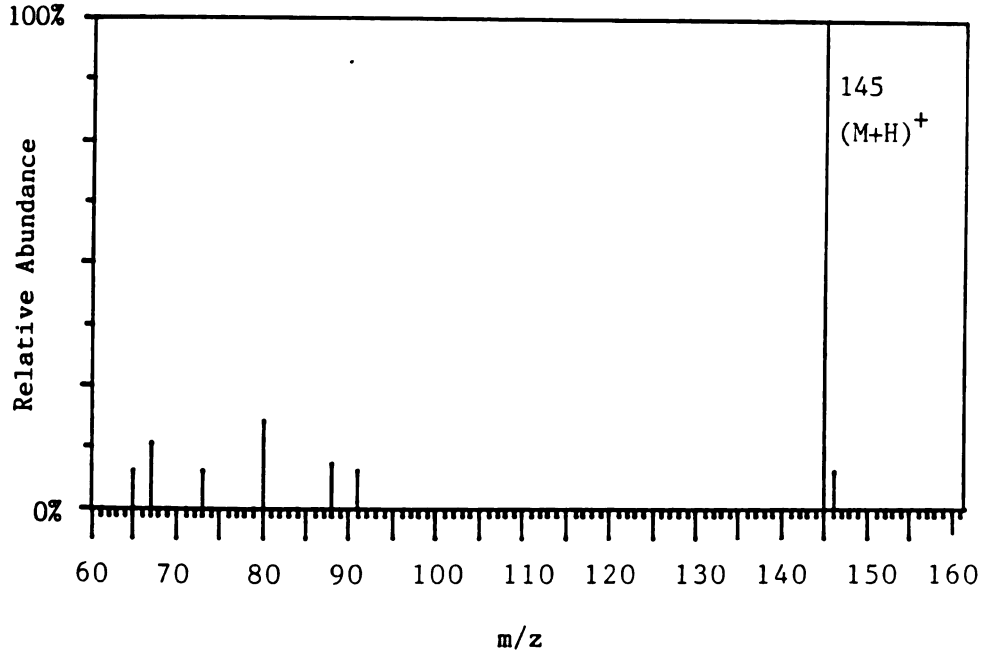

Figure 10. Isobutane CI Mass Spectrum of 2-Ethylhexanoic Acid

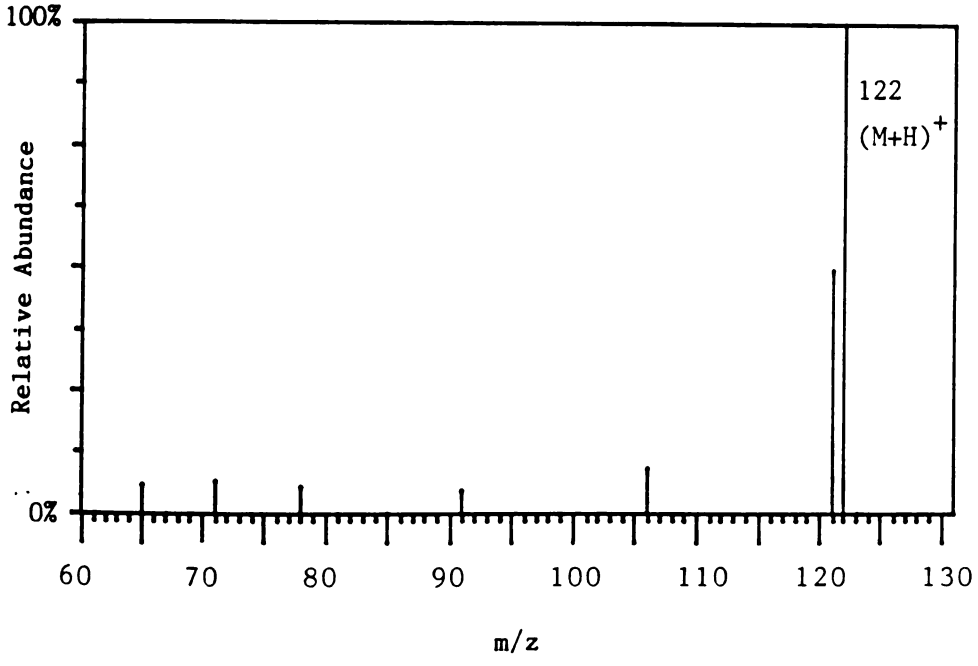

Figure 11. Isobutane CI Mass Spectrum of 2,6-Dimethylaniline

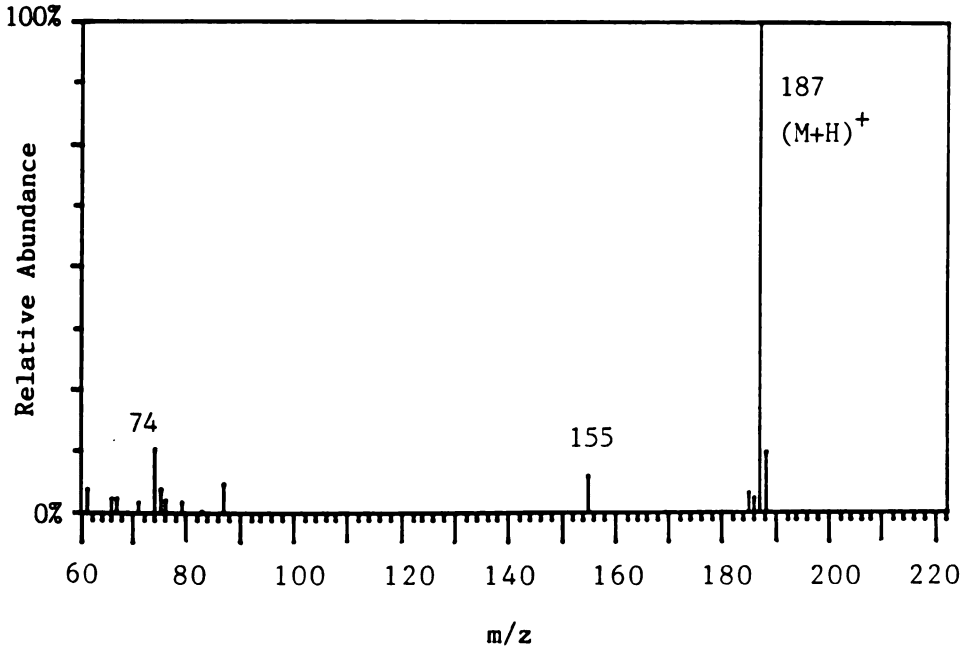

Figure 12. Isobutane CI Mass Spectrum C_{10}-Acid Methyl Ester

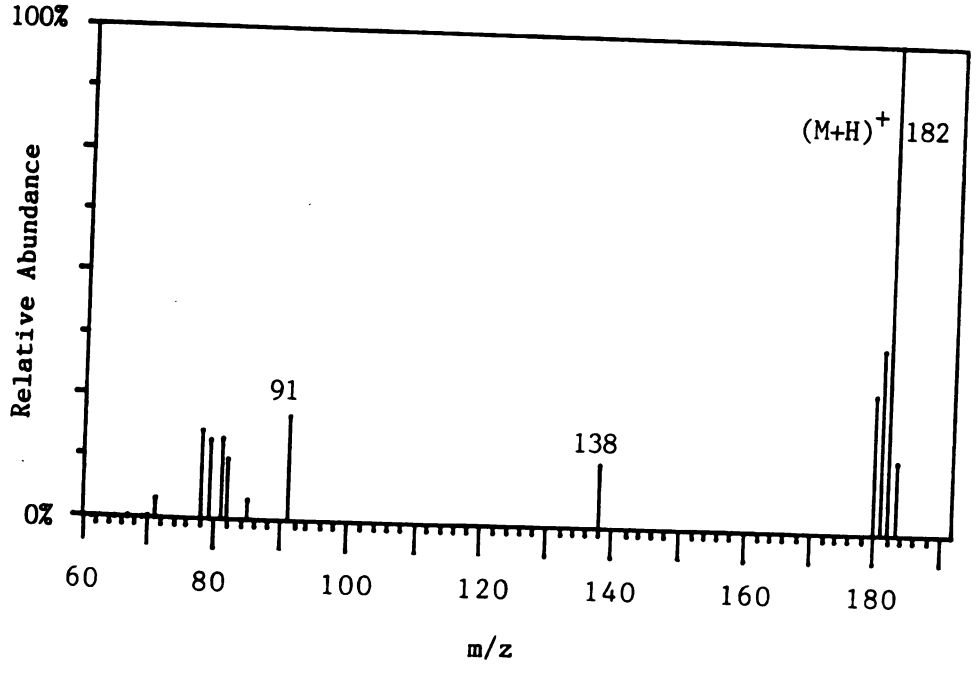

Figure 13. Isobutane CI Mass Spectrum Dicyclohexylamine

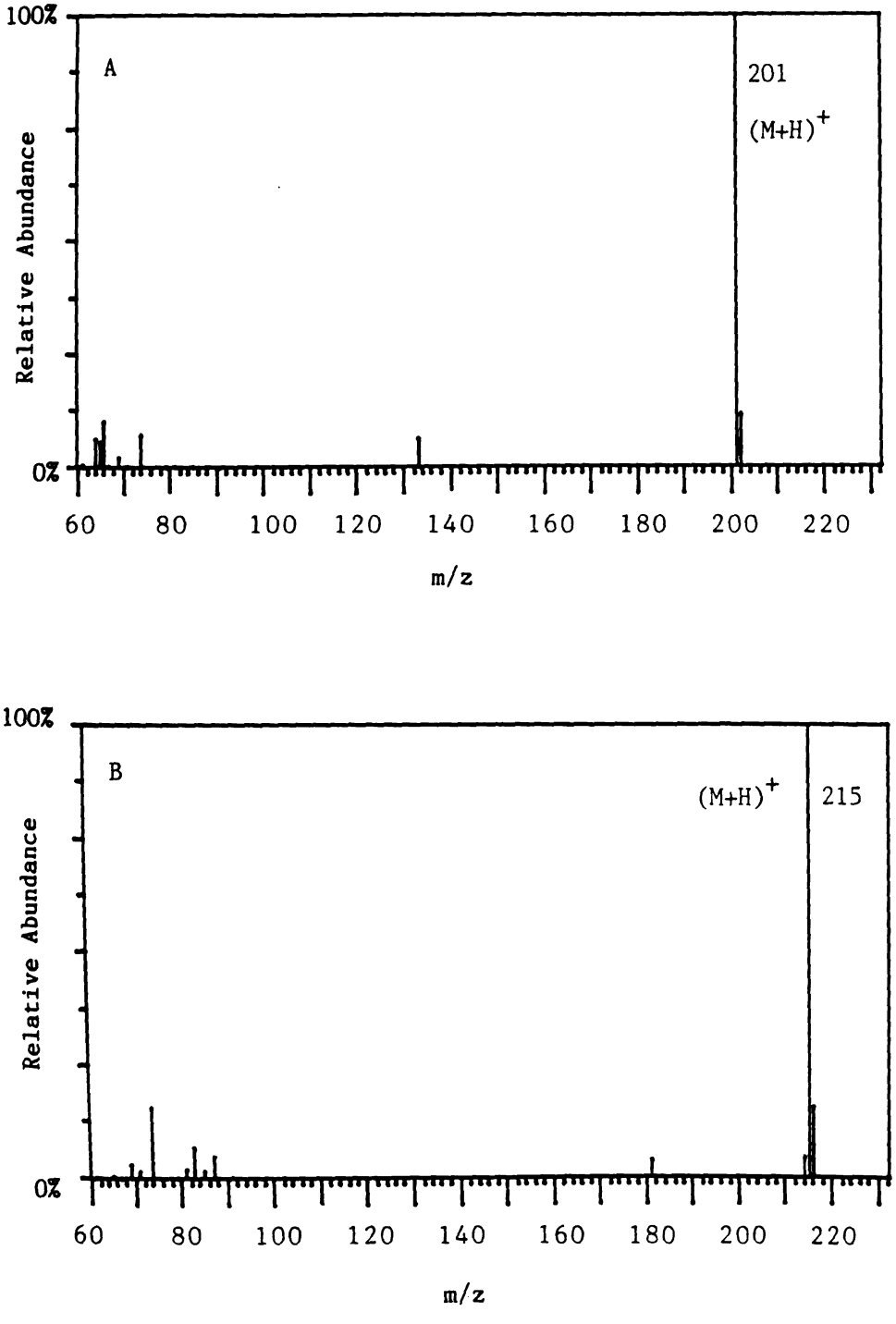

Figure 14. Isobutane CI Mass Spectrum C_{11}- and C_{12}-Acid Methyl Esters

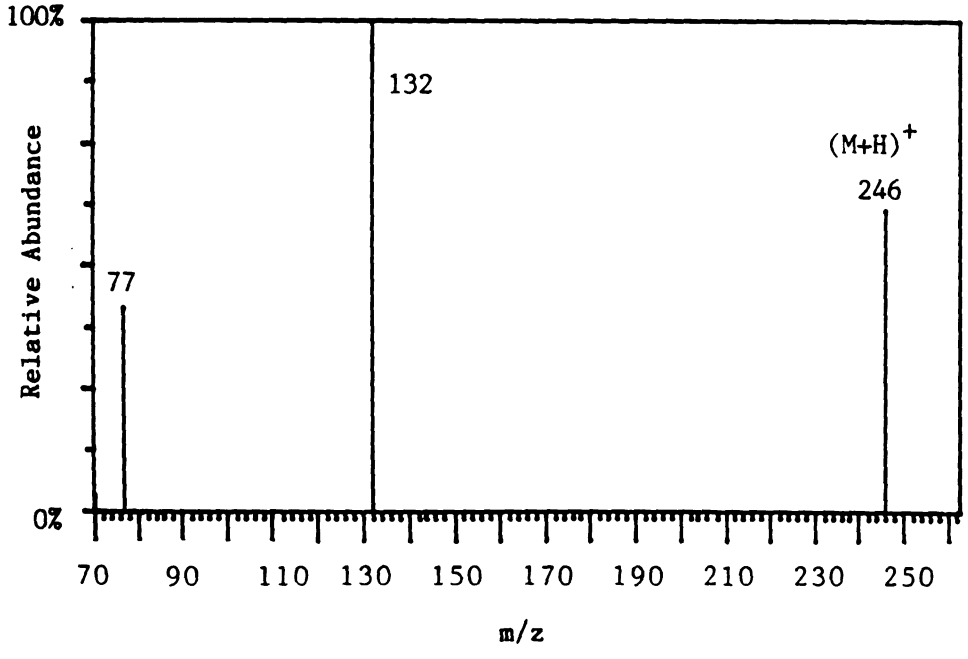

Figure 15. Isobutane CI Mass Spectrum of Impurity in the PTM

compound, but without more data it is difficult to identify the structure.

As expected, the isobutane CI of the PTM compounds provided no ion/molecule reaction products other than $(M+H)^+$ ions, $(M-H)^+$ ions, and a few fragment ions. Isobutane CI, therefore serves as a good blank against which all the reactions produced by other CI gases can be compared.

3. Methanol CI of the PTM

Methanol CI has been studied by M. Bauer in the MSU-NIH-MSF who has determined that it is a "softer" ionization method than methane or isobutane CI. This indicates that methanol CI produces fewer fragment ions, with more of the ion current concentrated in the $(M+H)^+$ ion. Methanol CI has, therefore, been suggested as a new method for quantitative analysis. The major reagent ions in methanol CI have m/z values of 33, 65, and 97, corresponding to the protonated monomer, and the proton-bound dimer and trimer of methanol respectively. Each of the three major ions loses water to form less abundant peaks at m/z 15, 47, and 79.

Figure 16 shows the reconstructed ion current chromatogram of the PTM as ionized by methanol CI. Because the reagent ions of methanol extend into the mass range of the ions collected for the compounds represented by the chromatogram in Figure 16, the reagent ions of methanol had to be subtracted from the total ion current so that one could observe the features of the chromatogram that were due to the presence of the PTM compounds. It is interesting to note that careful background subtraction decreases the amount of baseline noise in the

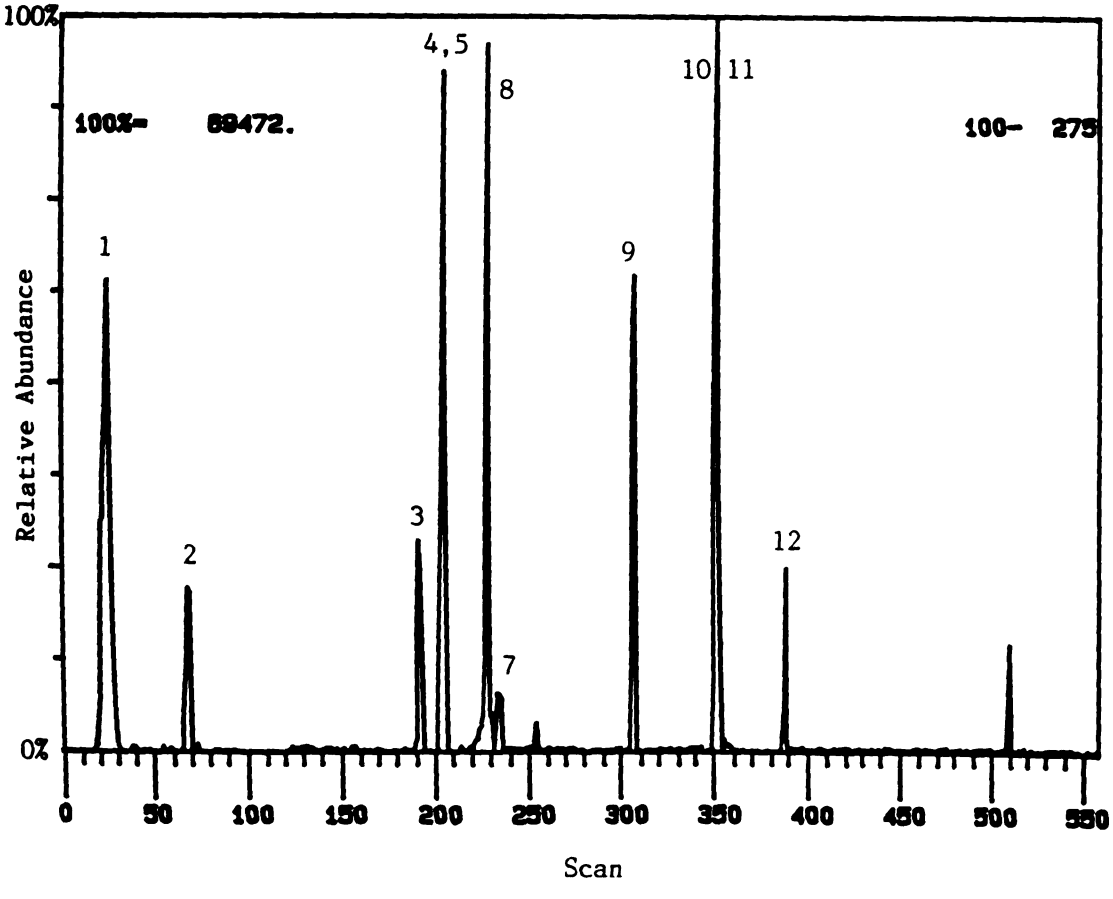

Figure 16. Reconstructed Total Ion Chromatogram of the PTM (Methanol CI)

reconstructed chromatogram, and that methanol CI produced a larger total ion signal than isobutane CI produced. The net result is an increase in signal-to-noise ratio of about one order of magnitude for the detection of the PTM compounds when one switches from isobutane to methanol CI.

The reconstructed total ion chromatograms of isobutane and methanol CI are similar for the most part, but a few notable differences exist. The methanol chromatogram exhibits a peak for the methylene chloride solvent, whereas the isobutane chromatogram does not. This difference, however, is only an artifact of the computer-assisted data processing; in one case the solvent ions were subtracted out, and in the other they were not. The major difference between the two chromatograms is that whereas undecane was ionized by isobutane CI and octanol was not, undecane was not ionized by methanol and octanol was. Therefore, peak 6 is absent from the methanol CI chromatogram and peak 3 is observed. Another difference in the two chromatograms is that peak 7 (2-ethylhexanoic acid) is even more poorly shaped in the methanol chromatogram than in the isobutane chromatogram. It is, in fact, split into two humps, one of which interferes with peak 8. The reason for this is unclear, but it probably lies in the chromatography (possibly the author's injection technique) and it probably has nothing to do with which CI gas was employed in the TQMS.

Figure 17 shows the methanol CI mass spectrum of 2,3-butanediol. One observes an $(M+H)^+$ ion and an $(MH-H_2O)^+$ ion as in isobutane CI, but one also observes several other ion/molecule reaction products at m/z values higher than the $(M+H)^+$ ion. The peak at m/z 123 probably represents the proton-bound adduct of methanol and the diol. The peak at m/z 105 would then be by analogy to methanol self-CI the (proton-

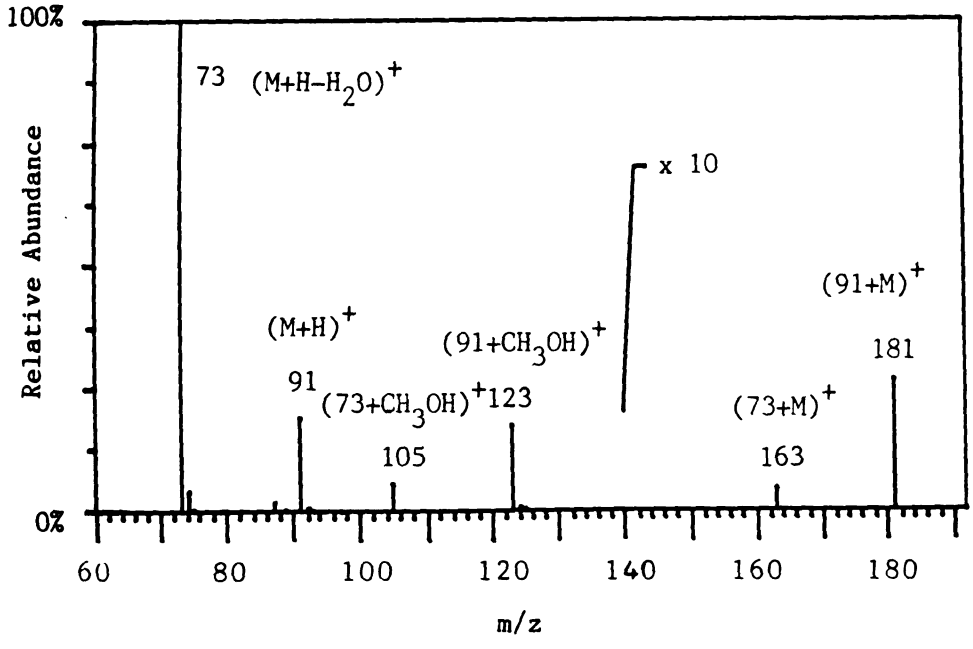

Figure 17. Methanol CI Mass Spectrum of 2,3-Butanediol

bound adduct - $H_2O)^+$ ion, presumably with an ether structure as is discussed in Chapter V. The $(M+H)^+$ ion of the diol is apparently in significant enough abundance that it is able to react with the neutral diol to form the protonated diol dimer ion at m/z 181, and the (protonated dimer - $H_2O)^+$ ion at m/z 163.

Figure 18 shows the methanol CI mass spectrum of 2-octanol. One observes very similar ion/molecule chemistry to that exhibited by the diol. A low abundance peak is present representing the $(M+H)^+$ ion of octanol, and two fragment ion peaks are also present: the $(MH-H_2O)^+$ ion at m/z 113 which is the base peak, and the $C_5H_{11}^+$ ion at m/z 71. One also observes a peak for the proton-bound adduct ion of methanol and octanol at m/z 163. The peak at m/z 177 is probably the result of the reaction between protonated dimethyl ether (m/z 47, a reagent ion in methanol CI) and octanol to form the proton-bound adduct ion.

Figure 19 shows the overlapping methanol CI mass spectra of 2,6-dimethylphenol and nonanal. The base peak (m/z 123) of Figure 19 is the $(M+H)^+$ ion of the phenol and there are no other major peaks attributable to the phenol. The peak at m/z 143 is the $(M+H)^+$ ion of the aldehyde. The peak at m/z 175 is the proton-bound adduct of the aldehyde and methanol, and the peak at m/z 157 is likely the (proton-bound adduct - $H_2O)^+$. The structure of the m/z 157 ion is possibly that of protonated octyl methyl ketone. The reaction of aldehydes and protonated alcohols to form ketones or acetals is discussed in more detail in Chapter VIII. There is also a peak of very low abundance at m/z 189 which is probably the protonated dimethylether and nonanal. The formation of this ion is analogous to that of the m/z 177 ion in Figure 18.

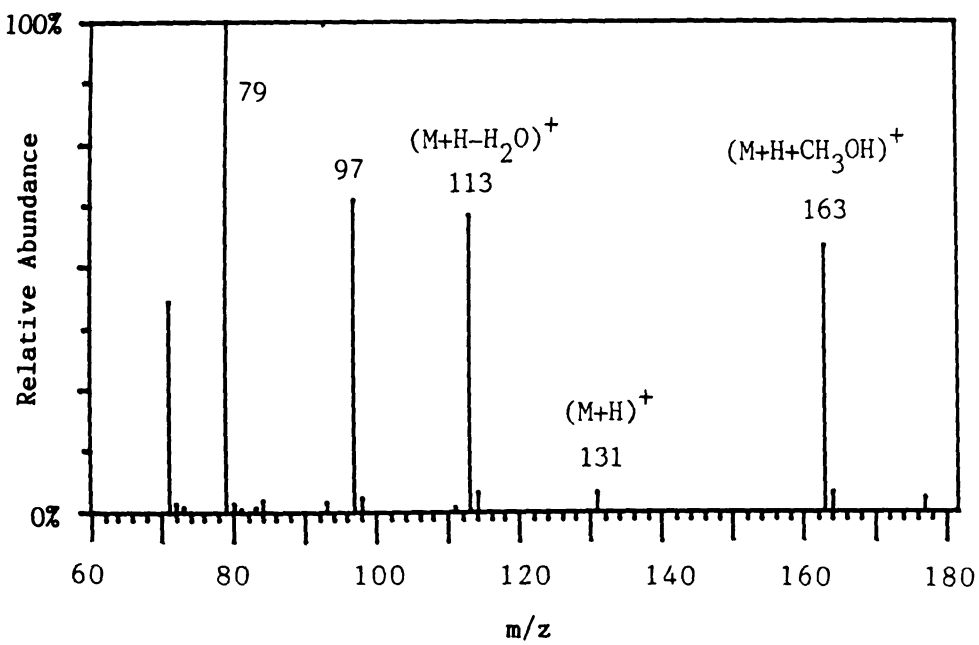

Figure 18. Methanol CI Mass Spectrum of 2-Octanol

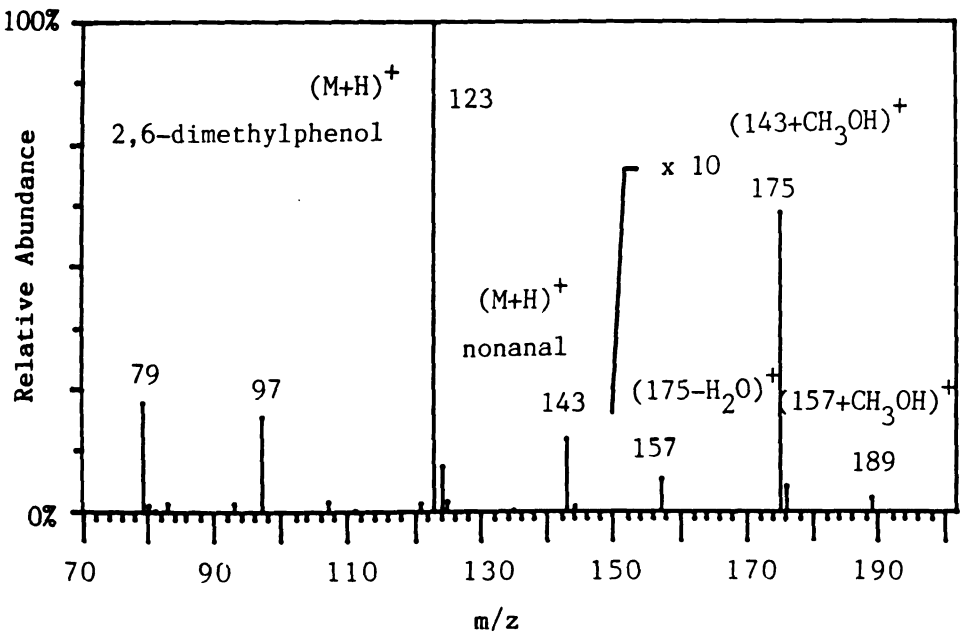

Figure 19. Methanol CI Mass Spectrum of a Mixture of 2,6-Dimethylphenol and Nonanal

Figure 20 shows the methanol CI mass spectrum of 2-ethylhexanoic acid. The peak at m/z 145 is the $(M+H)^+$ ion of the acid and the peak at m/z 127 is the $(MH-H_2O)^+$ ion. The peak at m/z 177 is the proton-bound adduct of the acid and methanol, and the peak at m/z 159 is the (proton-bound adduct - $H_2O)^+$ ion. The m/z 159 peak is the protonated methyl ester of the 2-ethylhexanoic acid, and the reaction that forms this type of ion is discussed in detail in Chapter V.

Compounds 8, 9, 10, 11, and 12 all react with some of the methanol CI reagent ions to give only the respective protonated molecules, so the mass spectra are not presented here in the interest of saving space. Clearly methanol is much more reactive in the gas phase than isobutane and produces a number of interesting ion/molecule reaction products with alcohols, aldehydes and acids.

4. Benzene CI of the PTM

Benzene CI has never to the author's knowledge been used as a technique for GC-MS, although ion/molecule reactions in benzene have been investigated by ICR (125). The author, however, was interested in exploring any reactions that might take place since benzene is such an important molecule in organic chemistry.

As it turned out, the most interesting part of the benzene CI investigation of the PTM was the reagent ions of benzene. The author had expected the reagent ions of benzene CI to be the molecular ion of benzene, the protonated molecule of benzene, and perhaps some fragment ions. Figure 21, which shows the self-CI mass spectrum of benzene indicates the presence of the expected ions and also many more. The structures of some of these ions and the mechanisms for their formation

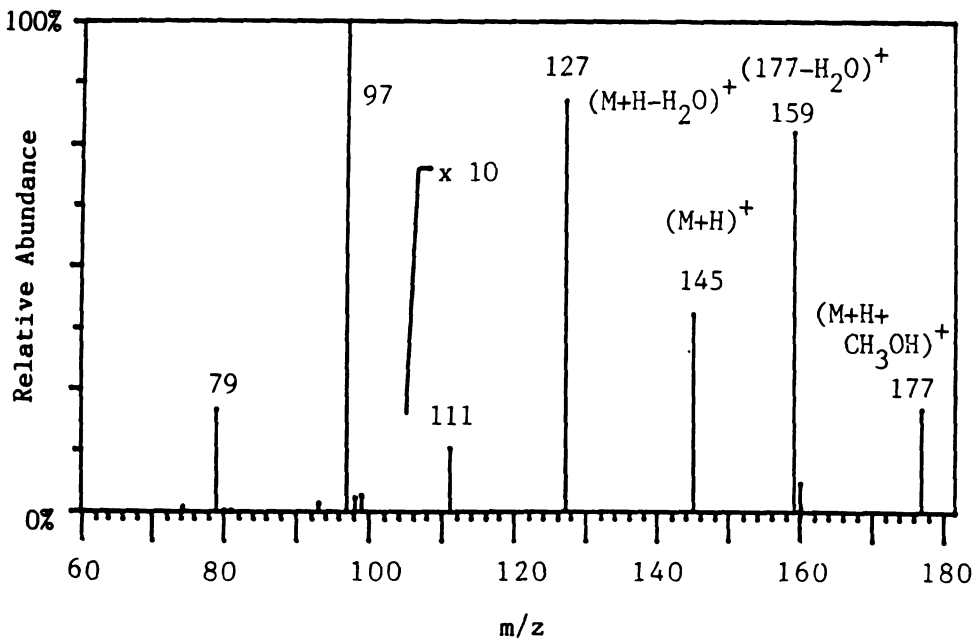

Figure 20. Methanol CI Mass Spectrum of 2-Ethylhexanoic Acid

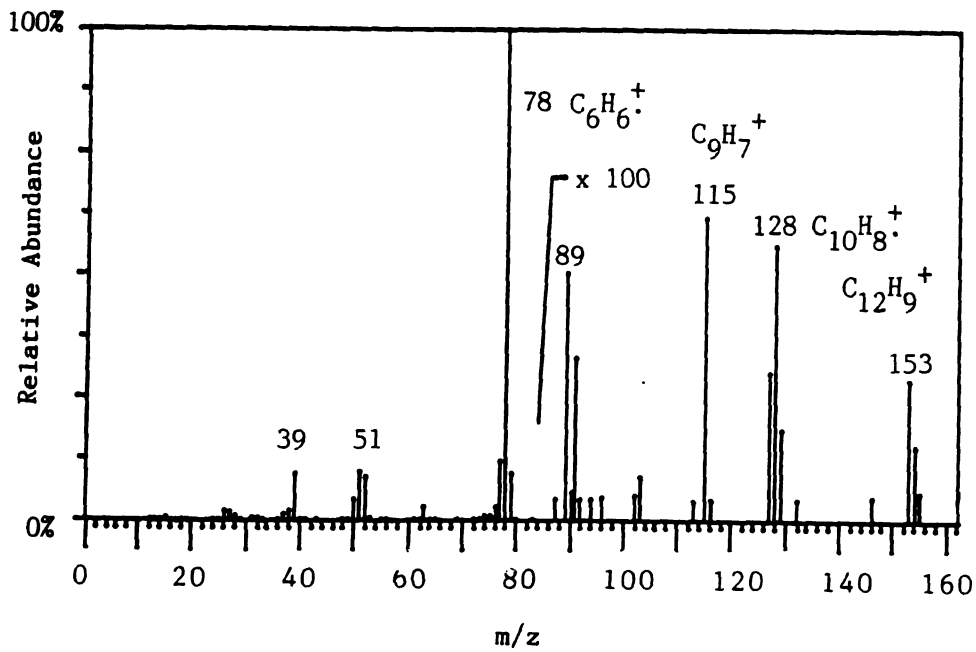

Figure 21. Self-CI Mass Spectrum of Benzene

were investigated during the course of this research project and are presented in Chapter VII.

The reconstructed total ion chromatogram of the ions generated from the PTM compounds by benzene CI is shown in Figure 22. The total ion chromatogram and the relevant mass chromatograms show that only seven of the PTM compounds are detected by benzene CI, with decane, 1-octanol, nonanal, undecane, and 2-ethylhexanoic acid missing. Of the PTM compounds detected, the two aromatic compounds are of greatest abundance. These data show that benzene CI is not a universal ionization technique, rather it tends to be selective for aromatic compounds.

Figure 23 shows the benzene CI mass spectrum of 2,3-butanediol. The base peak is the molecular ion at m/z 90. An $(M+H)^+$ ion at m/z 91 probably does exist in significant abundance, but one of the reagent ions of benzene also has an m/z value of 91, so the $(M+H)^+$ ion is missing due to background subtraction. One piece of evidence in support of the presence of a protonated molecule is the existence of a peak at m/z 73, which is probably the $(MH-H_2O)^+$ ion. In all of the benzene CI spectra there are several peaks of very low abundance with m/z values greater than that of the molecular ion. These ions are frequently the same in different spectra and do not correspond to logical neutral gains due to ion/molecule reactions. Therefore, the author suspects that they are due to minor artifacts of the computerized background subtraction process.

Figure 24 is the benzene CI mass spectrum of 2,6-dimethylphenol. The base peak is the molecular ion at m/z 122, and there is a much

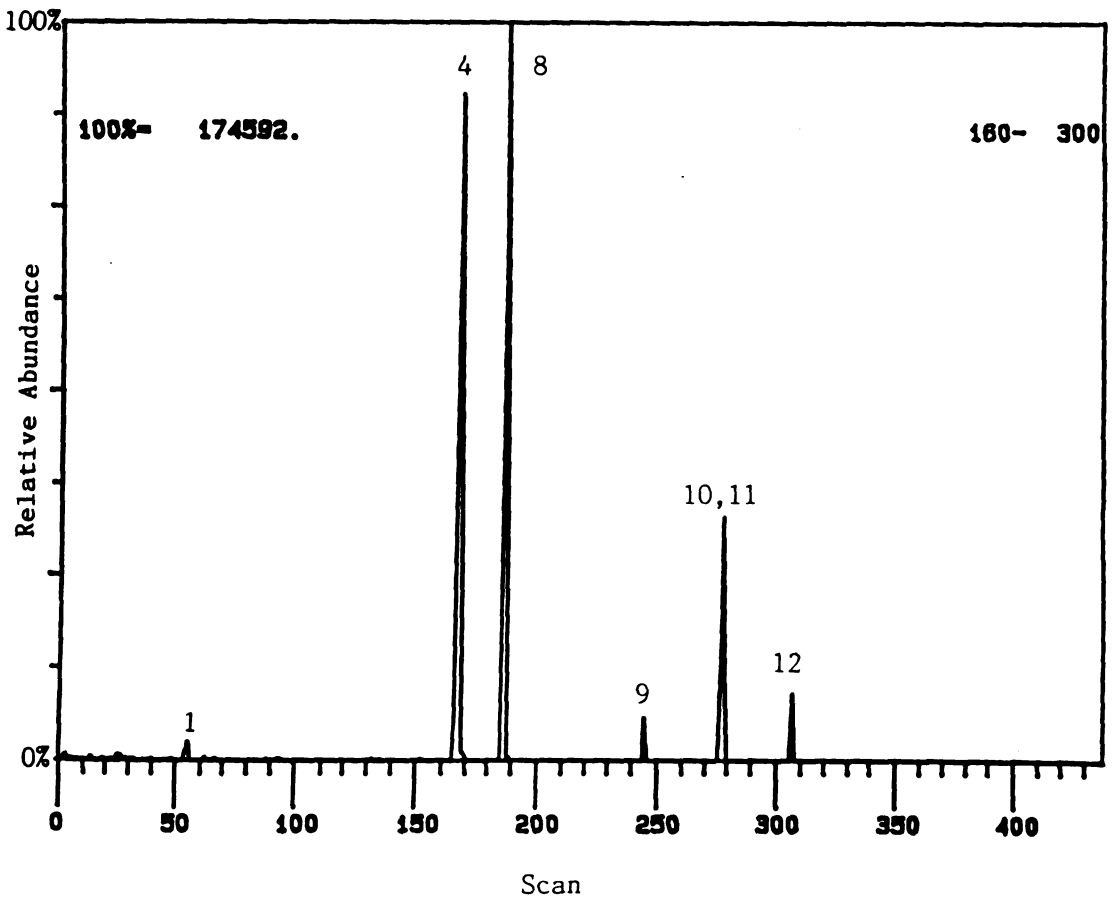

Figure 22. Reconstructed Total Ion Chromatogram of the PTM (Benzene CI)

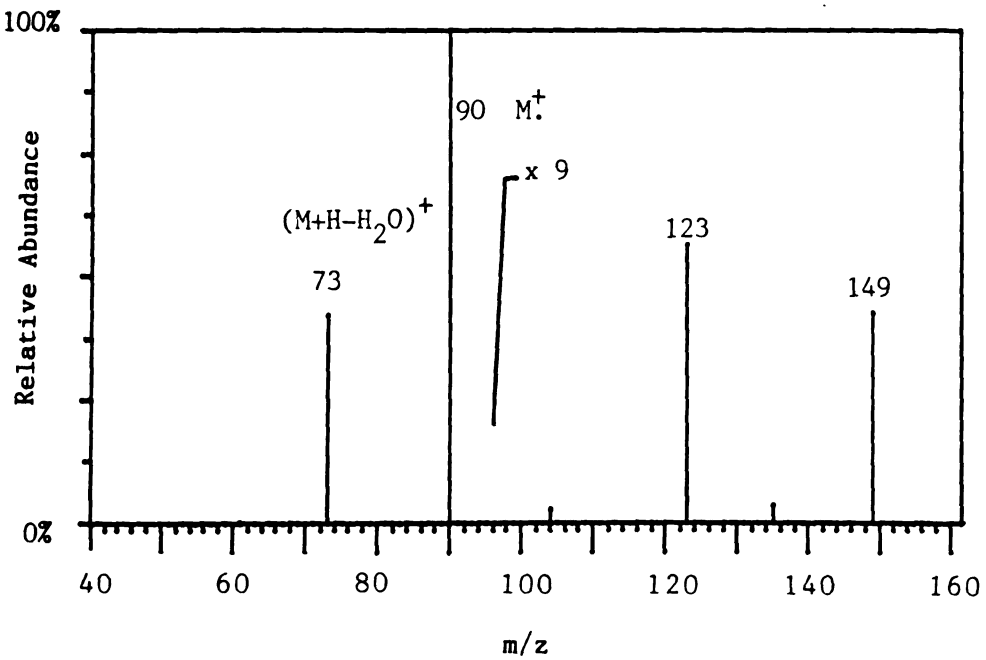

Figure 23. Benzene CI Mass Spectrum of 2,3-Butanediol

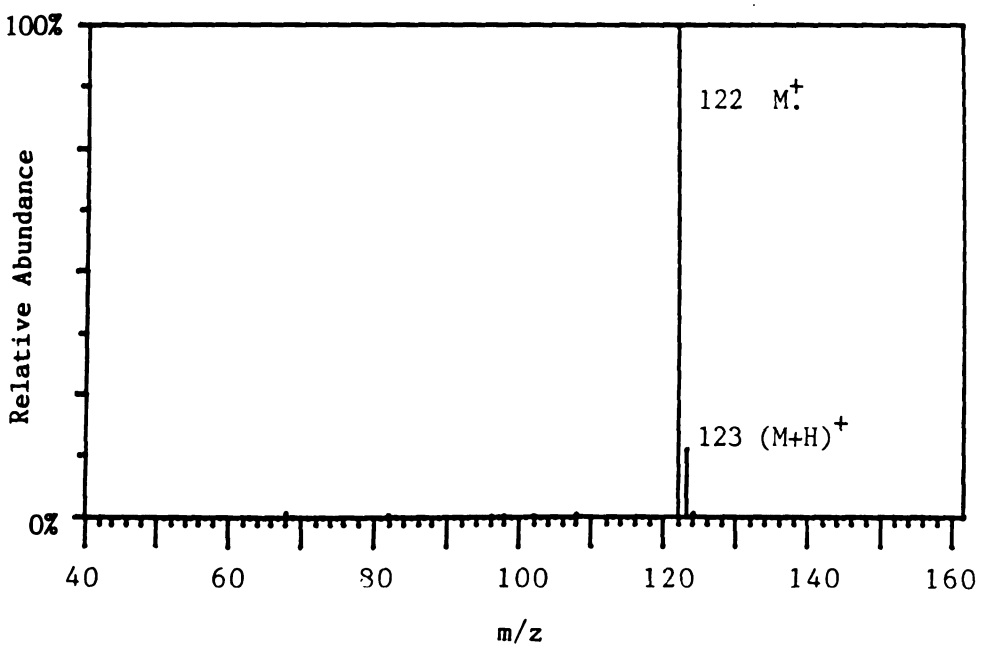

Figure 24. Benzene CI Mass Spectrum of 2,6-Dimethylphenol

smaller $(M+1)^+$ peak which is too abundant to be simply the ^{13}C isotope peak. Therefore, benzene CI must be producing both the molecular ion and protonated molecule of phenol.

Figure 25 is the benzene CI mass spectrum of 2,6-dimethylaniline. This spectrum is very similar to the one in Figure 24, in that the base peak at m/z 121 is the molecular ion and that the peak representing the $(M+H)^+$ ion is of low abundance. There is a fragment ion peak of significant intensity at m/z 106, probably $(M-CH_3\cdot)^+$, which matches with the fragment ion peak found in isobutane CI.

The benzene CI mass spectra of compounds 9, 10, and 11 follow the same pattern as in Figures 24 and 25: the protonated molecule is of low abundance and the molecular ion is the base peak of the spectrum. Compound 12, the C_{12}-acid methyl ester, has a slightly different pattern with the $(M-H)^+$, $M^+\cdot$, and $(M+H)^+$ ions in an abundance ratio of 1:2:3.

All things considered, benzene CI behaves very differently than any other chemical ionization gas the author has ever read about. It produces mainly molecular ions, few fragment ions, and no ion/molecule product ions other than the protonated molecules.

5. Acetone CI of the PTM

Acetone chemical ionization has not been used as an analytical technique, but ion/molecule reactions of acetone have been investigated by ICR (140). A mass spectrum of the acetone CI reagent ions is shown in Figure 26. The major peaks are the $(M+H)^+$ of acetone at m/z 59, the protonated dimer of acetone at m/z 117. There are two other less

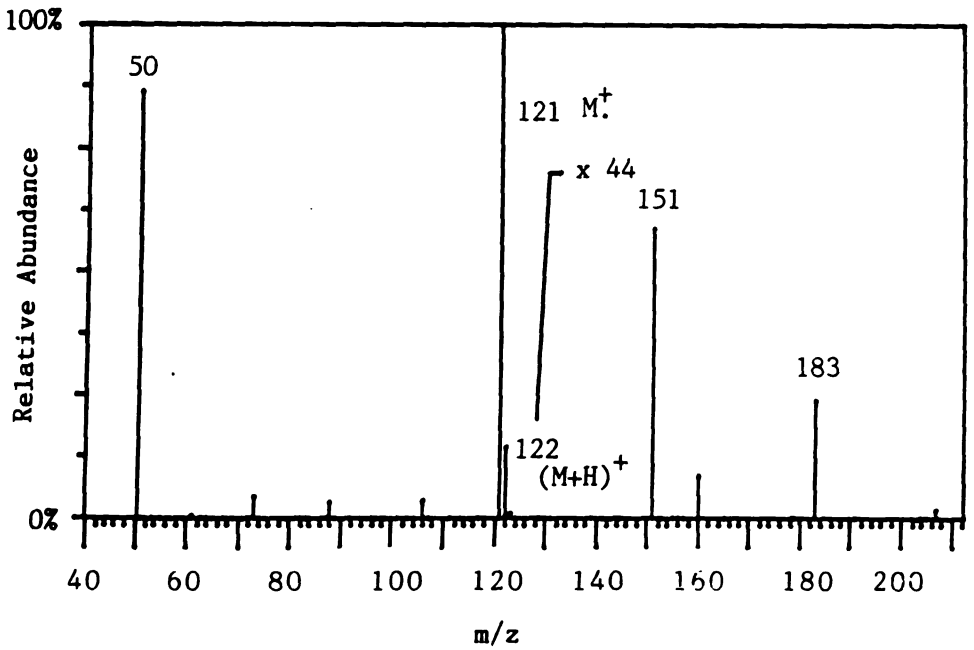

Figure 25. Benzene CI Mass Spectrum of 2,6-Dimethylaniline

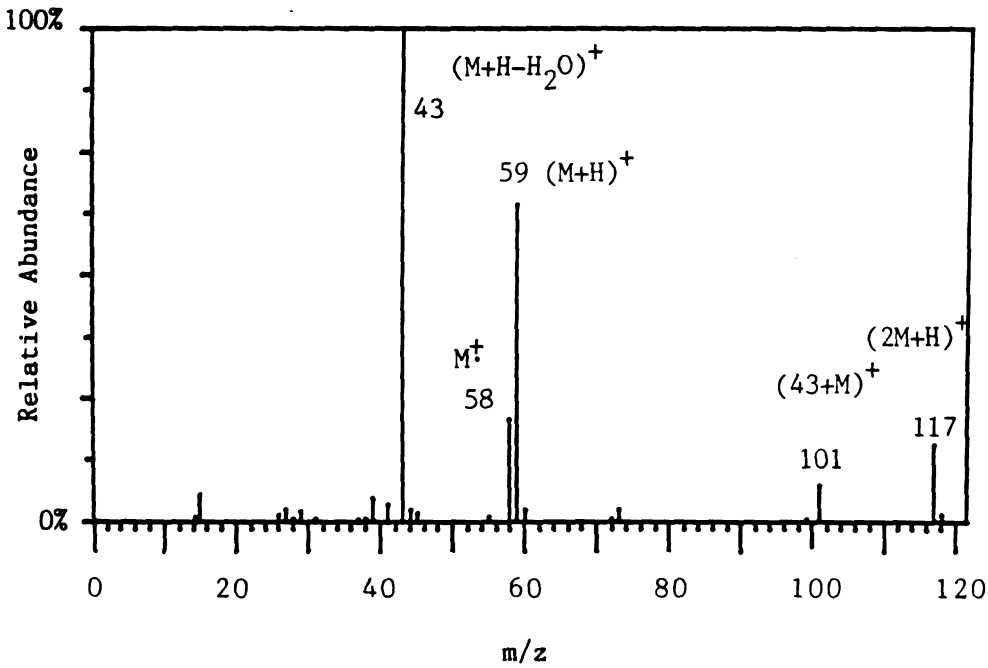

Figure 26. Self-CI Mass Spectrum of Acetone

abundant peaks at m/z 43 (the acetyl ion) and m/z 101 (the adduct of the acetyl ion and acetone). The structures and mechanisms for the formation of all these ions are discussed at length in Chapter VIII.

Figure 27 shows the reconstructed total ion chromatogram with the contribution from the reagent ions of acetone subtracted. The peaks missing from the chromatogram in Figure 27 correspond to the following molecules: decane, 1-octanol, nonanal, and undecane.

Figure 28 shows the acetone CI mass spectrum of the 2,3-butanediol. The $(M+H)^+$ ion of the diol is present in very minor abundance at m/z 91, but there are numerous other ion/molecule reaction products. The base peak of the spectrum at m/z 149 is the proton-bound adduct of acetone and the diol. The peak for the adduct between the acetyl ion and the diol is also very abundant. Peaks at m/z 131 and m/z 191 represent product ions of unknown structure.

Figure 29 shows the acetone CI mass spectrum of 2,6-dimethylphenol. Both the molecular ion and the protonated molecule of the phenol are present as abundant peaks. Also present in large abundance are the peaks representing the proton-bound adduct of acetone and the phenol at m/z 181, and the adduct of the acetyl ion and phenol at m/z 165.

Figure 30 shows the acetone CI mass spectrum of 2,6-dimethylaniline, which is extremely similar to the spectrum of 2,6-dimethylphenol. Again, both the molecular ion and the protonated molecule are present as high abundance peaks at m/z 121 and 122, as are the peaks representing the proton-bound adduct ion of acetone and the aniline at m/z 180 and the adduct ion of the acetyl ion and aniline at m/z 164.

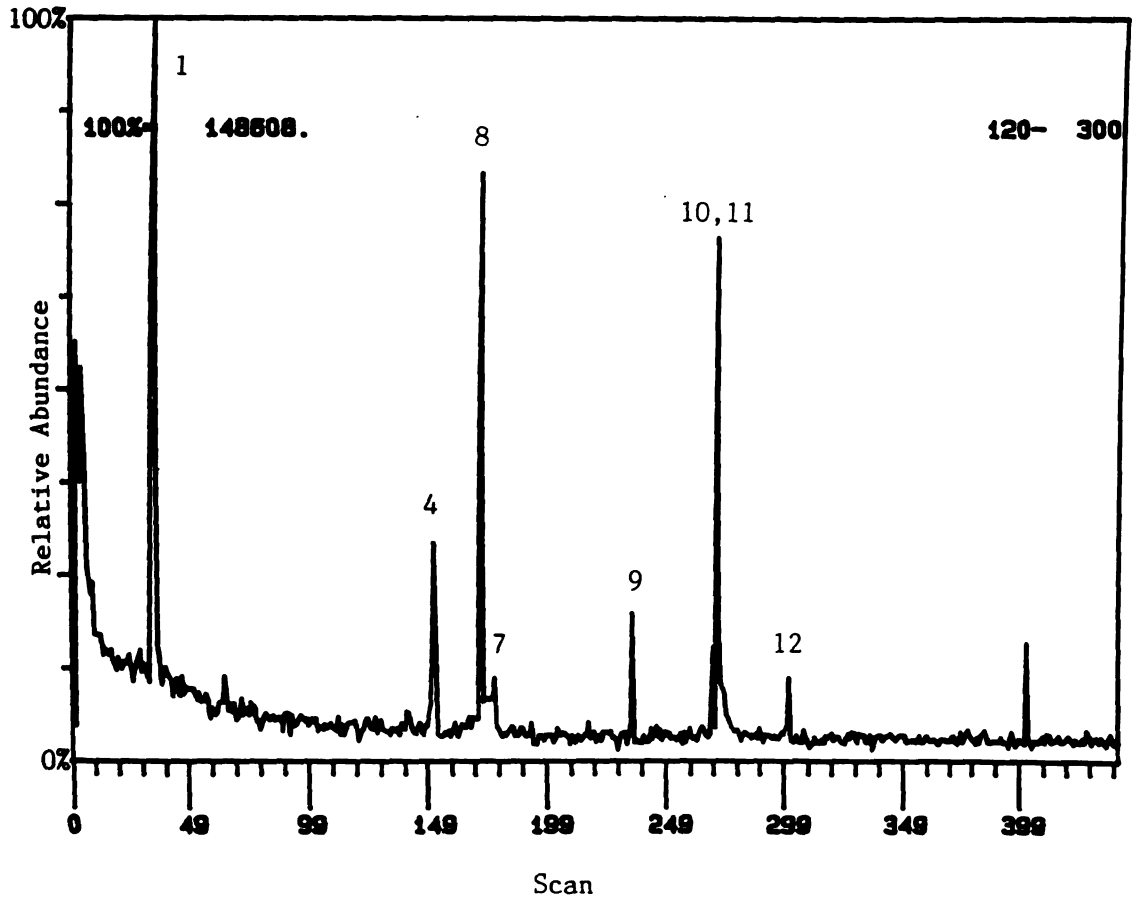

Figure 27. Reconstructed Total Ion Chromatogram of the PTM (Acetone CI)

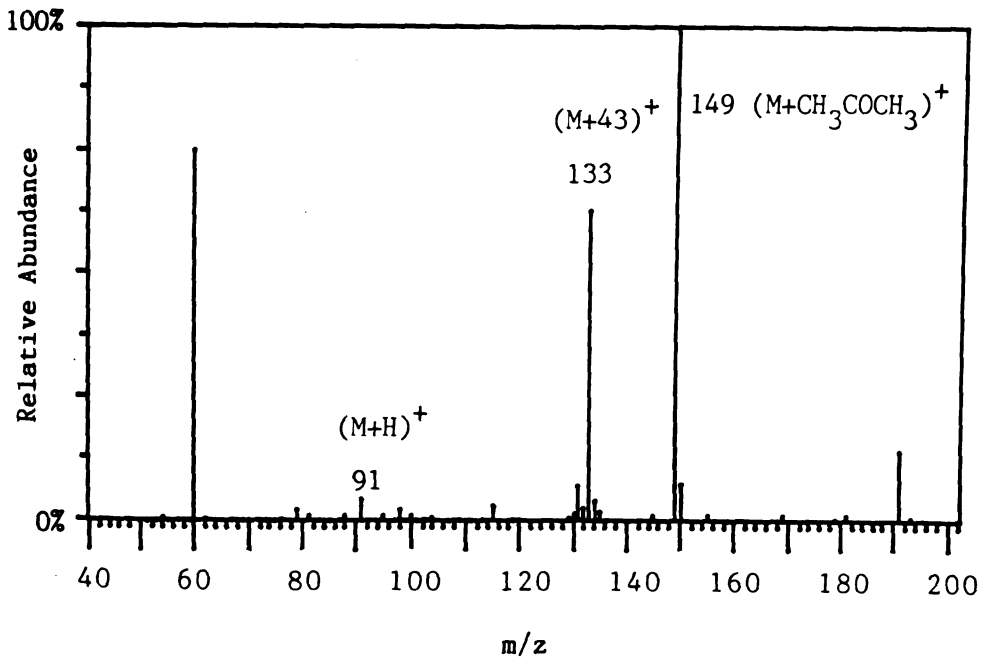

Figure 28. Acetone CI Mass Spectrum of 2,3-Butanediol

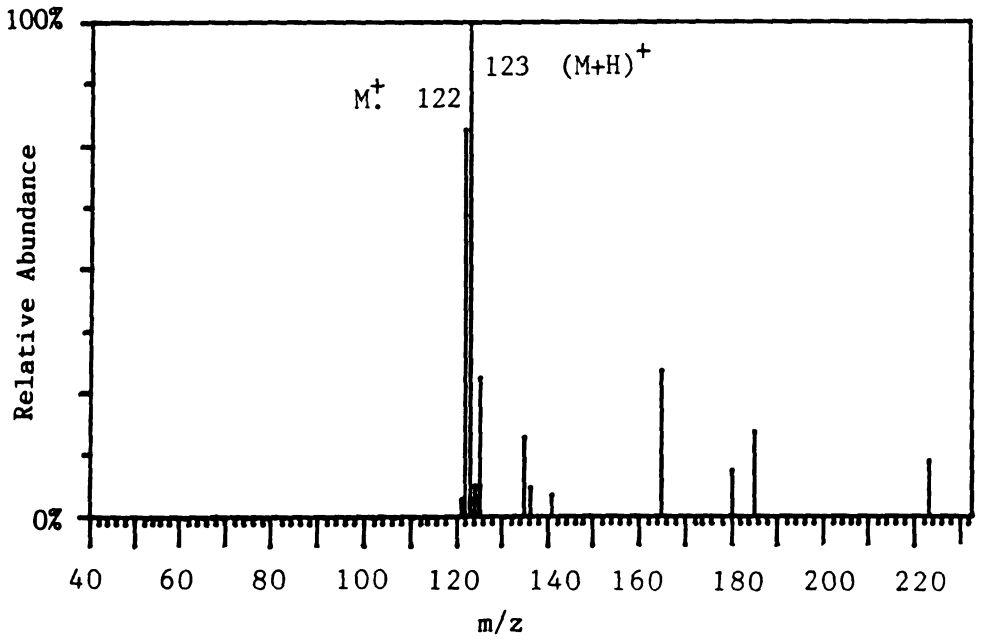

Figure 29. Acetone CI Mass Spectrum of 2,6-Dimethylphenol

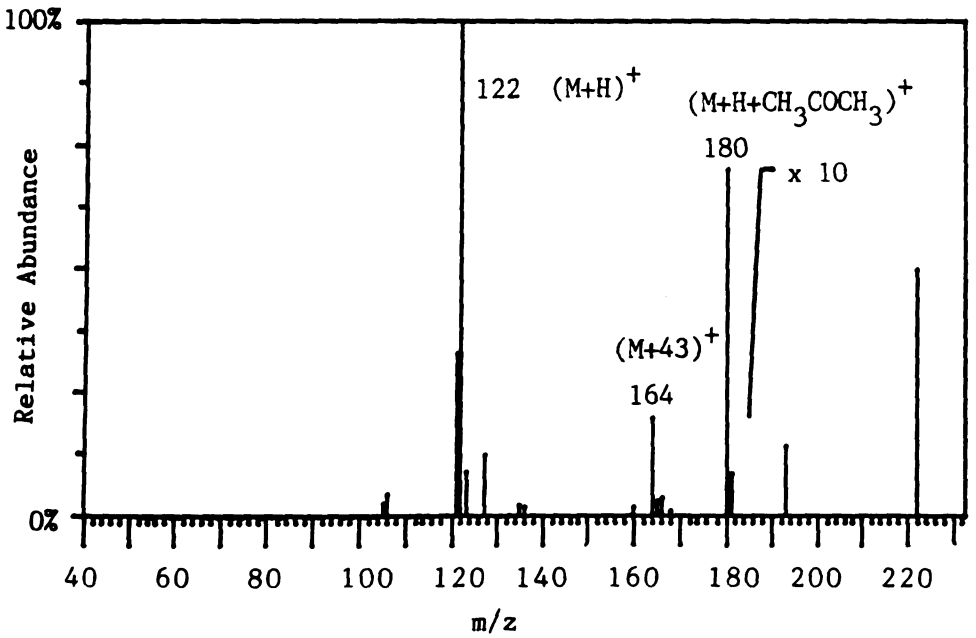

Figure 30. Acetone CI Mass Spectrum of 2,6-Dimethylaniline

Figure 31 shows the acetone CI mass spectrum of 2-ethylhexanoic acid. The $(M+H)^+$ ion is entirely absent from the spectrum, instead the $(MH-H_2O)^+$ ion at m/z 127 is the base peak. This is very different behavior from the spectra generated by the other CI gases in this chapter. Normally the $(M+H)^+$ ion of this acid is an important peak in the spectrum. It is possible that acetone selectively protonates the -OH site on the acid rather than the C=O site, predisposing the protonated molecule to lose a water molecule. Also present as a peak of low abundance is the proton-bound adduct of acetone and the acid.

Figure 32 shows the acetone CI mass spectrum of dicyclohexylamine. The $(M+H)^+$ ion is the base peak of the spectrum. No other peaks of significant intensity are present. This is the only compound of the PTM that forms an $(M+H)^+$ ion but does not form an abundant proton-bound adduct with acetone.

Figure 33 shows the three acetone CI mass spectra of the C_{10}-, C_{11}-, and C_{12}-acid methyl esters. The three are extremely similar, having the proton-bound adduct ion (at m/z 245, 259, and 273, respectively) as the base peaks, and having the protonated molecules (at m/z 187, 201, and 215, respectively) as a peak of roughly 50% relative abundance. Only the mass spectrum of the C_{10}-acid methyl ester shows an adduct of the acetyl ion with the ester as a peak of minor abundance at m/z 229.

In summary, the acetone CI mass spectrum of the PTM compounds are dominated by ion/molecule reactions that produce extremely abundant $(MH+acetone)^+$ adduct ions and $(M+acetyl)^+$ adduct ions. The reactions of carbonyl compounds are explored further in Chapter VIII. Because the

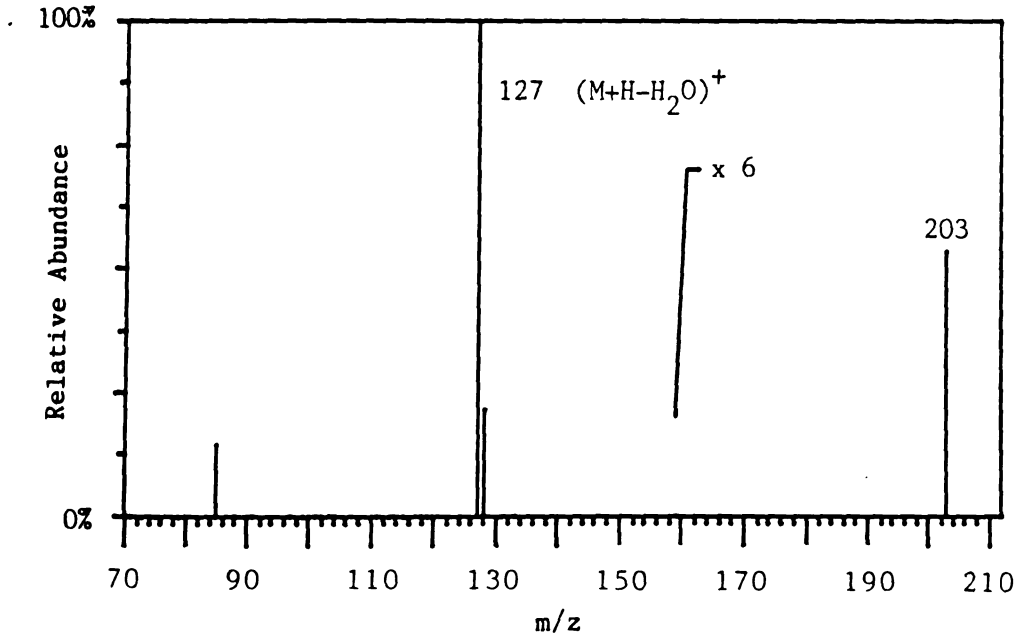

Figure 31. Acetone CI Mass Spectrum of 2-Ethylhexanoic Acid

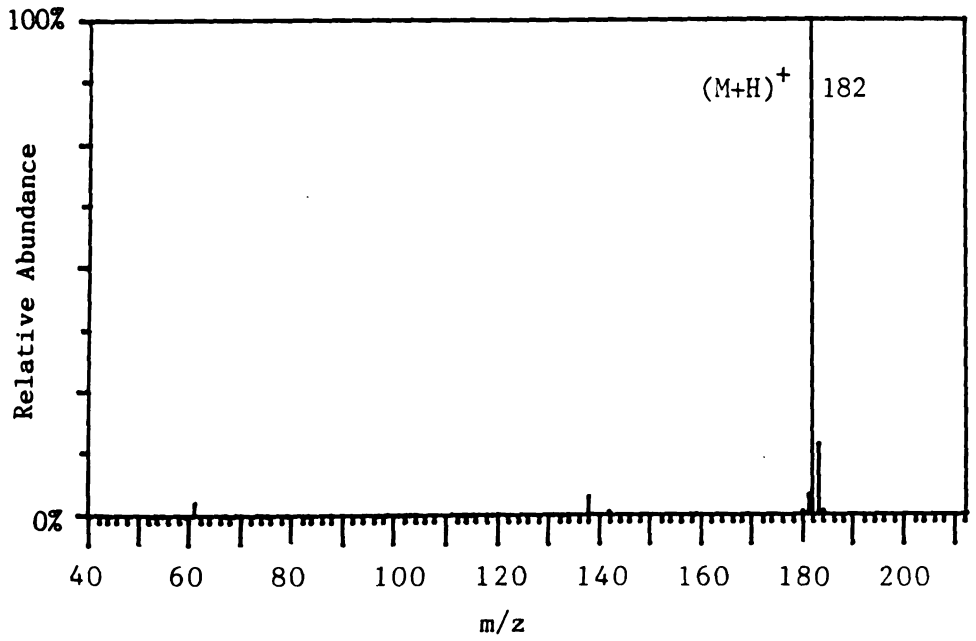

Figure 32. Acetone CI Mass Spectrum of Dicyclohexylamine

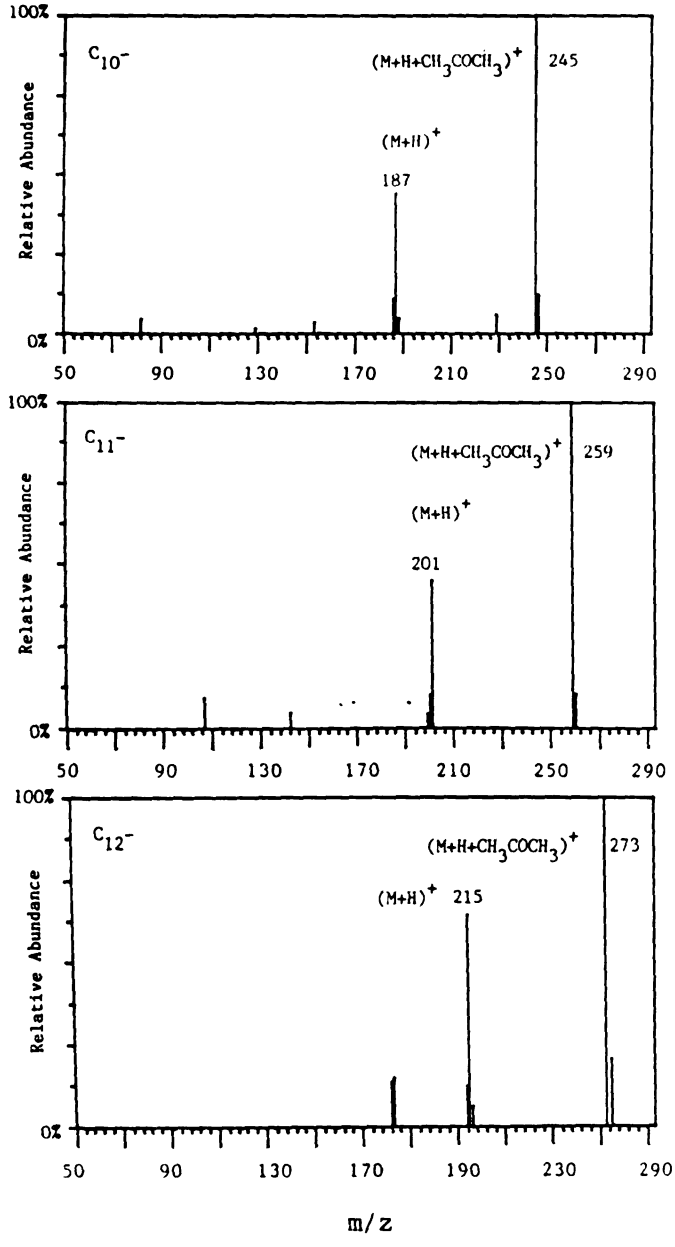

Figure 33. Acetone CI Mass Spectrum of of C_{10}^-, C_{11}^-, and C_{12}-Acid Methyl Esters

ion/molecule products formed by the reactions with acetone are so abundant, they may have some analytical utility. Unfortunately, the acetone ion/molecule reactions do not appear to be selective for any given class of compounds.

6. Reactive Gases in the Collision Chamber of the TQMS

Having examined the ion/molecule reactions of the PTM compounds by isobutane, benzene, methanol, and acetone CI, the author attempted to use these same four gases as reactive collision gases in the central quadrupole of the TQMS. Isobutane CI was chosen to produce the $(M+H)^+$ ions for the ion/molecule reactions in the central quadrupole.

In this mode both the first quadrupole and the third quadrupole were used as mass analyzers and the central quadrupole was set in rf-only mode. The first quadrupole was set to pass ions of one nominal mass (to select the parent ion) and the third quadrupole was then scanned from 70 to 275 amu to collect any reaction products that the parent ion generated in the central quadrupole. Before the next product scan the data system automatically instructed the first quadrupole to pass ions of a different nominal mass. In all, six parent ions were selected: the protonated molecules of 2,3-butanediol, 2,6-dimethylphenol, 2-ethylhexanoic acid, 2,6-dimethylaniline, C_{10}-acid methyl ester, and dicyclohexylamine. In this way each parent ion and its resulting product ions were observed every sixth scan (or every 12 seconds) during the run. Due to extreme difficulties with sensitivity in MS/MS mode, 20 ul of the PTM sample were evaporated down to 2 ul and this concentrated sample was injected onto the column. This procedure

overloaded the column causing broad overlapping peaks. The GC peaks for the parent ions chosen were, however, widely separated in time by the chromatography and did not overlap significantly.

The results of the interactions between the six $(M+H)^+$ ions chosen from the PTM and the reactive collision gases were very disappointing. Even with the large increases in the quantities of compounds injected and in the abundances of the $(M+H)^+$ ions, the signals due to the product ion were extremely weak. For the most part, no peaks of significant intensity were observed other than those representing parent ions. When benzene, isobutane, and methanol were used as the collision gas, the only other peaks observed were due to CID daughter ions. When acetone was used as a collision gas, both 2,3-dimethylphenol and 2,3-dimethylaniline did produce product ion peaks that corresponded to the $(MH+acetone)^+$ adduct ion and the $(M+acetyl)^+$ adduct ion. For all of the other compounds in the PTM, the only product ion peak of significant intensity was at m/z 117 which represents the protonated dimer of acetone and which arises from proton transfer to the collision gas.

These results are similar to those obtained previously by researchers who have attempted to use the central quadrupole of the TQMS for ion/molecule reactions. In general, the central quadrupole technique produces very low, or nonexistent yields of product ions, even in those cases where a reaction in known to occur in CI. In addition, the most abundant product ions formed are usually due to proton transfer to the reactive collision gas. These results mean that in the central quadrupole, one can only expect to observe ion/molecule product ions from extremely abundant parent ions that undergo extremely favorable

reactions. At this point in the research, it became clear to the author that either the ion/molecule research for this dissertation would have to rely heavily on chemical ionization (with its inherent lack of parent ion selectivity) or the technique for exploring ion/molecule reactions in the central quadrupole would have to improved significantly. As it turned out, the research into ion trapping in the central quadrupole detailed in Chapter IV. dramatically improved the performance of the central quadrupole technique. This improvement in turn has led to a new conception expressed in Chapters V. - IX. that the CI technique and the central quadrupole technique are complementary methods for studying ion/molecule reactions.

7. Conclusion

The results in this chapter indicate strongly that the technique of GC-CI/MS is a rapid and successful method for accomplishing a survey of organic ion/molecule reactions, and that the PTM is a highly useful mixture of compounds for accomplishing this kind of survey. Unfortunately, the results in this chapter also indicate that it is not possible to do a survey of ion/molecule reactions by GC/MS/MS using the central quadrupole of the TQMS as an ion/molecule reaction chamber. In fact, it is abundantly clear that the technique of using the TQMS collision chamber for ion/molecule reactions needs to be improved dramatically before it can be considered a valid method for studying ion/molecule reactions or become a useful analytical technique. The fundamental concern of the Chapters IV. - IX., therefore, is to show how

several novel alterations to the TQMS and its data system have improved the performance of the central quadrupole as an arena for studying ion/molecule reactions.

The results in this chapter also indicate that methanol, benzene, and acetone undergo many interesting ion/molecule reactions with the PTM compounds. Therefore, the bulk of this dissertation is concerned with the reactions of alcohols (see Chapters IV. - IX.), aromatic rings (see Chapter VII.), and carbonyl compounds (see Chapters IV., V., VI., and VIII.).

Since there appear at first glance to be ion/molecule reactions of the PTM compounds that mimic solution reactions, the author also decided to investigate in the gas phase two reactions that do occur in solution but were not addressed by the survey of reactions in this chapter. The first reaction is the silylation reaction of trimethylsilyl (TMS) compounds with alcohols and ketones to form trimethylsilylethers. This is an extremely common derivatization reaction for the purpose of making compounds amenable to GC-MS. The results of this investigation are shown in Chapter IV. The second reaction is the nucleophilic aromatic substitution reaction with ring opening and ring closing ($S_NANRORC$) of substituted pyridines with strong bases. This particular reaction is of interest mostly for the reason that it produces that produces stable negative ion intermediates. The author hoped to use the $S_N(ANRORC)$ reaction to investigate the capabilities of the TQMS for performing ion/molecule reactions in negative ion mode in both the CI volume and in the collision chamber. The results of the gas-phase $S_N(ANRORC)$ research are presented in Chapter IX.

The results of this chapter reiterate the well-known fact that chemical ionization is particularly well suited for studying ion/molecule reaction of organic molecules. Recent data (123) from other research groups have implicated ion/molecule reaction in the newly invented fast atom bombardment (FAB) process. Therefore, FAB has become a new area, like CI, in which one can study and perhaps make analytical use of ion/molecule chemistry. For this reason, the author introduced FAB as a technique to the TQMS in the MSU-NIH-MSF. Chapters II. - VII. of this dissertation show how FAB has been implemented on the TQMS, how the TQMS has been used to investigate the role of ion/molecule reactions in the FAB process, and how some of the unique ions produced by FAB have been investigated by means of ion/molecule reactions in the central quadrupole of the TQMS.

CHAPTER III.

FAB ON THE TQMS

A. Introduction

The gas chromatography and chemical ionization instrumentation used in the previous chapter were installed by the manufacturer of the TQMS, but a fast atom bombardment (FAB) ion source was not supplied with the instrument. The author designed and installed a FAB ion source from commercially available parts for the purpose of investigating the ion/molecule reactions involved in the FAB process and for surveying the kinds of ion/molecule reactions which are amenable for study in the central quadrupole of the TQMS.

Since the FAB ion source was new, the author decided to test its performance to determine whether it would produce results of sufficient quality and reproducibility to be useful for research into ion/molecule reactions. Tests were designed to measure the mass range and the signal-to-noise ratio for the ions produced by the new FAB ion source. Tests were also designed to determine whether it would produce both positive and negative ions, and whether it could be used in conjunction with MS/MS techniques. A further set of tests was designed to determine if the very new technique of thermally-assisted FAB (TA-FAB) (99) developed at the MSU-NIH-MSF could also be employed effectively with this new FAB ion source. The results of these tests are reported in this chapter.

B. Experimental

1. Solutions for Testing the Performance of FAB

Two solvents were used for the FAB tests: thioglycerol and a 1:1:1 by volume mixture of dithioerythritol, dithiotreotol and thiodiglycol. Both of these solvents are viscous liquids that are commonly used in FAB and have been well characterized in the MSU-NIH-MSF. A solution of 1 mg of CsI in 1 ml of glycerol was prepared by ultrasonicating the mixture in a glass vial. An acidified solution of glycerol was prepared by adding 1 ml of 6 N HCl to 10 ml of glycerol with vigorous stirring in a glass vial. A solution of the tripeptide alanyl-leucyl-glycine was prepared by dissolving 1 mg of pure tripeptide in 1 ml of the acidified glycerol with vigorous stirring in a glass vial.

2. Solutions for Testing the Performance of TA-FAB

The standard solvent for performing TA-FAB is a viscous solution of fructose in water. This solution is prepared by adding at least 1 gram of fructose to 1 ml of water. One then pipettes 1 ul of this solution onto the TA-FAB probe and concentrates the solution with a blow dryer until it forms a very thick gel. Another solution similar to this was prepared by adding 1 ul of H_2O^{18} water to the 1 ul of fructose-water solution on the TA-FAB probe before concentrating the solution with a blow dryer.

3. Conditions for FAB and TA-FAB

The source of energetic particles is a capillaritron probe gun manufactured by Phrasor Scientific. Xenon at a pressure of $5\text{-}7X10^{-5}$ torr was used to produce the energetic beam of primary particles which is responsible for the FAB and TA-FAB effect. The sample that is bombarded by the FAB beam is introduced into the TQMS at a right angle to the probe gun by means of any 1/2 inch diameter direct probe with an appropriate sample holder. The voltage on the capillaritron tip of the FAB gun was set at 10 kV. The ion source of the TQMS was very close to ground potential. Therefore, since xenon ions with charges ranging from +1 to +6 are produced by the capillaritron, the primary ions impinging on the sample ranged in energy from 10 keV to 60 keV. The FAB sample probe and the ion source were kept at room temperature, but the TA-FAB sample probe temperature was increased slowly (and not linearly) from 25°C to 100°C during the course of five minutes. The CI filament was actually used with the EI-TA-FAB experiment since it is closer to the sample probe and is therefore more likely to ionize neutral particles desorbed by the TA-FAB process. Since the CI volume was removed at the time, the ion source was open and the CI filament acted as the EI filament would have if it had been physically closer to the sample.

C. Results

1. Mass Range of FAB on the TQMS

The mass range of all ionization techniques on the TQMS in the MSU-NIH-MSF is limited by the 1-1000 dalton range of the first and third quadrupole power supplies. When this instrument was designed, the 1000

dalton mass range was more than sufficient for analyzing the types of compounds that can be transmitted through a GC and can be ionized by EI or CI. FAB, however, has been successful in desorbing organic ions to m/z 5000, and inorganic clusters to m/z 50000. Clearly, the TQMS cannot take full advantage of FAB, but the author was interested to determine whether the new FAB ion source, in combination with the TQMS, could produce and detect ions to the mass limit of the instrument.

Figure 34 shows two FAB mass spectra of common solvents with abundant peaks below m/z 300. The solvent in Figure 34A is thioglycerol and the solvent in Figure 34B is a 1:1:1 by volume mixture of dithiotreotol, dithioerithritol and thiodiglycol. Both of these solvents produced the expected low mass ions in roughly the expected intensity ratios. Figure 35 shows the FAB mass spectrum of CsI dissolved in glycerol. This solution has been used for several years as an m/z calibration standard for FAB on other instruments in the MSU-NIH-MSF. Figure 35 shows all of the peaks that are typical for CsI out to m/z 969, which is close to the mass limit of the TQMS.

2. Random Noise Due to FAB on the TQMS

The process of FAB has been observed both by this researcher to produce a high level of random noise at all m/z values throughout the mass range of the instrument. The reason for this appears to be that the line of sight arrangement of the quadrupoles in the TQMS allows energetic primary Xe^{o} and Xe^{+} particles and photons that are reflected from the FAB probe tip to pass undeflected through the mass filters to the electron multiplier detector. The detector in the TQMS is off-axis so that the energetic neutral particles and photons do not impinge upon

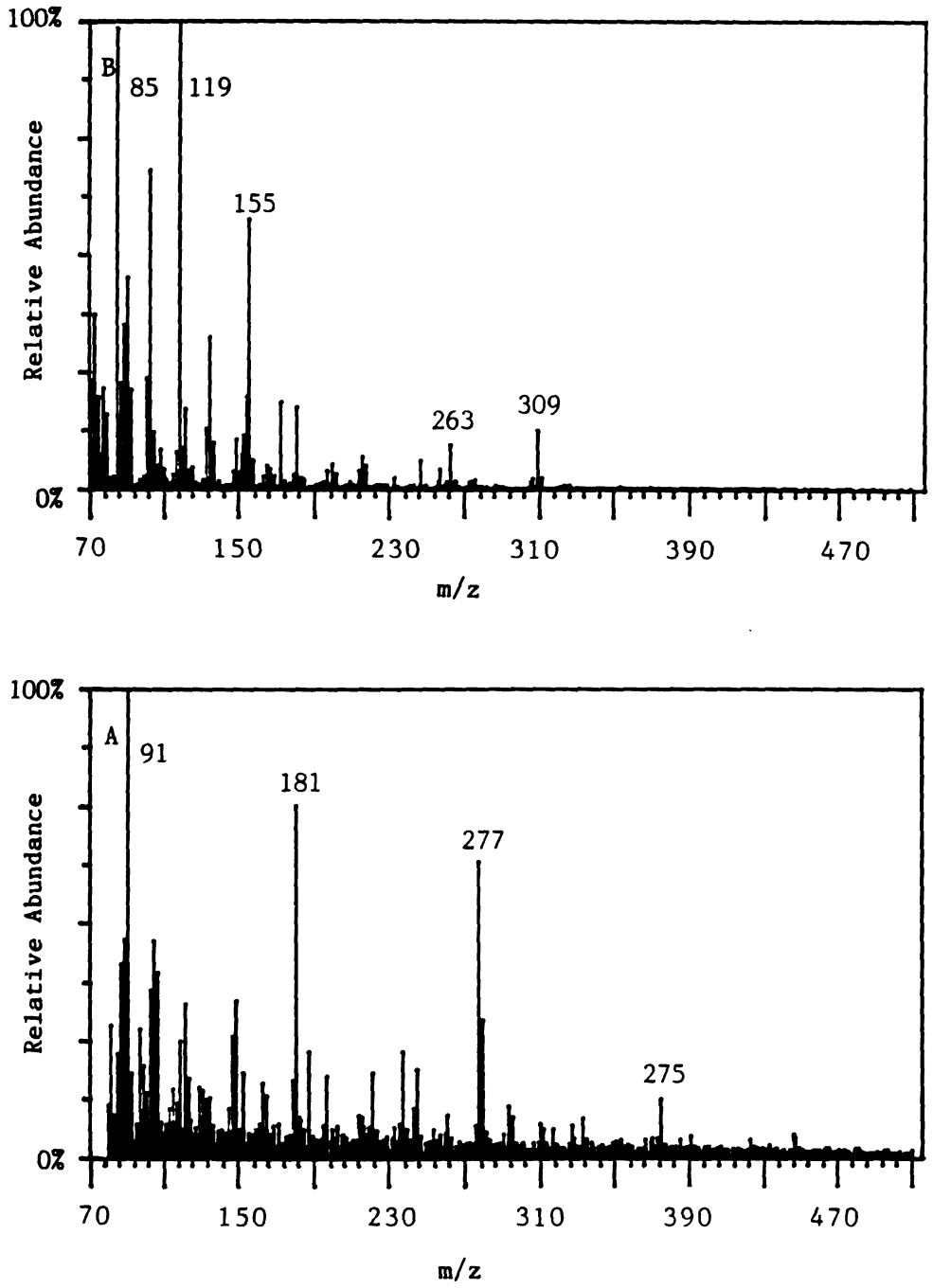

Figure 34. FAB Mass Spectra of (A) Thioglycerol and of (B) a Mixture of Dithiothreotol, Dithioerythritol, and Thiodiglycol

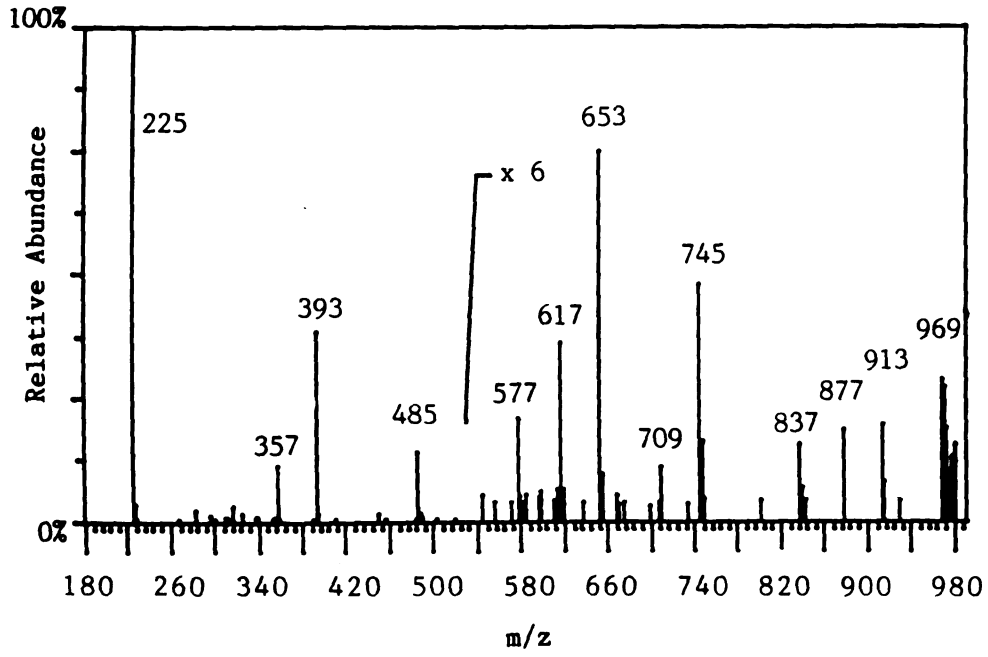

Figure 35. FAB Mass Spectrum of CsI in Glycerol

it. Slowly moving mass-filtered ions are attracted to a conversion dynode plate across from the electron multiplier which has a -3000 V voltage applied to it in positive ion mode and a + 3000V voltage in negative ion mode. Positive ions striking the conversion dynode create secondary electrons which are detected and amplified by the electron multiplier.

Some of the energetic Xe^+ ions that reach the end of the instrument have very high kinetic energies and probably pass by without striking the conversion dynode. Those energetic Xe^+ ions with less than 3 keV of kinetic energy, however, do strike the conversion dynode and the resulting secondary electrons are detected by the electron multiplier. Because the quadrupoles do not filter ions with more than approximately 100 eV of energy, these energetic Xe^+ ions are detected throughout the mass range of the TQMS.

The maximum signal of energetic Xe^+ ions in the instrument during FAB has been observed to be 1000 intensity units. Therefore, the random background noise in FAB is 10 to 100 times higher than in EI or CI. Fortunately, the FAB signal for a given analyte may last for up to one hour. The long-lived nature of the FAB signal allows extensive signal-averaging to be performed which can offset some of the problems of random noise. Because of the problems with background noise, and because the purpose of this research was to study ion/molecule reactions and not to develop analytical methods, the author chose never to use any concentration of FAB analyte below 100 ug/ug of matrix. Any researcher wishing to use FAB for analytical purposes on the TQMS would probably have to modify the FAB probe tip to reduce the number of reflected Xe^+

ions, or redesign the detector to discriminate against energetic ions by means of an energy analyzer.

3. Negative Ions by FAB on the TQMS

Glycerol has been reported to produce both positive and negative ions under FAB conditions (66). With the TQMS tuned to transmit and detect negative ions, the new FAB source generated the negative ion mass spectrum of glycerol shown in Figure 36. If one compares the positive and negative ion spectra of glycerol shown in this chapter, two facts are immediately apparent. First, the negative ion mass spectrum has many fewer large peaks than the positive ion spectrum; and second, the negative ions generated by FAB are deprotonated molecules $(M-H)^-$, not molecular anions, in the same way that positive ions generated by FAB are protonated molecules $(M+H)^+$, not molecular ions. Both of these facts are consistent with previously reported negative ion FAB data (66).

The focus for the negative ion FAB spectra was difficult to maintain and often the peaks would fade after only a few minutes, only to reappear if one moved the probe. This difficulty of maintaining a consistent focus can be attributed to the fact that, of the energetic particles produced by the capillaritron FAB gun, only about 50% are actually neutral Xe atoms, whereas the rest are Xe^+ ions. It seems likely that the constant large influx of positive ions into the ion source builds up positive charge on the glycerol droplet and decreases the abundance of negative ions produced by means of neutralization reactions. This drawback of the capillaritron gun can be overcome through deflection of the charged portion of the xenon primary beam away

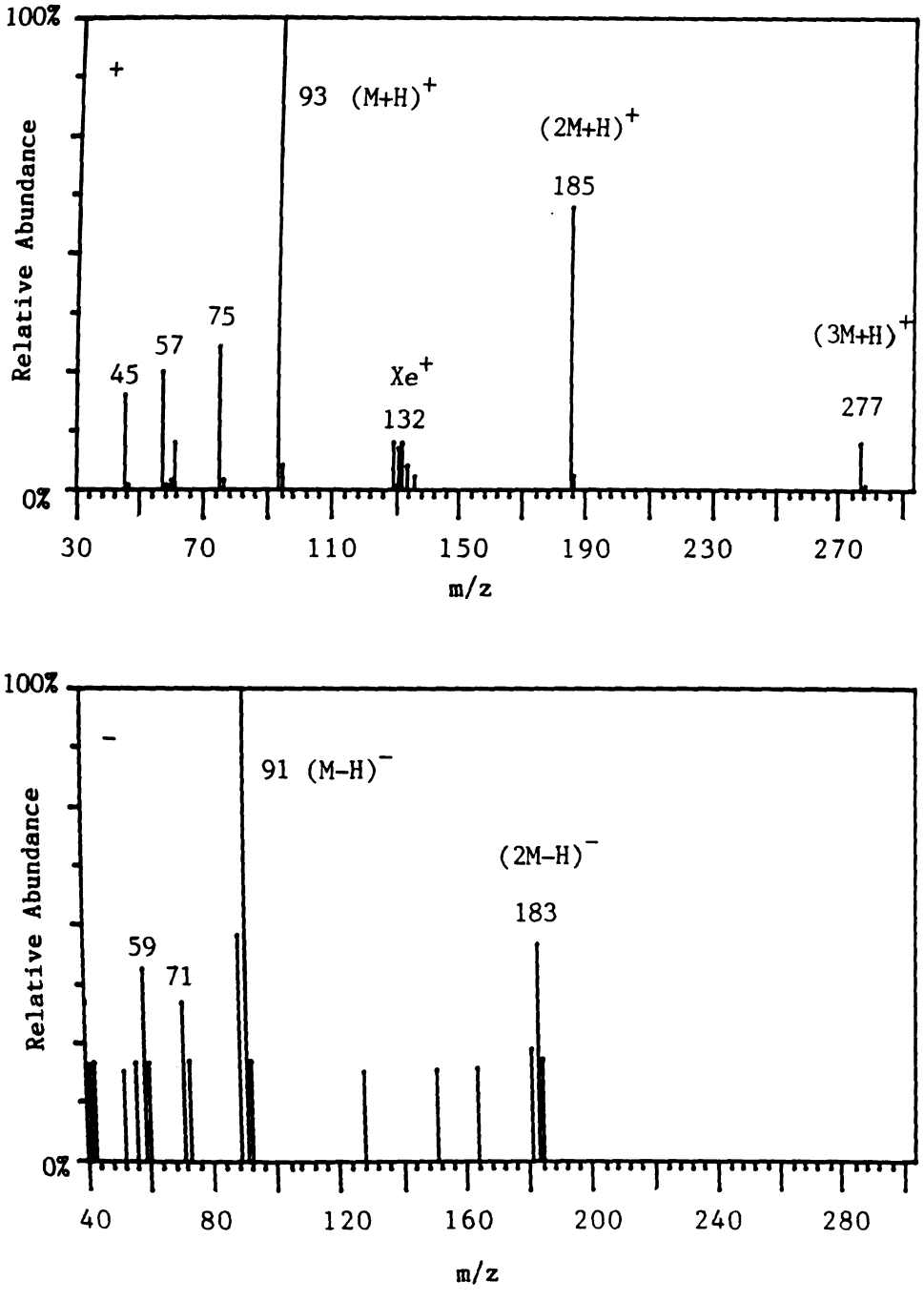

Figure 36. Positive and Negative Ion FAB Mass Spectra of Glycerol

from the ion source by means of electrostatic deflection plates. Another less difficult method of removing the positive charge build-up is to add salts to the glycerol to make it more conductive, thus allowing the excess charge to drain away into the metal probe.

4. FAB/MS/MS on the TQMS

Before embarking on ion/molecule studies using FAB, the author wanted to demonstrate that it was possible to operate the TQMS in MS/MS mode with FAB as the source of ions, with the purpose of obtaining high quality argon CID spectra of a model compound that was amenable only to FAB ionization. The model compound chosen was a tripeptide alanyl-leucyl-glycine, which has been characterized by FAB/MS and FAB/MS/MS on other types of mass spectrometers (99).

Figure 37A shows the FAB mass spectrum of glycyl-leucyl-alanine in acidified glycerol, showing a peak for the $(M+H)^+$ ion of the tripeptide at m/z 260. Figure 37B shows the argon CID daughter spectrum of the $(M+H)^+$ ion of the tripeptide. All of the daughter ion peaks in Figure 37B are characteristic of this particular molecule and have been documented in the literature by other techniques (99). Figure 37 demonstrates that the new FAB ion source is compatible with the normal operation of the TQMS, and that the results obtained by FAB/MS/MS on the TQMS are directly comparable to the results from other FAB/MS/MS techniques. Figure 37 also shows that, whereas the major peaks in the FAB/MS spectrum are due to the liquid matrix, all of the peaks in the FAB/MS/MS spectrum are due to the protonated molecule and fragment ions of the tripeptide. This demonstrates in a graphic manner the utility of

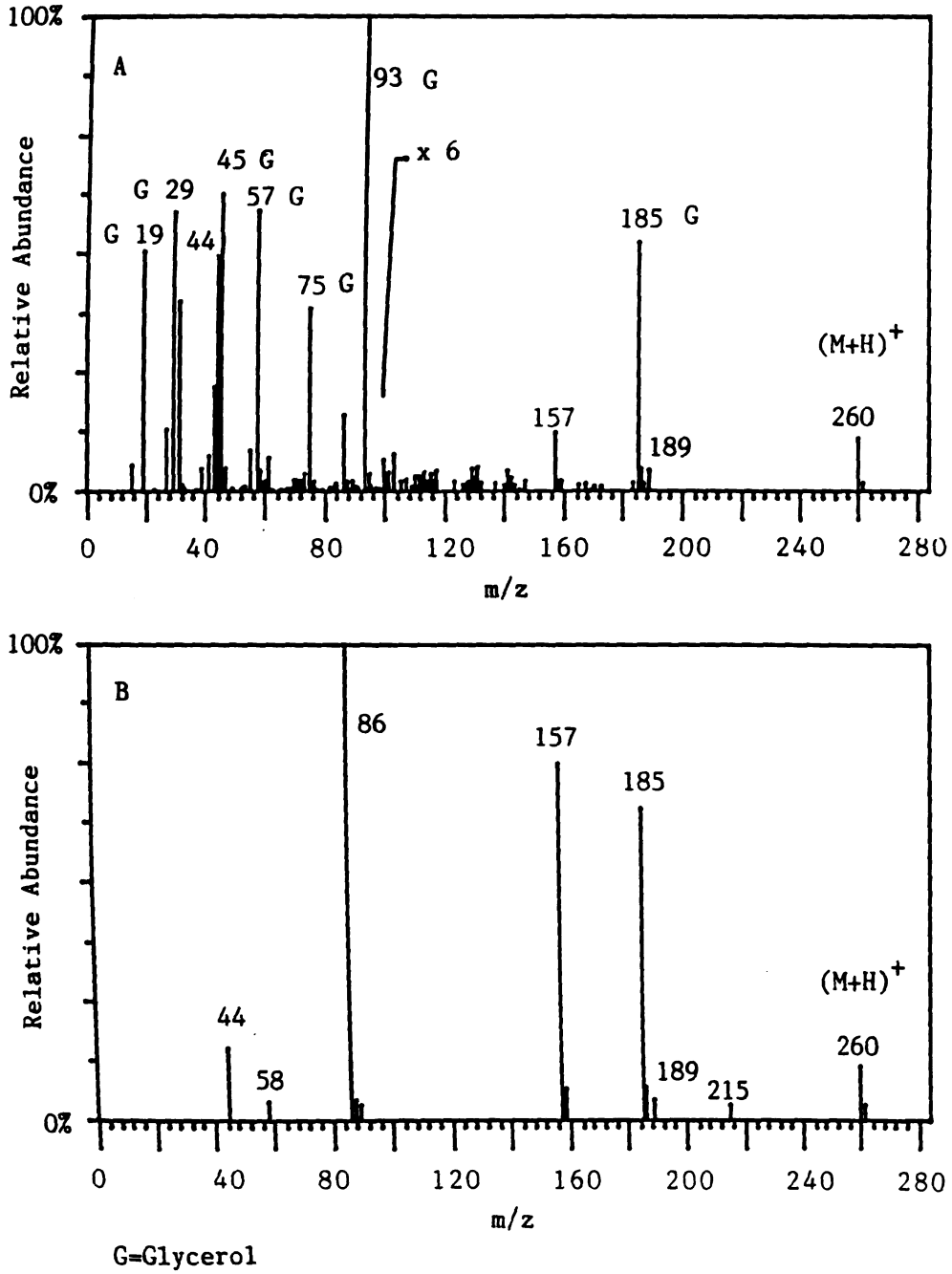

Figure 37. (A) FAB Mass Spectrum of Ala-Leu-Gly and (B) the Argon CID Daughter Spectrum of the $(M+H)^+$ of Ala-Leu-Gly

MS

io

ch

ki

im

fu

If

ge

cc

fi

wi

st

co

(S

wi

sc

sc

c

sy

pe

v

n

MS/MS for removing from the spectrum the interfering peaks due to FAB ionization of the liquid matrix.

One of the unique capacities of the TQMS is that it permits one to change the central quadrupole dc offset voltage, and thus regulate the kinetic energy of incoming parent ions. The amount of internal energy imparted to the parent ion in a collision with a target gas is a function of the kinetic energy the parent ion had before the collision. If one plots fragment ion abundance versus collision energy one can generate a reconstructed collision energy scan. When the optimal collision energy for the production of one fragment ion is different from that for another fragment, the ratio of the fragment ion abundances will vary with collision energy. Table 5 shows a CID collision-energy study of the m/z 189 and m/z 185 daughter ions of the tripeptide.

Table 5 indicates that the m/z 189 ion is favored at higher collision energies, which is consistent with data from other techniques (99). Table 5 also indicates that the new FAB source does not interfere with the ability of the TQMS to employ this kind of ion kinetic energy scan. Fortunately, the data in this section show that the new FAB source is compatible with the TQMS ion optics and ion detection system.

5. Thermally-Assisted FAB (TA-FAB) on the TQMS

Thermally-assisted FAB is an extremely new technique (99) which combines some of the best features of heated direct probe mass spectrometry with conventional FAB mass spectrometry which is usually performed at room temperature. The liquid matrix for TA-FAB is a viscous solution of fructose in water. At room temperature only the matrix provides a significant signal, but as the temperature is raised,

Table 5

Table of Fragment Ion Abundances for Two CID Daughter Ions of the Protonated Molecule of Ala-Leu-Gly Versus Collision Energy

Collision Energy (ev)	Percent Relative Abundance Ratio of m/z 189 / m/z 185
-1.4	15.3%
5.6	18.6%
10.4	34.2%
14.7	46.6%

the analyte also experiences desorption/ionization by the FAB process. If the temperature of the probe is programmed, however, the matrix ions exhibit a different ion abundance profile from the analyte ions. The differential desorption of matrix and analyte ions reduces the number of peaks due to matrix ions in the spectrum of the analyte and makes background subtraction feasible in TA/FAB. In ordinary FAB this is often not the case.

Ackermann's theory (99) for explaining the mechanism of TA-FAB claims that the mobility of the matrix increases with temperature and that water trapped in the fructose matrix is the key to the formation of ions. This view is partially substantiated by the fact that the maximum desorption of analyte ions always occurs close to 100°C, the boiling point of water. This point is called the best matrix temperature, and is comparable to the best anode temperature described in field desorption mass spectrometry. This mechanism, called ternary percolation, assumes that large amounts of water must be given off at the best matrix temperature. The mass spectrometer on which TA-FAB was pioneered, however, did not detect a large peak at m/z 19 corresponding to H_3O^+, and did not detect any peak at m/z 21 corresponding to $H_3{}^{18}O^+$ when the sample was spiked with $H_2{}^{18}O$. This led to the conclusion that either the model was incorrect or that the vast majority of the water given off was a neutral vapor and could not be detected by that instrument.

The TQMS, unlike the older instrument, is capable of using two ionization modes simultaneously. It is possible to perform FAB on a sample and to ionize any neutral products of the FAB process that escape into the gas phase either with the CI or EI filament. Figure 38A is a

100%

Relative Abundance

0%

100%

Relative Abundance

0%

Figur
With

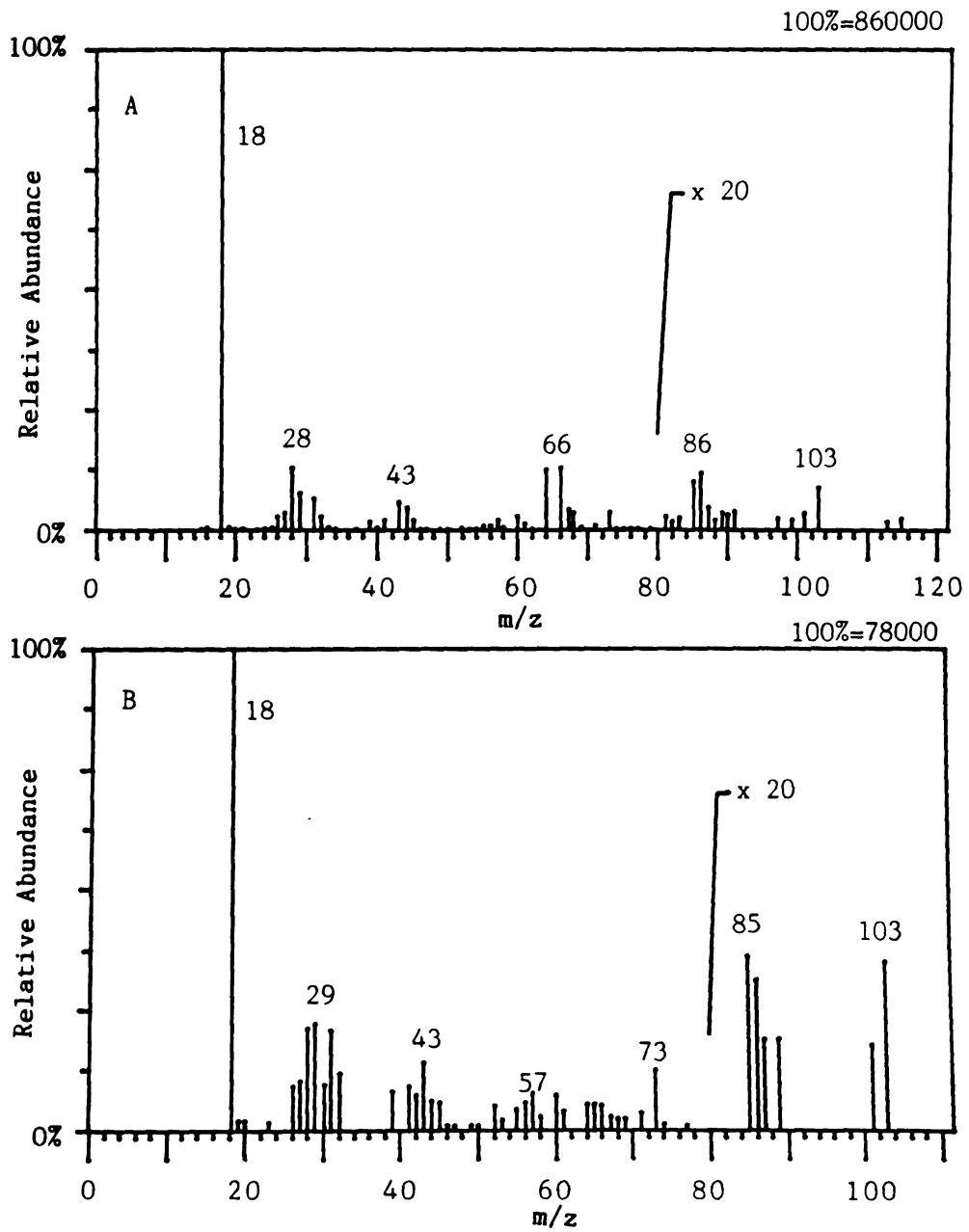

Figure 38. TA-FAB Mass Spectra of a Solution of Fructose in Water (A) With and (B) Without Subsequent EI

TA-FAB mass spectrum of the fructose-water matrix, and Figure 38B is and EI-TA-FAB mass spectrum of the fructose-water matrix. Figure 38 A and B show a large number of peaks due to fragmentation of fructose and also a major peak at m/z 18, which is likely due to the ion H_2O^+. When the filament is turned on, the m/z 18 peak increases over 100 times in abundance, indicating that the majority of the water molecules produced by TA-FAB are indeed neutral, not ionized. A similar EI-TA-FAB experiment using a fructose solution spiked with $H_2{}^{18}O$ yielded large peaks at both m/z 18 and m/z 20, indicating the presence in the gas phase of neutral H_2O and $H_2{}^{18}O$.

These TA-FAB experiments were conducted at the very end of this research project and are only preliminary results of a much broader investigation into TA-FAB which are being conducted currently by C. Heine at the MSU-NIH-MSF. Even these preliminary results, however, indicate that the TQMS with its tandem ion sources and tandem analyzers is an extremely valuable instrument for investigating the still mysterious mechanisms of both FAB and TA-FAB.

The major conclusion that one can draw from the data in this chapter is that the combination of FAB and the TQMS is sufficiently powerful and reproducible to justify its use for studying ion/molecule reactions as a complement to the established ion/molecule technique of CI/TQMS. Further research into the mechanism of FAB will be presented in Chapters V. and VI.of this dissertation.

CHAPTER IV.

ION-TRAPPING TECHNIQUE FOR ION/MOLECULE REACTION STUDIES IN THE TRIPLE QUADRUPOLE MASS SPECTROMETER

A. Introduction

The triple quadrupole mass spectrometer (TQMS) was developed initially to study laser photodissociation reactions in the region of the center quadrupole (101,102). Researchers soon discovered that by using the central quadrupole as a collision chamber it was also possible to study collision-induced dissociation (CID) (103) and ion/molecule reactions (104, 105). Of these three reaction modes, CID using nitrogen or argon has been used most frequently in scientific applications of the TQMS. Very recently, however, there has been renewed interest in using the TQMS to study ion/molecule reactions in the central quadrupole region (106-112) since interactions with a reactive collision gas may provide additional information about analyte ions that interaction with an inert gas cannot (107). Unfortunately, the majority of ion/molecule studies in the center quadrupole of the TQMS have produced low yields of product ions from reactions in the central quadrupole. Analyte ions entering the central quadrupole usually have low axial kinetic energies. Any ion/molecule products that do form by this process have very little axial kinetic energy, and they tend to remain in the central quadrupole region. In addition to this difficulty, the TQMS has poor control over the residence time of ions inside the central quadrupole (112). One can control the residence time only roughly by changing the pressure in the central quadrupole. Thus ion/molecule reactions products in the central

quadrupole are not observed except at relatively high pressures and low axial kinetic energies. The high pressures and the low kinetic energy of the ions' inhibit efficient transfer of the ion from the collision region through the third quadrupole to the electron multiplier. The standard technique is to use a drawout lens to extract ions near the exit of the central quadrupole. Ion/molecule product ion currents are limited by the rate of diffusion of product ions along the axis of the quadrupole.

This chapter describes a novel approach for increasing the residence time of ions inside the central quadrupole and for improving the intensity of signals representing ion/molecule reaction product ions. This technique stores product ions in the central quadrupole then extracts, in a pulse, those thermal ions present in the central quadrupole. One obtains an instantaneous current much greater than the steady state current. This technique requires no hardware modifications to the instrument, and can be applied to most TQMS instruments currently available.

The technique of ion trapping in a TQMS is illustrated with a reaction of methyl cations with neutral acetone. This reaction produces ten primary products as characterized by ICR spectrometry (114). The particular ion/molecule process used to characterize the effects of ion trapping in the central quadrupole is the reaction of protonated glycerol with neutral acetic acid. Similar ion/molecule reactions have been investigated by ICR spectrometry (115). A third ion/molecule reaction, the trimethylsilyl cation reacting with acetone, was used to compare the ion/molecule reaction data generated by two tandem quadrupole instruments of different internal design.

B. Experimental

1. Instrumentation

The instrument used for these studies is a prototype triple quadrupole mass spectrometer built by Extranuclear (now Extrel) Inc. The instrument has a dual EI/CI ion source that has been modified to permit fast atom bombardment (FAB) ionization. The fast atom gun is a capillaritron probe gun from Phrasor Scientific. All of the samples used in this study were introduced either through a volatile liquids inlet or by a direct probe. Collision gases were admitted into the collision region of the TQMS by means of a stainless steel vacuum line. The pressure of gas in the collision region was regulated by a model 216 pressure/flow controller from Granville-Phillips, Inc.

2. Computer System

An 8086-based microcomputer controls the TQMS and acquires data using a software control system built on the programming language FORTH. The control system, based on the work of C. Myerholtz (113) and adapted by Extrel, Inc., provides modular software which allows considerable flexibility in using the instrument. In addition the system can be programmed by the user. The authors easily modified the basic data collection algorithm to permit the trap and pulse data collection technique described in this section to be used with daughter scans, parent scans, and neutral loss/gain scans.

3. Chemicals Used

Glacial acetic acid was obtained from Mallinckrodt as an analytical reagent. Acetone and chlorotrimethylsilane were obtained from Fisher Scientific. Both were used without further purification. The glycerol used in this project was vacuum-distilled. Xenon obtained from Matheson Scientific was 99.99% purity.

4. Ion/Molecule Reactions

The phenomenon of ion trapping is illustrated in this chapter using the reaction of the methyl cation with neutral acetone. This reaction produces ten primary products and has been investigated by ICR spectrometry (114). The reaction was carried out in the TQMS by introducing $5x10^{-6}$ torr acetone into the ion source and $5x10^{-4}$ torr acetone into the central quadrupole region. The acetone in the ion source region was ionized by 70 eV EI which produced the methyl cation in addition to many other fragment ions. The methyl cation was mass-analyzed using the first quadrupole and reacted with the neutral acetone in the central quadrupole.

The particular ion/molecule process used to illustrate the effects engendered by ion trapping in the central quadrupole is the reaction of protonated glycerol with neutral acetic acid. Similar ion/molecule reactions between protonated alcohols and acetic acid have been investigated by ICR spectrometry (115). This reaction was implemented by protonating the glycerol with FAB in the ion source of the TQMS and by allowing a regulated pressure of acetic acid to enter the center quadrupole region. The ion source and central quadrupole regions are

differentially pumped so that there is little mixing of the neutral vapors of the glycerol and acetic acid. The protonated glycerol was mass-selected by the first quadrupole and reacted with the acetic acid in the second quadrupole to form the proton-bound adduct ion which in turn was mass-selected by the third quadrupole. This particular reaction was chosen because it represents a striking example of the effect of the trap and pulse technique. However, this technique is by no means limited to FAB. Similar effects have been observed for peaks representing the products of ion/molecule reactions that were the result of ions generated by CI and EI.

The ion/molecule reaction used to compare different tandem quadrupole instruments was the reaction of the trimethylsilyl cation (TMS^+) with acetone. The TMS^+ ion was generated by 70 eV EI from $5X10^{-6}$ torr of chlorotrimethylsilane leaked from the "liquids" inlet through a needle valve into the ion source of the TQMS. $9X10^{-4}$ torr acetone was admitted into the central quadrupole by means of the pressure controller described above. The ion source temperature was 150°C, and the central quadrupole temperature was 50°C.

5. Instrumental Conditions for Ion Trapping

A positive voltage on L5 (see Figure 39) prevents all low energy ions from reaching the detector and traps many of them inside the central quadrupole. For negative ions, of course, the L5 potential must be more negative than the dc offset of the central quadrupole to block the exit for ions. Ordinarily, the most reproducible results in the positive ion mode were obtained when the L5 potential was +100 V and then pulsed to -100 V, and in negative ion mode when L5 potential was -

100 V and then pulsed to +100 V. Typical TQMS instrument parameters for EI, CI, and FAB are shown in Table 6.

Table 6

Typical Conditions for Ion-Trapping
In the Center Quadrupole of the TQMS

Parameters	EI	+CI	-CI	FAB
Filament	70 eV	100 eV	100 eV	---
Repeller	14.3 V	33.0 V	-46.6 V	0.0 V
CI	2.7 V	32.2 V	-37.6 V	25.0 V
EI	14.9 V	-185.8 V	- 1.5 V	-104.0 V
EXT	23.7 V	-3.7 V	75.9 V	-141.4 V
L1	-30.0 V	-13.0 V	-23.3 V	17.3 V
L3	10.0 V	-191.3 V	110.4 V	100.0 V
Q1	-0.5 V	20.0 V	-33.0 V	-9.4 V
L4	15.9 V	-25.1 V	66.9 V	-59.5 V
Q2	20.0 V	32.2 V	-26.6 V	-1.8 V
L5	100.0 V	100.0 V	-100.0 V	100.0 V
Q3	4.0 V	20.0 V	-32.7 V	-13.2 V
Multiplier	-2 kV	-2 kV	-2 kV	-2 kV
Conversion Dynode	- 3 kV	-3 kV	3 kV	3 kV
FAB Gun	---	---	---	10 kV

C. Results and Discussion

1. Ion Trapping in the Central Quadrupole

Figure 39 is a diagram of the internal components of the TQMS used in this study. During a continuing long-term project to study ion/molecule reactions in the center quadrupole, it was observed that the signal intensity for ion/molecule product ions increased dramatically when the voltage on the drawout lens (L5) for the central quadrupole was decreased abruptly. For positive ions, the increase in peak intensity is greatest if the L5 potential is first increased to a value at least 10 V more positive than the dc offset voltage of the central quadrupole.

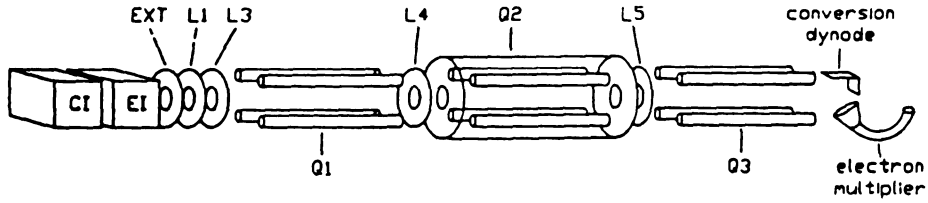

Figure 39. Schematic Diagram of the Internal Components of the TQMS

Apparently, the central quadrupole and its lenses, when "pressurized" can act as an ion trap for ion/molecule product ions with low kinetic energies. These trapped ions can then be drawn out toward the detector by means of a voltage pulse on L5 which gives a maximum signal intensity that may be many times greater than if ion/molecule product ions are drawn out by L5 under the normal steady-state operating conditions of the TQMS. This technique of detecting ion/molecule product ions will be referred to as the "trap and pulse" method. It must be emphasized at this point that in the trap and pulse method, parent ions are constantly being created in the ion source and being transmitted to the collision chamber by the first quadrupole. Because the third quadrupole cannot be scanned over its full range during the millisecond duration of the ion pulse generated by L5, these techniques are necessarily limited to collecting ions of a single nominal mass to charge value per pulse.

In a related technique, ions can be injected into the collision chamber as a discrete packet by pulsing the ion source, followed by ion trapping in the central quadrupole and a pulsed drawout of product ions by L5. This technique will be referred to as the "inject, trap, and pulse" method. The major difference between the two experiments is that trap and pulse admits parent ions continuously into the collision chamber, whereas inject, trap, and pulse admits only a discrete number of ions into the collision chamber. In both modes, L5 can block all ions with low axial kinetic energy from reaching the detector. The inject, trap, and pulse mode was used to determine the length of time that ions can be trapped inside the central quadrupole. The organic ion/molecule reaction chosen for this study was that of methyl cations

reacting with acetone (investigated previously by ICR (114)) to form the products listed in Table 7.

Table 7

Table of Ion/Molecule Products of the Reaction Between the Methyl Cation and Acetone

M/Z	Formula	
15.0	CH_3^+	(P)
29.0	$C_2H_5^+$	(1)
31.0	CH_3O^+	(1)
41.0	C_3H5^+	(1)
43.0	CH_3CO^+	(1)
44.0	$CH_3OCH_2^+$	(1)
57.0	$C_3H_5O^+$	(1)
58.0	$C_3H_6O^+$	(1)
59.0	$C_3H_7O^+$	(1)
117.0	$C_6H_{13}O_2^+$	(2)

(P) indicates the parent ion
(1) indicates a primary reaction product
(2) indicates a product formed by reaction of primary products with acetone

It is possible to trap stable ions such as those with peaks at m/z 59 (acetone + H)$^+$ and 117 (acetone dimer + H)$^+$ in the central quadrupole region for up to 20 seconds. The number of trapped ions drops off exponentially with trapping time. The time constant for this exponential decay (measured using the m/z 117 ion at $5X10^{-4}$ torr acetone) was 2.8 seconds. Attempts to perform the inject, trap, and pulse experiment on some of the other ion/molecule reaction products in Table 7, were unsuccessful (no ion currents detected above the background present in the instrument), until the acetone pressure in the central quadrupole was lowered to $7x10^{-6}$ torr. At these lower pressures, the less stable ions such as those of m/z 43 did not react as efficiently to form secondary products, and thus, could be trapped, albeit for short periods of time. The ion of m/z 43 was trapped for 100 msec before its signal faded into the background.

If one plots trapped ion abundance versus the axial kinetic energy of parent ions entering the central quadrupole, one obtains a sharp peak with a maximum at approximately 0 eV. This is the same type of energy effect found for most ion/molecule reactions observed without trapping in the central quadrupole (10).

In trap and pulse mode, parent ions enter the central quadrupole at a constant rate from the ion source. Therefore, a plot of the area under the ion pulse profile versus trapping time will reveal ion losses due to ion instability from its slope and losses due to approaching maximal trapping capacity from its linearity. If neither of these losses occurs, the ion/molecule product ion intensity should increase by an order of magnitude as the trapping time is increased by an order of magnitude. The area under the pulsed signal profile representing the protonated dimer of acetone of m/z 117 (from the reaction of CH_3^+ and acetone) does in fact, increase by an order of magnitude as trapping time in increased from 10 to 100 msec. Figure 40 shows a plot of analog to digital converter (ADC) counts (which represent the area under the pulse profile) versus trapping time. The linear nature of the plot in Figure 40 indicates that this ion is stable over the 100 msec experiment period and that the central quadrupole can effectively trap it without significant loss. This does not mean that one can detect all of the trapped ions since the ion extraction efficiency of L5 is probably fairly low.

If the parent ion flux is too high, the central quadrupole becomes filled with ions and the curve shown in Figure 40 is not linear. Instead it asymptotically approaches a steady state in which the rate of ions lost from the trap due to ion/ion repulsions is equal to the rate

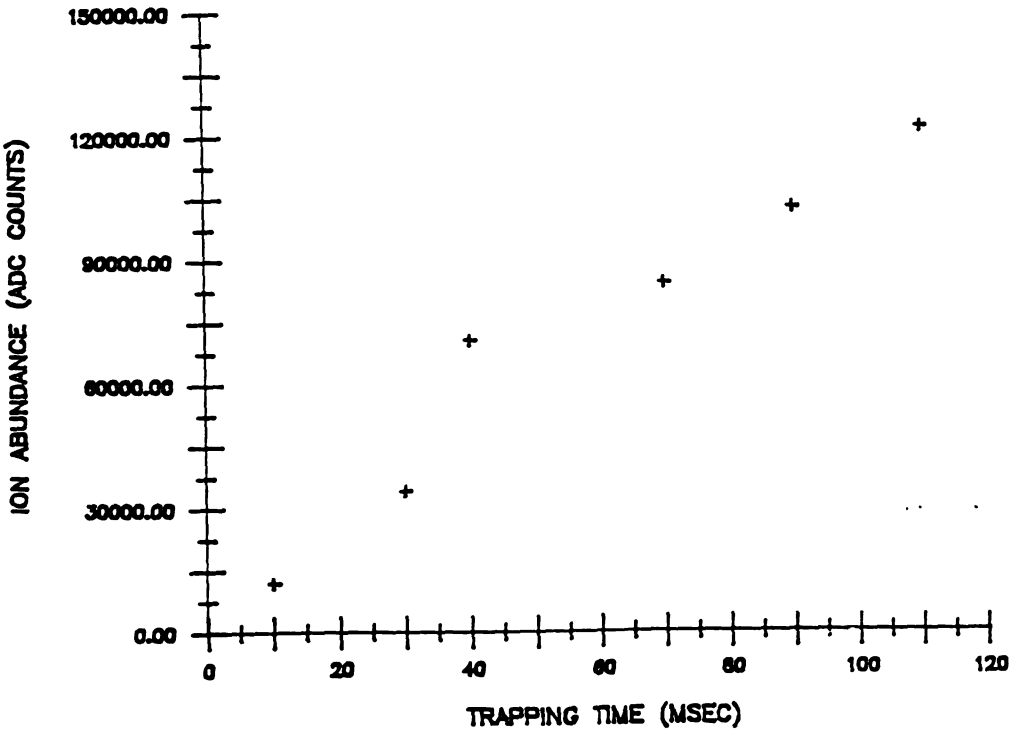

Figure 40. Plot of Ion Abundance (ADC Counts) Versus Trapping Time

of ions injected into the trap. The trap is usually filled within 100 msec at high parent ion fluxes. If the product ion decomposes unimolecularly or by collisions with neutral molecules, or if it reacts with neutral molecules to form other products, the curve in Figure 40 is still linear but its slope decreases. In either case (high parent flux or product decomposition) the apparent trapping efficiency for thermalized ions decreases. On the other hand, the apparent trapping efficiency for thermalized ions increases with decreasing collision gas pressure (increasing mean free path). Effective maximum pressures of reactive collision gases are in the range from 10^{-5} to 10^{-3} torr, but his depends on the particular ions and neutral gases chosen for study.

2. The Trapping Algorithms and their Effects on Data Acquisition

Figure 41 illustrates the time profiles of L3 voltage, L5 voltage, and product ion current in the inject, trap, and pulse mode. In this mode, the voltage on L3 is used as a gate to control parent ions leaving the ion source region and entering the collision chamber. The voltage on L5 is used to trap ions in the collision chamber and to pulse the stored ions toward the detector. Raising the L3 voltage does not cause ions to be stored in the ion source of the TQMS; rather it seems that parent ions are simply deflected from their original flight path.

Some of the characteristics of the MS/MS system in the trap and pulse mode are shown in Figure 42, which compares a product ion current profile and a corresponding plot of L5 voltage. During the trapping period no product ion current arrives at the detector, but following the drop in L5 voltage, there is an abrupt rise in the product ion current

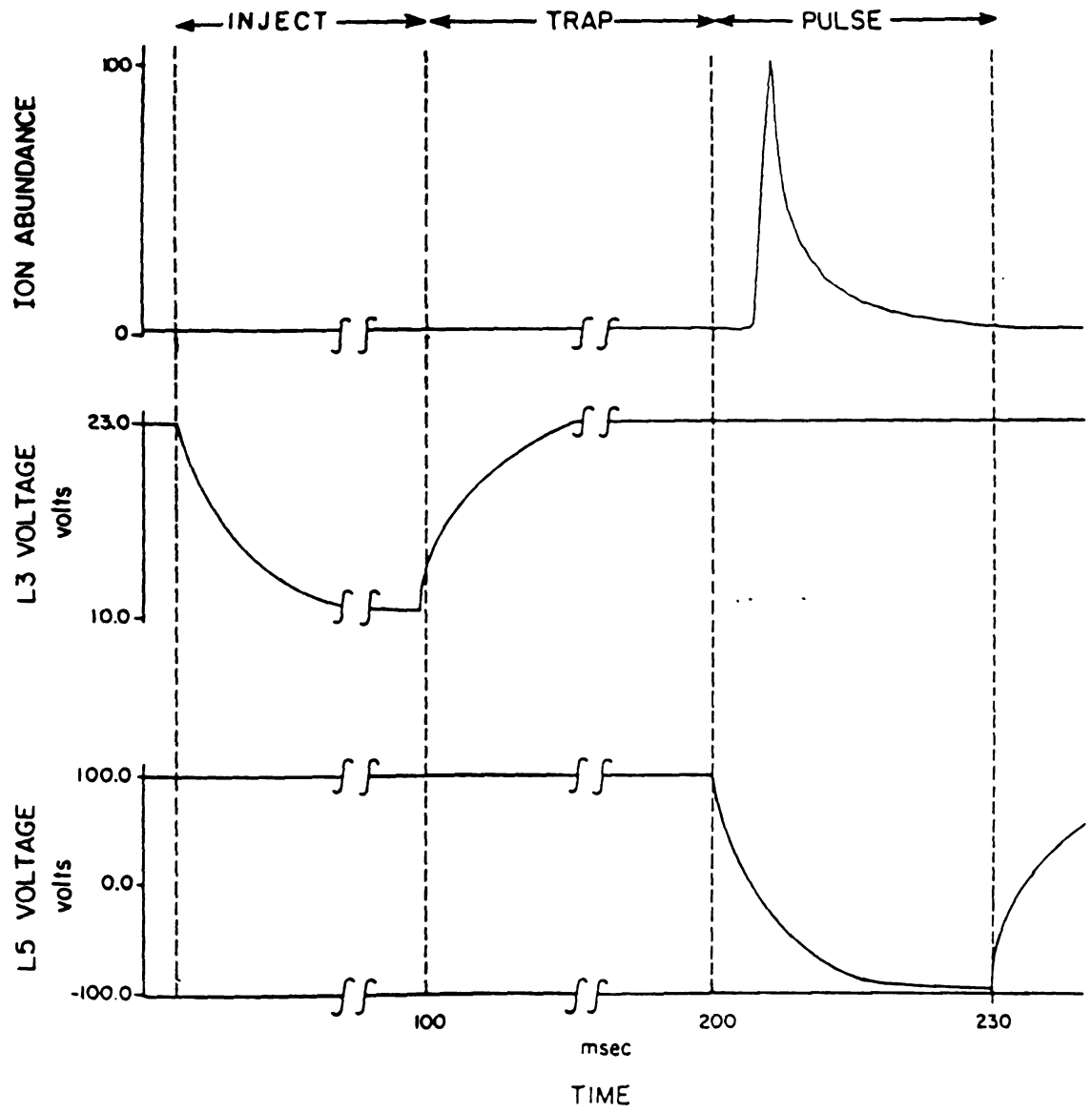

Figure 41. Plots of Ion Abundance Versus Time, and the L3 and L5 Voltages Versus Time, Showing One Full Inject, Trap, and Pulse Cycle

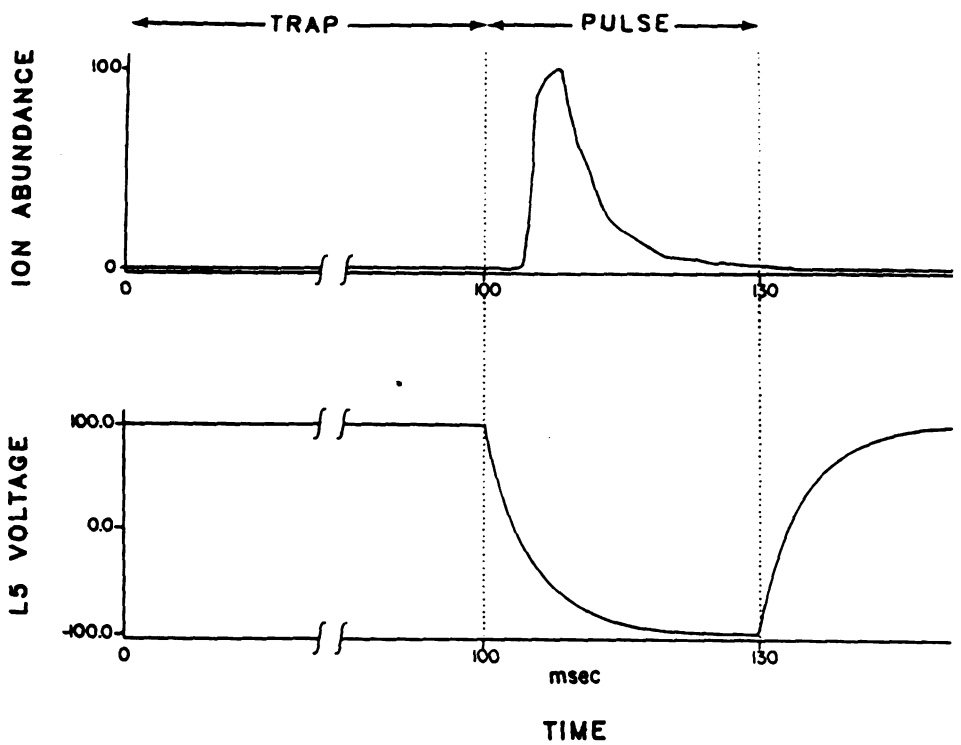

Figure 42. Plots of Ion Abundance Versus Time, and the L5 Voltage Versus Time, Showing One Full Trap and Pulse Cycle

followed by an decay to the level of product ion current produced during steady-state conditions (when L5 is set at -100 V and not pulsed). Unlike the decay observed in the inject, trap, and pulse mode, the decay of ion current in the trap and pulse mode is not cleanly exponential. The time constant of the decay increases with collision gas pressure (i.e., the ion current profile becomes wider during the pulse phase), which indicates that the shape of the ion current profile is controlled at least partially by diffusional effects.

The high voltages shown in Figures 41 and 42 for L5 are not necessary to observe the effects described. A pulse of 10 V to -10 V (for positive ions) is often just as effective, but the higher voltages ensure that the maximum number of ions is trapped in the central quadrupole and that the central quadrupole is purged of ions between storage intervals.

Also noteworthy in Figures 41 and 42 is the fact that the increase in ion current begins as the L5 voltage drops to approximately 0 V, which is the very near the offset voltage of the central quadrupole. Therefore, as the maximum ion current passes through the third quadrupole, L5 is not set at an extreme voltage, does not impart excess kinetic energy to the ions, and as a result does not degrade peak shape (see also Figure 43).

It is apparent from Figures 41 and 42 that the fall time of the L5 voltage pulse is about 20 msec. The rapid decay of the pulse has led the authors to develop a mass-scanning algorithm called a "reaction scan" that repetitively performs the trap and pulse technique and acquires data at least once per nominal mass unit to enhance the intensity of all ion/molecule products in an MS/MS spectrum.

Using the FORTH-based software control system of the TQMS, conventional MS/MS scans were easily modified to allow ion-trapping and pulsed data collection. In reaction scans, the ion source, detector, lens, and quadrupole potentials are set and the microcomputer then generates the sequence of voltage pulses to the lenses as illustrated in Figures 41 and 42. At each mass increment, the apex of the ion current pulse is determined; a series of these trap and pulse cycles at consecutive increments (0.1 mass unit) along the mass axis establishes the mass spectral peak profile. That is, immediately after the drawout pulse on L5, the microcomputer sequentially acquires a specified number of data points to establish the ion pulse profile of a given m/z increment. The data point with maximum magnitude during the data collection for that cycle is used as the ion current value for that mass increment in defining the profile of the mass spectral peak. Finally, a peak-finding algorithm processes the sequential values of the ion current along the mass axis to determine the peak intensity/mass value pairs for each mass spectral peak.

Alternatively, the microcomputer can integrate the area under the ion current profile. The integration algorithm, however, has been determined to decrease the signal-to-noise ratio of the measurement relative to that of simply finding the maximum ion current during the pulse. This means that the peak height is more reproducible than the peak area. The reason for this is that the data are in the form of an asymmetric peak with a long tail. The tail approaches a baseline which represents the steady-state product ion current. The low value of the steady-state current is sensitive to minor fluctuations in collision gas pressure and to random noise, such as that produced by the FAB gun.

Therefore, the baseline contains considerable noise and also varies from pulse to pulse, causing the peak areas to be irreproducible compared to peak height.

Reaction scans are necessarily slower than the corresponding conventional MS/MS scans because a finite time must be spent at each mass increment to trap ions and then to collect data during the pulse. Typical durations for reaction scans (50-500 u) vary from 1 - 2 minutes depending on the reaction being monitored. Therefore, collection of trap and pulse data over the complete mass range (50-500 u) cannot be achieved on the gas chromatographic time scale. One can collect limited trap and pulse data on the GC time scale by using an MS/MS technique called selected reaction monitoring in which the first and third quadrupoles are set to pass ions of one specific mass-to-charge ratio so that the TQMS selects for only one particular parent ion and one particular product ion at a time. One trap and pulse cycle can be accomplished in 50-100 msec, therefore, one can expect to obtain at least 10 data points across even the most narrow capillary gas chromatographic peaks by means of selected reaction monitoring.

3. Effects of Ion Trapping on the MS/MS Spectrum of an Ion/Molecule Reaction

In the trap and pulse mode, parent ions are accumulated continuously and all products are trapped in the central quadrupole. Therefore, ion-trapping time in the central quadrupole is an important parameter related to the magnitude of the signal for ion/molecule product ions. The peak intensity of the ion/molecule product ion increases rapidly with trapping time and then levels off. This

phenomenon reflects a limit to the accumulation of ions in the collision chamber due to space-charge. The same effect is observed frequently in other ion trapping techniques (16). Monitoring a parent ion with a significant abundance (such as the m/z 93 ion, the $(M+H)^+$ ion of glycerol generated by FAB) causes a high rate of parent ion influx into the central quadrupole. In this case, the space-charge limit can be exceeded in only 100 msec of trapping time. The trapping of lower abundance parent ions exceeds the space-charge limit more slowly. The major advantages of the trap and pulse technique over the conventional scanning techniques are illustrated in Figures 43 and 44. Figure 43 shows three MS/MS sweeps over two peaks representing the isotope peaks of the proton-bound adduct of glycerol and acetic acid that was produced by the ion/molecule reaction of protonated glycerol with acetic acid in the central quadrupole region. Sweep A was collected in the conventional mode by stepping the third quadrupole in 0.1 u intervals over the product ions of interest with no signal averaging (approximately 1 msec spent on each point). Sweep B was also collected in conventional mode but with 100 msec of real-time signal averaging per data point. Sweep C was collected using the trap and pulse mode with 100 msec of ion-trapping time per trap and pulse cycle. Figure 43 demonstrates that at the expense of scan speed, the trap and pulse technique can increase the signal-to-noise ratio for detecting ion/molecule product ions by 30 times over that achieved during conventional data acquisition. Figure 43 also demonstrates that at equivalent overall scan speeds, the trap and pulse technique can produce signal-to-noise ratios that are four times higher than those acquired by conventional data acquisition using real-time signal averaging over

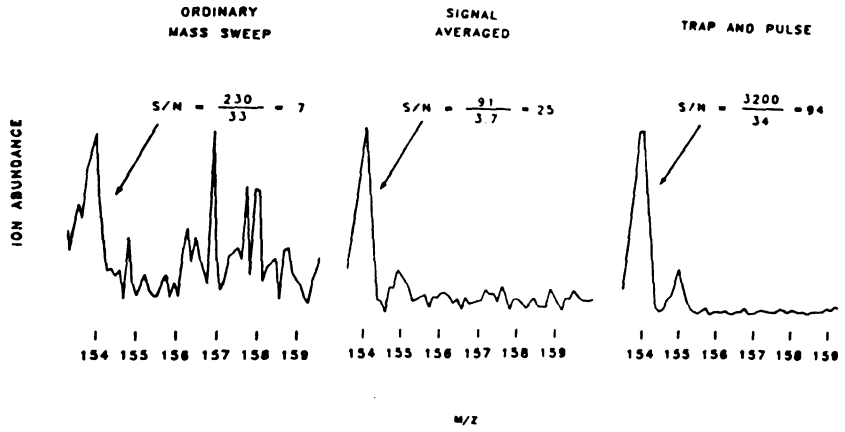

Figure 43. Three Mass-Sweeps of the Third Quadrupole Over the Isotope Peaks of the Proton-bound adduct of Glycerol and Acetic Acid, (A) by Conventional Data Collection (1 msec/point), (B) by Conventional Data Collection with Real-Time Signal Averaging (100 msec/point), (C) by Trap and Pulse Data Collection (100 msec/point)

equivalent time intervals. Signal averaging in the conventional mode improves the signal-to-noise ratio by discriminating against random noise while favoring the constant signal (S/N improves with square root of the number of averages). The trap and pulse technique does not discriminate against noise as such. It improves signal-to-noise by increasing the amount of signal by integrating ion current inside the central quadrupole. S/N theoretically improves linearly with trapping time. Therefore, if one increases trapping time by 100 times, one should observe a hundred fold increase in the signal-to-noise ratio. In Figure 43C we observe only about a third of this increase in S/N because the ion chosen for study decomposes to other products during the course of ion trapping as is shown in Figure 44. Only peaks representing ions which are stable for the entire period of ion trapping can exhibit the full theoretical increase in S/N. The total random noise in the system under trap and pulse mode can only be decreased by averaging consecutive pulse heights (or areas) together. Figure 43 also shows that the shape of the mass spectral peaks representing the ion/molecule products and the mass resolving power of the third quadrupole is not degraded by the trap and pulse technique.

Figure 44A is a conventional third quadrupole MS/MS scan of the ion/molecule reaction between protonated glycerol and acetic acid in the central quadrupole. Figure 44B shows a reaction scan of the same ion/molecule reaction using trap and pulse mode. Figure 44 illustrates that the appearance of ion/molecule product spectrum can be significantly different depending on the scan technique employed. In general, the ratio of product ion peak intensities to the parent ion peak intensity is greatly enhanced with the trap and pulse technique, as

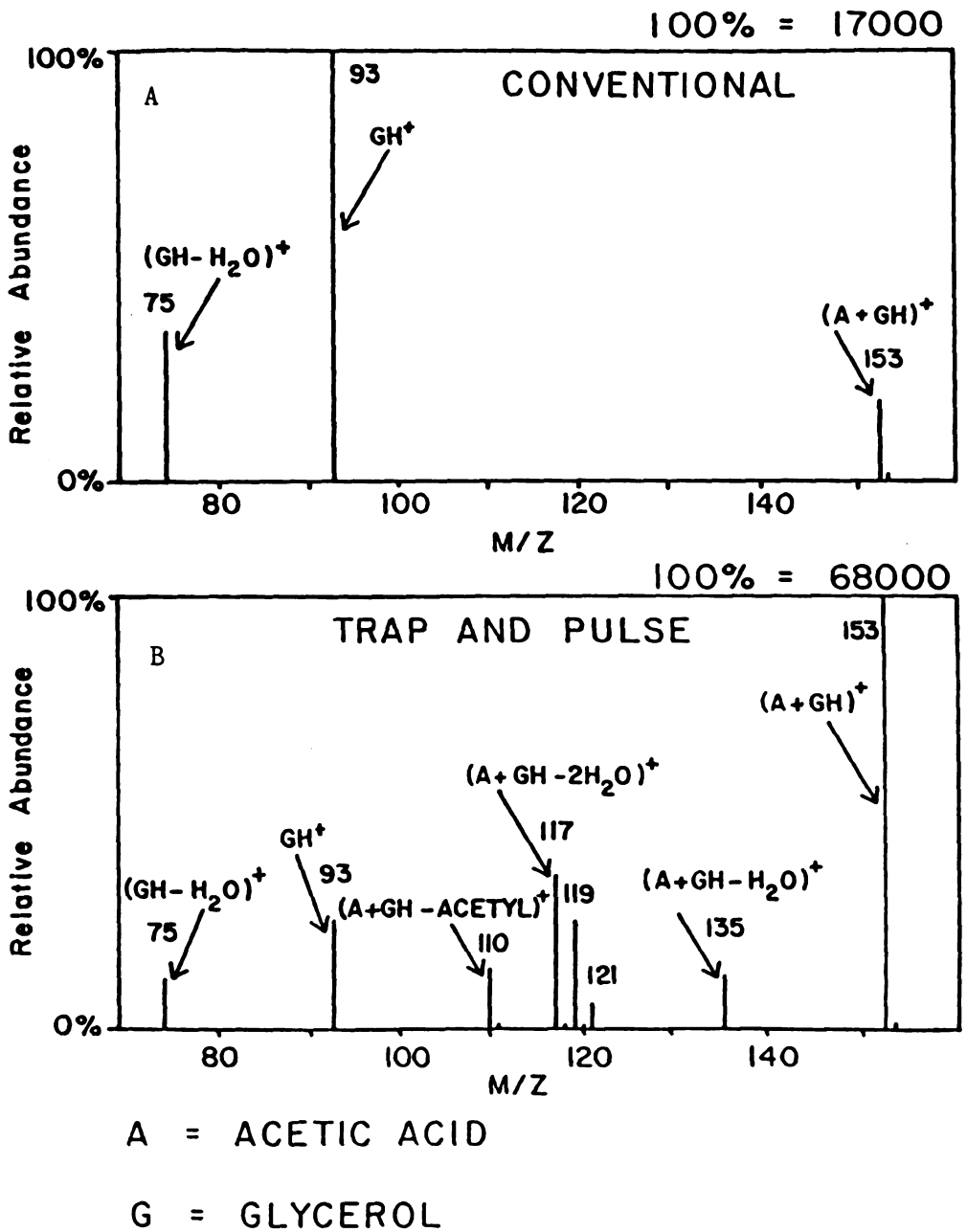

Figure 44. Two Product Scans of the Reaction Between Protonated Glycerol and Acetic Acid by (A) Conventional Data Collection and by (B) Trap and Pulse Data Collection

one would expect, since parent ions are being converted to products continuously during trapping.

Some ion/molecule product ions show more enhancement than others because at long trapping times unstable product ions can decompose or react with the collision gas to form secondary ion products. Therefore, trap and pulse tends to enhance dramatically the ion signals of stable ions, but may actually decrease the relative intensity of signals from less stable ions depending on the conditions in the collision chamber. Figure 44 also shows that at $7x10^{-5}$ torr of acetic acid in the collision chamber, the trap and pulse technique allows ion/molecule products to be observed that otherwise are not detectable at that pressure. The peaks at m/z 110, 117, 119, 121 and 135 are not present even in low abundance in the conventional spectrum. These ions are, however, present if one does CI of a mixture of glycerol and acetic acid. The ions represented by m/z 119 and 121 are the result of proton transfer to the acetic acid dimer, but the ions represented by m/z 117, and 135 are new ions that are the result of neutral losses from the proton-bound adduct of the glycerol and acetic acid. The ion/molecule chemistry between protonated alcohols and acids is discussed in detail in Chapter V. of this dissertation.

4. Comparison of Two Tandem Quadrupole Instruments with Regard to Ion/Molecule Reaction Studies

The research presented in this chapter has been presented to several scientific audiences and at least one researcher (116), responding to the results in this chapter, claimed that the TQMS in his laboratory (a Finnigan MAT TSQ) performed ion/molecule reactions in the

central quadrupole quite well without ion trapping. He, in fact, suggested that we perform on the Extrel TQMS a particular ion/molecule reaction experiment which had been performed with the Finnigan TSQ to determine whether the design of the Extrel TQMS was the cause of the poor sensitivity without ion trapping. The suggested reaction shown in Scheme 2 is the gas-phase analog of a common solution reaction used to derivatize some alcohol and ketone functional groups for the purpose of improving GC/MS performance.

The trimethylsilyl (TMS) ion was generated by EI in both instruments from chlorotrimethylsilane, and neutral acetone was leaked into the central quadrupole region. The Finnigan MAT TSQ and the Extrel TQMS produced virtually identical product spectra for the reaction in Scheme 2. The product spectrum without ion trapping is shown in Figure 45A, and the product spectrum with 50 msec of ion trapping is shown in Figure 45B. The signal enhancement for the peak representing the TMS-acetone adduct ion (m/z 131) is dramatic. Discussions with scientists from Finnigan MAT have recently confirmed that the trap and pulse effect can be observed on that instrument as well as on the Extrel TQMS, despite differences in design. This indicates that ion trapping in the rf-only quadrupole is a general phenomenon.

D. Conclusion

It is possible to trap ions with very low axial kinetic energies (such as ion/molecule product ions) with high efficiency in the central quadrupole region of the TQMS with no physical modifications to the instrument. The capacity to trap ions efficiently in the central quadrupole has several significant advantages for studying ion/molecule

Scheme 2

Reaction of the Trimethylsilyl Ion with Acetone to Form the Adduct Ion

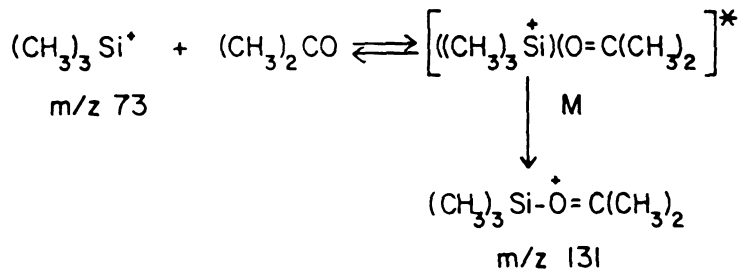

100%

Relative Abundance

0%

100%

Relative Abundance

0

MS

Fig
Cat
and

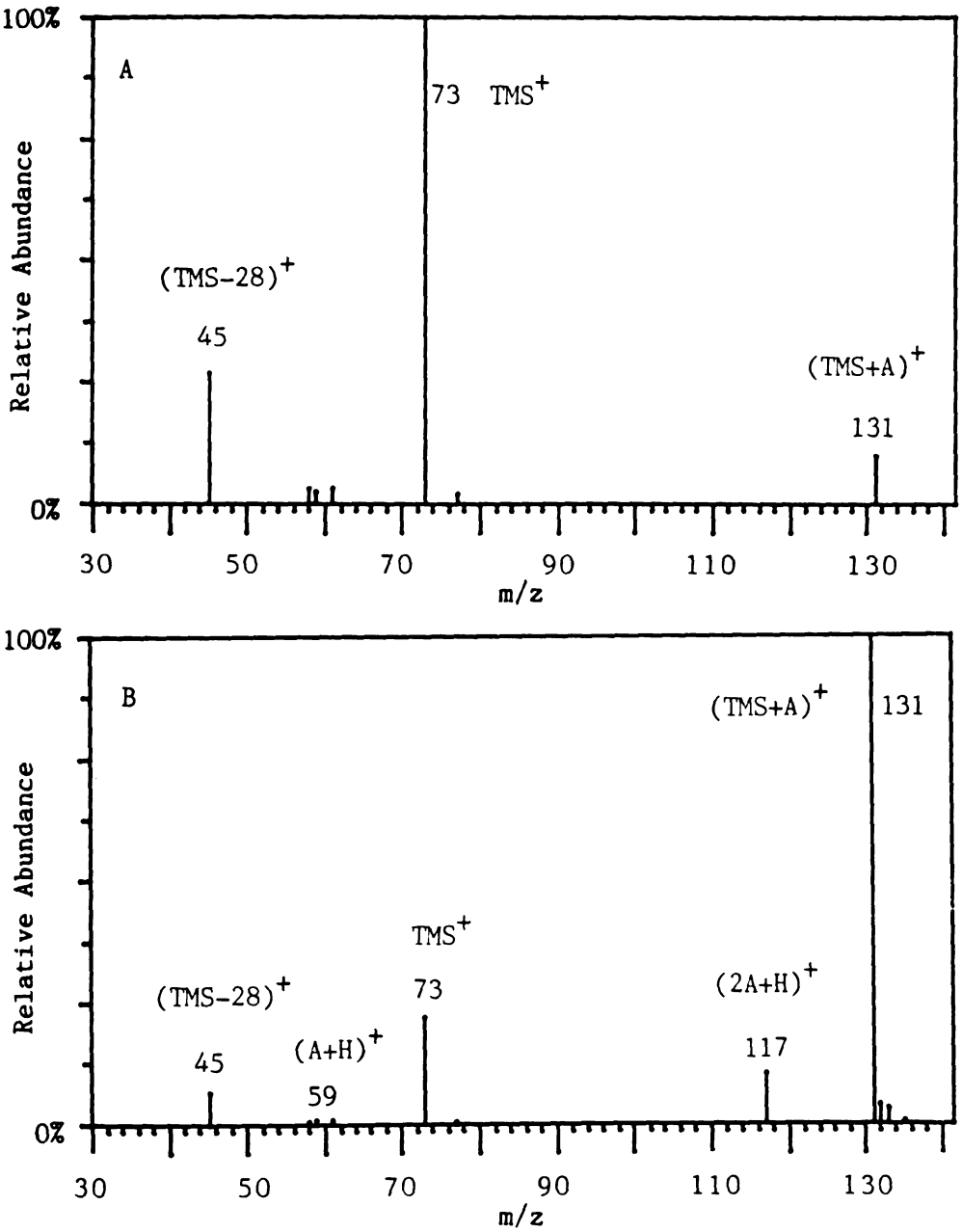

TMS=Trimethylsilyl

A=Acetone

Figure 45. Two Product Scans of the Reaction Between the Trimethylsilyl Cation and Acetone by (A) Conventional Data Collection and by (B) Trap and Pulse Data Collection

reactions in the TQMS: lower pressures of reactive collision gas can be used, the overall signal level and the signal-to-noise ratio for detecting ion/molecule reaction products can be improved, and ion/molecule products which are not easily observed by conventional TQMS data acquisition can be detected. The ion-trapping techniques described here could be used for enhancing the ion signals from other types of reactions in the collision chamber of the TQMS, such as charge transfer and photodissociation. Conceivably, ion trapping could be employed in other multi-quadrupole instruments such as the BEQQ (117,82) and the five-quadrupole instrument developed recently for ion/molecule reaction studies.

CHAPTER V.

ION/MOLECULE REACTIONS OF CARBOXYLIC ACIDS AND ALCOHOLS IN THE TQMS FOLLOWING IONIZATION BY CI AND FAB

A. Introduction

One of the classic reactions in organic solution chemistry is the acid-catalyzed Fisher esterification reaction (118). In a strongly acidic medium, one can protonate a carboxylic acid which will react readily with alcohols to form the protonated ester. By neutralizing the solution one obtains crystals of the neutral ester. This reaction has been used as a derivatization reaction in GC/MS applications to make the methyl esters of long-chain fatty acids (119) because the esters are more volatile and thermally stable than the acids and because the esters give molecular ions under EI, whereas the acids often do not. The Fisher esterification reaction is also commonly used in peptide synthesis as a method of protecting carboxylic acid functional group (120).

An analogous reaction of alcohols and acids has been demonstrated to take place in the gas phase by Tiedemann and Riveros using ICR spectrometry (90). Tiedemann and Riveros determined that alcohols and acids at approximately 10^{-5} torr react in the presence of protons to form protonated esters, and they published simple rules which allow one to predict whether a particular acid/alcohol pair will produce a protonated ester. The rules are: the reaction must be exothermic, and the proton affinity of the acid must be higher than that of the alcohol for the protonated ester to form. They also postulated that "the

initial position of the labile proton (on the acid or the alcohol) probably does not affect the mechanism, as rapid proton transfer very likely occurs in the collision complex."

Since this reaction is known to occur in the ICR technique and is amenable to study by the TQMS, the author considered it an ideal reaction to use for comparing the results obtained from ion trapping in the TQMS to the results obtained from ion trapping in the ICR. This is necessary because use of the TQMS without ion trapping has sometimes produced results that were contradictory to other more established ion/molecule techniques. The dubious quality of non-ion-trapped TQMS data has previously led at least one author to dismiss the TQMS as a useful tool for observing ion/molecule reactions (121).

The first question which this chapter seeks to answer is whether the TQMS technique with ion trapping can be validated as an analytical method for studying ion/molecule reactions. The second question is: assuming that it is possible to study ion/molecule reactions productively using the TQMS, what can the particular ion/molecule reaction chosen for this study reveal about current unresolved issues in mass spectrometry, such as the mechanism of FAB, and the ability of ion/molecule reactions to function as probes for structural analysis in complex molecules.

B. Experimental

1. Conditions for FAB

Due to the fact that the experiments in this section were carried out over three years, the conditions varied more from experiment to experiment than in other sections of the dissertation. Nevertheless,

the conditions were relatively constant throughout. The voltage to the capillaritron FAB gun was 10 kV, the Xe pressure in the ion source chamber varied from $5X10^{-5}$ to $8X10^{-5}$ torr, and the distance from the FAB gun was approximately 10 cm. The repeller voltage applied to the sample probe varied from 0 to 15.6 volts. Fortunately, this variation affected only the total ion current and not the relative abundances of product ions, since it was possible to keep the average axial kinetic energy of the parent ion constant from experiment to experiment by varying the central quadrupole offset voltage to match the changes in repeller voltage.

Vacuum distilled glycerol was the most commonly used FAB matrix, but it was necessary to use a 1:1:1 mixture by volume of dithioerythritol, dithiothreotol, and thiodiglycol as a matrix to achieve satisfactory results with ibuprofen. The reason for this was that the (glycerol dimer + Na)$^+$ ion obscures the protonated molecule of ibuprofen at m/z 207. However, no major ion is present from the thiol matrix.

All of the FAB samples except for ibuprofen were pure compounds obtained as analytical grade reagents. The ibuprofen was obtained from a local drug store as tablets with the brand name Nuprin. One Nuprin tablet was placed in 1 ml of 6 N HCl and shaken vigorously. This procedure creates a yellow suspension which settles out to leave a yellow solution. 1 ul of the yellow solution was pipetted onto 5 ul of the thiol mixture and was immediately placed in the TQMS for FAB analysis since the thiol mixture is more volatile than glycerol and has an offensive odor. Once inside the TQMS, the thiol mixture gives superb

FAB spectra of ibuprofen but the ions usually are produced for no more than five minutes since the matrix dries out quickly under the vacuum.

2. Conditions for CI and GC

Whenever possible, the author used self-CI to create $(M+H)^+$ parent ion of gases and volatile liquids. The standard ion source chamber pressure for self-CI was $5X10^{-5}$ torr of the appropriate gas such as methanol, ethylene glycol, ethanol, ethylacetate, and acetic acid. Whenever a reagent gas was necessary, as in the GC experiment, the author employed $1X10^{-4}$ torr isobutane as the reagent gas. The ion source temperature for CI was generally 75°C, but was set at 130°C for the GC experiment. For the GC experiment, the heated transfer line from the GC was set at 200°C, the GC oven was programmed from 50°C to 250°C at 10°C per minute. The column was a narrow-bore analytical fused-silica bonded-phase column coated with a DB-5 stationary phase.

3. Conditions in the Central Quadrupole

For ion/molecule reactions in the central quadrupole, the average axial kinetic energy of parent ions was nearly always in the vicinity of 4 eV. The actual energies varied from 2.6 to 5.3 eV as calculated by subtracting the central quadrupole offset voltage from the ion source voltage (either the CI volume voltage or the FAB repeller depending on the ionization technique). There is only marginal control over the axial kinetic energy in this TQMS design, so the parent ions exhibit an energy spread of at least 3 eV in all experiments. Therefore, to a first approximation, the average kinetic energy of the parent ions was held constant throughout the experiments in this section.

Table 8

Typical Operating Conditions for EI/MS/MS and CI/MS/MS Using Ar CID

EI/MS/MS

Parameter	Value	Parameter	Value
Mode	+CI	M1	m/z of Parent Ion
EV	70eV	M2	M1÷2
REP	16.0V	M3	m/z of Daughter Ion
CIV	15.0V	DM1	3.3
EIV	15.0V	DM3	7.6
EXT	23.7V	RM1	—
L1	-30.0V	RM2	—
L2	—	P2	—
L3	10.0V		
Q1	9.5V	THR	150
L4	12.0V	PWD	5
Q2	13.0V	MWD	30
L5	0.5V	RTE	6
Q3	10.3V		
MHV	1900.0V		

CI/MS/MS

Parameter	Value	Parameter	Value
Mode	+CI	M1	m/z of Parent Ion
EV	70eV	M2	M1÷2
REP	37.9V	M3	m/z of Daughter Ion
CIV	37.2V	DM1	3.3
EIV	-70.2V	DM3	7.6
EXT	40.8V	RM1	—
L1	-10.4V	RM2	—
L2	—	P2	—
L3	-63.0V		
Q1	21.0V	THR	170
L4	-12.2V	PWD	5
Q2	28.8V	MWD	30
L5	-11.8V	RTE	6
Q3	23.1V		
MHV	2000.0V		

regi

of r

For

coll

quac

C.

numb

both

are

pres

subt

whic

acid

with

alco

its

deco

mole

usua

pres

abun

spec

The standard pressure of acetic acid in the central quadrupole region was $8X10^{-4}$ torr as measured by an ionization gauge. The pressure of methanol in the central quadrupole was regulated to be $2X10^{-3}$ torr. For CID experiments, $1X10^{-3}$ torr argon was used as the non-reactive collision gas. The pressures of all gases entering the central quadrupole were regulated with a Granville-Phillips pressure controller.

C. Ion/Molecule Chemistry Results from the TQMS Compared to Other Techniques

1. Ion/Molecule Reactions in Methanol

Both alcohols and acids in the gas phase exhibit a considerable number of self-CI type ion/molecule reactions. These reactions occur both in the CI volume and in the central quadrupole of the TQMS. They are of interest in this chapter primarily because the self-CI reactions present a chemical background (rather like that in FAB) which must be subtracted from the product spectra to reveal the ion/molecule reactions which take place between alcohols and acids. With both alcohols and acids, the self-CI reactions are initiated by any incoming parent ion with a labile proton that can undergo proton transfer to the neutral alcohol or acid. The protonated alcohols or acids can then react with its neighboring neutral molecules to form product ion which can decompose to form fragment ion which in turn can react with neutral molecules to form still more product ions. All of the product ions usually lose water readily, forming still more product ions. At higher pressures (as in CI) one can generate many different product ions of low abundance up to approximately m/z 200. Figure 46 shows two product spectra of protonated methanol (m/z 33) obtained while reacting with

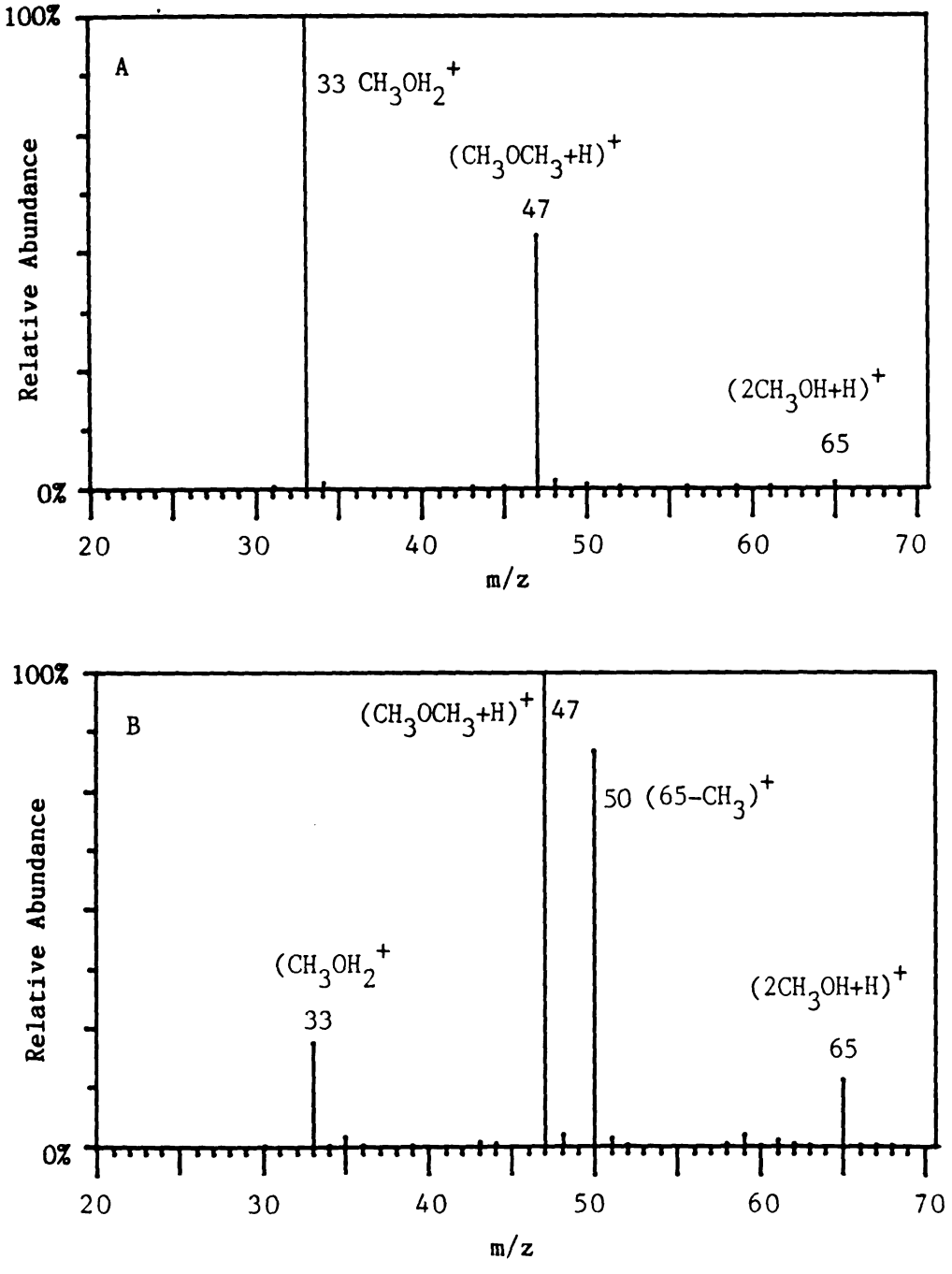

Figure 46. Product Spectra of Protonated Methanol Reacting with Methanol in the Central Quadrupole (A) Without Ion-Trapping and (B) With Ion-Trapping

methanol in the central quadrupole. Figure 46A was obtained without ion trapping and Figure 46B was obtained with 100 msec of ion trapping.

It is immediately obvious from Figure 46 that ion trapping increases the number and the total ion abundance of the self-CI ions produced in the central quadrupole. The major product ion peaks one observes are the protonated dimer of methanol at m/z 65, the protonated trimer of methanol at m/z 97, and the protonated dimethylether ion at m/z 47, and the adduct of water and methanol at m/z 50.

In Figure 47, the self-CI spectrum of methanol generated in the CI volume shows product ions peaks that are nearly identical to those generated by ion trapping in the central quadrupole.

2. Ion/Molecule Reactions in Acetic Acid

Figure 48 shows the product spectrum of the reaction between protonated acetic acid (m/z 61) and neutral acetic acid in the central quadrupole with 100 msec of ion trapping. Figure 48 demonstrates that acetic acid produces many more product ions than methanol and that these ions extend over a much wider mass range. The base peak of the spectrum is the acetyl ion at m/z 43 which is the result of neutral water loss from the protonated acid. In fact, it is very difficult to obtain the protonated molecule of any monofunctional carboxylic acid in any ionization technique due to this facile water loss. Other major peaks in Figure 48 include the protonated dimer of acetic acid at m/z 121 and the adduct of H_2O^+ and acetic acid at m/z 78. Acetic acid cluster ions have received considerable attention in the scientific literature (122).

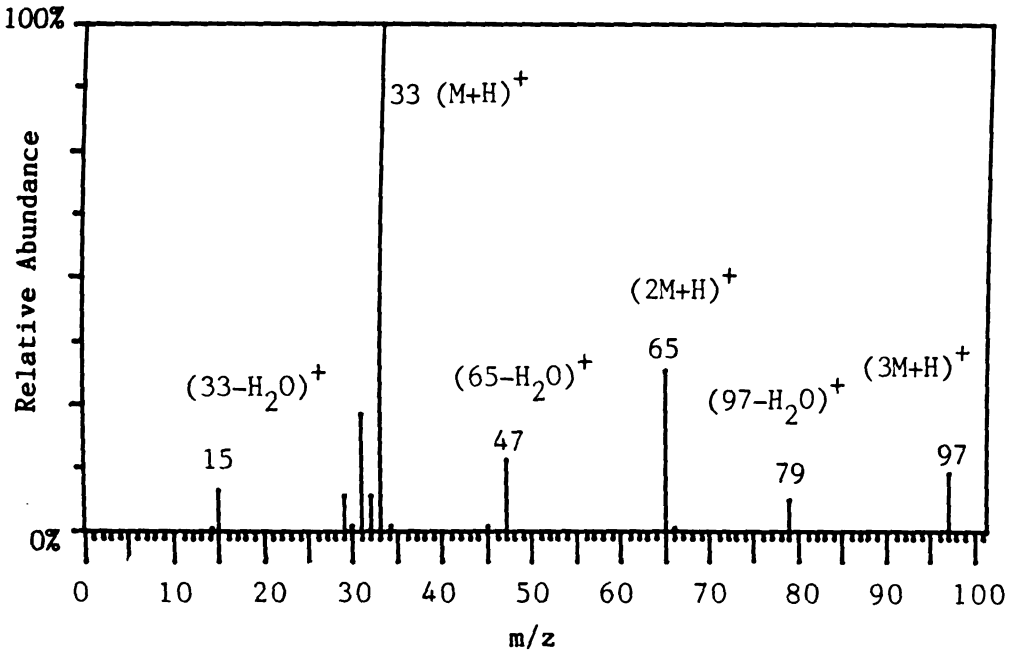

Figure 47. Self-CI of Methanol

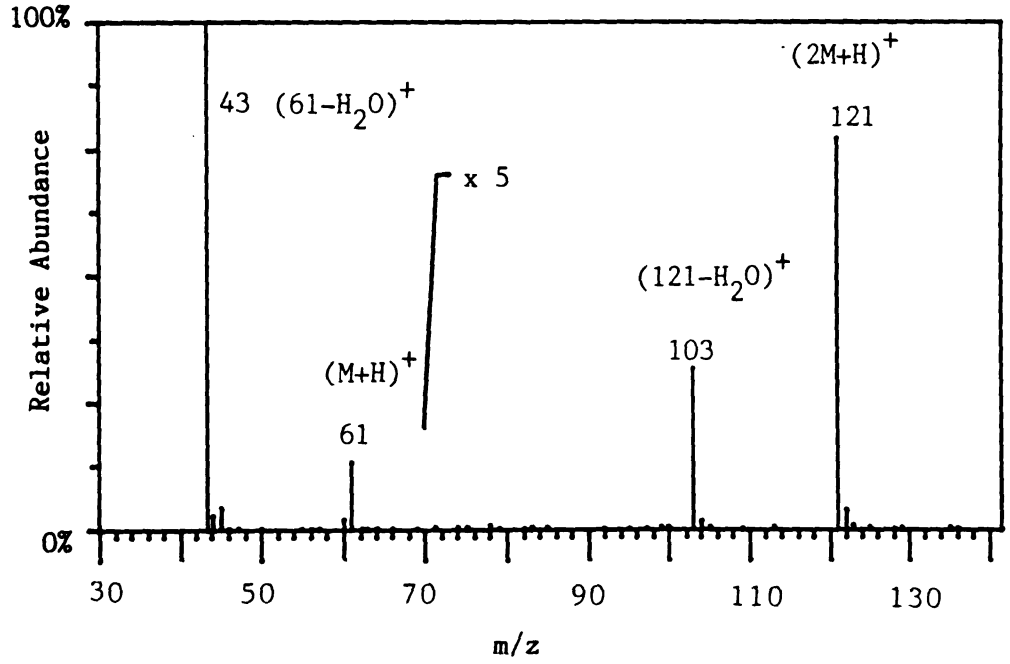

Figure 48. Product Spectrum of Protonated Acetic Acid Reacting with Acetic Acid in the Central Quadrupole with Ion Trapping

3. Background Subtraction to Remove the Self-CI Contribution from the Product Spectrum

Since the pattern of the self-CI product spectrum of acids and alcohols in the central quadrupole is quite reproducible at a given reactive collision gas pressure and at a given trapping time, the self-CI spectra can be stored in a file on a magnetic disk and can be subtracted from any other product spectrum by means of computer routines to give product spectra which are free from contributions to peaks that are due to ion/molecule reactions from to the collision gas. This spectral background subtraction strategy is used in this chapter and in other places in this dissertation to aid in spectral interpretation. If the background peaks are much larger than the ion/molecule reaction product peaks with the same nominal mass, the ion/molecule reaction product peaks will tend to be subtracted from the spectrum along with the background peak. This difficulty can only be overcome completely by isotopically shifting the mass of the product ion (by addition of ^{2}H or ^{13}C to the parent ion) or by using an instrument such as the JEOL HX-110 with high resolution capabilities for product ion scans that actually can resolve the product peaks from the background peaks.

4. Reactions of Protonated Alcohols with Acetic Acid

When one protonates ethanol by self-CI in the CI source and reacts the protonated molecule with acetic acid in the central quadrupole, one obtains the ion-trapped product spectrum in Figure 49A. The base peak of Figure 49A is m/z 43, representing the acetyl ion, which is the major peak produced by background ion/molecule reactions in acetic acid. Therefore, the author used the program MSOUT to subtract the product

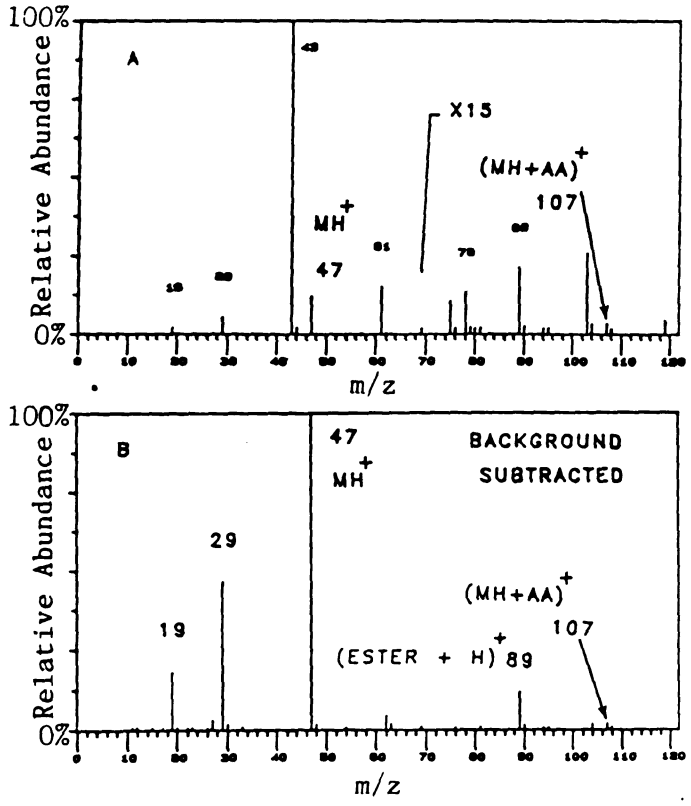

Figure 49. Ion-Trapped Product Spectrum of Protonated Ethanol Reacting with Acetic Acid (A) With and (B) Without Background Subtraction

spectrum of reactions in acetic acid (Figure 47) from the spectrum in Figure 49. In order to obtain the correct peak heights in the background-subtracted spectrum, the peaks in Figure 47 were normalized to the height of the base peak in Figure 49A. The background subtracted spectrum is shown in Figure 49B. It is free of the peak for the acetyl ion and of all other peaks which represent ion/molecule reactions in acetic acid. The parent ion, the protonated molecule of ethanol, (m/z 47) is the base peak in the background-subtracted spectrum. There are two peaks that are the result of CID processes: m/z 19 (H_3O^+) and m/z 29 ($CH_3CH_2^+$). The most abundant ion/molecule product ion peak with an m/z value greater than the parent ion is at m/z 89. This corresponds to the mass expected for the protonated ester reaction product of protonated ethanol and acetic acid. The structure of this ion is probably that of protonated ethylacetate. There is also a peak at m/z 107 in Figure 49B which represents the proton-bound adduct of ethanol and acetic acid.

Combining acetic acid and ethanol in the CI volume with the CI filament "on" produces the spectrum shown in Figure 50. The m/z 89 peak produced by the reaction of acetic acid and protonated ethanol at high pressure in the CI volume has in all likelihood the same ion structure as the m/z 89 peak produced by the reaction of protonated ethanol and acetic acid in the central quadrupole. In order to determine the structure of the m/z 89 product ion peak, the author performed the argon CID experiments shown in Figure 51A and 51B. Figure 51A shows the argon CID daughter scan of the m/z 89 ion produced by the ion/molecule reactions between ethanol and acetic acid in the CI volume, and Figure 51B shows the argon CID daughter spectrum of the m/z 89 ion produced by isobutane CI of ethylacetate. One can see that the two daughter spectra

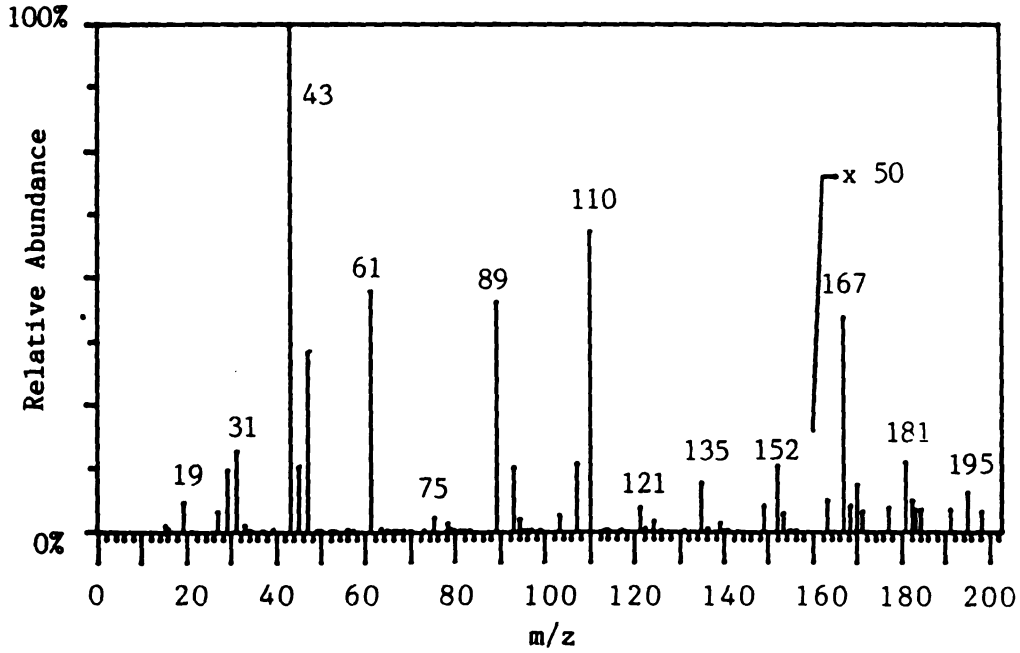

Figure 50. CI Mass Spectrum of a Mixture of Ethanol and Acetic Acid

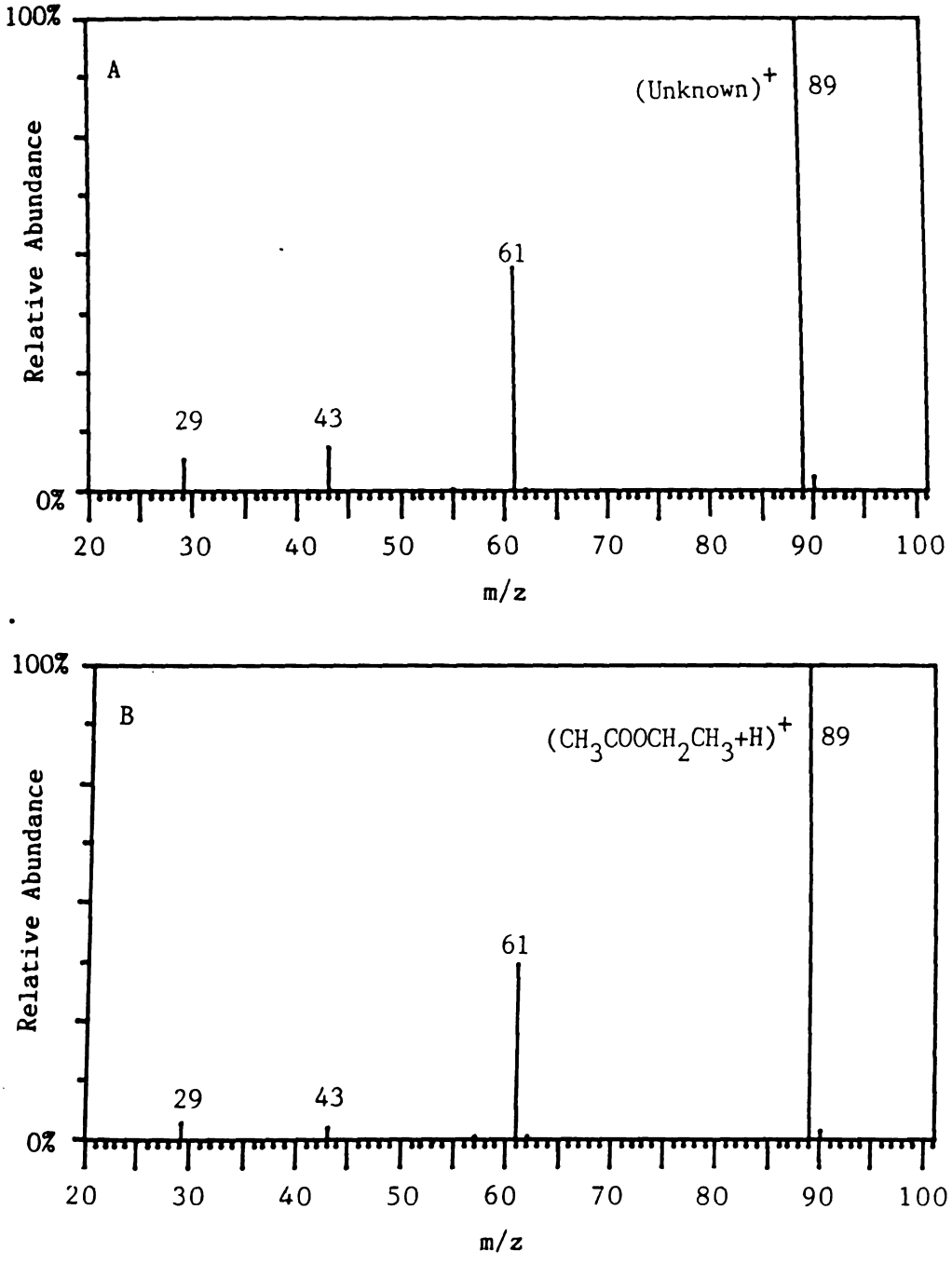

Figure 51. CID Daughter Spectrum of the m/z 89 Product Ion Peak (A) Compared to a Daughter Spectrum of Protonated Ethylacetate (B)

shown in Figure 51 are extremely similar. This evidence substantiates the ICR evidence that the m/z 89 product ion peak produced by the reaction of protonated ethanol and acetic acid is, indeed, protonated ethylacetate.

In addition, the spectra in Figures 49, 50, and 51 show how the central quadrupole and the CI volume can be used to produce more information about a given reaction than either one alone can produce. When an ion/molecule reaction is accomplished using the central quadrupole, one has control over which parent ion reacts with the neutral gas, therefore, one can determine which products arise from particular parents. One cannot, however, perform CID subsequently to determine the structure of the products (unless one has a pentaquadrupole instrument). On the other hand, when an ion/molecule reaction is accomplished using the CI volume, one cannot choose a parent ion, but one can perform CID subsequently to determine the structure of the product ions by spectral interpretation and by comparison of the CID spectrum of the product ions to those of reference compounds. This technique of using the CI volume and the central quadrupole in a complementary fashion is employed repeatedly in this dissertation to determine the structures of product ions which are produced by a given ion/molecule reaction.

5. Ion/Molecule Reaction of Protonated Acids with Alcohols

The article by Tiedemann and Riveros (90) indicates that whether the proton is initially located on the alcohol or the acid is inconsequential to the mechanism of the reaction, since they postulate

rapid proton transfer in the intermediate complex. The author was interested in testing the validity of this view by means of the unique geometry of the TQMS. One can easily protonate the acid by means of CI or FAB instead of the alcohol, and then react the protonated acid with a neutral alcohol in the central quadrupole. If one protonates the acetic acid by either self-CI or by FAB (acetic acid dissolved in glycerol) and reacts the protonated molecule of acetic acid with methanol in the central quadrupole, one obtains the ion-trapped product spectrum shown in Figure 52. The base peak (m/z 43) in Figure 52 is the acetyl ion due to CID. There is another CID peak at m/z 59 which is due to loss of H_2 from the protonated acetic acid. The only ion/molecule reaction product is m/z 75 which corresponds to the protonated methyl acetate, which is the same peak one obtains from the reaction of the protonated alcohol and the neutral acid. One obtains approximately the same yield of the protonated ester whether the proton is initially located on the acid or on the alcohol. These data agree with Riveros and Tiedemann's (90) assertion that the mechanism of the gas-phase reaction is independent of the initial location of the proton.

6. Effect of the Acid's Proton Affinity on the Esterification Reaction

Tiedemann and Riveros (90) observed in the ICR that whereas acetic acid reacted with protonated ethanol to form the protonated ester, formic acid did not. Formic acid has a lower proton affinity than ethanol (see Chapter XI.), so the rules stated in the introduction of this chapter for the production of protonated esters appear to be obeyed in the ICR. The author was interested in whether the same result would

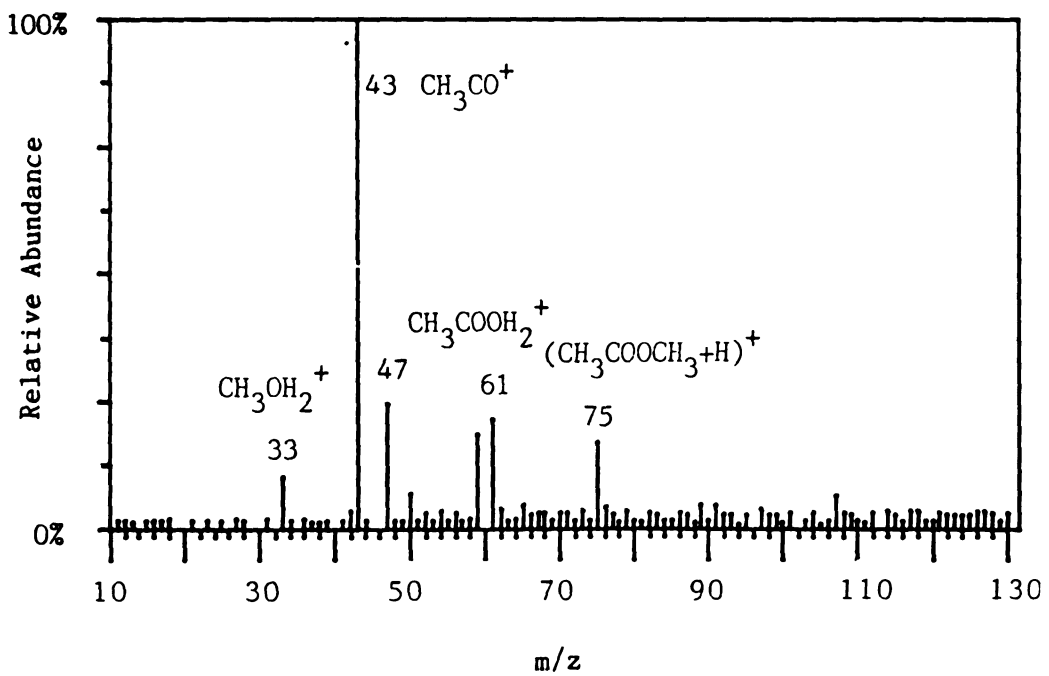

Figure 52. Ion-Trapped Product Spectrum of Protonated Acetic Acid Reacting with Methanol in the Central Quadrupole

be obtained in the TQMS. The first pieces of information obtained in this regard were that commercial formic acid is usually contaminated with small amounts of acetic acid, and that residual acetic acid remains in the TQMS vacuum lines for hours after they have been evacuated. It was, therefore, extremely difficult to obtain a formic acid product spectrum that was entirely from peaks due to acetic acid. The major difficulty presented by the presence of acetic acid was that the ion/molecule reactions in acetic acid create peaks that have the same m/z values as the esterification products one wishes to observe due reactions between formic acid and protonated alcohols.

To avoid the problems presented by acetic acid, the author chose an alcohol (ethylene glycol) whose expected esterification products with both acetic acid and formic acid would be at m/z values that were not observed by background peaks from residual acetic acid. Figure 53 shows a product spectrum of protonated ethylene glycol reacting with formic acid and residual acetic acid in the central quadrupole of the TQMS. Figure 53 shows the parent ion peak at m/z 63 and numerous product ion peaks since this spectrum is intentionally not background-subtracted. Notice in particular that although there is a peak at m/z 105 which would represent the protonated ester of ethylene glycol and acetic acid, there is no peak at m/z 91 which would represent the protonated ester of ethylene glycol and formic acid. According to this data the lower proton affinity of the formic acid appears to inhibit the esterification reaction in the TQMS.

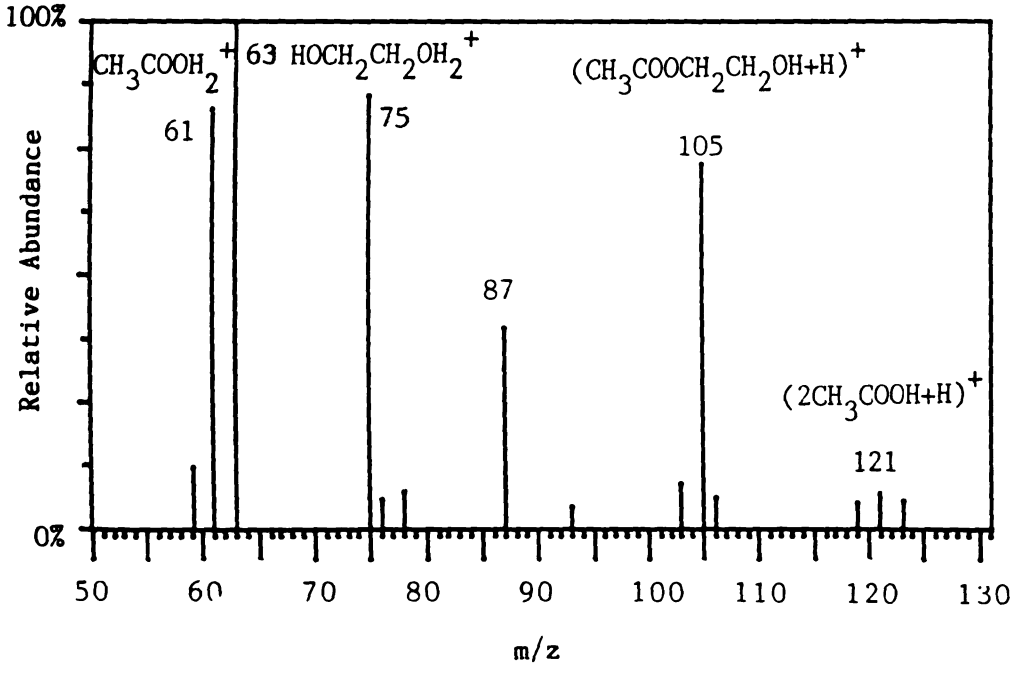

Figure 53. Product Spectrum of Protonated Ethylene Glycol Reacting with Formic Acid and Residual Acetic Acid in the Central Quadrupole

7. Mechanism of the Gas-Phase Esterification Reaction

Tiedemann's and Riveros' mechanism (90) for the formation of the ester is that protonated alcohol and the acid come together in the gas-phase to form an activated intermediate which is a proton-bound adduct of the two molecules, but which is not observed in the ICR because it either dissociates back to the reactants or it loses a water molecule to release its excess energy forming the protonated ester. In the TQMS one often does observe the proton-bound adduct because the pressure in the central quadrupole and in the CI volume is often high enough to stabilize the activated intermediate through collisions with neutral molecules that transfer excess energy away from the proton-bound adduct. The mechanism for the reaction of acetic acid with protonated ethanol in the TQMS is illustrated in Scheme 3.

Several researchers (158) in the field had doubts about this mechanism for two reasons. First, the data in this chapter used to support the mechanism in scheme 3 show that the product ion with m/z 89 has the protonated ester structure. However, the protonated molecule of an ester is usually thought to have a structure in which the proton is attached to the carbonyl oxygen, not the structure shown for the product ion in scheme 3 in which the proton is attached to the ester oxygen. Furthermore, the proton transfer from one oxygen to the other is considered unlikely as a unimolecular event.

It is possible to address this point that the wrong form of the protonated ester is produced, by observing that the protonated ester is produced in both the ICR and the TQMS only at relatively high pressures. This indicates that the proton may be transferred intermolecularly to the more stable position after the formation of the ester. Scheme 4

Scheme 3

Reaction of Protonated Ethanol with Acetic Acid to Form Protonated Ethylacetate

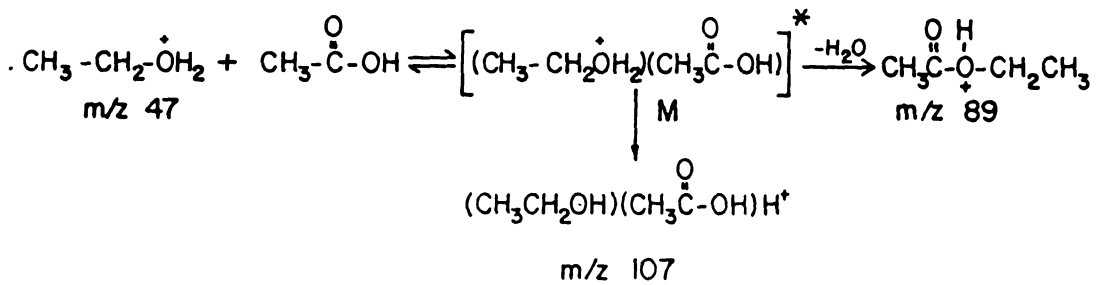

Scheme 4

Intermolecular Hydrogen Transfer Reactions in Esters

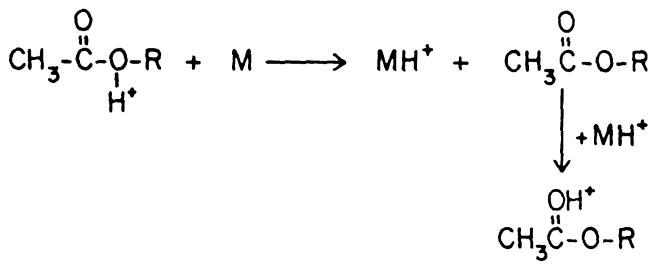

shows this mechanism. Both of the steps in scheme 4 can be exothermic if the neutral species, M, has a proton affinity which is intermediate between that of the carbonyl oxygen and the ester oxygen.

The second criticism of the mechanism in scheme 3 was that the data in Figure 49 show that the acetyl ion is the base peak in all the product spectra that produce esters. Perhaps the protonated ester formation is the result of the acetyl ion reacting with the neutral alcohol. It is possible to test this hypothesis experimentally in the TQMS. Figure 54 shows the product spectrum of the acetyl ion reacting with methanol in the central quadrupole of the TQMS. The reaction of the acetyl ion with methanol produces numerous products of low abundance but does not produce a product ion peak at m/z 75 which would indicate the production of protonated methyl acetate. Therefore, it seems that the acetyl ion does not cause the formation of protonated esters. The combined reactions in schemes 3 and 4 appear to be the mechanism whereby small monofunctional protonated alcohols react with acetic acid to form protonated esters in the TQMS.

Unfortunately, Tiedemann's and Riveros' (90) paper does not show any spectra of the reaction between acids and alcohols, so it is not possible to compare the data produced by the ICR and the TQMS for the esterification in a quantitative fashion. However, the data in this chapter show that, at least for the esterification reaction, the ICR and the TQMS methods yield the same qualitative results. Every detail of the esterification reaction that was revealed by ICR was substantiated by the TQMS, and both techniques appear to point toward the same reaction mechanism. ICR and its modern cousin, FT-MS, have for many years been used as the premier methods for studying ion/molecule

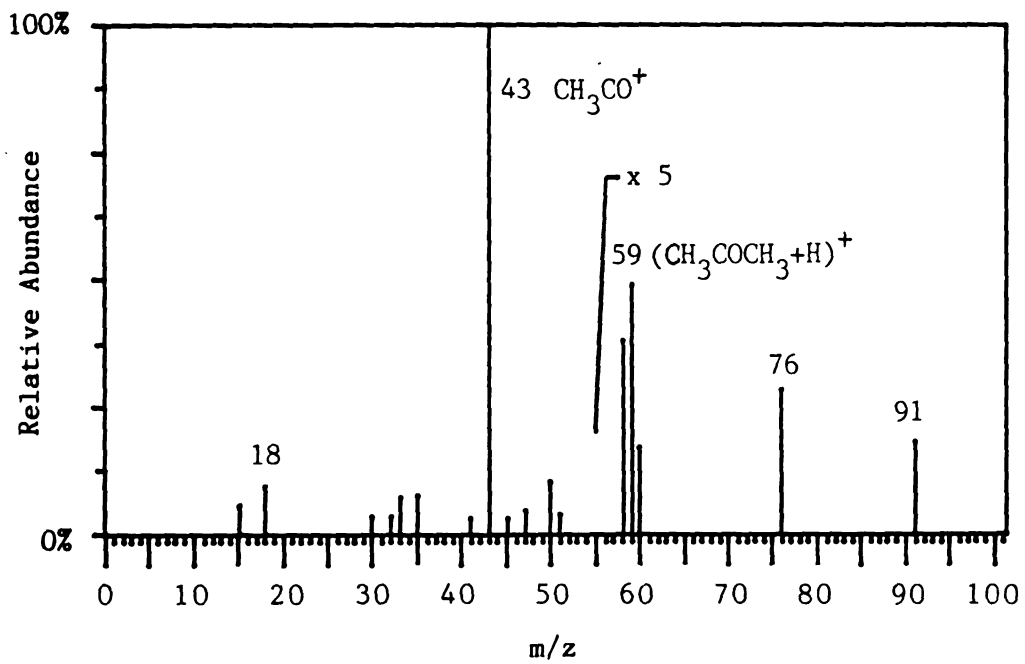

Figure 54. Product Spectrum of the Acetyl Ion Reacting with Methanol in the Central Quadrupole

reactions, and it is gratifying to this author that the TQMS technique with the addition of ion trapping is capable of producing data which are comparable and complementary to ICR data.

D. Applications of the Esterification Reaction to FAB

1. Esterification Reactions in the FAB Process

Protonated glycerol (1,2,3-trihydroxypropane) and acetic acid have been found to react in the central quadrupole in Chapter IV., probably by the esterification reaction discussed in this chapter. Glycerol and acids also react in solution to form esters. These facts prompted the author to investigate the interaction of glycerol and acetic acid in FAB to determine whether esterification products could be produced in the FAB process, and if so, whether the products resulted from a solution or a gas-phase reaction with the hope that this data might illuminate the mechanism of the FAB process.

If one mixes glacial acetic acid with glycerol 1 to 1 by volume and immediately performs a FAB/MS analysis of the solution, one obtains the spectrum shown in Figure 55. The peaks at m/z 75, 93, and 185 are typical of the FAB spectrum of pure glycerol, but the peaks at m/z 61, 117, 121, 135, and 153 are typical of the reactions between protonated glycerol and acetic acid that occur in the central quadrupole of the TQMS (see Chapter IV.) These data were obtained on a JEOL-HX-110 double focussing mass spectrometer which was focused to collect only those ions which were formed near the surface of the matrix, so it is very unlikely that the peaks shown in Figure 55 are due to processes occurring elsewhere in the instrument. Therefore, the presence of these peaks

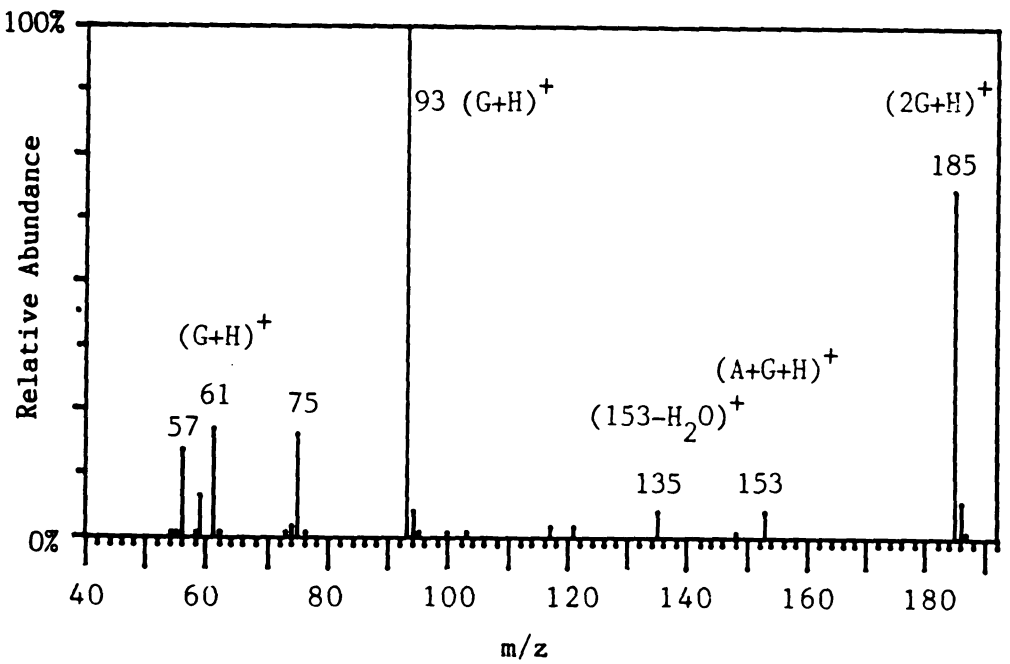

G=Glycerol

A=Acetic Acid

Figure 55. FAB Mass Spectrum of a Freshly Mixed Solution of Glycerol and Acetic Acid

suggests that they were produced by gas-phase ion/molecule reactions in the FAB process.

If one lets the same glycerol/acetic acid solution mentioned above sit covered for several days, one obtains an entirely different FAB spectrum which is shown in Figure 56. The typical glycerol peaks at m/z 93, and 185 are greatly diminished with respect to those in Figure 55. The major peaks in Figure 56 are m/z 57, 61, 75, 117, 135, 159, 177, 227, and 269. The peaks at m/z 159, 177, 227, and 269 are all new, and the peaks at m/z 121 and 153 from Figure 55 are missing. Clearly time has changed the nature of the solution. Since the most prominent peaks from the ion/molecule reactions of protonated glycerol, the protonated dimer of acetic acid (m/z 121), or the protonated glycerol adduct with acetic acid (m/z 153), are missing, it is unlikely that the peaks that do appear are the results of the same kind of ion/molecule reactions observed in the central quadrupole of the TQMS. Instead, it seems very likely that the peaks in Figure 56 are the result of slow solution reactions between glycerol and acetic acid. The peak at m/z 135, can therefore, be explained as the protonated monoester of glycerol, and the peak at m/z 177 can be explained as the protonated diester of glycerol. There is a minor peak at m/z 219 which may indicate the presence of the triester of glycerol. The peaks at m/z 117 and 159 can then be explained as the $(MH-H_2O)^+$ fragments of the protonated mono- and diesters. No $(MH-H_2O)^+$ peak is observed for the triester, but this may simply be due to the peak for the protonated triester being of such low abundance. The peak at m/z 227 is apparently due to the $(M+H)^+$ ion of the monoester reacting in the gas phase with the neutral glycerol to form the (monoester+glycerol)H^+ adduct ion. Likewise, the peak at m/z

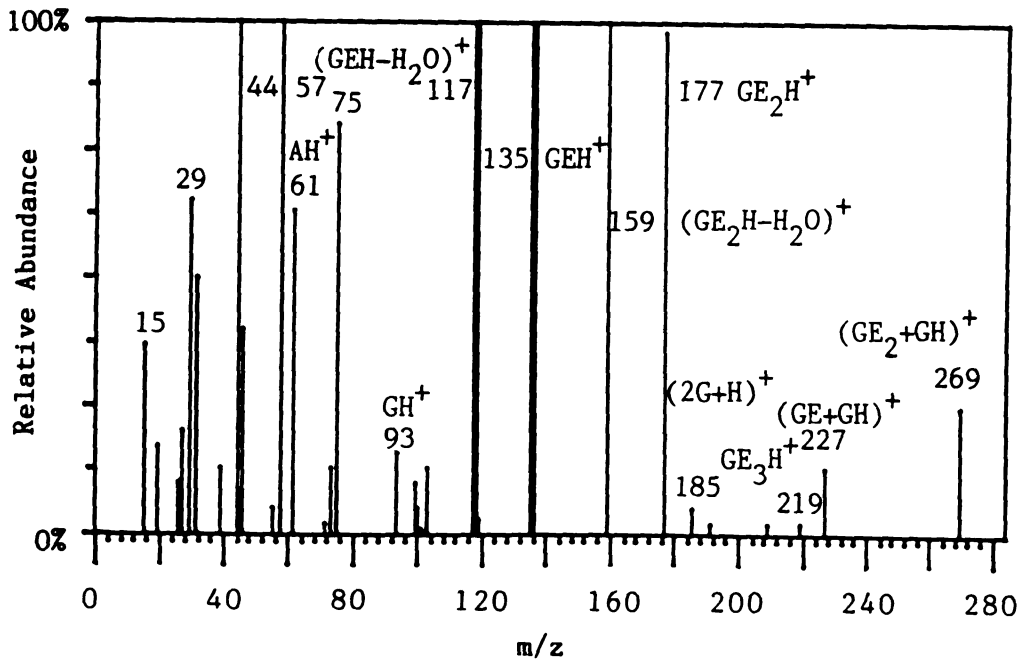

G=Glycerol

A=Acetic Acid

GE=Glycerolmonoester

GE_2=Glyceroldiester

GE_3=Glyceroltriester

Figure 56. FAB Mass Spectrum of a Week Old Solution of Glycerol and Acetic Acid

269 can be explained as the (diester+glycerol)H^+ adduct ion. The solution reaction with acetic acid has therefore transformed the simple mixture of the two reactants into a solution composed primarily of mono-, di-, and triglycerides of acetic acid.

These data indicate that both the gas-phase esterification and the solution esterification reactions can take place in the FAB process. This implies that any given peak in a FAB spectrum may originate directly from the solution or from gas-phase ion/molecule reactions subsequent to desorption of the analyte from the liquid matrix. Therefore, it is fair to say that the chemistry of the FAB process can be extremely complex if one uses a reactive matrix such as glycerol. Because of this rich chemistry one cannot account for all the ions observed in FAB with a simple sputtering model which is normally used to explain secondary ion spectra from solid matrices.

It has occurred to the author that the ion/molecule reactions observed in FAB between acetic acid and glycerol may be due to the vapor pressure of acetic acid causing a kind of CI-FAB (157) process to occur, in which the FAB beam causes desorption/ionization followed in tandem by ion/molecule reactions. In order to eliminate the complications caused by the possibility of acetic acid CI, the author chose to study the ion/molecule reactions of some nonvolatile alkali metal salts which are often present in the FAB process. The results of these investigations are presented in Chapter VI. of this dissertation.

2. Ion/Molecule Reactions of Protonated Multifunctional Acids with Methanol

It was documented earlier in this chapter that acetic acid will react in the gas phase with protonated molecules of small aliphatic alcohols, diols and triols to form protonated esters. These findings led the author to explore the reactions of more complex molecules containing the carboxylic acid functional group in order to determine whether the esterification reaction could be used to characterize this functional group in the types of molecules frequently studied by FAB.

FAB ionization is used for compounds of biochemical or pharmacological interest because these molecules often cannot be ionized intact by any other method. Therefore, the author chose the following two compounds, which are of biomedical interest, as test materials for the esterification reactions of multifunctional ions.

Table 9

Multifunctional Acid Test Compounds

1. alpha-methyl-4-[2-methyl propyl]-benzeneacetic acid
(also called ibuprofen)

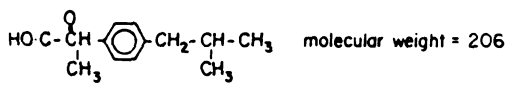

molecular weight = 206

2. alanyl-leucyl-glycine (abbreviation: ala-leu-gly)

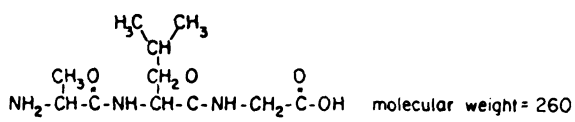

molecular weight = 260

Both ibuprofen and ala-leu-gly are moderately complicated molecules with carboxylic acid functionalities which are amenable to FAB analysis and within the mass range of the TQMS. Figure 57 shows the FAB/MS spectrum of ibuprofen. Most of the peaks are due to the matrix background, but the cluster of peaks at m/z 205, 206, and 207 represent the $(M-H)+$, $M+\cdot$, and $(M+H)^+$ ions formed from ibuprofen. Both direct

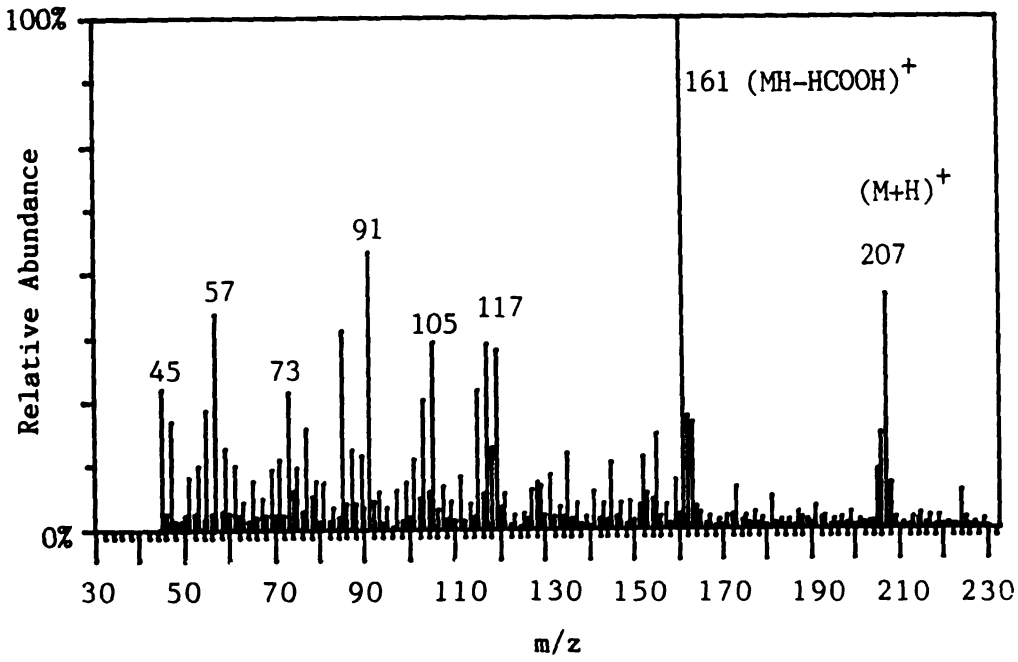

Figure 57. FAB Mass Spectrum of Ibuprofen (From a Nuprin Tablet)

analysis of daughter ions (DADI) on the Varian MAT CH5-DF instrument and argon CID on the TQMS confirmed that the m/z 161 peak present in Figure 58 is the only fragment observed. All three ions for ibuprofen at m/z 205, 206, and 207) produce the m/z 161 peak by unimolecular decomposition and by CID. Figure 58 shows the ion-trapped product spectrum of the protonated molecule of ibuprofen (m/z 207) after reaction with methanol in the central quadrupole. The base peak as expected is the m/z 161 daughter ion, and the peak at m/z 239 is the adduct ion of methanol and ibuprofen. There is, however, no peak at m/z 222, which would be the m/z value expected for the protonated methyl ester of ibuprofen.

Figure 59 shows the FAB/MS spectrum of ala-leu-gly. As in Figure 57, most of the peaks are from the matrix background (although this is a different matrix), but the peak for the protonated molecule of ala-leu-gly is clearly visible at m/z 260. Figure 60 shows an argon CID daughter scan of m/z 260. The daughter ions at m/z 215, 189, 185, 157, and 86 have been used by other researchers to characterize the sequence of amino acids in this compound (99). Figure 61 shows the ion-trapped product spectrum of the reaction of $(ala\text{-}leu\text{-}gly + H)^+$ with methanol in the central quadrupole. All of the CID peaks from Figure 60 are present in Figure 61, and there are an additional three peaks at m/z 245, 277, and 292. The peak at m/z 292 is the proton-bound adduct of ala-leu-gly and methanol but the other two peaks are rather mysterious. In any event, none of the new peaks are at m/z 275 which would correspond to the protonated peptide methyl ester. It would appear from the two examples of ibuprofen and ala-leu-gly that one cannot assume that ion/molecule reactions which occur with small monofunctional ions will

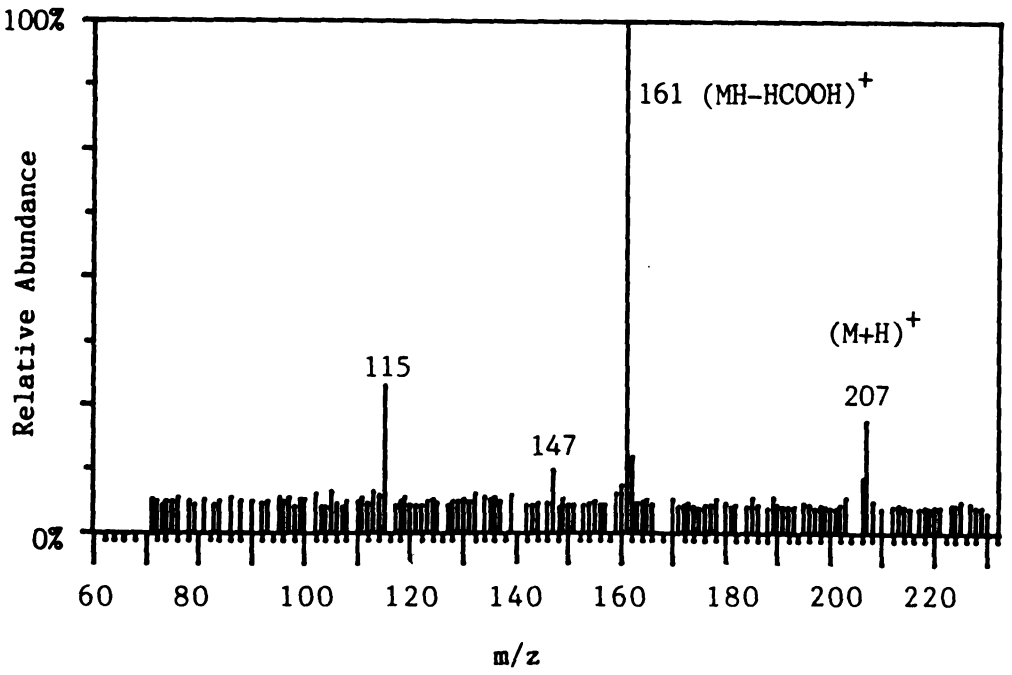

Figure 58. Protonated Ibuprofen Reacting with Methanol in the Central Quadrupole

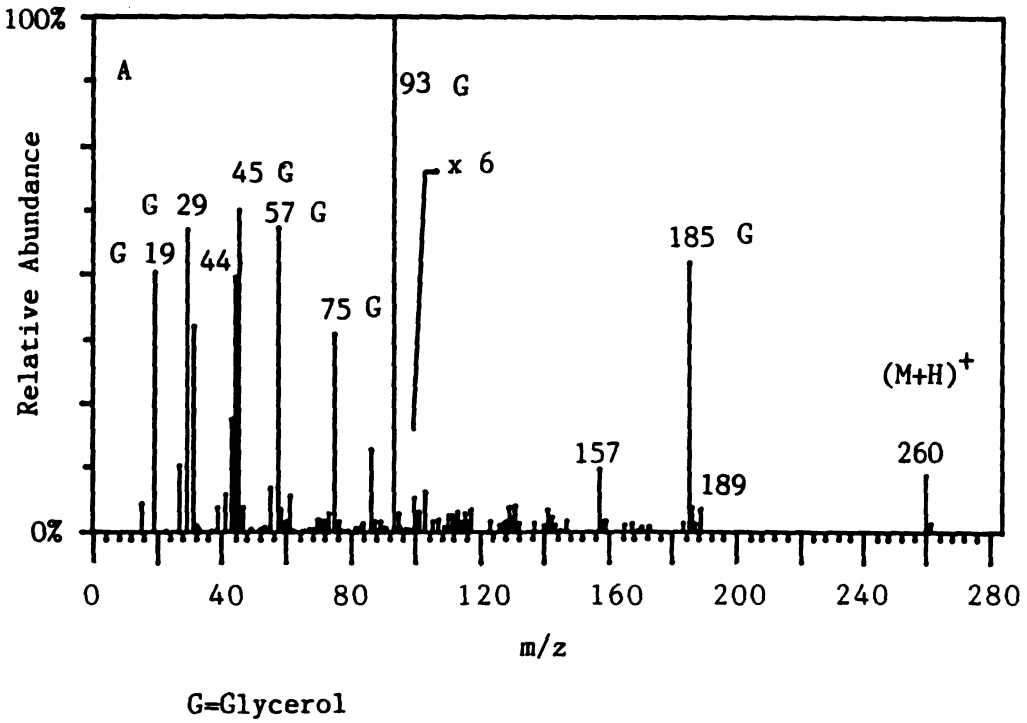

Figure 59. FAB Mass Spectrum of Ala-Leu-Gly

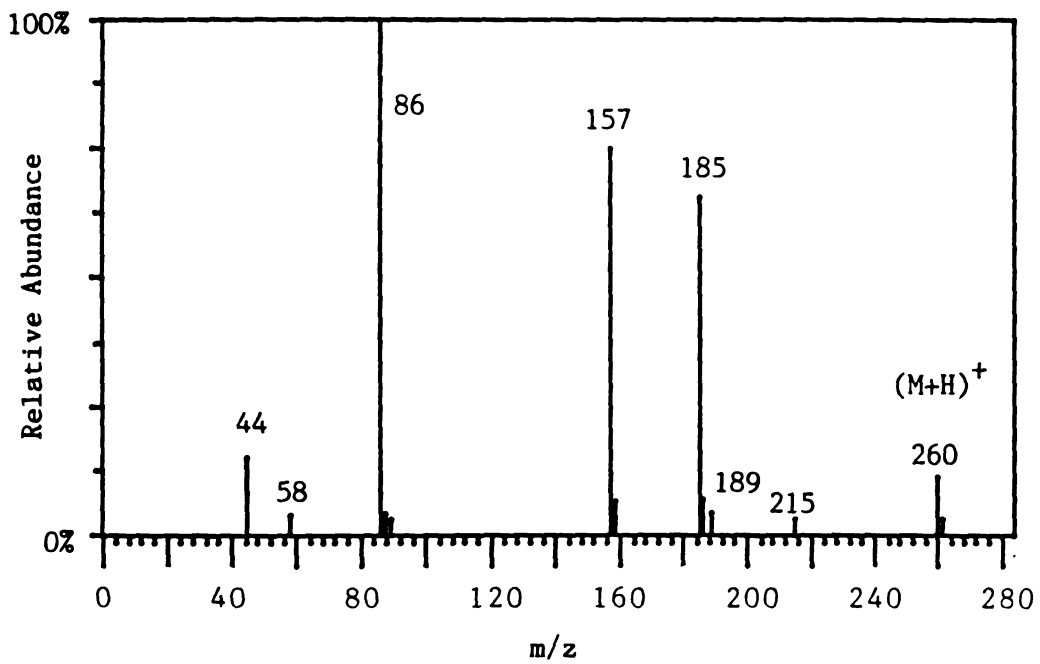

Figure 60. Argon CID Daughter Spectrum of Protonated Ala-Leu-Gly

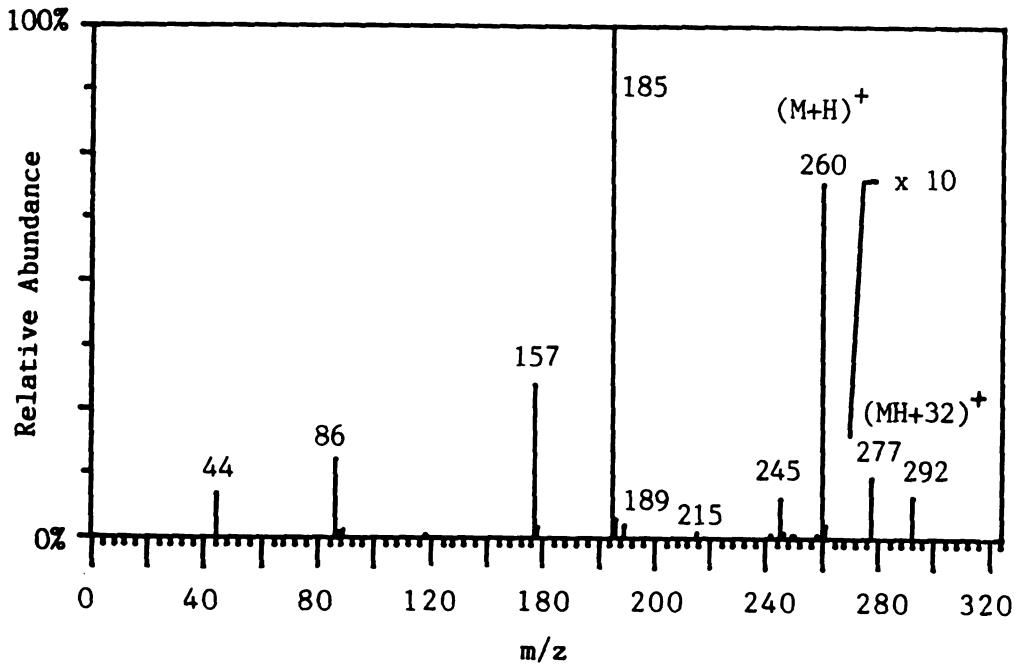

Figure 61. Protonated Ala-Leu-Gly Reacting with Methanol in the Central Quadrupole

also occur with larger polyfunctional ions, even if one could expect to use an analogous reaction in solution (as in the case of the esterification of peptides). The location of the proton on the ala-leu-gly and ibuprofen ions may in fact be critical to the success of this particular ion/molecule reaction. In order for the esterification reaction to take place, it may be necessary to protonate selectively the acid functional group.

Clearly, the esterification reaction cannot be used as general structural probe for the acid functional group on a complex molecule. However, the esterification reaction does appear to be specific for certain kinds of acids and alcohols. In fact, the greatest usefulness of this particular reaction is probably as selective reaction detector in GC-MS as shown in Chapter II., and in GC-MS/MS as shown in the following section of this chapter.

E. Analytical Applications of the Esterification Reaction

1. Application of Esterification to Mixture Analysis by MS/MS

Protonated methanol, ethanol, and propanol all react with acetic acid in the central quadrupole to form the respective protonated esters. Figure 62 demonstrates that if one ionizes a mixture of methanol, ethanol, and propanol by isobutane CI, one can then have the TQMS perform a linked scan of quadrupoles one and three to produce a neutral gain spectrum (with ion trapping and a fixed neutral gain of 42 amu) to detect those parent ions in the mixture which produce protonated esters when they react with acetic acid in the central quadrupole. Figure 62 shows three peaks, one for each of the three protonated alcohol

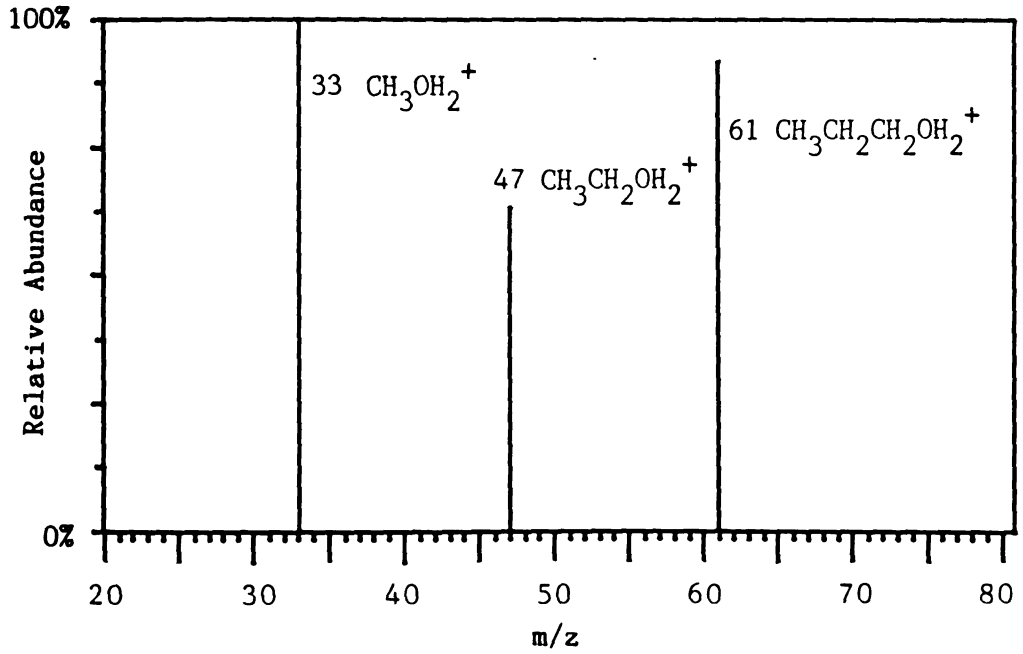

Figure 62. Detection of a Mixture of Alcohols by Means of the Esterification Reaction and a Neutral Gain Scan With a Fixed Neutral Gain of 42 amu

molecules in the mixture. None of the numerous other ions produced by the CI process, including the reagent ions of isobutane and the fragment ions of the three compounds, were detected because the esterification reaction in acetic acid is specific for protonated alcohols. In this way one could use ion/molecule reactions in the TQMS as a selective method for mixture analysis.

2. The Esterification Reaction as Mixture Analysis Technique in GC-MS/MS

The multiple reaction monitoring program, R-MRM, for doing ion/molecule reactions with ion trapping in the central quadrupole on the GC time scale, has already been discussed in Chapter IV. of this dissertation. R-MRM allows the user to monitor the products of several ion-trapped ion/molecule reactions that may be occurring in the central quadrupole of the TQMS. The computer instructs the TQMS to trap a particular parent ion with a reactive collision gas for a predetermined period of time in the central quadrupole, then detects a particular product ion which is pulsed out from the reaction chamber. The computer then instructs the TQMS to select a new parent/product pair and executes the trap and pulse method again. Because each trap and pulse cycle takes less than 100 msec, eight ion/molecule reactions can be monitored in a single GC run, producing eight separate GC-MS/MS ion current profiles.

R-MRM was used to demonstrate the feasibility of employing ion/molecule reactions for the purpose of performing GC-MS/MS mixture analysis on the TQMS. The two reactions chosen for illustrating the potential of the R-MRM approach were the acetic acid proton-bound adduct

formation reaction, and the acetic acid esterification reaction. The idea behind this selection was that the esterification reaction should be the more selective reaction of the two for alcohols, since presumably acetic acid could form proton-bound adducts with virtually any protonated parent ion, but only the proton-bound adducts with alcohols would decompose to protonated esters.

The programmed test mixture (PTM) discussed in detail in Chapter II. of this dissertation was used as the source of compounds for isobutane CI (for protonation) followed by reaction with acetic acid in the central quadrupole (for proton-bound adduct formation and protonated ester formation). The parent ions chosen for this R-MRM study were the protonated molecules of 2,3-butanediol (m/z 91), 2,6-dimethylaniline (m/z 122), 2,6-dimethylphenol (m/z 123), nonanal (m/z 143) and 2-ethylhexanoic acid (m/z 145). Both the $(MH+60)^+$ product ions (proton-bound adducts) and the $(MH+42)^+$ product ions (protonated esters) were monitored for each parent ion.

Figure 63 shows the GC-MS/MS profiles for each of the ten ion/molecule reactions in the central quadrupole. The data in Figure 63 were collected in two separate runs because all ten profiles could not be collected simultaneously. Figure 63 shows clearly discernible peaks well above noise level for the acetic acid adduct reaction of 2,3-butanediol, 2,6-dimethylaniline, and 2,6-dimethylphenol. It also shows a clearly discernible peak for the esterification reaction of 2,3-butanediol, but not for any other compound. For this set of parent ions, representing five different polar functional groups, the esterification reaction appears to be selective for the single aliphatic alcohol in the group.

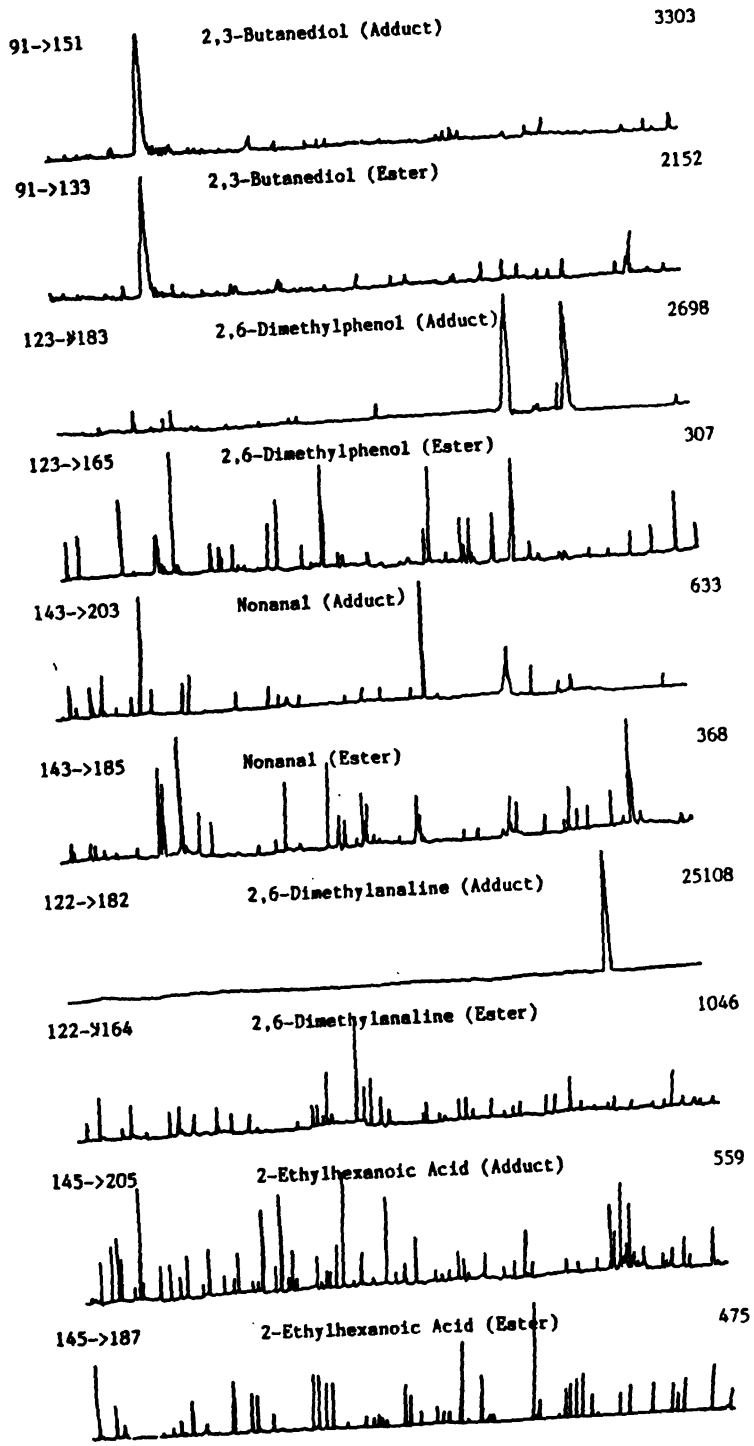

Figure 63. R-MRM GC-MS/MS Profiles of Selected PTM Compounds Using Acetic Acid as a Collision Gas

As an analytical method, the esterification reaction using ion-trapping in the central quadrupole is capable of detecting selectively, 1 ug of 2,3 butanediol by GC-MS/MS with a signal-to-noise ratio of approximately seven. By no means does this demonstrate exceptional sensitivity, but using the same conditions without ion-trapping produces no discernible peak above noise level for any of the compounds. Clearly, ion-trapping is essential for producing any kind of useful GC-MS/MS analyses by means of ion/molecule reactions in the central quadrupole of the TQMS.

This section demonstrates that it is possible to detect analytically useful quantities of compounds from mixtures in either a selective or non-selective fashion by means of GC combined with well chosen ion/molecule reactions in the TQMS. This study shows that given a suitable ion/molecule reaction or set of ion/molecule reactions and optimized conditions of pressure, temperature, and tuning of the ion-optics, an assay based on the ion-trapped GC-MS/MS method could potentially be used to detect trace quantities of target compounds in complex mixtures.

F. Summary

The gas-phase ion/molecule reactions of alcohols and acids have served in this chapter as model reactions for studying the behavior of ion/molecule processes in FAB and in the central quadrupole of the TQMS. There are three major conclusions to be drawn from this chapter. First, ion/molecule reactions and CID in the TQMS have confirmed the protonated ester structure of the products from and the mechanism for the reactions between acetic acid and protonated alcohols. Second, FAB can produce

ions that are the product of both solution and gas-phase reactions. Third, ion/molecule reactions in the center quadrupole of the TQMS can be used for selective detection of target compounds in mixtures through an ion-trapped multiple reaction monitoring GC-MS/MS approach.

CHAPTER VI.

ION/MOLECULE REACTIONS OF FAB-GENERATED GLYCEROL-ALKALI METAL ADDUCT IONS WITH METHANOL AND ACETIC ACID

A. Introduction

It has been established in this dissertation that it is possible to perform ion/molecule reactions with ion trapping in the central quadrupole of the TQMS, and that the results of this technique are in agreement with those of other techniques for observing ion/molecule reactions. One of the methods of producing ions for these ion/molecule reactions is FAB, which commonly produces protonated ions $(M+H)^+$ of both the liquid matrix and the analyte dissolved in that matrix. When soluble metal salts are added to the liquid matrix, many researchers observe metal cationized species of the form $(matrix+metal)^+$ or $(analyte+metal)^+$. Alkali metal salts, in particular, are widely used as additives in FAB, and a recent publication (123) describes in detail the effects that the alkali metal salts have on the FAB process. Since the $(M+metal)^+$ ions generated by FAB are a prominent feature of FAB spectra, it is possible to determine whether $(M+metal)^+$ ions undergo ion/molecule reactions that are similar to the reactions of $(M+H)^+$ ions. Investigations of this kind can shed light on the nature of the bonds formed in ion/molecule reactions, and since ion/molecule reactions have been implicated in the FAB process (123), investigations of this kind may also help to explain the FAB process itself.

Using the central quadrupole of the TQMS is an ideal method for studying ion/molecule reactions of ions generated by FAB, because the ion/molecule reactions and the FAB process are located in two physically

separate chambers and cannot interfere with each other. The reactions described in this chapter are of the (glycerol+metal)$^+$ ions (where metal = H, Li, Na, K, Rb, or Cs) with acetic acid.

The author fully expected the presence of alkali metals to interfere with the reactions that are typical of the protonated ions since bonds to alkali metal ions have much less covalent character than bonds to the proton (124). One could predict that either the metals would inhibit the reactions, or that the metals would act more subtly to change the distribution of the products which were formed. In fact, both predictions are true depending on the metal, and one can therefore observe periodic trends in the ion/molecule products that are produced.

B. Experimental

1. FAB Conditions in the Ion Source

As described earlier in this dissertation, the FAB ion source is a combination of a commercially available capillaritron probe FAB gun and a locally-manufactured sample probe with an electrically isolated tip. The voltage applied to the capillaritron was 9 kV and the distance from the gun to the sample was approximately 10 cm. The ion-repeller voltage applied to the sample tip was 14.7 V for the acetic acid reaction and 15.7 V for the methanol reaction (see below, Experimental, Section b). The FAB gas used for this experiment was Xe, and its pressure in the ion source chamber was measured to be $8X10^{-5}$ torr. The FAB source was operated at room temperature. The glycerol used as the liquid matrix and sample was vacuum distilled. The alkali metals were introduced as a glycerol solution of LiCl, NaCl, KCl, RbCl, or CsI.

2. Conditions for Ion/Molecule Reactions in the Central Quadrupole

As described earlier in this dissertation, the reactive collision gases were regulated by a Granville-Phillips pressure controller and were introduced into the central quadrupole through a stainless steel vacuum line. Both the methanol and the acetic acid were analytical grade reagents and were used without further purification. The pressure of methanol in the central quadrupole collision chamber was $8.5X10^{-4}$ torr and the pressure of the acetic acid was $1X10^{-3}$ torr.

The quadrupole offset voltage for the acetic acid reaction was 10.7 V and 12.7 V for the methanol reaction. Therefore, the $(glycerol+metal)^+$ parent ions entered the central quadrupole with 4 eV axial kinetic energy in the acetic acid reaction and with 3 eV in the methanol reaction. Parent ions entering the central quadrupole were trapped inside it for 50 msec by means of dc voltages on an entrance lens and on an extraction lens. For ion-trapping, the entrance lens was set at 15.8 V and the exit lens at 100 V. Because of the ion-trapping, the initial axial kinetic energy of the parent ions is dissipated through multiple collisions with neutral molecules. Product ions were detected by the trap and pulse method described earlier in this dissertation. The electron multiplier is a continuous dynode type and was operated with 1.8 kV applied across it.

C. Results and Discussion

1. FAB of the Alkali Metal Salts

The FAB/MS spectrum of the mixture of the Li, Na, K, Rb, and Cs salts in glycerol is shown in Figure 64. Figure 64 illustrates that one can observe all of the (glycerol+metal)$^+$ ions from the mixture in a single spectrum. Since all of the ions needed for this study were produced from a single solution, the results were obtained rapidly (without withdrawing the sample probe) and thus both the FAB conditions and the central quadrupole conditions remained constant for each of the different (glycerol+metal)$^+$ parent ions.

2. Reactions of (glycerol+H)$^+$ and (glycerol+metal)$^+$ Ions with Acetic Acid

Table 10 shows that the major ionic products in the reactions of the (glycerol+metal)$^+$ and (glycerol+H)$^+$ parent ions with acetic acid. The data in Table 10 were collected by the ion-trapping method described in Chapter IV. Protonated glycerol reacts with acetic acid to form three ion/molecule reaction products including a protonated ester. Glycerol cationized by the alkali metals ions does not react with acetic acid to form any ion/molecule reaction products. The reason for this is that proton affinities of organic molecules rival covalent bond energies, whereas metal ion affinities do not. The alkali metal ions simply do not behave like the proton in any regard due to their weak interactions with organic molecules.

All of the cationized glycerol ions transfer a cation to acetic acid, and also produce the acetyl ion due to dissociation of the

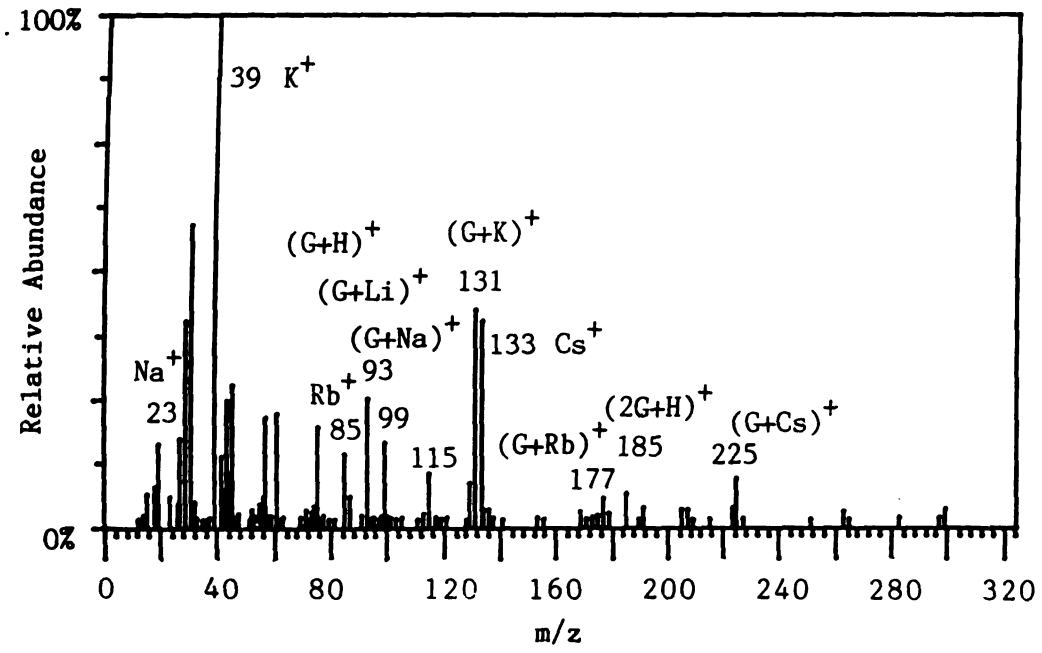

Figure 64. FAB Mass Spectrum of Li, Na, K, Rb, and Cs Salts Dissolved in Glycerol

Table 10

Reaction Products of the (Glycerol+Metal)$^+$ Ions with Acetic Acid

Parent Ion	Product Ions						
	Collision-Induced Dissociation	Dissociative Charge Transfer	Charge Transfer	Adduct of Acetic Acid	Hydration of Glycerol	Protonated Ester Formation (Loss of Water)	Loss of 2 Waters
GH^+	—	$Acetyl^+$	AH^+	$(GH+A)^+$	$(G+H_2O)^+$	$(GH+A-H_2O)^+$	$(GH+A-2H_2O)^+$
GLi^+	—	$Acetyl^+$	ALi^+	$(GLi+A)^+$	—	—	—
GNa^+	—	$Acetyl^+$	ANa^+	$(GNa+A)^+$	—	—	—
GK^+	K^+	$Acetyl^+$	AK^+	—	—	—	—
GRb^+	Rb^+	$Acetyl^+$	ARb^+	—	—	—	—
GCs^+	Cs^+	$Acetyl^+$	ACs^+	—	—	—	—

G = Glycerol
A = Acetic Acid

cationized acetic acid. The cation-bound adduct of glycerol and acetic acid was detected when the cation was H^+, Li^+, or Na^+, but not when the cation was K^+, Rb^+, or Cs^+. In fact, the K^+, Rb^+, and Cs^+ ions were detected as CID products. The $(GK+A)^+$, $(GRb+A)^+$, and $(GCs+A)^+$ ions apparently have very weak bonds and decompose so readily by CID that they are not observed in the spectrum. Presumably, if the collision energy were raised, the H^+, Li^+, and Na^+ ions would also be observed as CID products, but at the low collision energies used the $(GH+A)^+$, $(GLi+A)^+$, and $(GNa+A)^+$ ions remained intact.

3. Conclusions about FAB and Ion/Molecule Reactions

The implications of this study to organic ion/molecule reactions by FAB in the TQMS are fairly obvious. First, one cannot expect cationized species in FAB to undergo typical organic ion/molecule reactions. Second, the products that do form depend on the identity of the metal cation and the energy of the system. These two results mean that studying the cationized species present in FAB spectra will not tend to increase our understanding of the organic ion/molecule chemistry of the analyte with the reactive gas. Rather, the results are more likely to increase our understanding of the interactions of the metal cations with the reactive collision gas. The fact that ion/molecule reactions of species containing a metal are dominated by the metal is quite analogous to the organometallic ion/molecule chemistry results that have been investigated by ICR spectrometry for the last decade (83).

The implication of this study for the mechanism of FAB is more interesting. One can observe the following adduct ions both in FAB

(123) and in the TQMS collision chamber: $(G+Y+A)^+$ where G=glycerol; Y=H^+, Li^+, or Na^+; and A=analyte. One cannot observe the following adduct ion in either the FAB (123) or the TQMS collision chamber: $(G+N+A)^+$ where G=glycerol; N=K^+, Rb^+, or Cs^+; and A=analyte. These similarities exist despite the fact that whereas the analyte is in the gas phase (and is neutral) in the TQMS collision chamber, the analyte is in solution (and possibly pre-charged) in FAB.

A new model of the FAB process called the gas-phase collision model (GCM) (123) explains why the TQMS and FAB results are the same despite the apparent differences in phase and in the charge of the analyte. The GCM model states that neutral particles are desorbed by FAB in much greater concentration than are ions, and that the result of this process is a "hot gas" formed in the crater generated by the impact of the FAB beam. In this hot gas, numerous collisions between ions and neutrals occur, yielding gas-phase ion/molecule reactions between the analyte and the matrix. The GCM model also states that if alkali metal salts create preformed ions in the matrix, these alkali metal ions will be rapidly transferred through many ion/molecule reactions to the molecules and adducts with the greatest affinity for them, or they will be released as free atomic ions into the vacuum if they form only weak bonds with neutral molecules. The similarity of the ion/molecule results observed in the collision chamber of the TQMS to the results of other research groups investigating FAB (123) substantiates the GCM assertion that ion/molecule reactions do play an important role in the FAB process and that added alkali metal ions necessarily dominate those ion/molecule reactions.

CHAPTER VII.

ION/MOLECULE REACTIONS OF ARYL CATIONS IN THE TQMS

A. Introduction

The ion/molecule reactions of the benzene radical cation and its fragment ions with benzene and with other molecules have been probably the most intensively studied group of organic ion/molecule reactions. A wide variety of techniques have been used in studying these reactions including ion cyclotron resonance (ICR)(125), trapped-ion mass spectrometry (TI/MS) (126), chemical ionization mass spectrometry (CI/MS) (127), rf-plasma discharge mass spectrometry (RPD/MS) (128), and gas-phase radiolysis (GPR) (129). The operating pressures for ion/molecule studies in ICR and TI/MS are in the range from 10^{-7} to 10^{-5} torr, and all three techniques permit ions to be stored for several milliseconds to allow ion/molecule reactions to occur by means of multiple collisions between neutrals and trapped ions.

In the two ICR techniques, increasing the pressure of the reactive neutral gas degrades mass resolution since ionization and mass analysis occur in a single chamber. However, these techniques can trap ions under very low pressure conditions for hundreds of milliseconds. In ultra-low pressure ICR at cryogenic temperatures ions can be trapped for hours or even days. In the ICR techniques a combination of magnetic and dc fields fields trap ions with very little kinetic energy in cycloidal orbits, and it is possible to select parent ions by double resonance techniques. In addition, tandem Dempster-ICR (125) and tandem quadrupole-ICR (130) have made true tandem mass spectrometry possible on ICR instruments.

The TI/MS technique traps ions in the space charge field of an electron beam and since this technique relies on a conventional magnetic mass spectrometer for collecting data, the mass resolution is independent of pressure in the ion source. It is not practical, however, to trap ions for longer than 2 milliseconds with TI/MS. Since TI/MS is a pulsed ion technique on a magnetic instrument, the advent of time-resolved ion-momentum spectrometry (TRIMS) developed at the MSU-NIH-MSF by Stults et al. (31) has created TI/MS/MS.

Ion/molecule reactions in CI/MS/MS, RPD/MS, and GPR occur at pressures in the range from 0.1 - 760 torr. CI is used with both magnetic sector instruments and with quadrupole instruments (as in this study). The rf-plasma instruments use quadrupole MS exclusively, and the GPR experiments do not use mass spectrometers at all. None of these techniques traps ions, but rely instead on the high neutral gas pressure to provide the number of collisions necessary for ion/molecule reactions to occur. The major drawback of these three techniques is that selecting a parent ion for a particular reaction is often difficult or impossible. This lack of parent ion selection often leads to complex mixtures of products that must be separated or distinguished in some fashion. The CI and RPD techniques rely on MS and CID MS/MS for distinguishing and characterizing products, and GPR relies on radioactive labeling and gas chromatography for separating the neutralized products. The major advantage of these three techniques is that they provide collisional stabilization of product ions with excess energy which would ordinarily decompose to fragments in ICR, FT-ICR, and TI/MS. Therefore, these high pressure techniques often can detect

unstable intermediate products of ion/molecule reactions, a feat which helps enormously in determining reaction mechanisms.

The ion/molecule reactions that occur in pure benzene are quite numerous and have been investigated by several research groups for over 15 years. A complete listing of all the ion/molecule reactions in benzene as investigated by ICR is presented by R. D. Smith et. al. (125). The techniques used to study these reactions produce results which differ markedly from one another. Table 11 demonstrates this lack of agreement between three techniques in the reaction of the phenyl cation with benzene.

The disparity of the results shown in Table 11 has led several authors to suggest that the $C_6H_5^+$ and $C_6H_6^+$ ions may be present in the gas phase in a variety of vibrational states and as a combination of isomers. As a result of these suggestions there have been several studies of the gas-phase structures of the $C_6H_5^+$ and $C_6H_6^{+\cdot}$ ions and careful investigation of their isomers. These studies suggest strongly that the $C_6H_5^+$ ions formed in all of the MS techniques rapidly rearrange to form the phenyl cation (132). It is possible, however, to generate in sequential ion/molecule reactions in acetylene a linear $C_6H_5^+$ isomer which undergoes different ion/molecule reactions from the phenyl cation (133), and which fragments differently under CI conditions.

All of the positions on the phenyl cation ring are equivalent due to extremely rapid 1,2 hydrogen transfers around the ring. $C_6H_5^+$ ions produced from a variety of compounds with a variety of ionization techniques exhibit identical CID spectra and undergo identical ion/molecule reactions. The $C_6H_6^{+\cdot}$ ion isomers such as the molecular ions of fulvene and benzvalene, however, undergo very different sorts of

Table 11

Reaction of the Phenyl Cation with Benzene

Technique	Reactants	Products	Branching Ratio
ICR (125)	$C_6H_5^+ + C_6H_6$	---> $C_{12}H_{11}^+$	<0.02
		---> $C_{12}H_{10}^+ + H$	<0.02
		---> $C_{10}H_{10}^+ + C_2H$	0.25
		---> $C_{10}H_9^+ + C_2H_2$	0.4
		---> $C_{10}H_8^+ + C_2H_3$	0.25
		---> $C_9H_7^+ + C_3H_4$	0.1
		---> $C_6H_6^+ + C_6H_5$	<0.1
TI/MS (126)	$C_6H_5^+ + C_6H_6$	---> $C_{12}H_{11}^+$	0.184
		---> $C_{12}H_{10}^+ + H$	0.114
		---> $C_{12}H_9^+ + H_2$	0.490
		---> $C_{10}H_9^+ + C_2H_2$	0.05
		---> $C_{10}H_8^+ + C_2H_3$	0.03
		---> $C_9H_7^+ + C_3H_4$	0.06
RPD/MS (128)	$C_6H_5^+ + C_6H_6$	---> $C_{12}H_{11}^+$	
		---> $C_{10}H_9^+ + C_2H_2$	

reactions from benzene. In fact, some very interesting gas-phase analogs to the condensed-phase Diels-Alder cyclo-addition reactions have been discovered that involve fulvene as a reactant (131). Therefore, it appears that the differences in the branching ratios observed for the reactions of the phenyl cation are due to differences in the techniques used to observe the reactions not due to the structural characteristics of the phenyl cation.

It is remarkable that despite all of this research, there is no consensus on the structures of most of the product ions from the ion/molecule reactions in benzene. The only product ion whose structure has been investigated extensively is the $C_{12}H_{11}^+$ ion. Some studies claim that it has a ring-opened structure (133), and others support a protonated biphenyl structure (127). The latter structure currently has more support due to CID studies. In fact, the CI/MS/MS method has received the endorsement of several research groups as the ideal method of determining product ion structures since the CID spectrum provides a "fingerprint" of the product ion that can be compared with the CID spectra of ions formed from authentic reference compounds. This CI/MS/MS technique has already been demonstrated in Chapter V. of this dissertation to be fruitful for investigating the structures of ionic products formed in the TQMS, and it will be used in this chapter for the purpose of trying to unravel some of the product ion structures from the ion/molecule reaction in benzene.

The phenyl cation has been reacted with a number of molecules besides benzene, including methanol (48), NO_2 (89), alkyl halides (47), H_2O and D_2O (57). Except for ammonia and water, none of these reagents has ever been used in the central quadrupole of the TQMS as a reactive

collision gas, and the methanol reaction with the phenyl cation has never been investigated by TQMS. Therefore, the author was interested in investigating as many of these reactions as possible in the TQMS due to the novelty of the technique and the unusual nature of the reactions.

The reaction of the phenyl cation with methanol produces a wide variety of hydrocarbon and oxygenated products at very high pressure in the GPR technique including phenol, anisole, and toluene. At the outset of this research, it was not certain if any of these products would be formed at lower pressures in the TQMS. This reaction does have analogs in solution chemistry, but the extreme difficulty of producing phenyl cations in solution makes the comparison to solution chemistry difficult in this case, unlike in the case of the reactions of acids and alcohols in the preceding chapter. Nevertheless, the reaction of the phenyl cation and methanol is intrinsically interesting, due to its unusual nature and due to possible analytical applications for selective mass spectrometric detection of aromatic compounds.

B. Experimental

1. CI Conditions

Benzene CI was studied over a range of pressures from $1X10^{-5}$ to $4X10^{-4}$ torr benzene (measured at the throat of the ion source turbomolecular pump). The benzene pressure in the CI volume itself was of course much higher, in the range from 0.1 to 1.0 torr. The benzene pressure was set at $6X10^{-5}$ torr for investigating the structures of ion/molecule reaction products by benzene CI. In the CI experiments concerning the reactions of benzene and methanol, the partial pressure of benzene was $3X10^{-5}$ torr and the partial pressure of methanol was

$2X10^{-5}$ torr. In the CI experiments concerning the reactions of benzene and ammonia, the partial pressure of benzene was $1X10^{-5}$ torr and the partial pressure of ammonia was $1X10^{-5}$ torr. In all of the experiments in this chapter the temperature of the CI volume was 75°C.

2. EI Conditions

For the purpose of comparison, CID spectra were obtained from the molecular ions of several aromatic compounds that were likely to be products of the ion/molecule reactions discussed in this chapter. Naphthalene, anthracene, biphenyl, catechol, aniline, phenol, o-,m-, and p-xylenes, o-,m-, and p-dichlorobenzenes, and pyridine were all analyzed by EI with samples pressures in the EI volume of $5X10^{-5}$ torr. Naphthalene, anthracene, and biphenyl were all introduced as pure solids by direct probe. The other compounds were sufficiently volatile to be leaked into the ion source through the liquids inlet using a needle valve.

3. FAB Conditions

The FAB spectrum of arachidonic acid contains ions of interest to this study. One microliter of neat arachidonic acid was pipetted onto the FAB probe and inserted without addition of a liquid matrix since arachidonic acid is a viscous liquid itself. Xenon was used as the FAB gas. The xenon pressure in the ion source region was $5X10^{-5}$ torr, and the capillaritron voltage was 9.5 kV. The ion source was at room temperature and the probe tip was connected to the instrument ground potential.

4. Conditions in the Central Quadrupole

All of the argon CID experiments were performed at an argon pressure of $4X10^{-3}$ torr, which is higher than normal for the TQMS, and represents multiple collision conditions. The elevated pressure of collision gas was made necessary because of the low abundance of fragment ion from the aromatic ions studied in this chapter. In all of the CID experiments reported in this chapter, the axial kinetic energy of parent ions entering the central quadrupole was in the range from 4-5 eV.

Ion/molecule reactions in the central quadrupole were accomplished using $4X10^{-3}$ torr methanol, $2X10^{-3}$ torr ammonia $2X10^{-3}$ torr methane, or $2X10^{-3}$ torr benzene. For these ion/molecule reactions the axial kinetic energies of parent ions entering the central quadrupole were in the range from 0-1 eV. In those product spectra that were acquired by the trap and pulse method, all ions were trapped for approximately 100 msec. The temperature of the central quadrupole region was held constant at 50°C in all CID and ion/molecule reaction experiments, except in those circumstances in which FAB ionization was employed. In the FAB experiments, the entire instrument was allowed to cool to room temperature.

C. Results and Discussion

1. Reactions of Aryl Cations with Benzene

Except for the molecular ion, the most abundant ion in the EI and CI spectra of benzene is the phenyl cation, $C_6H_5^+$, at m/z 77. The phenyl cation produced by EI of benzene reacts with neutral benzene in

the collision chamber of the TQMS yielding the product spectrum shown in Figure 65. The distribution of product ions generated by this reaction appears to be similar but not identical to those produced by other ion/molecule techniques (compare Figure 65 with Table 11). The greatest similarity is to the products detected by TI/MS. The structures of the m/z 78 and 79 ions are no doubt those of benzene and protonated benzene, but the structures of the ions at higher m/z values are in considerable doubt, and will be discussed at length later in this chapter.

The next most abundant ion in the EI spectrum of benzene is the $C_4H_3^+$ ion at m/z 51. The reaction of this ion with benzene in the central quadrupole yields the product spectrum in Figure 66. Again, the benzene and protonated benzene ions are prominent, but the sole high mass product ions is at m/z 128, corresponding to the $C_{10}H_8^+$ ion. This reaction has also been observed in TI/MS (126). None of the other ions in the EI spectrum of benzene were sufficiently abundant to be used successfully as parent ions.

The MS/MS data in Figures 65 and 66 substantiate some of the aryl cation reactions surmised from the results of other techniques. Figure 67 shows the reaction products in benzene as investigated by CI/MS in the TQMS. The pressure is higher in the CI volume than in the central quadrupole and there is no selection of parent ions, but the CI spectrum shows many of the same features that are observed in Figures 65 and 66. There are some prominent new peaks as well, including m/z 89 ($C_7H_5^+$) and m/z 91 ($C_7C_7^+$) which are not observed either in the central quadrupole or in other methods that have been published in the literature. The m/z 91 peak, however, is produced by the reaction of the phenyl cation with methane in the central quadrupole as in shown in Figure 68. Also, m/z

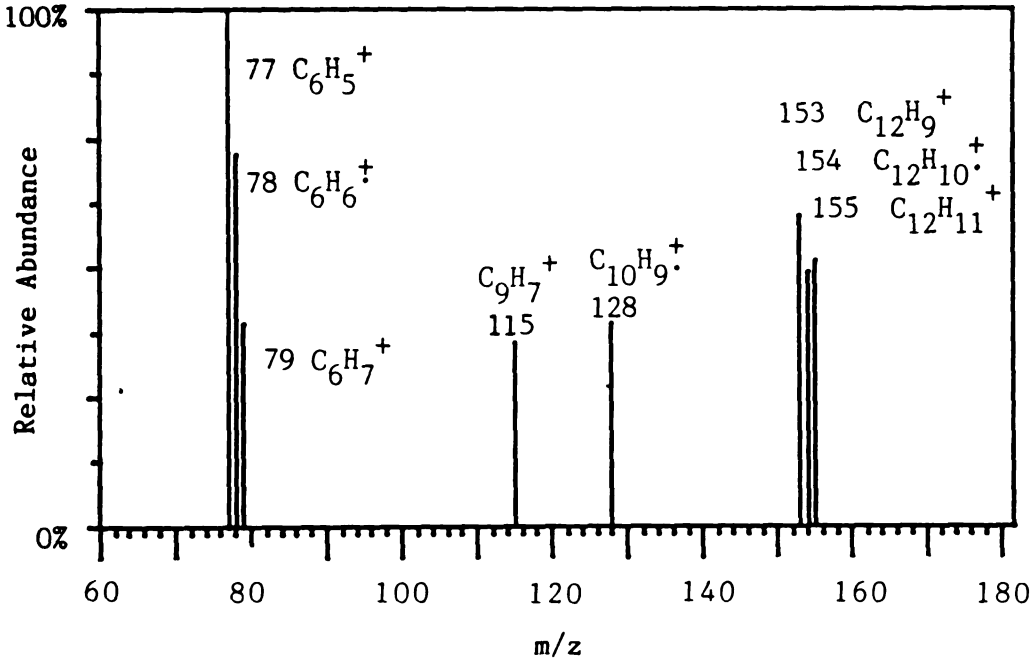

Figure 65. The Product Spectrum of the Phenyl Cation Reacting with Benzene in the Central Quadrupole

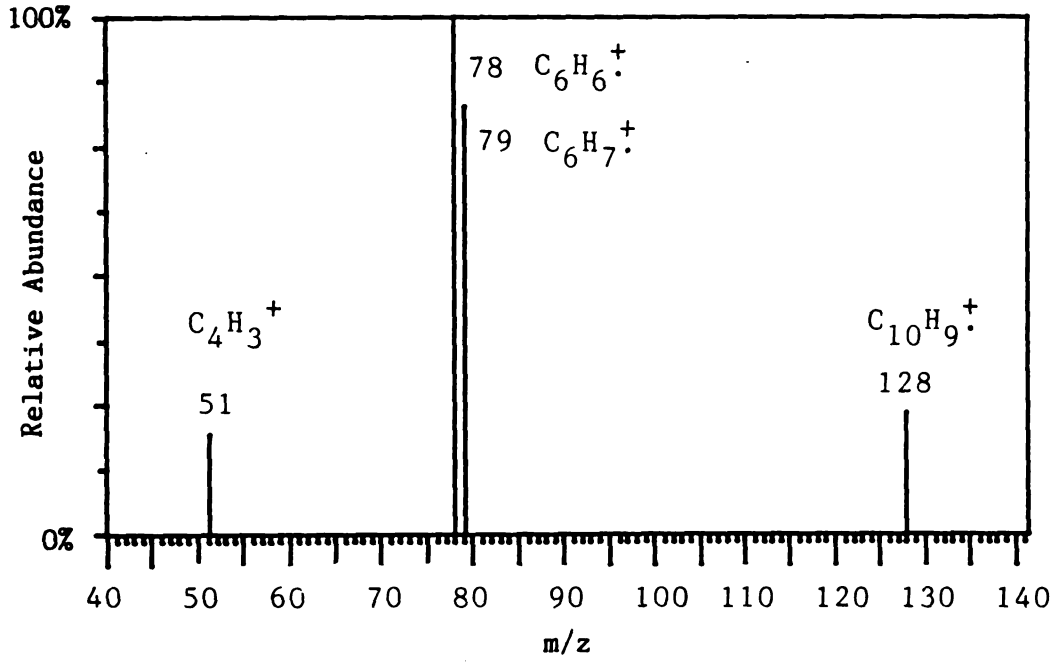

Figure 66. The Product Spectrum of the $C_4H_3^+$ Ion Reacting with Benzene in the Central Quadrupole

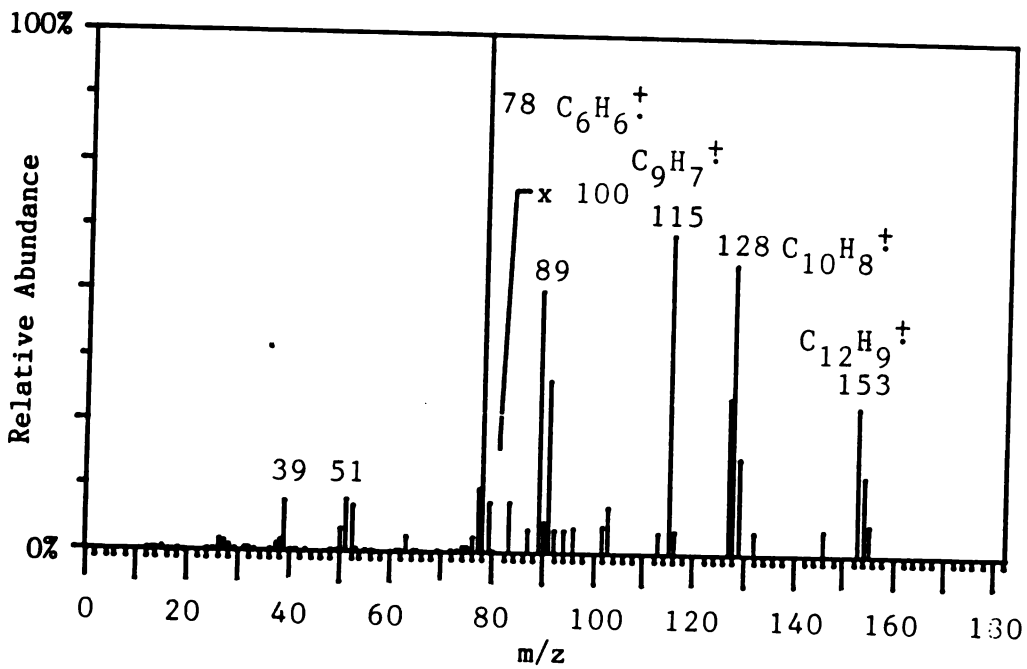

Figure 67. The Self-CI Mass Spectrum of Benzene

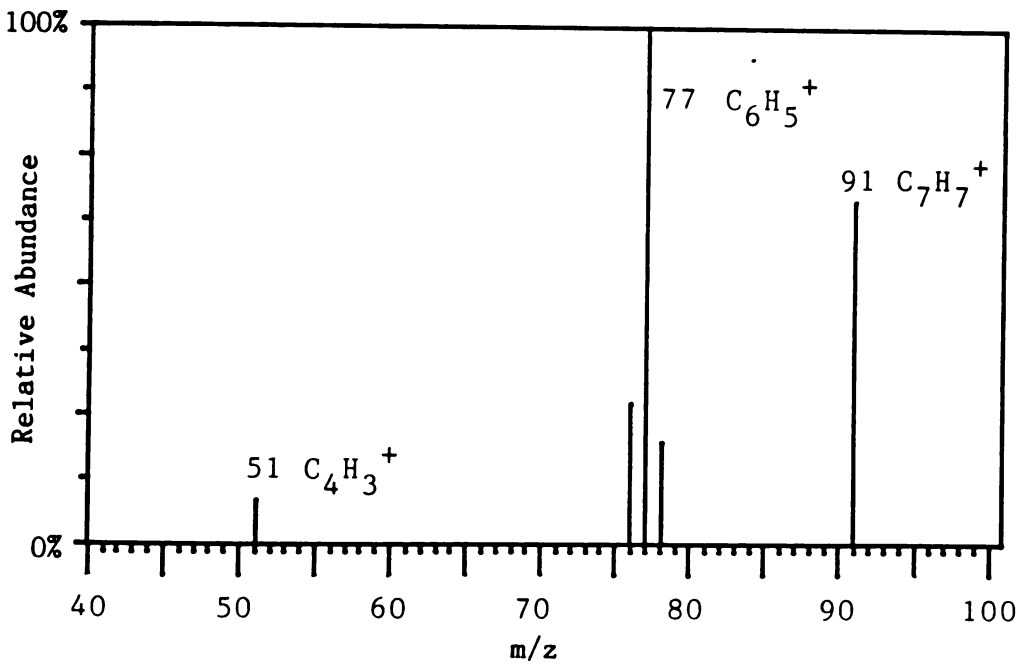

Figure 68. The Product Spectrum of the Phenyl Cation Reacting with Methane in the Central Quadrupole

89 and 91 are produced in other ion/molecule reaction techniques by reactions of the phenyl cation with other saturated hydrocarbons such as cyclopropane (135). Therefore, it is very likely that the peaks at m/z 89 and 91 are due to the reaction of the phenyl cation with residual saturated hydrocarbon impurities in the CI source.

All of the abundant ions in the CI spectrum of benzene were investigated by argon CID. Figure 69 shows the CID spectra of the peaks at m/z 153 (Fig. 76a), 154 (Fig. 76b), and 155 (Fig. 76c). The m/z 155 ion has been identified as protonated biphenyl by other researchers (127). This indicates that the m/z 154 ion should be the molecular ion of biphenyl, and that the m/z 153 ion should be $(M-H)^-$ ion of biphenyl. Pure biphenyl was volatilized into the EI source of the TQMS and ionized by 70 eV EI. The CID daughter scans of the m/z 154 and 153 ions of biphenyl are shown in Figure 70. If one compares the CID spectra in Figures 69 and 70, it is abundantly clear that the m/z 153 and 154 ions produced by the ion/molecule reactions in benzene do not have the same CID spectra as the m/z 153 and 154 ions produced by authentic biphenyl. This leads the author to believe that the $C_{12}H_{10}^+$ and $C_{12}H_9^+$ ions produced by ion/molecule reaction in benzene do not have the biphenyl structure. The largest difference between the reference CID spectrum and the ion/molecule product CID spectrum of m/z 154 is the absence of the m/z 77 peak in the reference compound indicating the presence of a strong covalent bond between rings. On the other hand, the presence of an abundant m/z 77 peak in the ion/molecule product CID spectrum indicates the absence of a strong covalent interaction between rings.

Since the CID spectrum of m/z 155 peak of the ion/molecule reaction also contains a prominent m/z 77 peak, indicating a weak bond

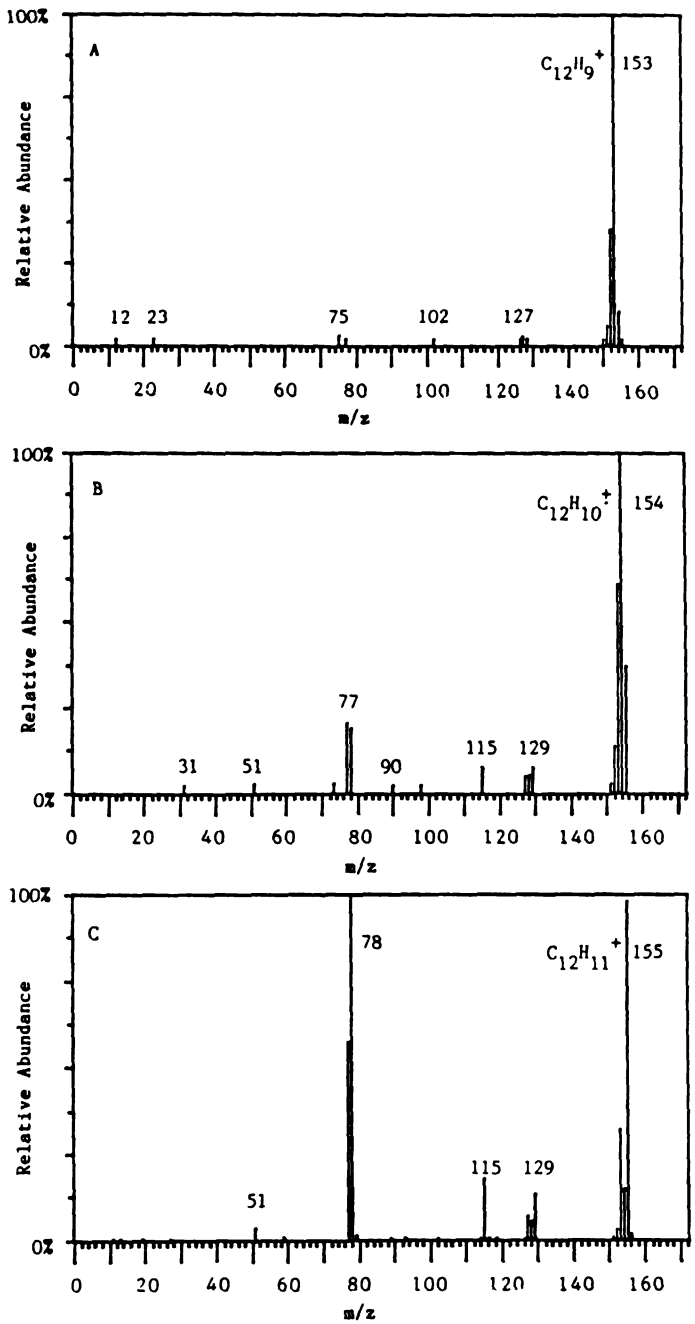

Figure 69. Argon CID Daughter Spectrum of the (A) m/z 153, (B) m/z 154, and (C) m/z 155 Peaks from the Self-CI Mass Spectrum of Benzene

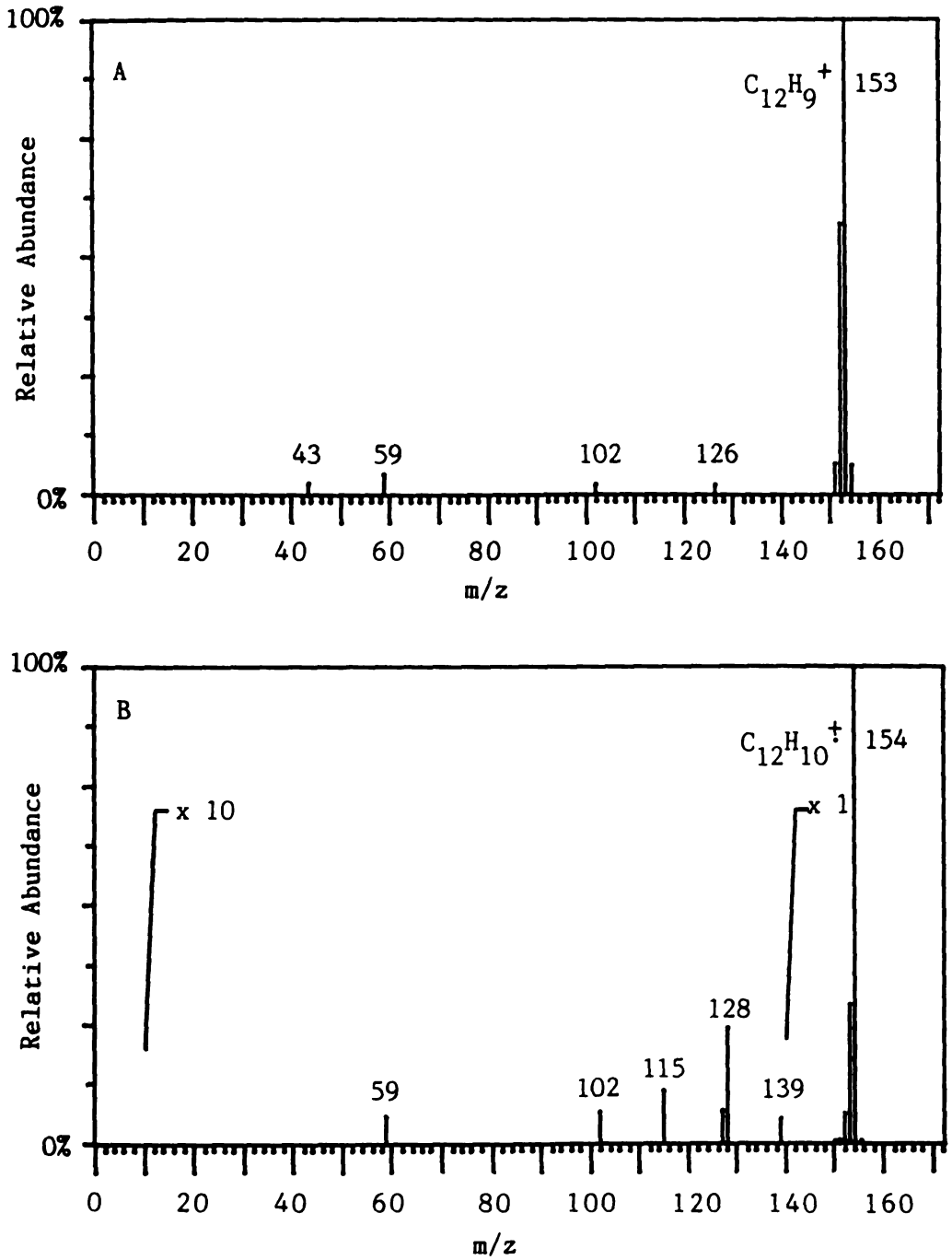

Figure 70. Argon CID Daughter Spectra of the (A) $(M-H)^+$ Ion and (B) M^+ Ion of Biphenyl

between rings, it hardly seems likely based on the CID evidence that the structure of the $C_{12}H_{11}^+$ ion is that of protonated biphenyl.

As is shown in Figures 65 and 66, both the phenyl cation and the $C_4H_3^+$ ion react with benzene to form the m/z 128 ion, $C_{10}H_8^+$. The CID daughter spectrum of the $C_{10}H_8^+$ ion produced by ion/molecule reactions in the CI volume is shown in Figure 71A. The CID daughter spectrum of the naphthalene molecular ion, generated by 70 eV EI is shown in Figure 71B. The fact that the two CID spectra in Figure 71 are virtually identical indicates that the ion/molecule reaction product $C_{10}H_8^+$ has the naphthalene structure. This is a very different case from the $C_{12}H_{10}^+$ ion discussed earlier. $C_4H_6^+$ ions have been shown to undergo gas-phase Diels-Alder cycloaddition reactions (131) but the $C_4H_3^+$ ion cannot form the naphthalene radical cation by the Diels-Alder mechanism. The two ion/molecule reactions that produce the naphthalene molecular ion in the TQMS are shown in Scheme 5.

The mechanism of these reactions is unknown. In the case of reaction 1 from Scheme 5, the intermediate must be an ion of m/z 155, which may have a protonated biphenyl structure (127) or a ring opened structure (133). The m/z 155 ion found in the ion/molecule reactions in benzene is presumably the collisionally stabilized intermediate of this reaction. Reactivating the m/z 155 ion by energetic collision with argon in the central quadrupole should lead to decompositions that indicate the mechanisms of the reaction. The CID spectrum of m/z 155 (Figure 69) does indeed contain the m/z 128 ion as a daughter. The m/z 154 ion also decomposes by CID to form m/z 128, as does the m/z 129 ion, which is presumably the intermediate of reaction 2 from Scheme 5. It may be that all of these decompositions to form the $C_{10}H_8^+$ ion happen by

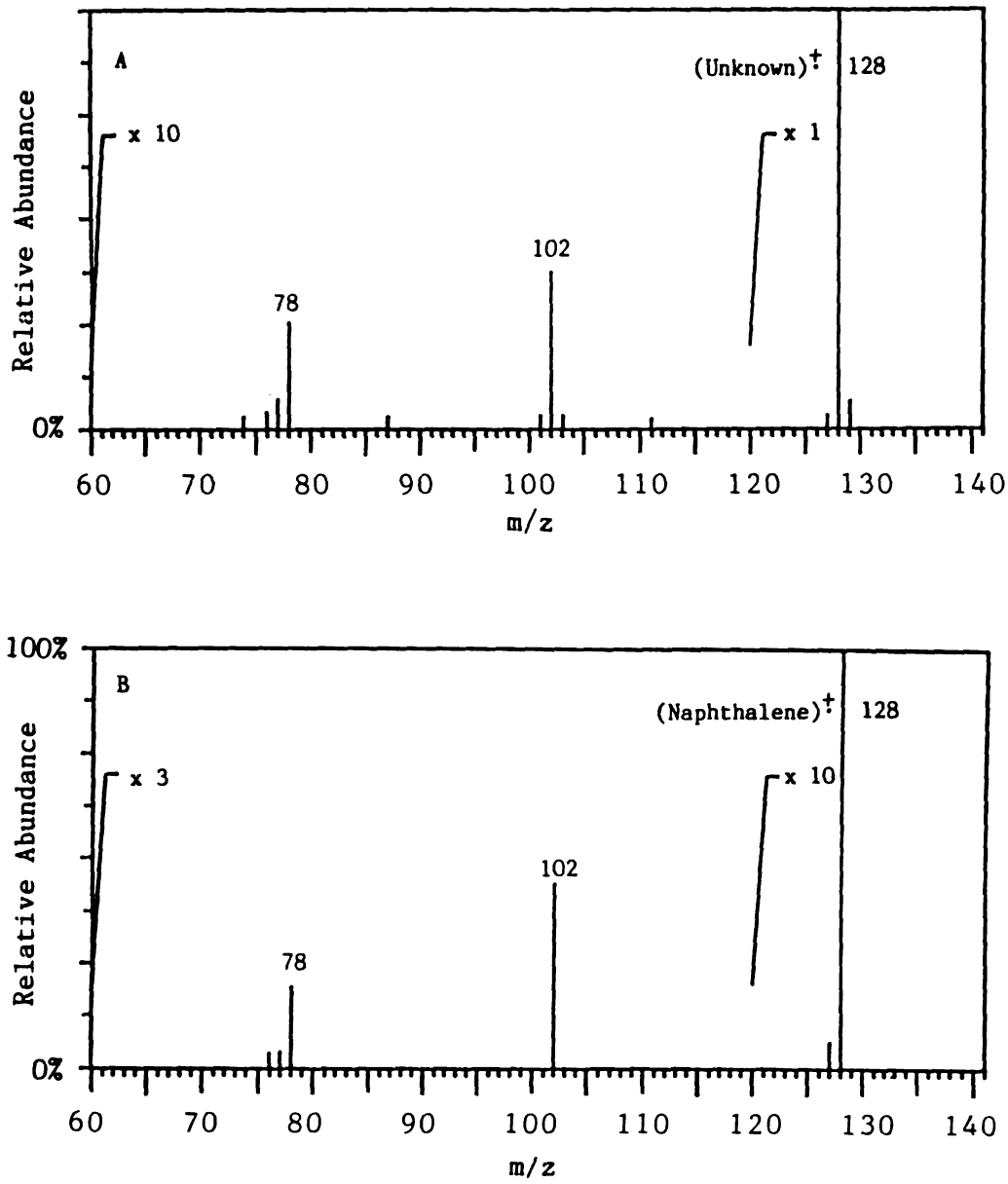

Figure 71. Argon CID Daughter Spectra of the (A) $C_{10}H_8^+$ Ion Generated by Benzene Self-CI, and (B) the $M^{+\cdot}$ of Naphthalene

Scheme 5

Two Reactions in the TQMS that Produce the $C_{10}H_8^{+\cdot}$ Ion

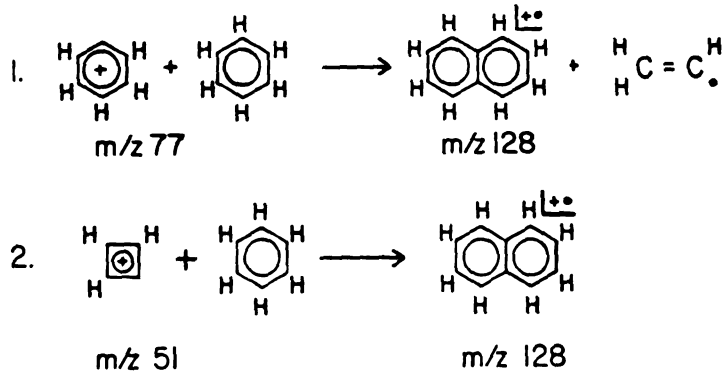

different mechanisms and that the products rearrange in the end to form the most stable isomeric structure, which in this case is the naphthalene molecular ion. This view is analogous to the example of the m/z 77 ion mentioned in the introduction to this chapter (132), in which the isomers of $C_6H_5^+$ rearrange in the gas phase to form the phenyl cation irrespective of parent ion structure.

Another prominent peak in the ion/molecule reactions of benzene is found at m/z 115. Figure 72 shows the CID daughter spectrum of this ion. McLafferty (136) suggests that this ion may have the indene structure. Unfortunately, the author was unable to acquire a reference sample of indene, but it would be interesting to compare the CID spectrum of indene to the spectrum in Figure 72. Clearly, though, the structure of the m/z 115 ion is very much like that of naphthalene in that its CID spectrum shows the same neutral losses as in the CID spectrum of naphthalene. It is certainly a covalently bonded aromatic species like naphthalene, and unlike the more weakly-bonded m/z 155 and m/z 154 ions. As such, the indene structure is a likely candidate.

In summary, the TQMS data in this chapter support the idea that the ions m/z 155, 154 and 153 from the ion/molecule reactions in benzene do not have a biphenyl structure, but may be ring-opened structures or may simply be ionic adducts. The TQMS data concerning the ion/molecule reactions in benzene also indicate that the m/z 128 ion has the naphthalene structure, and that it is plausible that the m/z 115 ion has the indene structure.

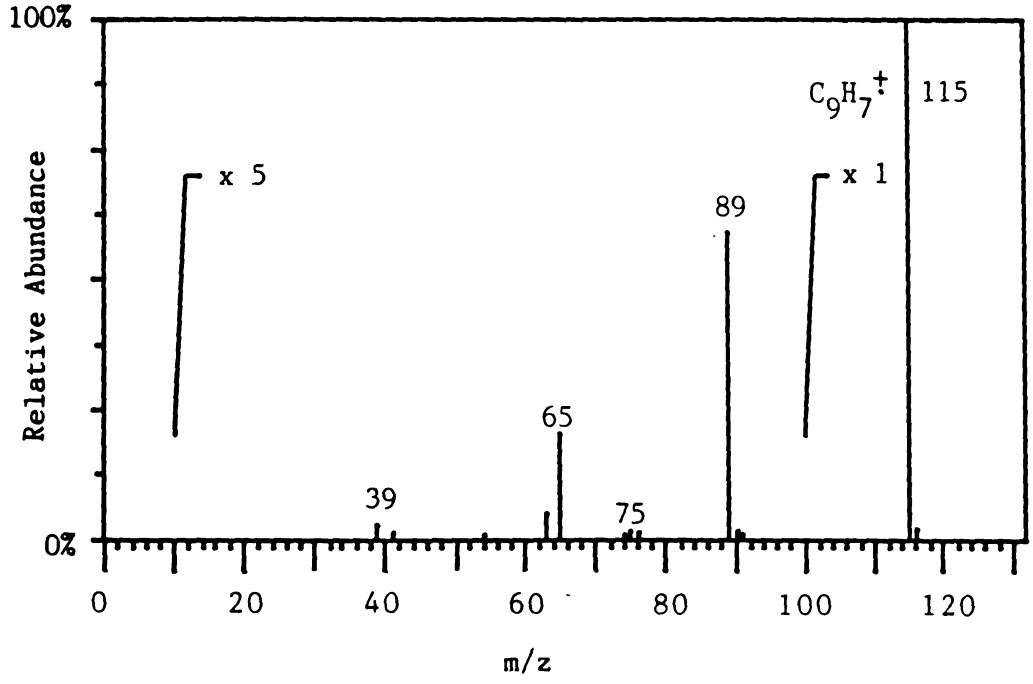

Figure 72. Argon CID Daughter Spectrum of the m/z 115 Peak from Benzene Self-CI

2. Reactions of Aryl Cations with Ammonia

From the data shown in this chapter and from the data in the literature it was apparent that the phenyl cation is a highly reactive ion that will generate interesting ion/molecule reactions even with relatively unreactive molecules such as benzene. For this reason, the author chose to investigate the reactions of the phenyl cation with other more reactive molecules. Figure 73 shows the product spectrum of the reaction of the phenyl cation with ammonia in the central quadrupole of the TQMS. The chemical equations that can be written from the observed products in Figure 73 appear in Scheme 6.

There is little doubt that the m/z 18 ion has the ammonium ion structure. It is not immediately obvious, however, whether the m/z 93 and m/z 94 ions have the aniline and protonated aniline structures (41). Therefore, the structures of the m/z 93 and m/z 94 ions were investigated by CID.

Figure 74 shows the products of mixing benzene and ammonia in the CI volume. Only the ions above m/z 80 are shown, since the reagent ions of benzene are off-scale in order to achieve the abundance of ion/molecule products necessary for performing CID. Figure 74 shows that the m/z 93 and m/z 94 ions are present as expected, but since there is no parent ion selection in CI, the base peak is m/z 95, which apparently arises from the reaction of the benzene molecular ion with ammonia. Figure 74 also shows the products of the reactions between aryl cations and benzene discussed previously in this chapter as peaks at m/z 115, 128, and a cluster around m/z 154. There is an unexplained peak at m/z 138.

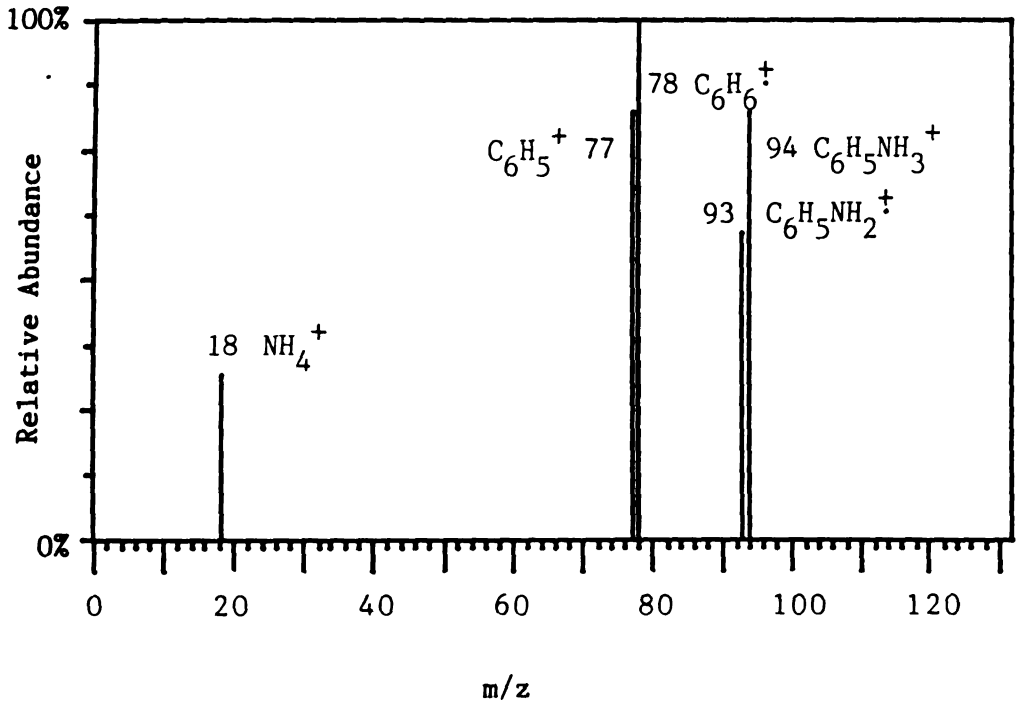

Figure 73. The Product Spectrum of the Reaction Between the Phenyl Cation and Ammonia in the Central Quadrupole

Scheme 6

Reactions Between the $C_6H_5^+$ Ion and NH_3

1. $C_6H_5^+ + NH_3 \longrightarrow C_6H_6^{+\bullet} + NH_2$
   m/z 77 m/z 78

2. $\longrightarrow C_6H_4 + NH^+$
   m/z 18

3. $\longrightarrow C_6H_5NH_2 + H\bullet$
   m/z 93

4. $\longrightarrow C_6H_5NH_3^+$
   m/z 94

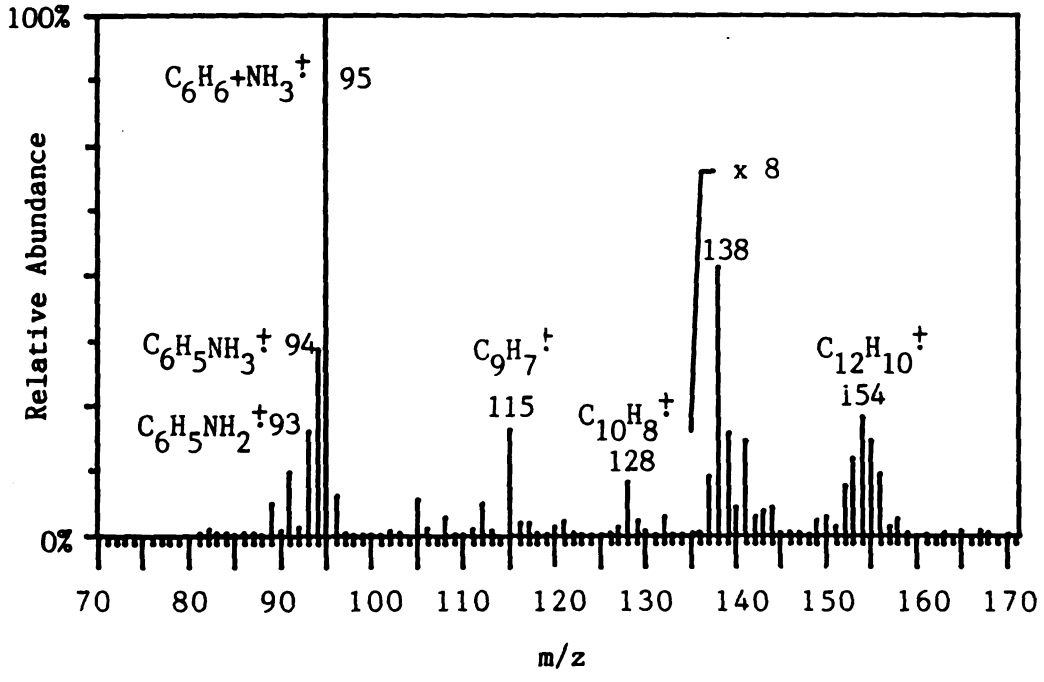

Figure 74. Partial Mass Spectrum Resulting from the Mixture of Benzene and Ammonia in the CI Volume

Figure 75 shows the argon CID daughter scan of the m/z 95 ion produced by benzene/ammonia CI. Figure 75 shows a single very large peak which is the benzene molecular ion at m/z 78, indicating that the m/z 95 ion is a weakly-bonded adduct of ammonia and benzene. Figure 76A shows the CID daughter scan of the m/z 93 ion produced by benzene/ammonia CI, and Figure 76B shows the CID daughter scan of the molecular ion of authentic aniline produced by EI. The spectra in Figure 76 are virtually identical, so it seems likely that the phenyl cation does react with ammonia in the gas phase to produce an ion with the aniline structure. Figure 77 shows the CID daughter spectrum of the m/z 94 ion produced by benzene/ammonia CI. Since the phenyl cation is produced by CID in considerable yield for this relatively unstable ion, the m/z 94 ion must be considered to be a loosely bound adduct of the phenyl cation and ammonia. This ion is the collisionally stabilized intermediate of the reaction that produces the aniline molecular ion from the phenyl cation reacting with ammonia (see Scheme 7).

3. The Reactions of Aryl Cations with Methanol

Since the phenyl cation has been shown to react with methanol to form numerous products at pressures of about 1 torr by the GPR technique (129), the author was very interested to determine whether similar reactions occur at approximately one order of magnitude lower pressures in CI and at three to four orders of magnitude lower pressures in the central quadrupole. The products of the reactions of the phenyl cation with methanol, in both the gas phase and in solution, are listed in Table 12 (129). The results in Table 12 were obtained by the following reaction scheme (Scheme 8) (129).

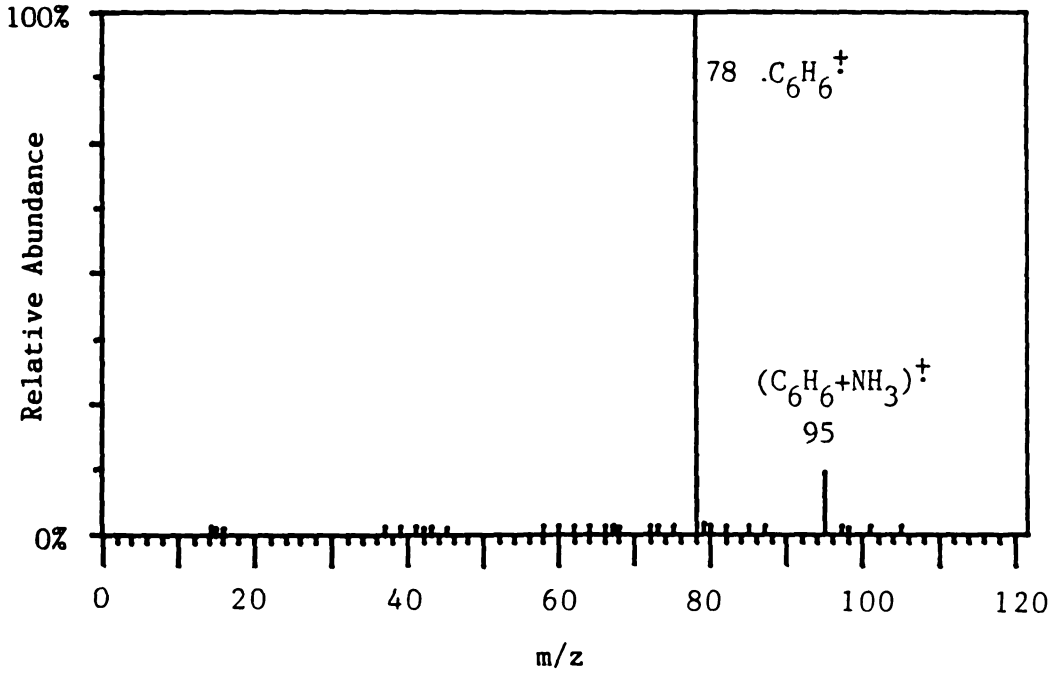

Figure 75. Argon CID Daughter Spectrum of the m/z 95 Peak Produced by Ion/Molecule Reactions of Benzene/Ammonia CI

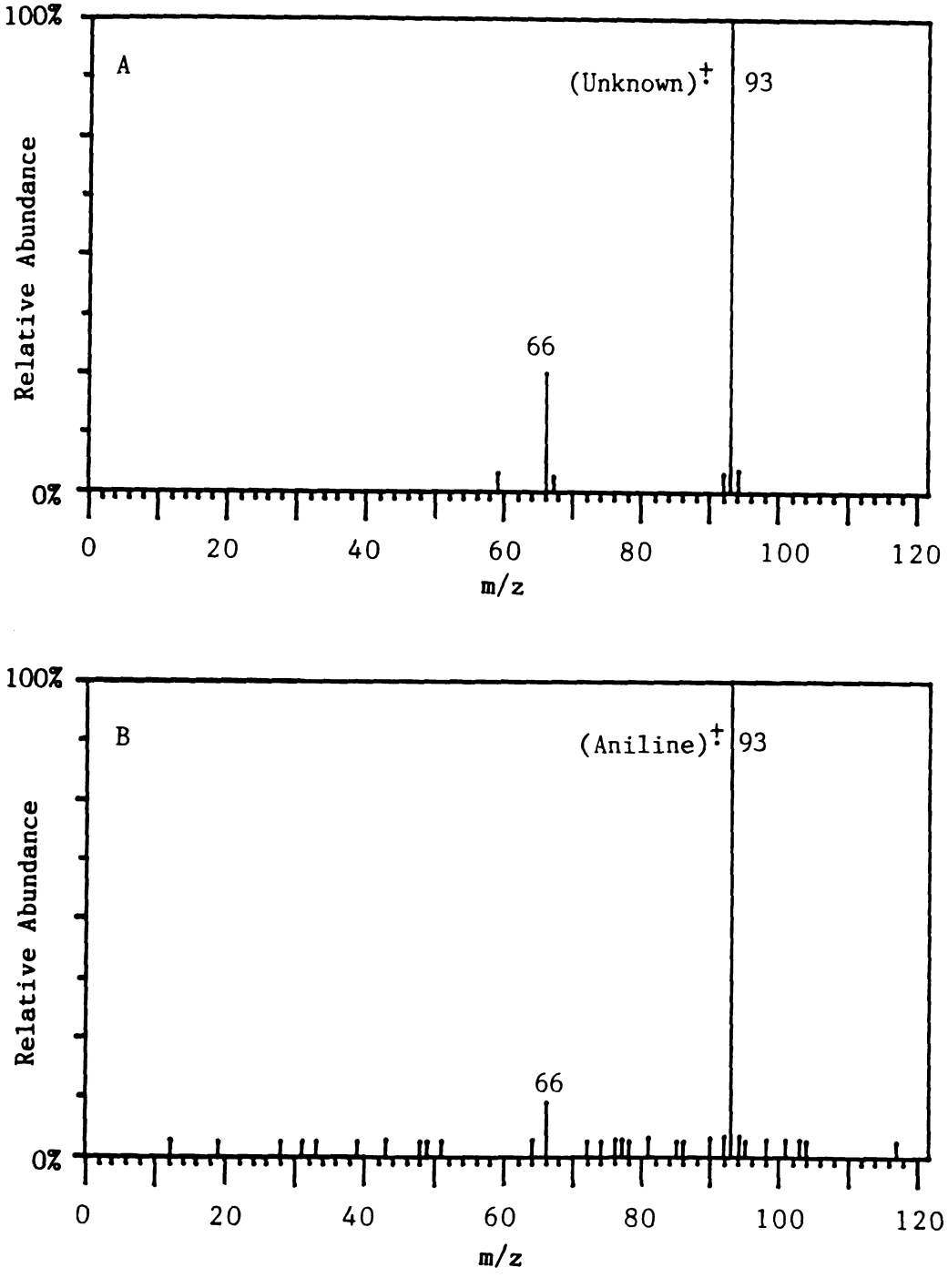

Figure 76. Argon CID Daughter Spectrum of (A) the m/z 93 Peak Produced by Benzene/Ammonia CI and of (B) the $M^{+\cdot}$ Ion of Aniline Produced by EI

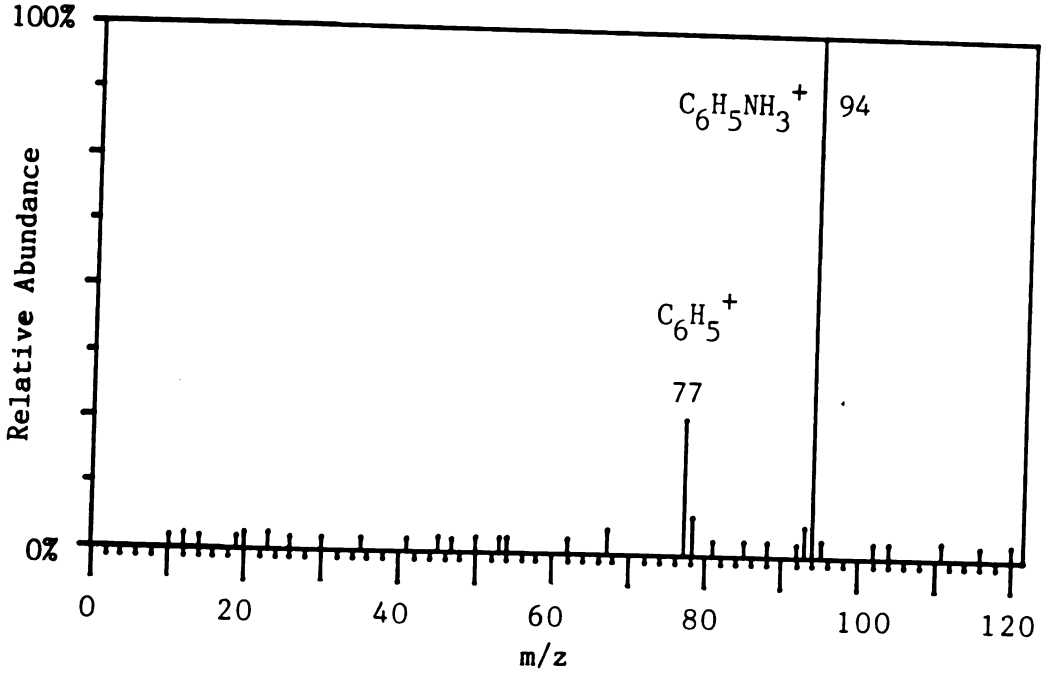

Figure 77. Argon CID Daughter Spectrum of the m/z 94 Peak Produced by Benzene/Ammonia CI

Scheme 7

Mechanism for the Formation of Aniline from $C_6H_5^+$ and NH_3

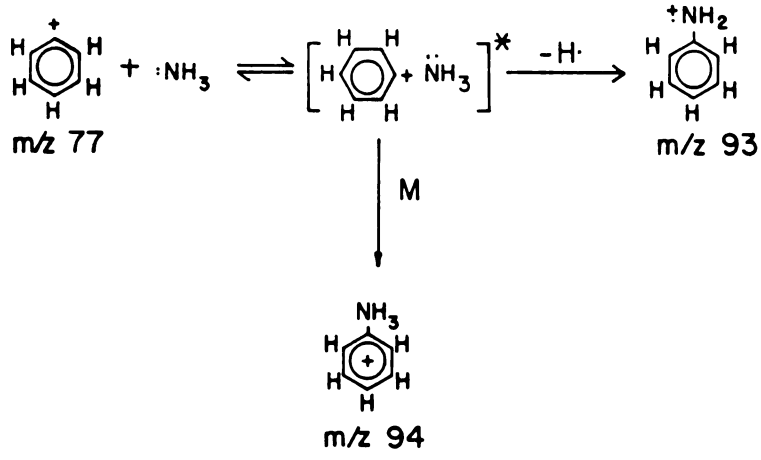

Table 12

Relative Distribution of Products from the Reaction of $C_6H_5^+$ and CH_3OH

	Products	5 torr	50 torr	Solution
1.	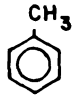	1%	1%	4%
2.	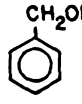	1%	1%	5%
3.	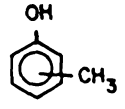	3%	1%	2%
4.	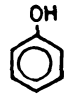	20%	5%	5%
5.	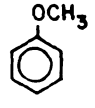	75%	90%	80%

Scheme 8

Reactions of Tritiated Phenyl Ion with Methanol (129)

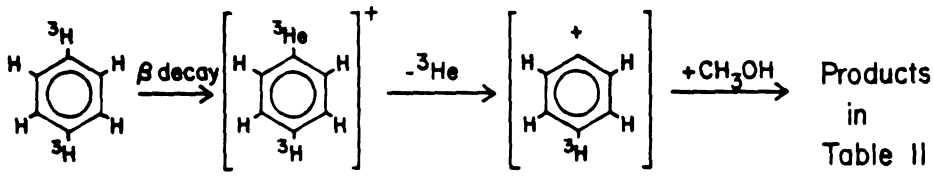

The bitritiated benzene molecule was prepared by Angelini, et al. (129) and mixed either in the gas phase or in solution with methanol. When one of the tritium nuclei decays to ^3He, the energy released breaks the bond to the benzene ring and forms the tritiated phenyl cation, which reacts with the surrounding molecules of methanol. The advantages of the technique are that one can prepare charged species in their ground state without the presence of a massive counter ion and one can trace the products formed by means of their radioactive label. The disadvantage is that this technique is experimentally laborious and extremely time-consuming (up to a year for a single reaction). In gas-phase studies, changing the pressure of methanol also changed the relative distribution of products from Table 12. The amount of products 1 and 2 stays steady with changes in pressure from 1 to 70 torr. The amount of products 3 and 4 increases with decreasing pressure and the amount of product 5 decreases with decreasing pressure. From this data one would expect the same reaction would produce primarily the products 3 and 4 at the much lower pressure used in the mass spectrometer.

The phenyl cation in this chapter was generated from benzene by 70 eV EI in the TQMS. Methanol was leaked into the central quadrupole. There was little mixing of the two gases due to the fact that the ion source and central quadrupole of the TQMS are differentially pumped. The product spectrum of the reaction between the phenyl cation and methanol is shown in Figure 78. The only ionic products formed with m/z values greater than the parent ion are the $C_7H_7^+$ ion at m/z 91 and the $C_6H_5OH^+$ ion at m/z 94. These probably correspond to products 1 and 4 of the GPR reaction. Obviously the low pressure ($4X10^{-3}$ torr methanol) changes the reaction dramatically. If the other ionic products are

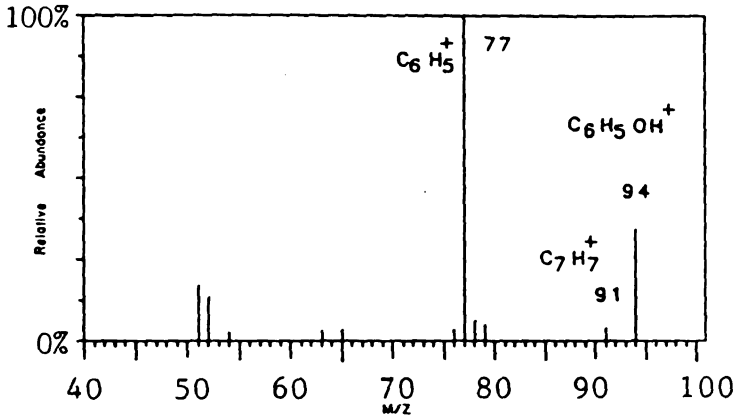

Figure 78. The Product Spectrum of the Reaction Between the Phenyl Cation and Methanol in the Central Quadrupole

formed in the central quadrupole they are not sufficiently stabilized by collisions with other molecules for them to be detected before they decompose.

Since all of the reaction products were not observed in the central quadrupole, the author implemented the same reaction at higher pressure (0.1-1 torr) in the CI volume. Figure 79 shows the reaction products of a mixture of benzene and methanol in the CI volume. Because the parent ion is not selected and the reaction is done in a single chamber, all of the product ions from reactions in methanol (see Chapter V.) and all of the product ions from reactions in benzene appear in the spectrum along with the product ions from the reaction of the phenyl cation with methanol. If we remove from consideration all of the methanol and benzene self-CI products, the reaction products left are at m/z 91 ($C_7H_7^+$), m/z 94 ($C_6H_5OH^+$), and a group of ions from m/z 107 to m/z 111. Both products 2 and 3 occur at m/z 108, and the m/z value of product 5 is 107. It would appear, therefore, that raising the pressure has in fact produced the products which were missing in the central quadrupole reaction due to lack of collisional stabilization. The peaks at m/z 109, m/z 110 and m/z 111 in the CI spectrum were, however, rather mysterious.

It seems reasonable that the m/z 94 ion should have the phenol structure and that the m/z 110 ion should have the catechol structure. In order to determine the structures of these two ions, the author obtained the argon CID daughter spectra of these two ions as produced by ion/molecule reactions in benzene/methanol CI and compared them with the CID spectra of reference compounds. Figure 80A shows the CID daughter spectrum of the m/z 94 ion produced by ion molecule reactions in CI, and

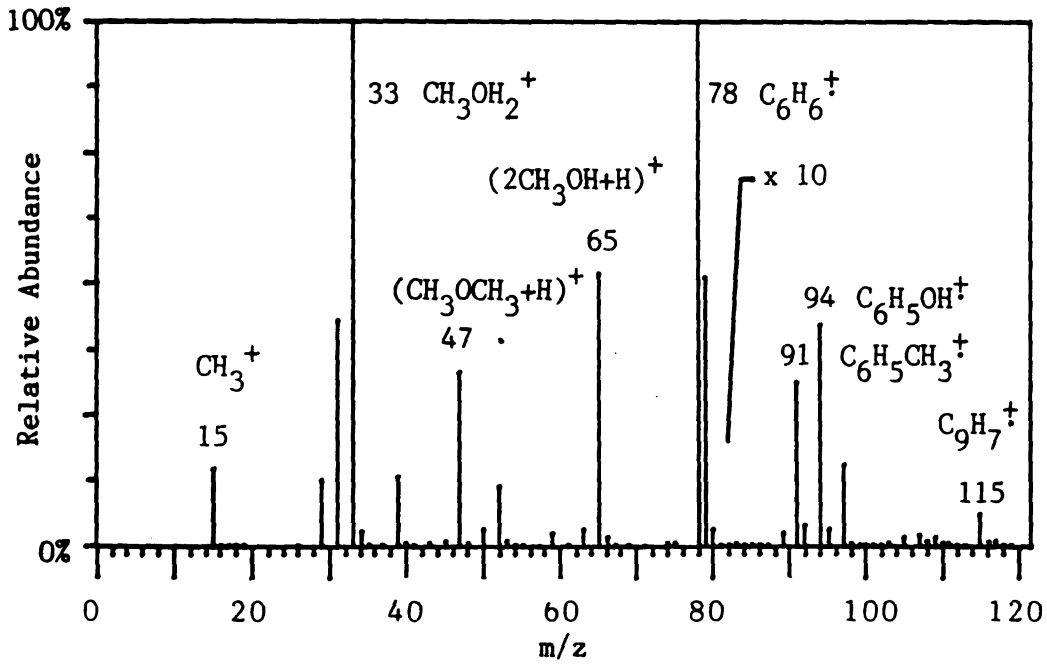

Figure 79. Mass Spectrum Resulting from the Mixture of Benzene and Methanol in the CI Volume

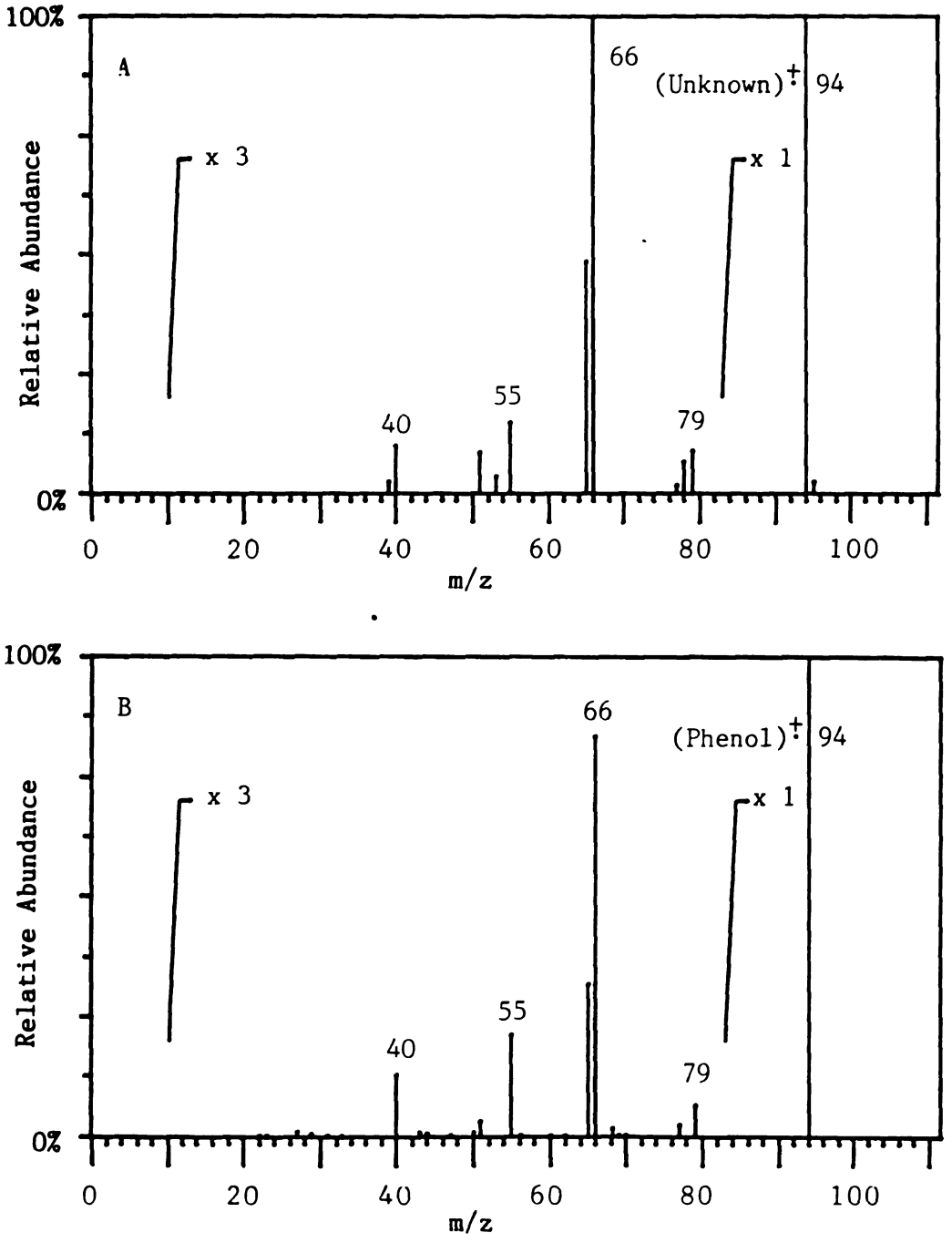

Figure 80. Argon CID Daughter Spectra of the (A) m/z 94 Peak Produced by Benzene/Methanol CI, and of (B) the $M^{+\cdot}$ of Phenol Produced by EI

Figure 80B shows the CID daughter spectrum of the phenol molecular ion produced by 70 eV EI. The match between the reference compound CID spectrum and the ion/molecule products CID spectrum is very good. Thus the identification of the m/z 94 ion as phenol is quite certain.

Figure 81A is the CID daughter spectrum of the m/z 110 ion from the ion/molecule reactions in benzene/methanol CI, and Figure 81B is the CID daughter spectrum of the molecular ion of catechol by 70 eV EI. In this case, the match between the reference compound and the ion/molecule product is very poor, so the m/z 110 product ion definitely does not have the catechol structure. In fact, since the major daughter ion in Figure 81A is the benzene molecular ion and the neutral loss is 32u, the most likely structure for the m/z 110 ion is the methanol adduct of benzene.

Figure 82 shows the CID daughter spectrum of the m/z 111 ion in the ion/molecule reactions of benzene/methanol CI. The neutral loss of 32 u to form protonated benzene indicates that m/z 111 is the proton-bound adduct of benzene and methanol. Figure 83 shows the CID daughter spectrum of the m/z 109 ion in the ion/molecule reactions of benzene/methanol CI. The neutral loss of 15 u to form the phenol molecular ion is strong evidence that this ion has the structure shown for the intermediate in the mechanism of the reaction that forms $(phenol)^+$ (see Scheme 9).

By identifying the presence of the collisionally stabilized intermediate in the reaction, the CID spectrum of the m/z 109 ion confirms the mechanism in Scheme 8 which was postulated (129) for phenol formation. Unfortunately, a similar analysis of the peak at m/z

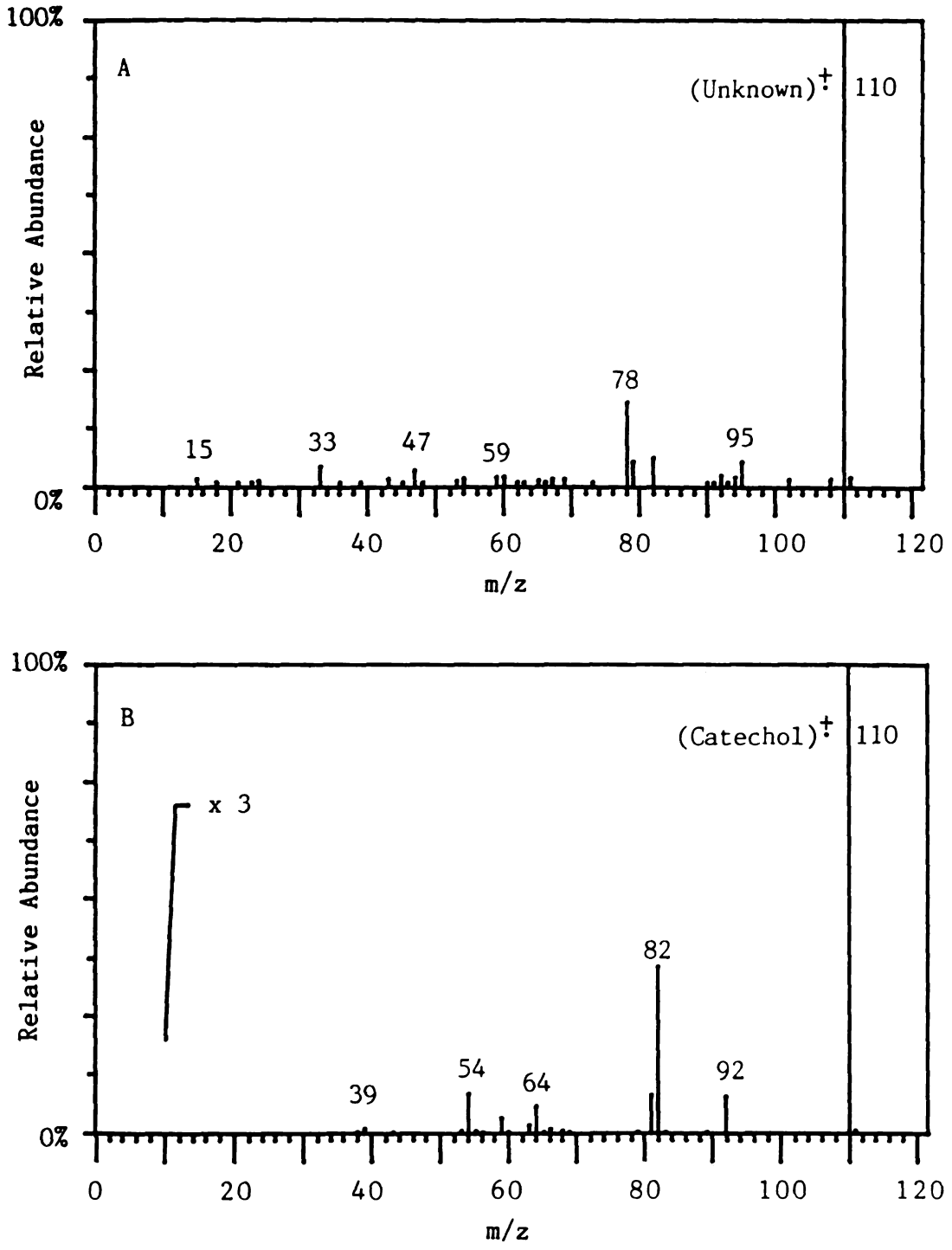

Figure 81. Argon CID Daughter Spectra of the (A) m/z 110 Peak Produced by Benzene/Methanol CI and of (B) the M^+ of Catechol Produced by EI

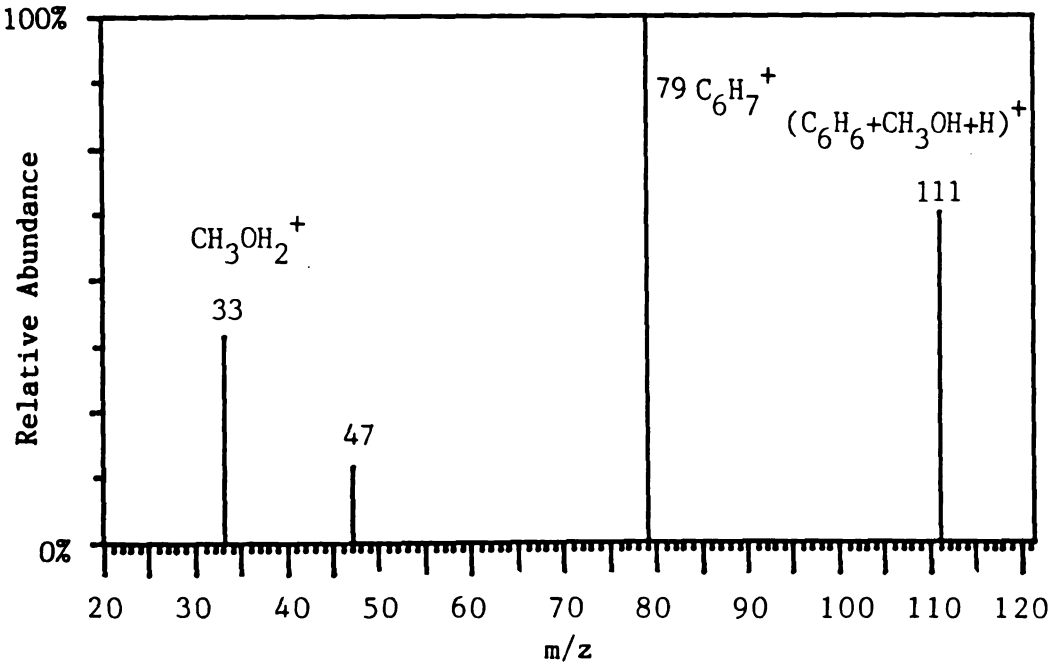

Figure 82. Argon CID Daughter Spectrum of the m/z 111 Peak Produced by Benzene/Methanol CI

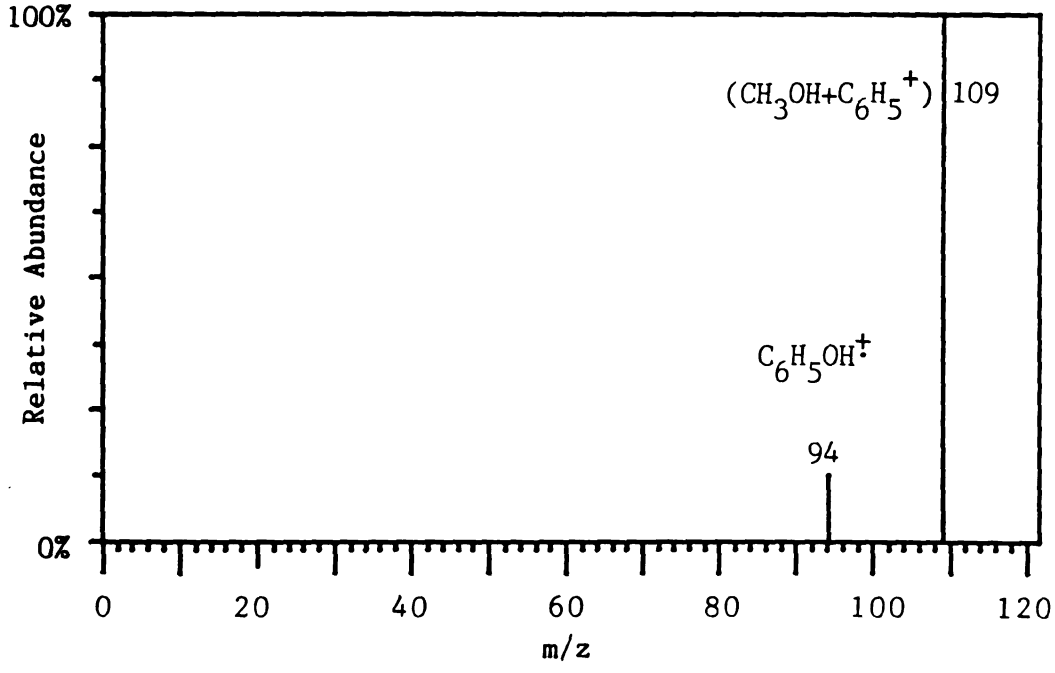

Figure 83. Argon CID Daughter Spectrum of the m/z 109 Peak from Benzene/Methanol CI

Scheme 9

Reaction of the Phenyl Cation with Methanol to form Phenol

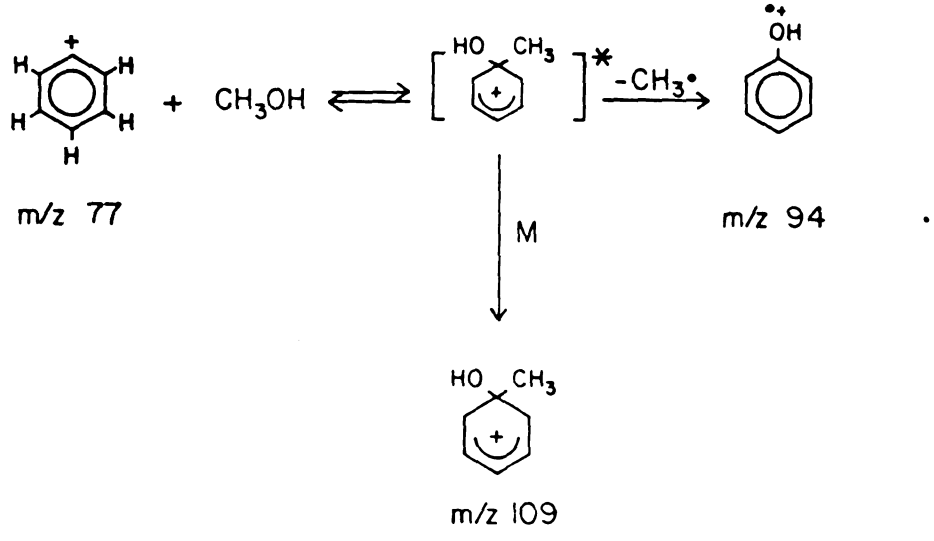

108 is impossible due to the fact that products 2 and 3 are isomeric and produce overlapping CID spectra.

The benzene/methanol CI experiment was also performed on the JEOL HX-110 instrument and the molecular formulas of all the ions discussed in this section were confirmed by exact mass measurements. Even though CID experiments on the TQMS were not performed on the m/z 108 ion in the CI ion/molecule reactions of benzene and methanol, the identification of its molecular formula as C_7H_8O strongly points to its identity as the anisole molecular ion which is compound 5 in Table 11. The results from CI and GPR for this reaction of the phenyl cation and methanol are as similar as one could hope for considering the vast differences between the techniques.

The data collected from the central quadrupole in this chapter so far were done without ion-trapping. The reason for this is that the most stable product ion by far in the product spectrum of the reaction of the phenyl cation with methanol is the benzene molecular ion. The result of this fact is that ion-trapping simply favors the production of m/z 78 at the expense of the more interesting products. This is the only example that the author has yet discovered in which ion-trapping was of little or no benefit for the study of ion/molecule reactions. Rather, this study points out the importance of high pressure for analyzing ions which would normally decompose under mass spectrometric conditions.

In fact, Mahle, et al. (138) used an atmospheric pressure ionization (API), also called atmospheric pressure CI) source to study the reaction of the benzene molecular ion with air. Apparently, the benzene molecular ion reacts with molecular oxygen at extremely high

pressures to form the phenol molecular ion in very high yield. They also observed this hydroxylation reaction with xylenes, naphthalene, toluene and chlorobenzene, but not for hexane, cyclohexane or pyridine. These observations led the author to investigate the reactions of other cations with methanol under CI and central quadrupole conditions to determine whether or not the methanol reaction was unique to the phenyl cation.

Toluene, naphthalene, anthracene and pyridine are all aromatic molecules which under EI conditions readily form $(M-H)^+$ ions which are analogous to the phenyl cation derived from benzene. Figure 84 is the product spectrum of the reaction between the $(M-H)^+$ ion (m/z 91) of toluene ($C_7H_7^+$) and methanol in the central quadrupole of the TQMS. The spectrum in Figure 84 was obtained with 100 msec of ion-trapping. In the following figures, ion-trapping was essential for observing the ion/molecule reaction products, unlike in the case of phenyl cations.

The product ions observed are the protonated dimer (m/z 65) and trimer (m/z 97) of methanol due to proton transfer from the parent ion to collision gas; the $C_7H_7OH^+$ ion is due to the hydroxylation reaction of methanol with the parent ion.

Figure 85 shows the product spectrum of the pyridine $(M-H)^+$ ion (m/z 78) $(C_5H_4N)^+$ with methanol in the central quadrupole. This reaction was accomplished with 100 msec of ion-trapping. The product ions observed are the protonated molecule of pyridine (m/z 80), the hydroxylation product from the reaction of methanol and $C_5H_4N^+$ to form the $C_5H_4NOH^+$ ion at m/z 95 (presumably with the OH group attached to a C not the N), and the adduct ion of the parent ion and methanol at m/z 110.

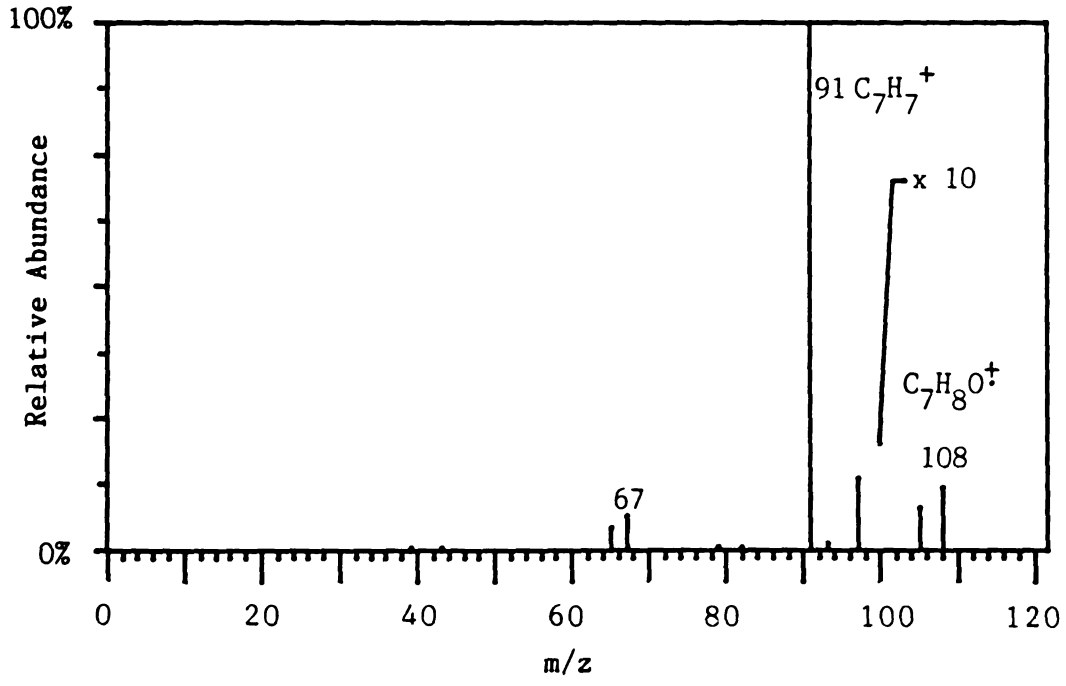

Figure 84. The Product Spectrum of the Reaction Between the $C_7H_7^+$ Ion and Methanol in the Central Quadrupole

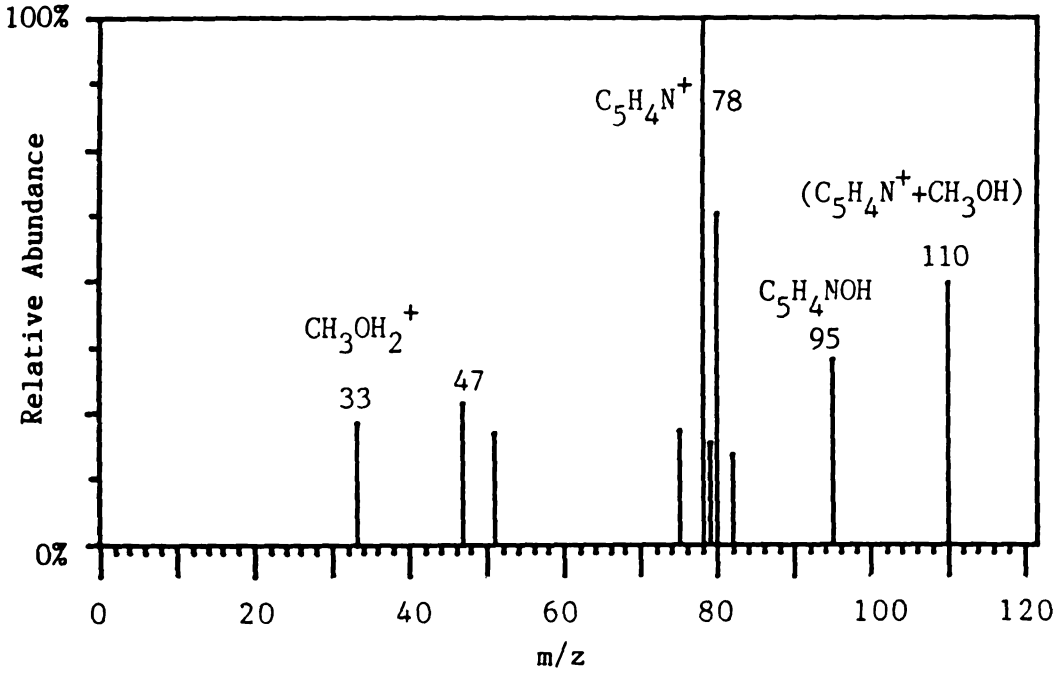

Figure 85. The Product Spectrum of the Reaction Between the $(M-H)^+$ Ion of Pyridine and Methanol in the Central Quadrupole

Figure 86 shows the product spectrum of the $(M-H)^+$ ion of naphthalene (m/z 127) $(C_{10}H_7)^+$ with methanol in the central quadrupole. The productions observed are the naphthalene molecular ion (m/z 128), and the hydroxylation product (m/z 144) from the reaction between methanol and the parent ion.

Figure 87 shows the product spectrum of the $(M-H)^+$ ion of anthracene (m/z 177) $(C_{14}H_9)^+$ with methanol in the central quadrupole. The product ions observed with 100 msec of ion-trapping are the anthracene molecular ion (m/z 178), the hydroxylation product m/z 194 from the reaction of the parent ion with methanol, and the adduct ion of methanol with the parent ion.

Figure 88 shows the product spectrum of the $(M-H)^+$ ion of p-xylene (m/z 105) reacting with methanol in the central quadrupole. The m/z 122 peak corresponds to the hydroxylation product of the parent ion reacting with methanol. The peak at m/z 154 is due to a further reaction of the hydroxylated product with methanol to form the methanol adduct, and the peak at m/z 135 is due to the loss of $CH_3\cdot$ from the adduct ion. The hydroxylated product reacted because the 100 msec of ion trapping employed in this scan gave rapid side reactions a chance to occur. The product spectra of the $(M-H)^+$ ions o-, m-, and p-xylenes with methanol are identical.

In all of the cases of aromatic compounds, the reaction of methanol with the $(M-H)^+$ ion in the central quadrupole formed the expected hydroxylation product, but did not form most of the other products that are typical of the phenyl cation reaction with methanol. Occasionally, the methanol adduct ion, which is thought to be the intermediate in the hydroxylation reaction, was also observed.

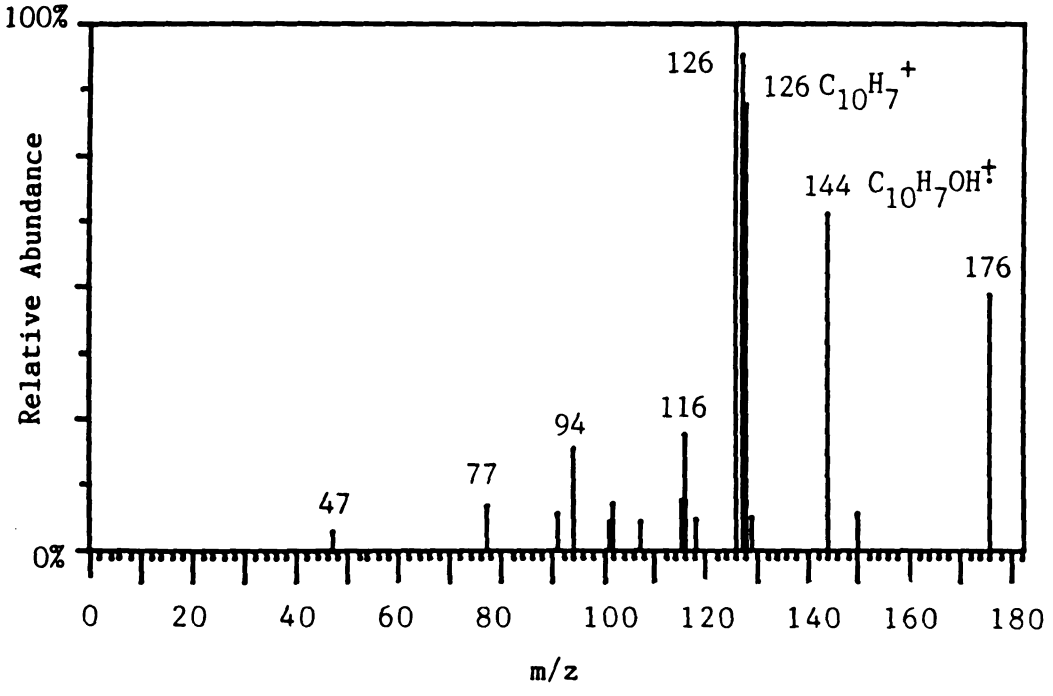

Figure 86. The Product Spectrum of the Reaction Between the $(M-H)^+$ Ion of Naphthalene and Methanol in the Central Quadrupole

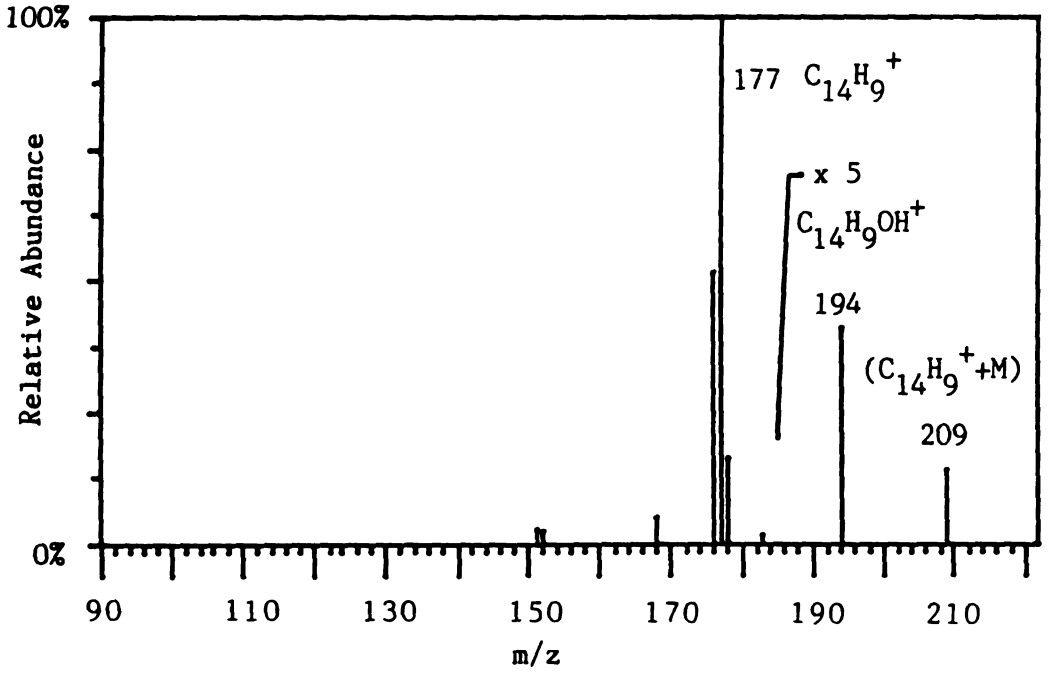

M=Methanol

Figure 87. The Product Spectrum of the Reaction Between the $(M-H)^+$ Ion of Anthracene and Methanol in the Central Quadrupole

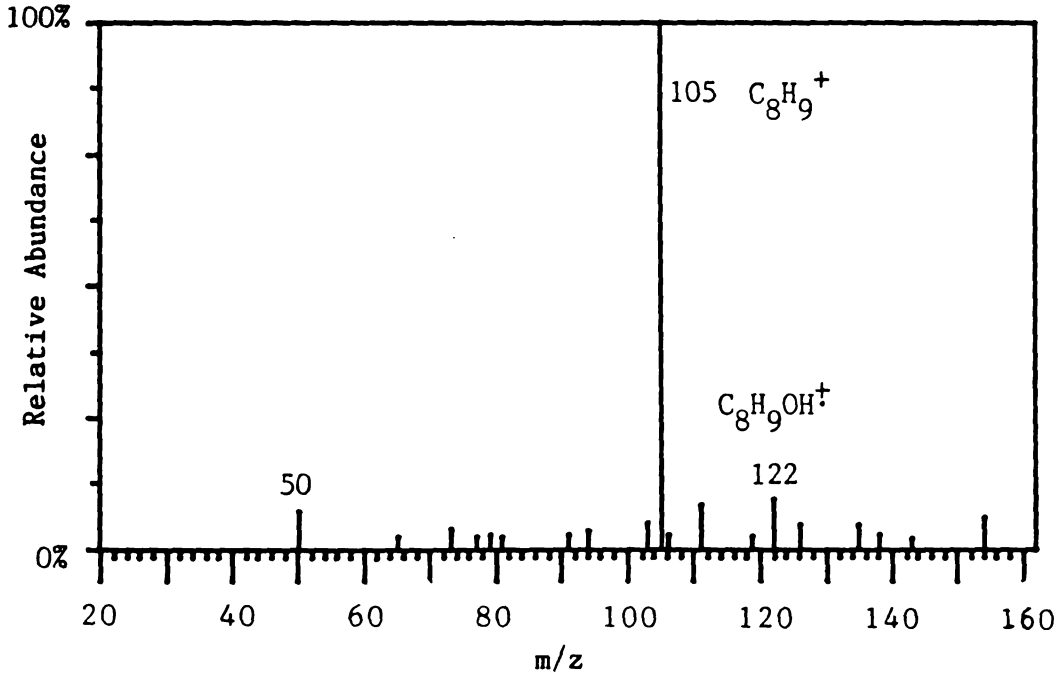

Figure 88. The Product Spectrum of the Reaction Between the $(M-H)^+$ Ion of p-Xylene and Methanol in the Central Quadrupole

Therefore, one can expect to observe the hydroxylation reaction with virtually all $(M-H)^+$ ions from unsubstituted or substituted aromatic compounds, whether they are polycyclic or heteroaromatic. A major condition for the reaction is, however, that a radical must be lost from the ring if the aromatic compound contains an aliphatic substituent, or the reaction will not proceed. This phenomenon is illustrated by the fact that the hydroxylation product is not formed by the reaction of the $(M-H)^+$ ion of hexane (m/z 85) with methanol in the central quadrupole. Figure 89 shows the product spectrum of the hexyl$^+$/methanol reaction taken with 100 msec of ion trapping. The only product peaks formed are due to proton transfer to methanol (m/z 33, 47, 50, and 65). The remaining peaks (m/z 57 and 75) are due to ions produced by CID of the parent ion. In fact, the hydroxylation reaction appears to be specific for aromatic ions that have a vacant position on the ring carbon. This vacancy need not be due to an H· radical loss, but can also be due to the loss of a Cl· radical as is shown in Figure 90. Here the $(M-Cl)^+$ ion of para-dichlorobenzene $(C_6H_4Cl)^+$ (m/z 111) is reacted with methanol in the central quadrupole. The product spectrum in Figure 90 was taken with 100 msec of ion trapping and shows a number of peaks (m/z 33, 47, 50, 65, and 97) which are due to proton transfer to methanol, and a few CID fragment ions of the parent ion (m/z 75, 76, 77, and 79). Figure 90 also shows the hydroxylation product $(HOC_6H_4Cl)^+$ (m/z 128) to be the base peak of the spectrum, as well as numerous side reaction products. For example, the m/z 77 ion produced as a CID fragment has had time to react (due to ion trapping) with the excess methanol in the central quadrupole to form the phenol ion (m/z 94). The m/z 128 product ion apparently has reacted further with methanol to form a methanol adduct

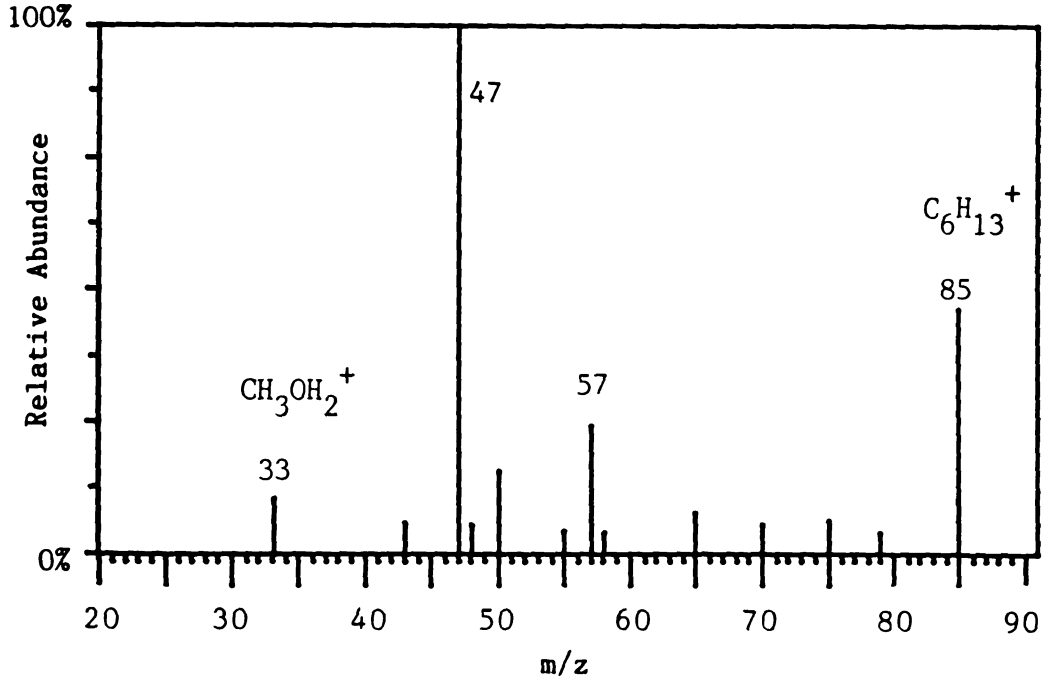

Figure 89. The Product Spectrum of the Reaction Between the $(M-H)^+$ Ion of Hexane and Methanol in the Central Quadrupole

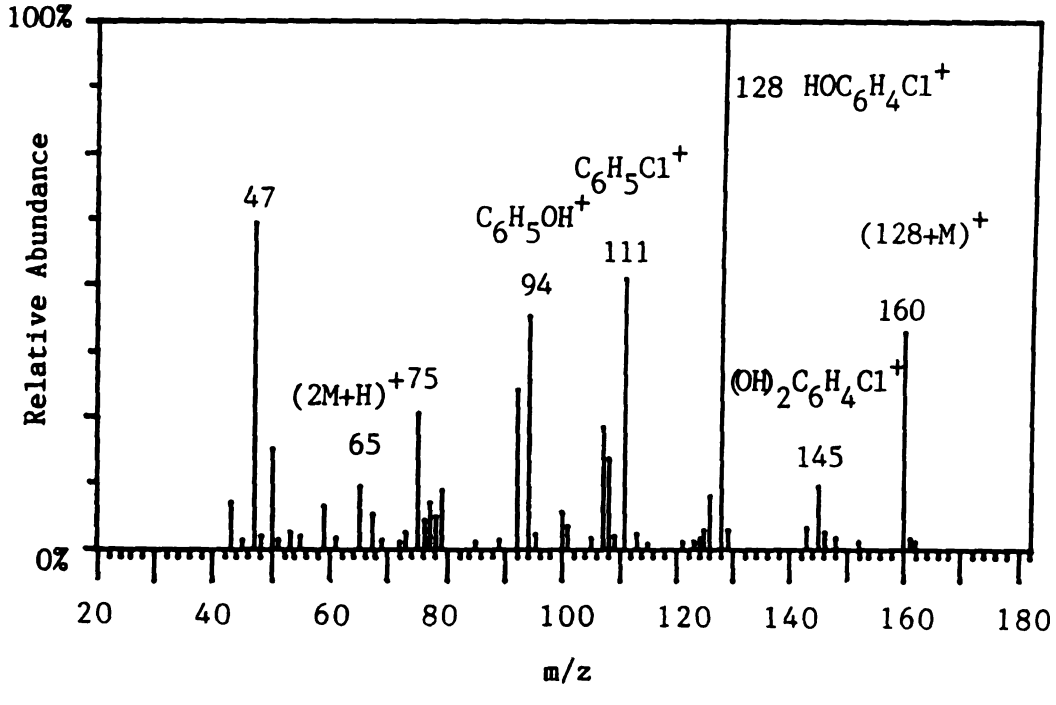

M=Methanol

Figure 90. The Product Spectrum of the Reaction Between the $(M-Cl)^+$ Ion of p-Dichlorobenzene and Methanol in the Central Quadrupole

ion at m/z 160 which has acted as an intermediate to form the $[(HO)_2 C_6H_4Cl]^+$ ion (m/z 145) through a $CH_3\cdot$ radical loss.

Identical reaction product scans are obtained when one uses o-, m, or p-dichlorobenzene, probably because of extremely rapid H and Cl 1,2 transfers around the ring. The dichlorobenzenes, however, do not produce an $(M-H)^+$ ion under 70 eV EI. In fact, many chlorinated or multi-substituted aromatic molecules do not produce $(M-H)^+$ ions. Therefore, when studying these more complicated aromatic molecules, one must be judicious in choosing which fragment ion to use if one wishes to observe the hydroxylation reaction.

The following example shows that one can also observe the hydroxylation reaction in the fragment ions of molecules that are not aromatic, but whose structural features can rearrange to form aromatic fragment ions. Arachidonic acid is a polyunsaturated fatty acid that is essential in human metabolism. Its structure and the FAB mass spectrum of the neat liquid are shown in Figure 91A. The FAB process produces in this case a large number of fragment ions and no protonated molecule. Most of the fragment ions are due to the unsaturated hydrocarbon chain, and when these fragment ions are reacted with methanol in the central quadrupole, the only product ions (besides CID ions) are due to proton transfer methanol. However, the product spectrum shown in Figure 91B is generated when the fragment ion from arachidonic acid (m/z 77) reacts with methanol in the central quadrupole. The appearance of the hydroxylation product (m/z 94) indicates that the m/z 77 fragment ion is the phenyl cation.

It is clear from all of the reactions studied in this chapter that the hydroxylation reaction of methanol is specific for aromatic ions

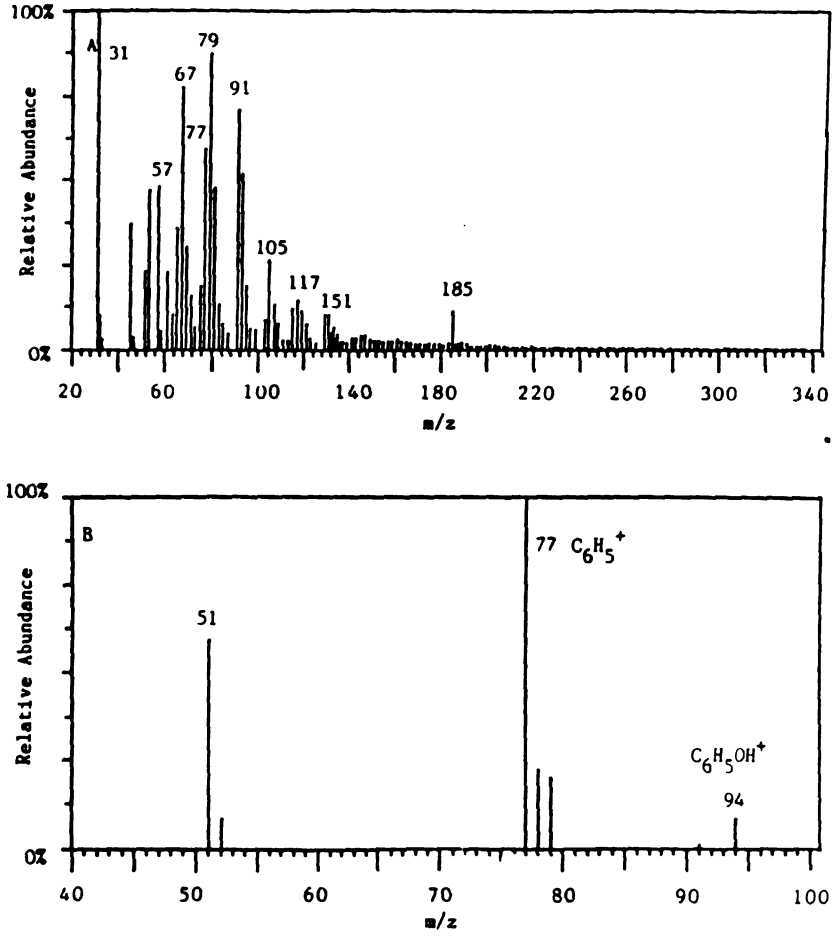

Figure 91. (A) FAB Mass Spectrum of Arachidonic Acid, and (B) the Product Spectrum of the m/z 77 Fragment Ion of Arachidonic Acid and Methanol in the Central Quadrupole

with vacant carbon sites on the ring, and that aliphatic or unsaturated carbocations simply do not react with methanol in this fashion. All of the ions tested that fit the criterion above do react to form the hydroxylation product. Therefore, the hydroxylation reaction is a technique for selective detection of aromatic compounds. Because of rapid scrambling of ring substituents, the hydroxylation reaction is not capable of distinguishing o-, m-, and p-isomers. The yields of the hydroxylation reaction in both the central quadrupole and the CI volume tend to be rather low except in the case of halogenated aromatic compounds in which the peak for the hydroxylated ion is frequently the base peak of the spectrum. For this reason, the hydroxylation reaction in either CI or the central quadrupole has significant potential as an analytical technique for the selective detection of halogenated or polyhalogenated aromatic and polycyclic aromatic compounds.

CHAPTER VIII.

ION/MOLECULE REACTIONS OF CARBONYL COMPOUNDS IN THE TQMS

A. Introduction

Reactions of carbonyl compounds in solution are among the most commonly used synthetic reactions in organic chemistry. As a result, there has been interest in the gas-phase chemistry of carbonyl compounds, particularly ketones, for over two decades. M. S. B. Munson (139) studied the reactions in acetaldehyde and in acetone by chemical ionization and speculated that the condensation products observed in gas-phase might have the same structure as those observed in solution, namely, those of acetaldol and diacetone alcohol.

The condensation reaction and the self acylation reaction of acetone have received considerable attention in the chemical literature. These reactions have been studied by ICR (140,141) and CI (142) with much emphasis on the kinetics and mechanisms. Some of the proposed mechanisms contradict one another (140,141), and even today the exact structures of the intermediates and products of these reactions remain in doubt.

The ion/molecule reactions of protonated carbonyls have also been studied (143), as have the reactions of carbonyls with other compounds such as ammonia (144), methanol (90), catechol (145), methyl ions (114), and amines (86) (Schiff base synthesis). The carbonyl reactions with ammonia (91) have been performed recently using the central quadrupole of triple quadrupole mass spectrometers (without ion trapping).

There has also been considerable interest in the negative ion reactions of carbonyls. Initially, the research into negative ion reactions employed fluorinated and chlorinated species (53,146) to carry the charge. More recently, species such as the NH_2^- and O^- ions have been reacted with carbonyls (159), and there has been interest in the reactions of carbonyl negative ions with other carbonyls (91) as a gas-phase analog of the Claisen condensation.

The thrust of the research in this chapter is to examine the structures of some of these products of carbonyl reactions that are currently in doubt by CI/CID, and to investigate in the central quadrupole of the TQMS some of the less studied carbonyl reactions, such as the ion/molecule reactions in esters and mixed carbonyl systems, and also the reactions of carbonyls with alcohols.

B. Experimental

1. Conditions for EI and CI

In those cases in which the parent ions were generated by EI, the pressure of the gas in the EI source was set at $5X10^{-6}$ torr by means of a needle valve. All of the compounds ionized by EI and CI in this study (acetone, ethylacetate, acetaldehyde, acetylacetone, methanol, and propanol) were volatile liquids that could be admitted through the liquids inlet of the TQMS.

In the cases where parent ions were generated by self-CI, the pressure of gas (as measured at the ion gauge at the throat of the ion source turbomolecular pump) was set at $8X10^{-5}$ torr by means of the same needle valve mentioned above. Several experiments were conducted using a mixture of gases in the CI volume. The partial pressures of the gases

(as measured by the ion gauge) were as follows: $1X10^{-4}$ torr acetone and $2X10^{-4}$ torr methanol; $5X10^{-5}$ torr ethylacetate and $5X10^{-5}$ torr propanol; $5X10^{-5}$ torr acetaldehyde and $5X10^{-5}$ torr methanol.

2. Conditions in the Central Quadrupole

The pressure of collision gas in the second quadrupole was regulated by a Granville-Phillips pressure controller. In all cases where EI or CI was the ionization method, whether the gas in the second quadrupole was argon for CID or a reactive gas for ion/molecule reactions, the pressure was regulated to be $8X10^{-4}$ torr. In all of the ion/molecule reactions carried out in the central quadrupole, ions were trapped for 50 msec unless specified otherwise in the text.

C. Results and Discussion

1. Ion/Molecule Reactions in Acetone

The mechanism proposed by W. J. van der Hart and H. A. van Sprang (141) for the reaction of the acetone molecular ion with acetone in the gas phase is shown in Scheme 10. The authors (141) who proposed Scheme 10 suggest that this scheme may be incomplete, but basically they postulate two separate and competing processes for the production of the acylated ketone product. These two pathways as shown in Scheme 12 are the self acylation reaction of the molecular ion with the neutral ketone, and the clustering reaction of the acetyl ion with the neutral ketone. Both of these reactions were observed in an ICR.

Another research group (143) investigated the reactions of protonated acetone in high pressure (up to 3 torr) mass spectrometry with photoionization. The reactions they observed are shown in Scheme

Scheme 10

Ion/Molecule Reactions in Acetone

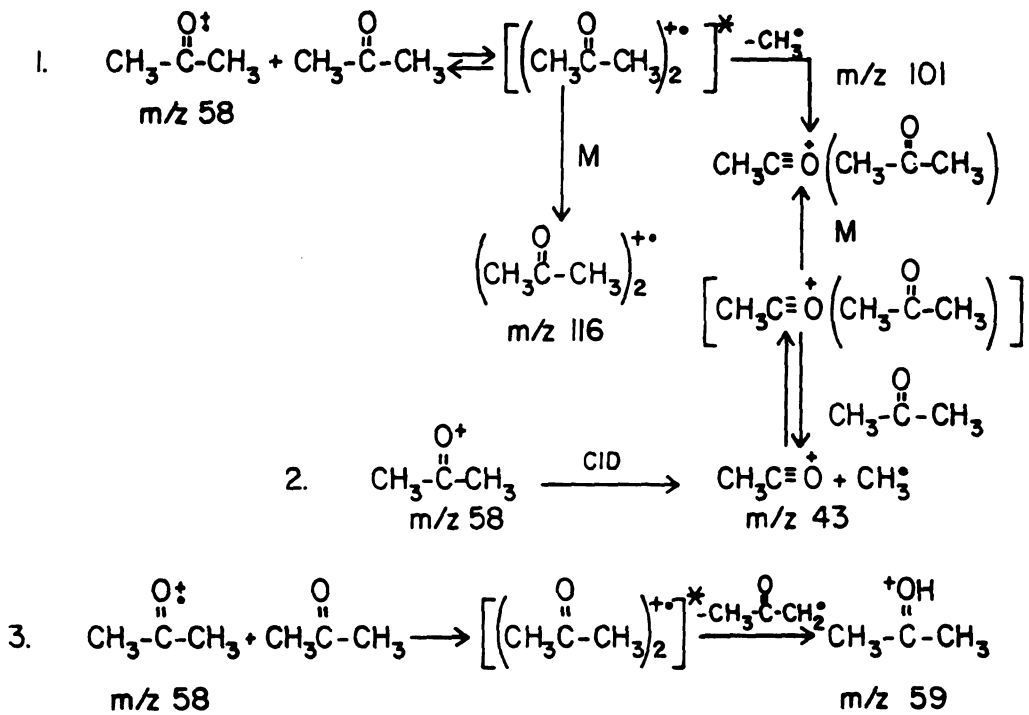

11. The equations in Scheme 11 reveal two mechanisms at work in the high pressure gas-phase reactions of acetone. The first is a reaction of the protonated molecule of acetone with up to five neutral acetone molecules to form protonated multimers, which in turn all lose water to form a $C_6H_{11}O^+$ ion of unknown structure that is coordinated with up to four neutral acetones. The second reaction is of protonated acetone with neutral acetones and water (which may be either adventitious or produced by the previous reaction) to form cluster ions which consist of a proton solvated with water and acetone molecules.

The author was very interested to determine whether the same reactions would be observed in the TQMS. The product spectrum of the reaction between the acetone molecular ion and neutral acetone in the central quadrupole shown in Figure 92 indicates that the self acylation reaction does, indeed, occur in the TQMS. The peak at m/z 101 is the correct mass for the self acylation product of acetone, $CH_3CO^+(CH_3COCH_3)$, and the acetone dimer (m/z 116) which is the proposed intermediate from Scheme 10 is observed. The proton-bound dimer of acetone is also observed because the molecular ion of acetone can transfer a proton to neutral acetone (see Scheme 10) which can then react according to Scheme 11 to form the proton-bound dimer.

Another possible explanation for the peak at m/z 101 is the formation of a covalently bonded species such as acetylacetone by an entirely different and unknown mechanism. To test this hypothesis, the author obtained the argon CID spectrum of the m/z 101 ion/molecule reaction product ion produced by acetone self-CI (see Figure 93A) and also obtained the CID spectrum of protonated acetylacetone (see Figure 93B). The CID daughter spectra in Figure 93 clearly show that the m/z

Scheme 11

Reactions of Protonated Acetone with Acetone

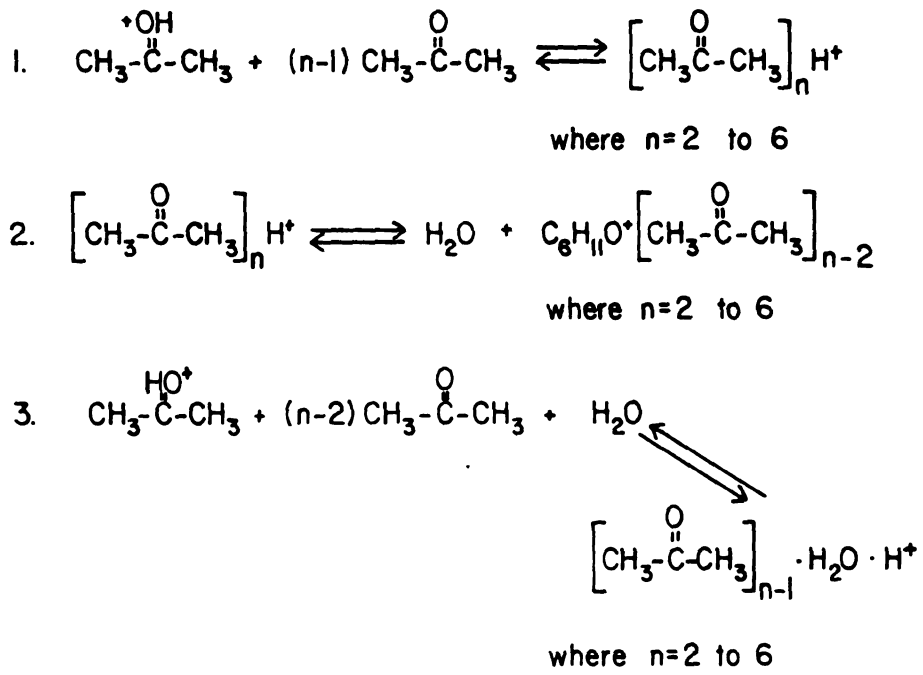

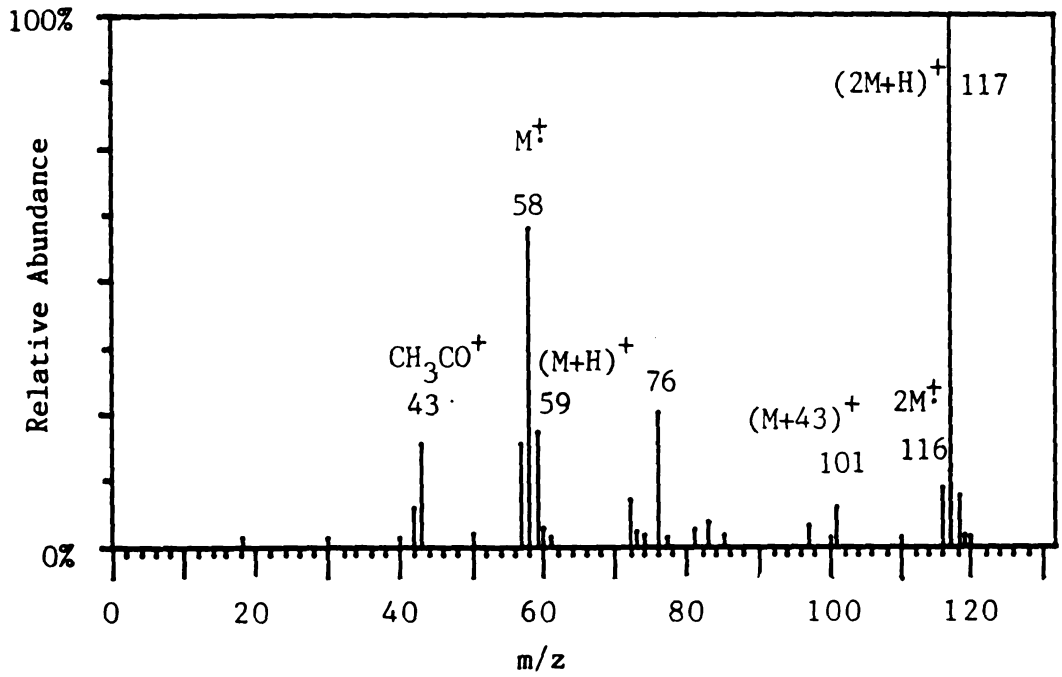

Figure 92. The Product Spectrum of the Reaction Between the M^+ Ion of Acetone and Neutral Acetone in the Central Quadrupole

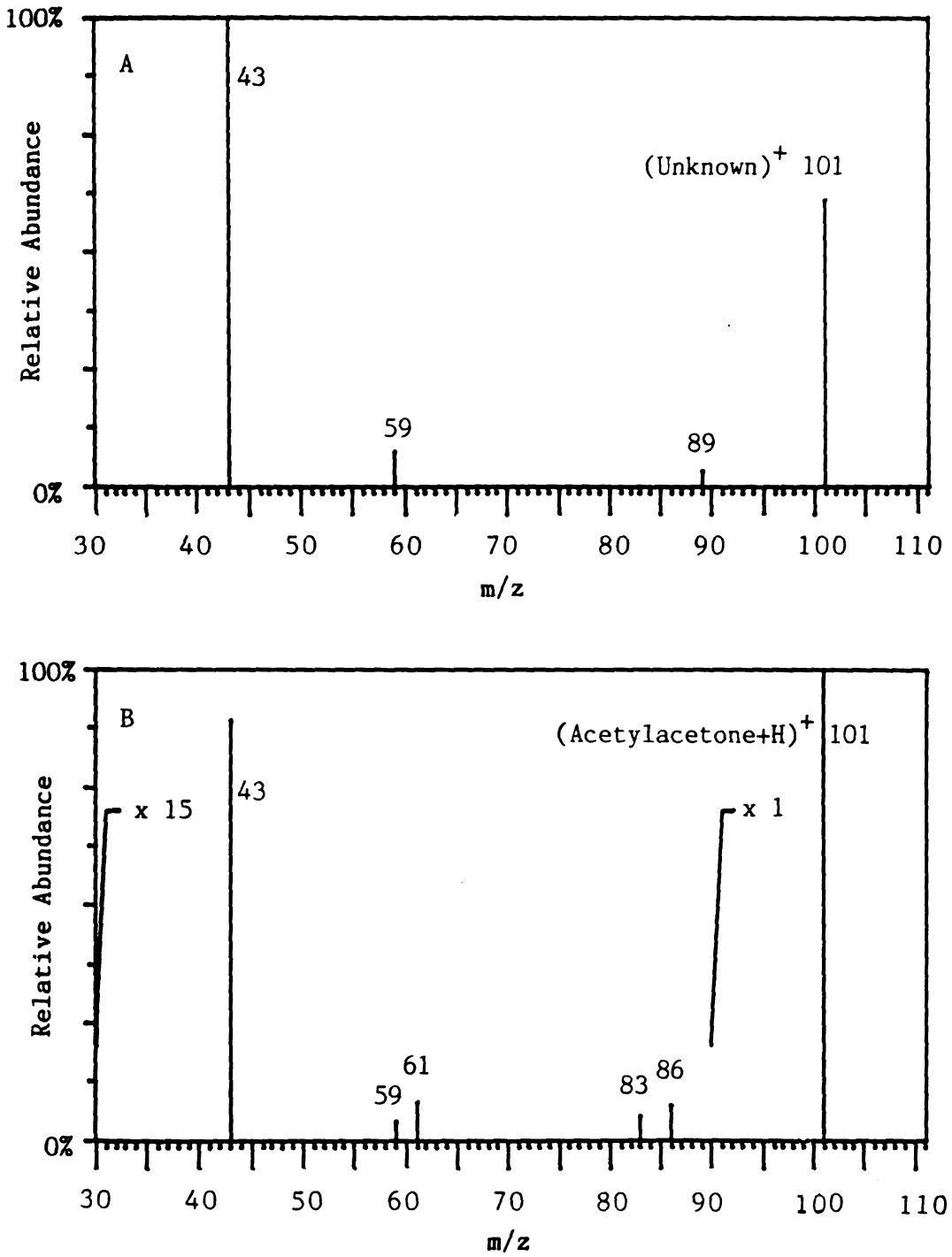

Figure 93. Argon CID Daughter Spectrum of (A) the m/z 101 Peak from Acetone Self-CI, and of (b) the Protonated Molecule of Acetylacetone

101 ion produced by the ion/molecule reactions in acetone is not protonated acetylacetone. This fact and the prominence of the acetyl ion (m/z 43) in ion/molecule product CID spectrum indicate that the structure of the m/z 101 ion is indeed that of a weakly bound cluster ion of the acetyl ion and acetone. These data add credence to the mechanism in Scheme 10.

When one chooses, instead, the protonated molecule of acetone as the parent to be reacted with acetone, the product spectrum shown in Figure 94 is the result. Figure 94 shows that the proton-bound dimer of acetone (m/z 117) is formed and that the dimer of acetone (m/z 116) is not. Both of these facts are in accordance with Scheme 11. The peak at m/z 101 is still present, however, because the acetyl ion reacts with neutral acetone to form the clustering product from Scheme 10.

The higher coordination number products suggested by Scheme 11 are not observed in Figure 94, and neither are the products due to loss of water or the mixed water and acetone clusters. These differences between the central quadrupole data and the high pressure MS data are probably due chiefly to the great difference in the pressure of neutral acetone in the two techniques.

The self-CI spectrum of acetone is shown in Figure 95. The products in the self-CI spectrum are similar to those in the central quadrupole for the reaction of protonated acetone with neutral acetone. As mentioned in the introduction to this chapter, Munson has proposed that some of the ion current in the m/z 117 peak in the self-CI spectrum of acetone (see Figure 95) might be due to diacetone alcohol. To test this hypothesis, the author obtained the argon CID daughter spectrum of the m/z 117 parent ion (see Figure 96). Unfortunately, the author was

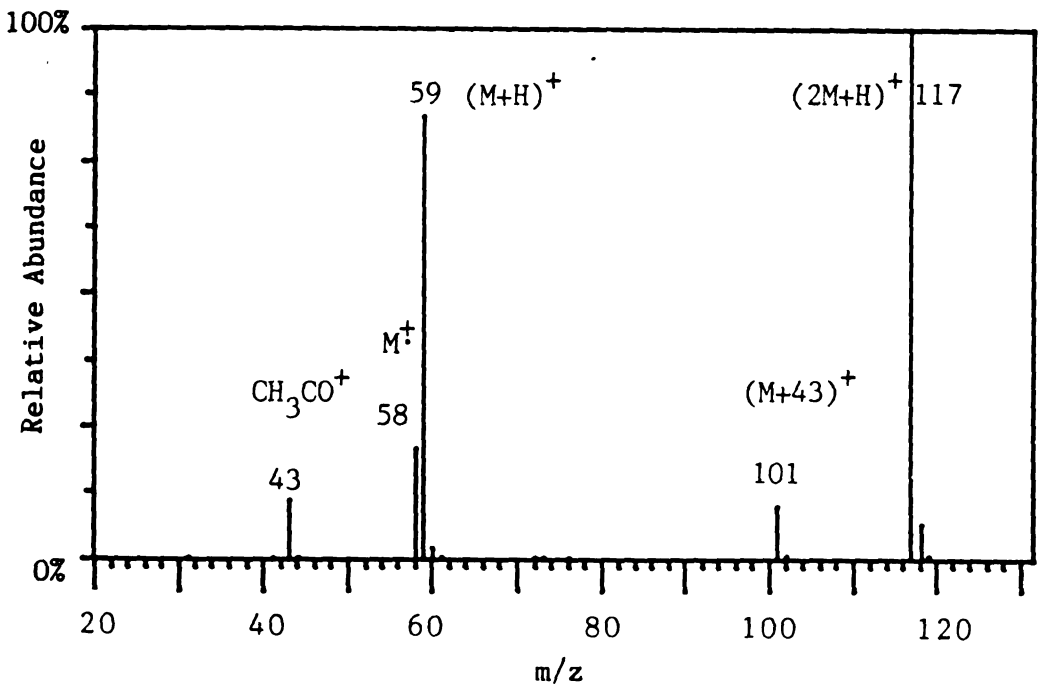

Figure 94. The Product Spectrum of the Reaction Between the Protonated Molecule of Acetone and Neutral Acetone in the Central Quadrupole

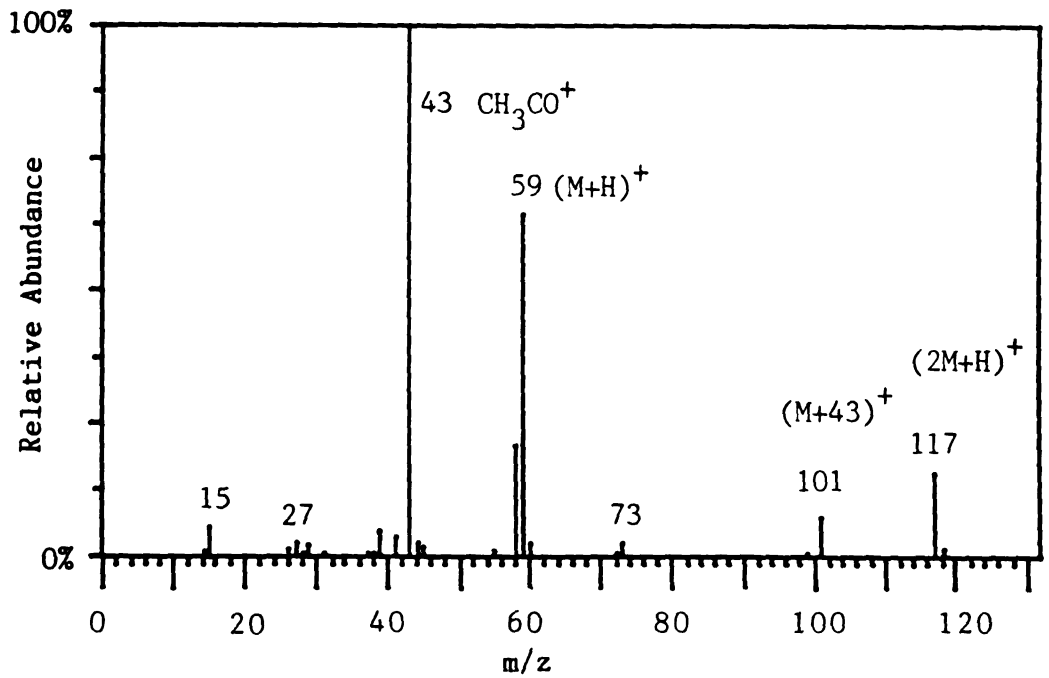

Figure 95. Self-CI Mass Spectrum of Acetone

not able to obtain a sample of pure diacetone alcohol, but the extremely large abundance of protonated acetone (m/z 59) as the sole daughter ion in Figure 96 argues strongly against the presence of more than a trace of the diacetone alcohol, and argues strongly for the proton-bound acetone dimer structure of the ion at m/z 117.

The major difference between the self-CI spectrum of acetone and the reaction of protonated acetone with neutral acetone in the central quadrupole is the presence of a peak at m/z 99 which according to Scheme 12 would represent the $C_6H_{11}O^+$ ion formed by water loss from the proton-bound dimer of acetone. The argon CID daughter spectrum of the proton-bound dimer shown in Figure 96 suggests, however, that the ion represented by the peak at m/z 99 does not arise from the decomposition of the proton-bound dimer. The argon CID daughter spectrum of the peak at m/z 99 is shown in Figure 97. The single prominent daughter ion peak at m/z 41 indicates that the parent ion originates from the clustering reaction of an acetone molecule with the C_2HO^+ ion (m/z 41) which is present in the acetone CI spectrum (see Figure 95). These data clearly do not support the mechanisms derived from high pressure MS studies (Scheme 12) except for the initial formation of the proton-bound dimer ion. Also, the lack of a peak at m/z 77 in the self-CI spectrum of acetone (see Figure 95), even at the highest pressures available in the TQMS, indicates that the clustering reaction of water and acetone (see Scheme 12) does not occur unless either the pressure is much higher or a considerable partial pressure of adventitious water is present in the system.

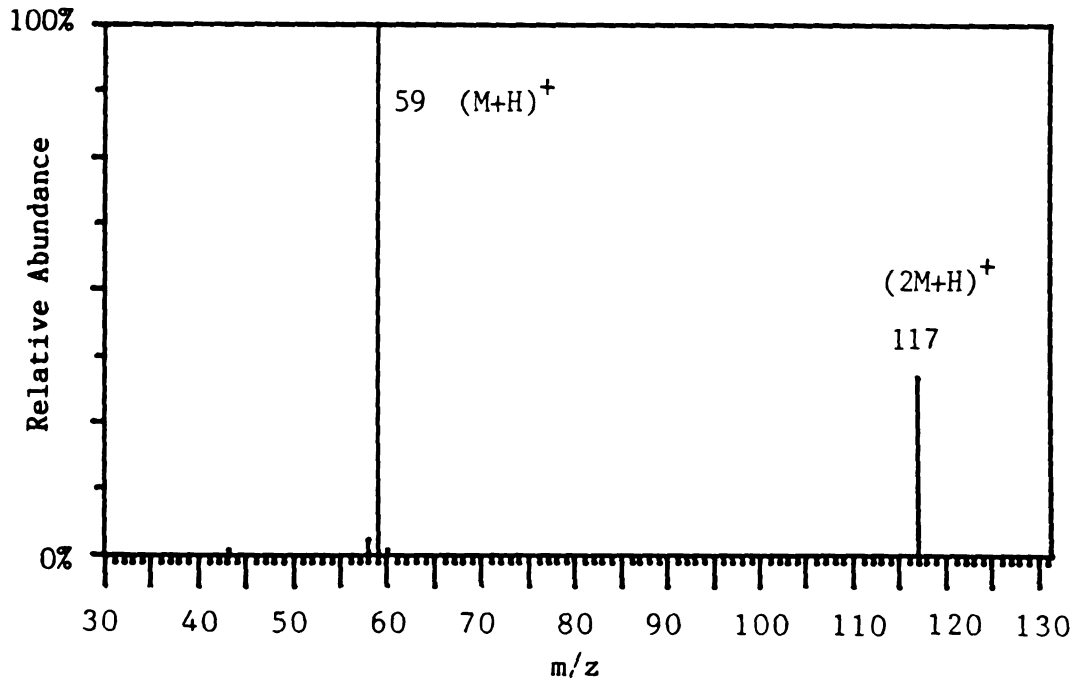

Figure 96. Argon CID Daughter Spectrum of the m/z 117 Peak from Acetone Self-CI

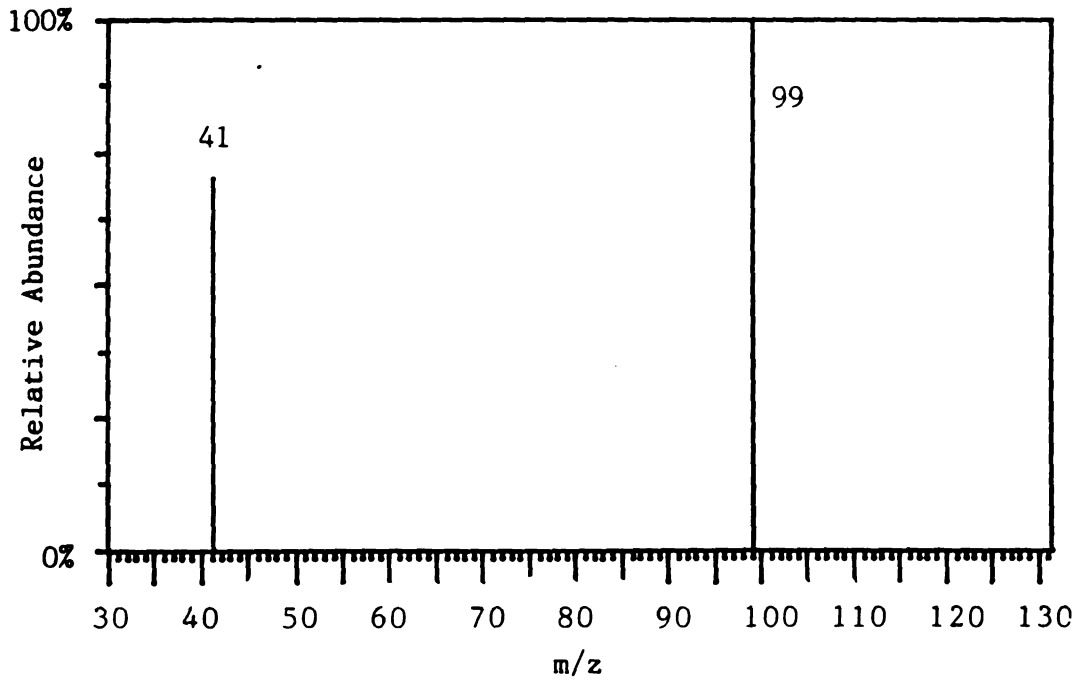

Figure 97. Argon CID Daughter Spectrum of the m/z 99 Peak from Acetone Self-CI

2. Ion/Molecule Reactions in Ethylacetate

The ion/molecule reactions that are typical of ketones should also be possible in other types of carbonyl compounds. This section investigates the ion/molecule reactions in the ester, ethylacetate. Figure 98 shows the product spectrum of the reaction between the protonated molecule of ethylacetate (m/z 89) and neutral ethylacetate in the central quadrupole of the TQMS. The product spectrum in Figure 98 does not employ ion trapping, unlike all of the other product spectra in this chapter. There are three CID daughter ions, at m/z 15, 29, 43, and 61. The ethyl ion (m/z 29), and the acetyl ion (m/z 43) are due to single bond cleavages. The m/z 61 ion is protonated acetic acid formed by a McLafferty rearrangement with a hydrogen shift and a bond cleavage. All four CID processes are shown in Scheme 12.

In addition to the CID daughter ions, one observes in Figure 98 two ion/molecule product ion peaks at m/z 131 and 177. The m/z 177 peak represents the proton-bound dimer ion of ethylacetate by analogy to the same reaction in acetone. The m/z 131 peak is probably the result of the reaction between the acetyl ion and protonated ethylacetate again by analogy to the same reaction in acetone. From this data, however, one cannot rule out that the m/z 131 peak is due to loss of ethanol from m/z 177. When one conducts the ion trapping experiment in the central quadrupole, the peaks at m/z 43 and 131 disappear from the spectrum as is shown in Figure 99. From Chapter IV. we know that the acetyl ion is difficult to trap since it is readily consumed by ion/molecule reactions, so its absence is not surprising. The interesting fact is that the m/z 131 peak has disappeared as well, indicating that the acetyl ion is its precursor ion.

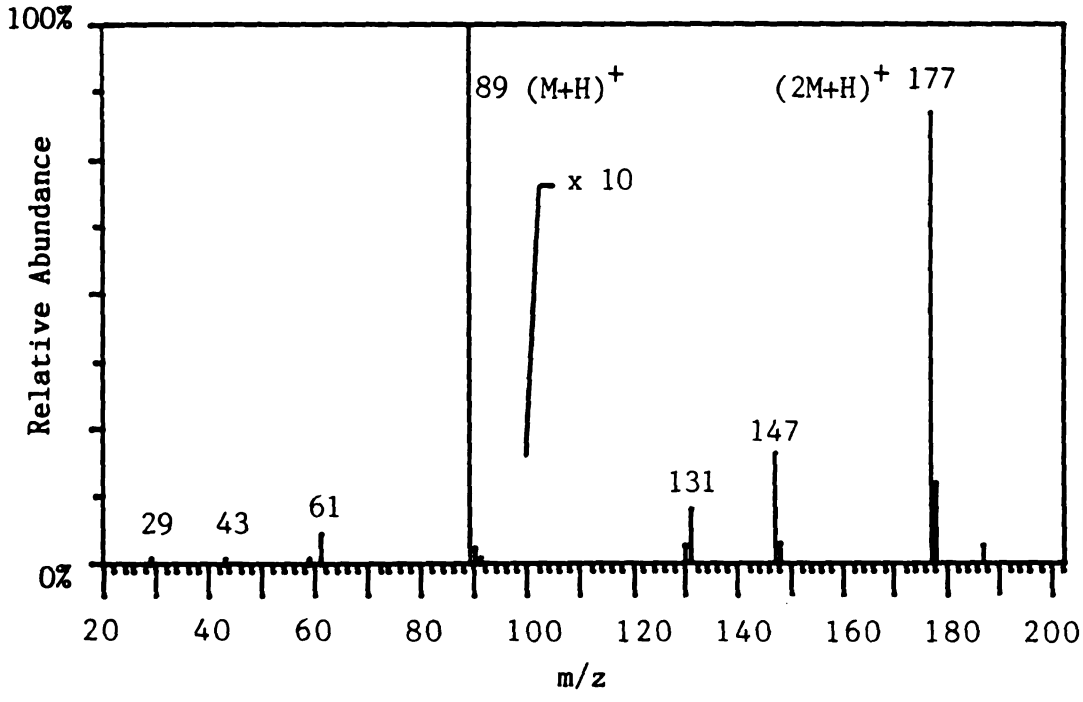

Figure 98. The Product Spectrum of the Reaction Between the Protonated Molecule of Ethylacetate and Neutral Ethylacetate in the Central Quadrupole Without Ion Trapping

Scheme 12

CID Processes in Protonated Ethylacetate

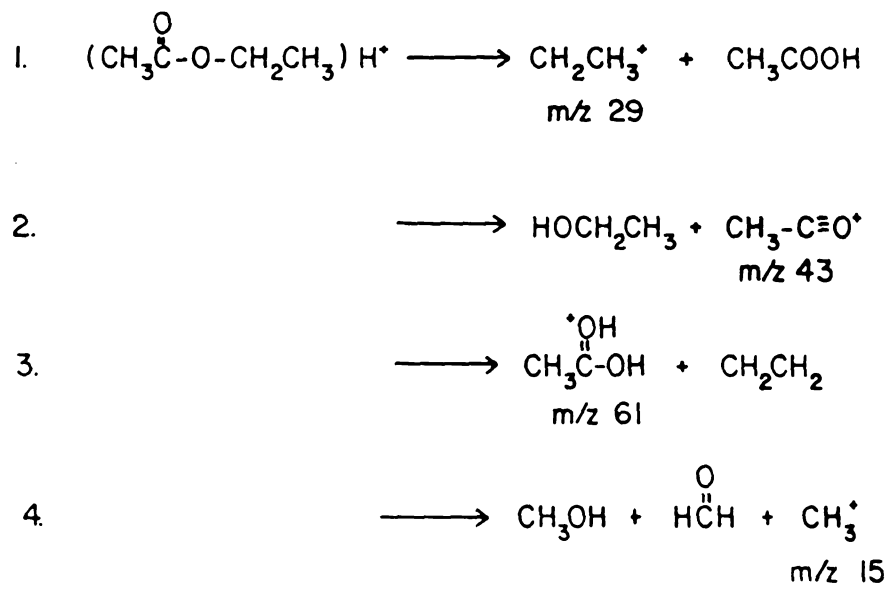

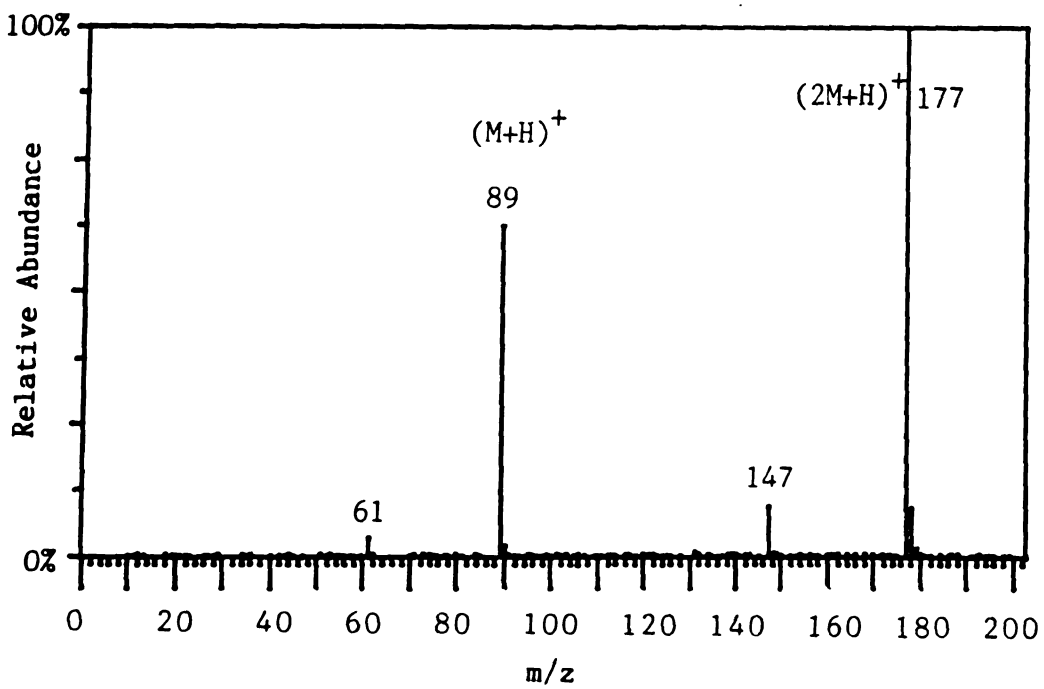

Figure 99. The Product Spectrum of the Reaction Between the Protonated Molecule of Ethylacetate and Neutral Ethylacetate in the Central Quadrupole With Ion Trapping

The spectrum in Figure 100 is the self-CI spectrum of ethylacetate. At the higher pressures present in CI, the fragment ions of ethylacetate are more abundant, but otherwise the product spectra generated in the central quadrupole and the CI volume are quite similar. The argon CID daughter spectrum of the peak at m/z 177 in the CI spectrum is shown in Figure 101. The extremely intense daughter ion peak at m/z 89 indicates that the parent ion is indeed the weakly bound proton-bound dimer of ethylacetate. The fact that no peak at m/z 131 is observed in the CID spectrum of the proton-bound dimer is confirmation that the m/z 131 ion does not result from decomposition of the proton-bound dimer.

The argon CID spectrum of the m/z 131 product ion peak from the self-CI spectrum of ethylacetate is shown in Figure 102. The presence of both protonated ethylacetate and the acetyl ion as abundant ions in this spectrum indicates that the ion at m/z 131 has a weakly bound cluster ion with the following structure: $CH_3CO^+(CH_3COOCH_2CH_3)$. Mechanisms for the formation of the major ion/molecule products in ethylacetate are shown in Scheme 13. The data in this section indicate that identical mechanisms form the major ion/molecule products in both acetone and ethylacetate.

3. Ion/Molecule Reactions in a Mixture of Acetone and Ethylacetate

Since acetone and ethylacetate appear to react with the same mechanism, one would predict that they react with one another to form products similar to those observed in this chapter. It has already been

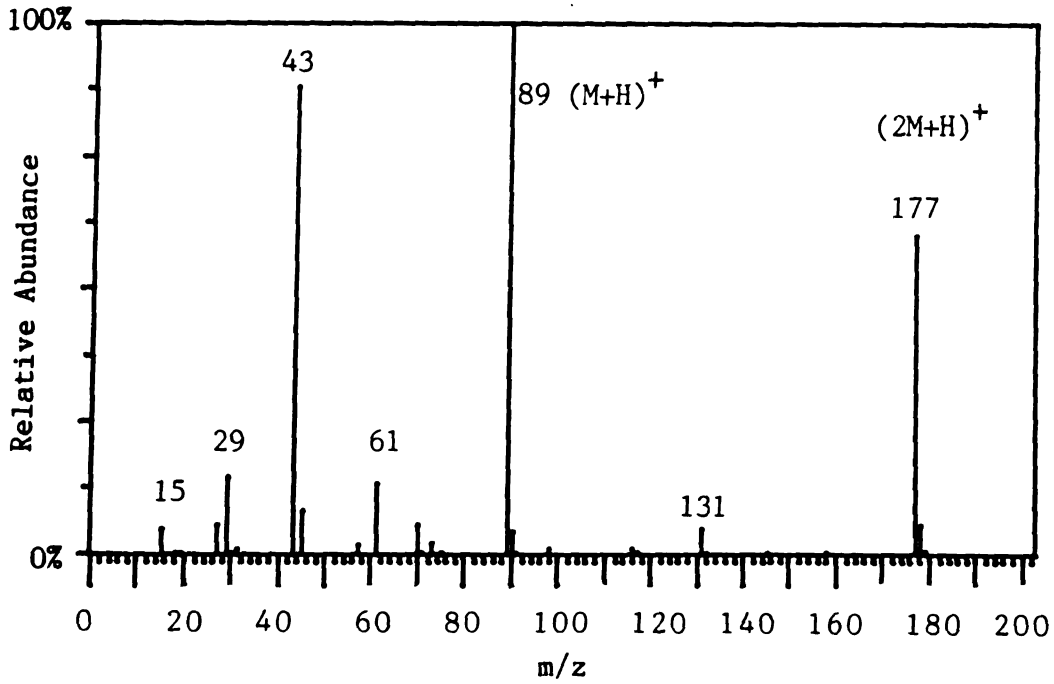

Figure 100. Self-CI Mass Spectrum of Ethylacetate

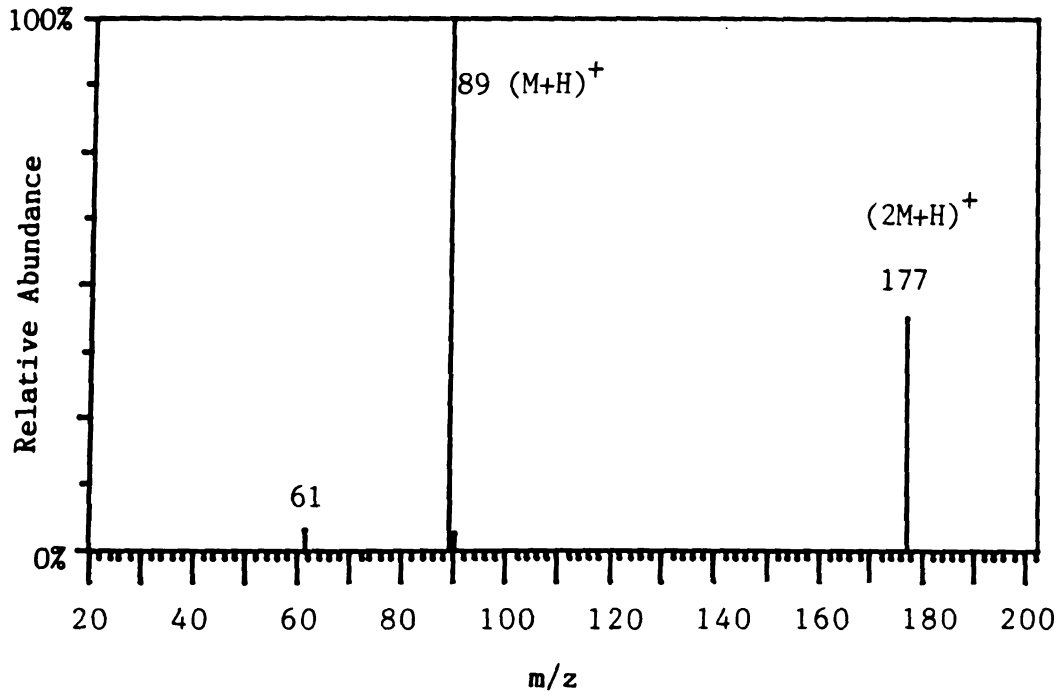

Figure 101. Argon CID Daughter Spectrum of the m/z 177 Peak from the Self-CI of Ethylacetate

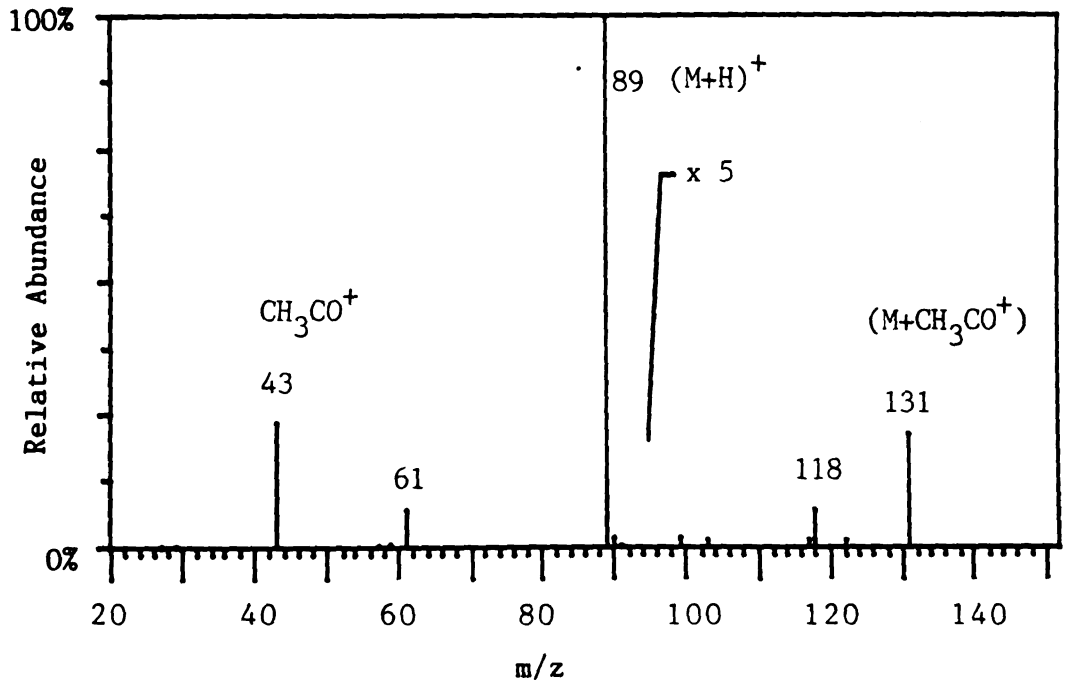

Figure 102. Argon CID Daughter Spectrum of the m/z 131 Peak from the Self-CI of Ethylacetate

Scheme 13

Reactions of Protonated Ethylacetate with Ethylacetate

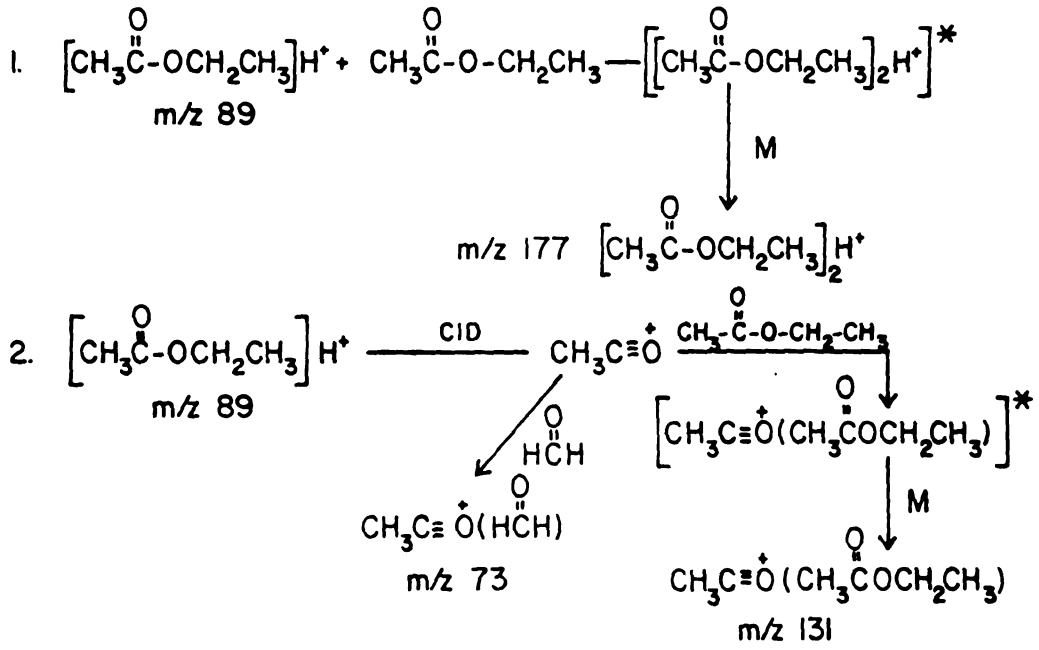

reported in Chapter II. that methyl esters react with protonated acetone in CI to form chiefly the proton-bound adducts of the ester and acetone. Therefore, this section will concern itself with reactions of the molecular ions, not the protonated ions.

The product spectrum of the reaction between the molecular ion of ethylacetate and neutral acetone in the central quadrupole is shown in Figure 103. The most prominent product peaks are those at m/z 59 and 117, representing the protonated monomer and dimer of acetone, respectively. A minor peak at m/z 146 is the adduct of acetone and ethylacetate, but it is important in that it serves as the intermediate in the reactions that produce the peaks at m/z 59, 117, and also m/z 131. The peak at m/z 131 represents the acylated ethylacetate ion. The ethylacetate molecular ion does not decompose as readily as acetone by CID, so the acetyl ion which is often a major peak in carbonyl spectra is quite diminutive. One can ascribe the peak at m/z 101 to the reaction of the acetyl ion with neutral acetone to form the clustering ion. One cannot, however, consider the peak at m/z 131 to be produced from the clustering reaction of the acetyl ion and ethylacetate because there is no appreciable amount of neutral ethylacetate in the central quadrupole. Scheme 14 shows the major reactions that occur as a result of reacting the acetone molecular ion with ethylacetate.

Reactions 1-4 in Scheme 14 are the major pathways in the reactions between the ethylacetate molecular ion and acetone, and reactions 5 and 6 are minor pathways due to the relatively low abundance of the acyl ion. A number of peaks with minor abundances in Figure 103 are not taken into account in Scheme 14 , so the processes occurring in the central quadrupole are probably even more complicated than indicated.

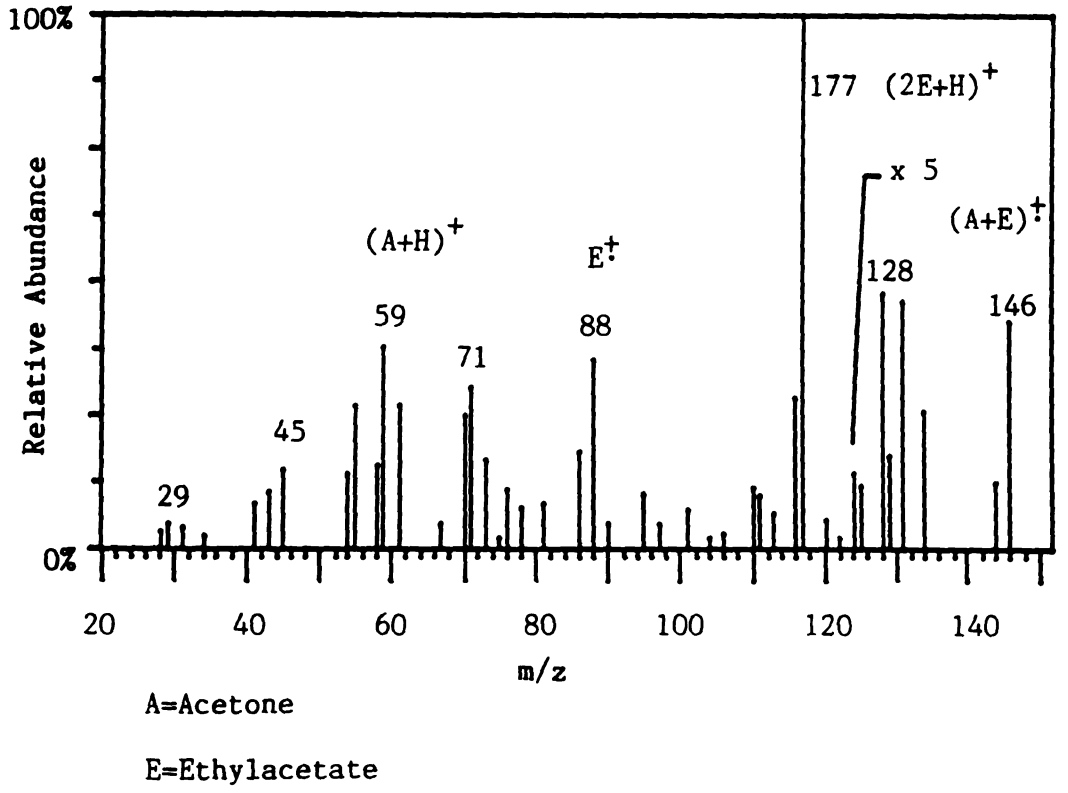

Figure 103. The Product Spectrum of the Reaction Between the $M^{+\cdot}$ of Ethylacetate and Acetone in the Central Quadrupole

Scheme 14

Reactions of the Ethylacetate Molecular Ion with Acetone

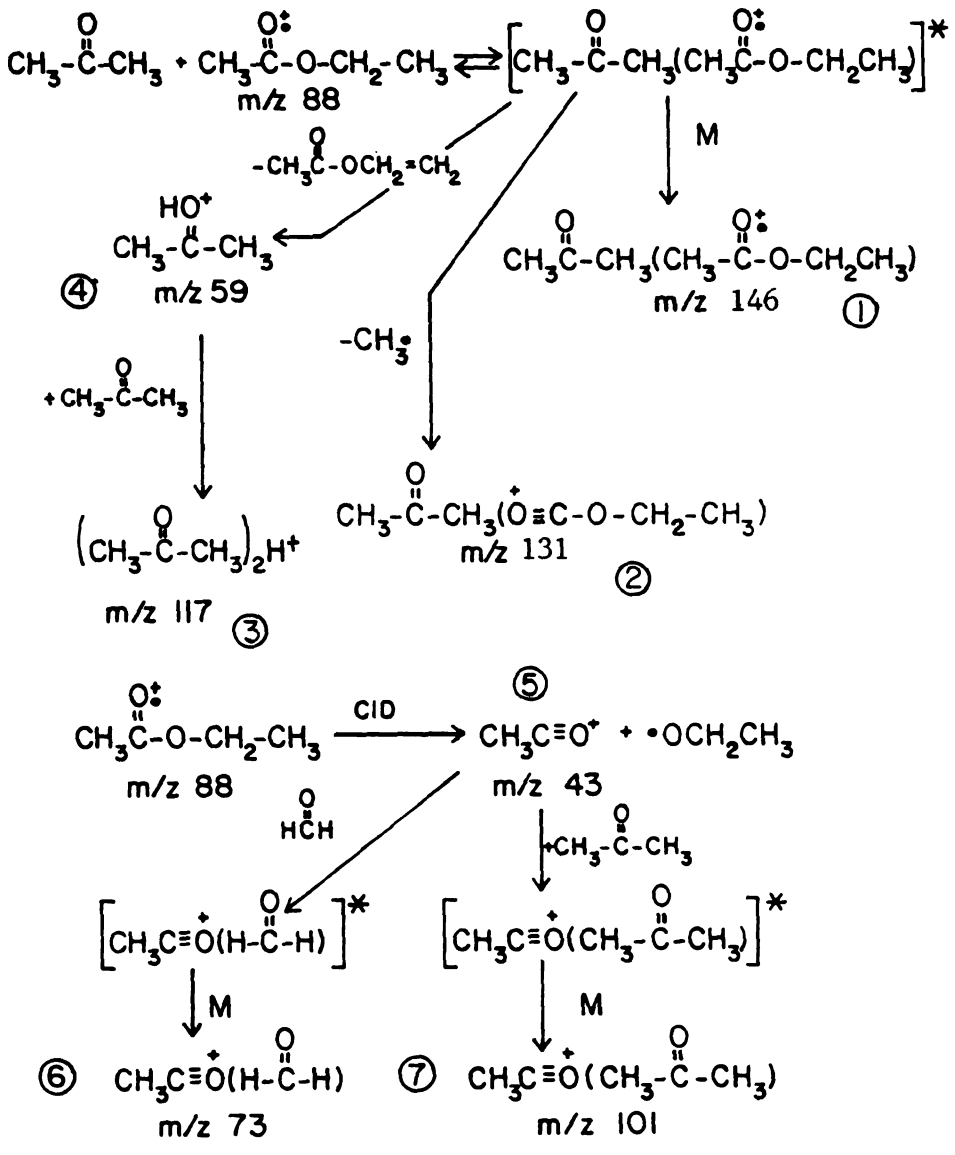

The TQMS has the unique ability to select either reactant as the charged species because the ionization occurs in a separate chamber from the ion/molecule reaction. In some cases, (as in the reaction between alcohols and acids in Chapter V.) choosing which reactant carries the charge has no effect on the products of the reaction. In this case, however, choosing acetone to carry the charge instead of ethylacetate changes the product spectrum dramatically. Figure 104 shows the products spectrum that results from the ion/molecule reaction between the molecular ion of acetone and neutral ethylacetate in the central quadrupole. The most abundant product ion peak in Figure 104 is m/z 43, the acetyl ion, which arises from the facile CID of the acetone parent ion. The acetyl ion dominates the product ion spectrum to the extent that one does not observe the m/z 146 peak which was the intermediate ion to the major pathways in Scheme 14. Instead one observes a peak at m/z 147, which corresponds to the proton-bound adduct of acetone and ethylacetate. One also observes a greatly increased relative intensity for the peaks at m/z 89 (protonated ethylacetate), m/z 131 (cluster ion of acetyl and ethylacetate), and m/z 73 (cluster ion of m/z 43 and formaldehyde; see Scheme 12 for the origins of neutral formaldehyde). Scheme 15 shows a proposed mechanism for the production of these ions.

The fact that the molecular ion of acetone dissociates more readily than the ethylacetate molecular ion to form the acetyl ion changes the products of the reaction between acetone and ethylacetate and changes the mechanism by which the products are formed. In a single chamber ion/molecule reactor (like CI), these changes are difficult to observe, but in the central quadrupole of the TQMS the differences are

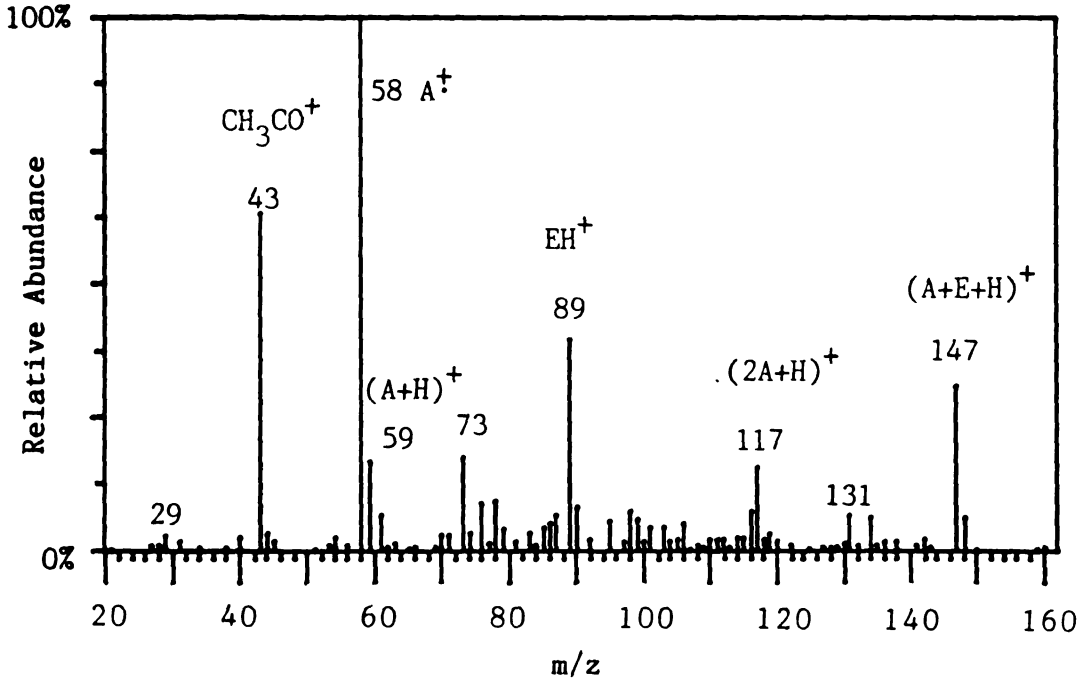

A=Acetone

E=Ethylacetate

Figure 104. The Product Spectrum of the Reaction Between the $M^+\cdot$ of Acetone and Ethylacetate in the Central Quadrupole

Scheme 15

Reactions of the Acetone Molecular Ion with Ethylacetate

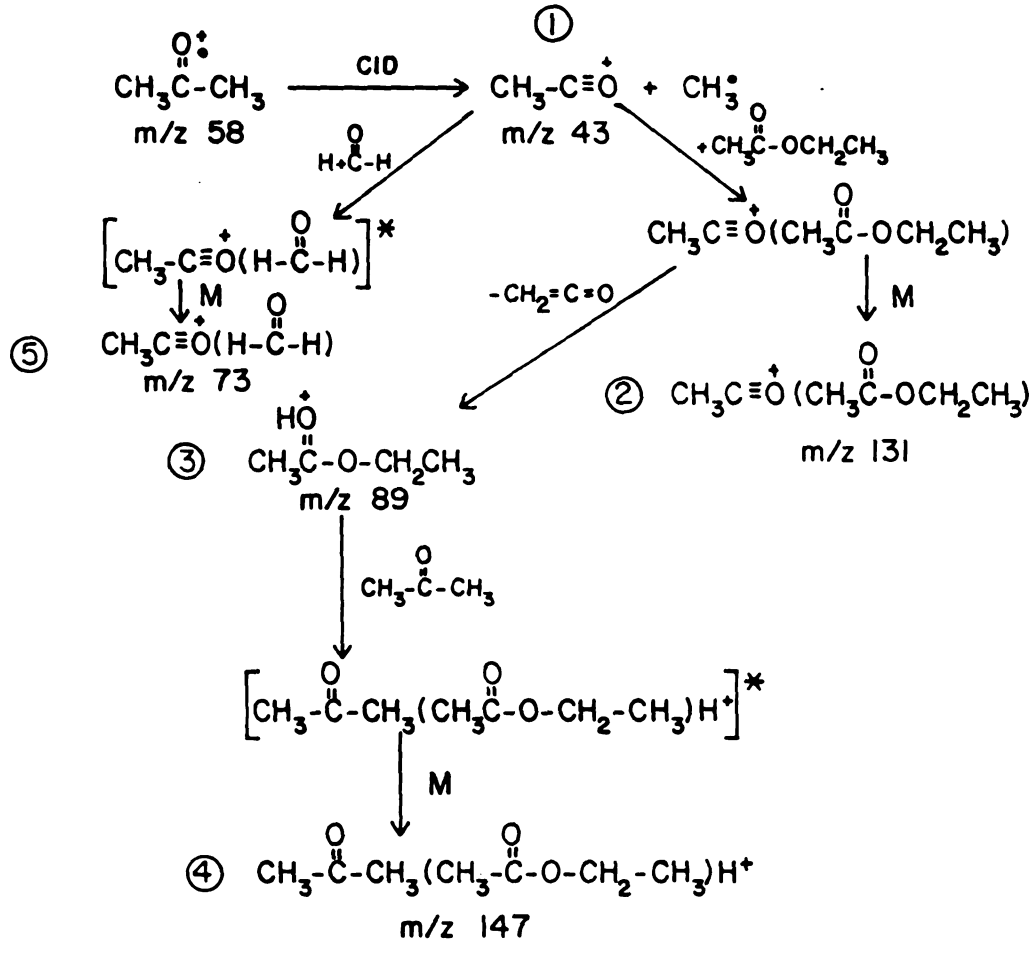

obvious because one can choose which of the two reactants carries the charge.

4. Ion/Molecule Reactions in Acetaldehyde

The ion/molecule reactions in acetaldehyde CI are very similar to those in acetone and ethylacetate CI. Figure 105 shows the self-CI spectrum of acetaldehyde. One observes the protonated molecule of acetaldehyde at m/z 45, the molecular ion of acetaldehyde at m/z 44, and three fragment ions at m/z 43 (CH_3CO^+), m/z 29 (CHO^+), and m/z 15 (CH_3^+). One also observes numerous cluster ions above the mass of the protonated molecule. The most prominent of these cluster ions is at m/z 89 which represents the proton-bound dimer of acetaldehyde. The argon CID daughter spectrum of the peak at m/z 89 (see Figure 106) shows that the parent ion is indeed the proton-bound dimer since the only daughter ion is the protonated molecule of acetaldehyde (m/z 45). It also shows that the low intensity peaks at m/z 59 and 87 in the CI spectrum are not due to decomposition of the proton-bound dimer. The daughter spectrum of m/z 87 is shown in Figure 107 and indicates that this ion is the cluster ion of the acetyl ion and neutral acetaldehyde. Scheme 16 shows the mechanism for the production of ions in acetaldehyde CI.

The mechanism in Scheme 16 is very similar to the mechanisms for acetone and ethylacetate with the exception that the acetaldehyde molecule seems to form protonated multimers more easily than either acetone or ethylacetate.

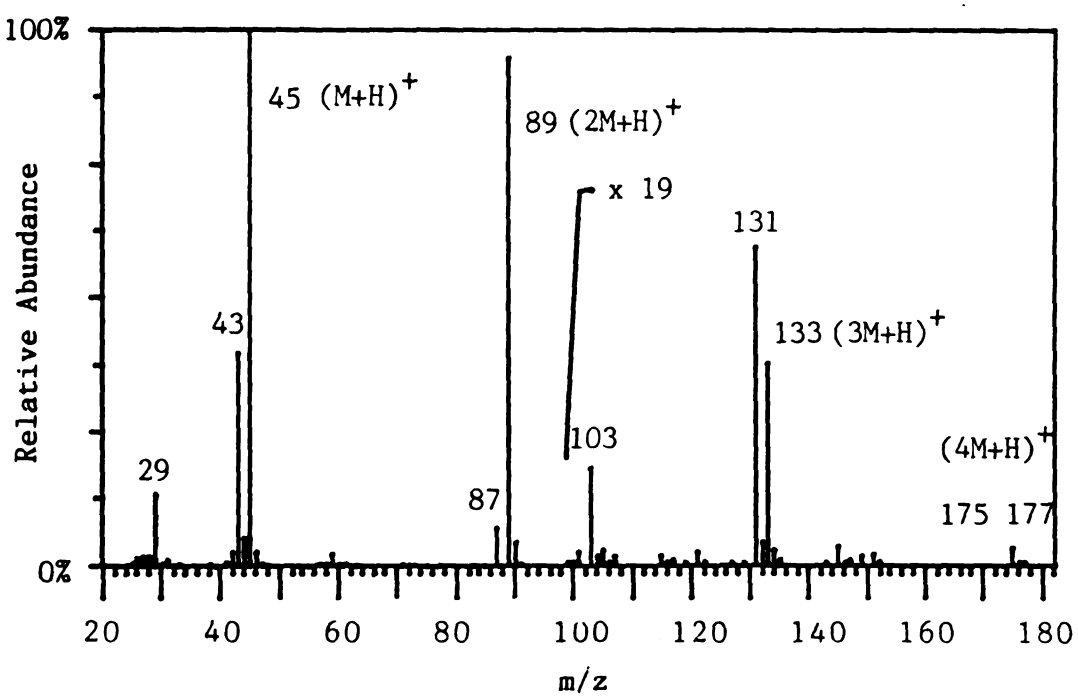

Figure 105. Self-CI Mass Spectrum of Acetaldehyde

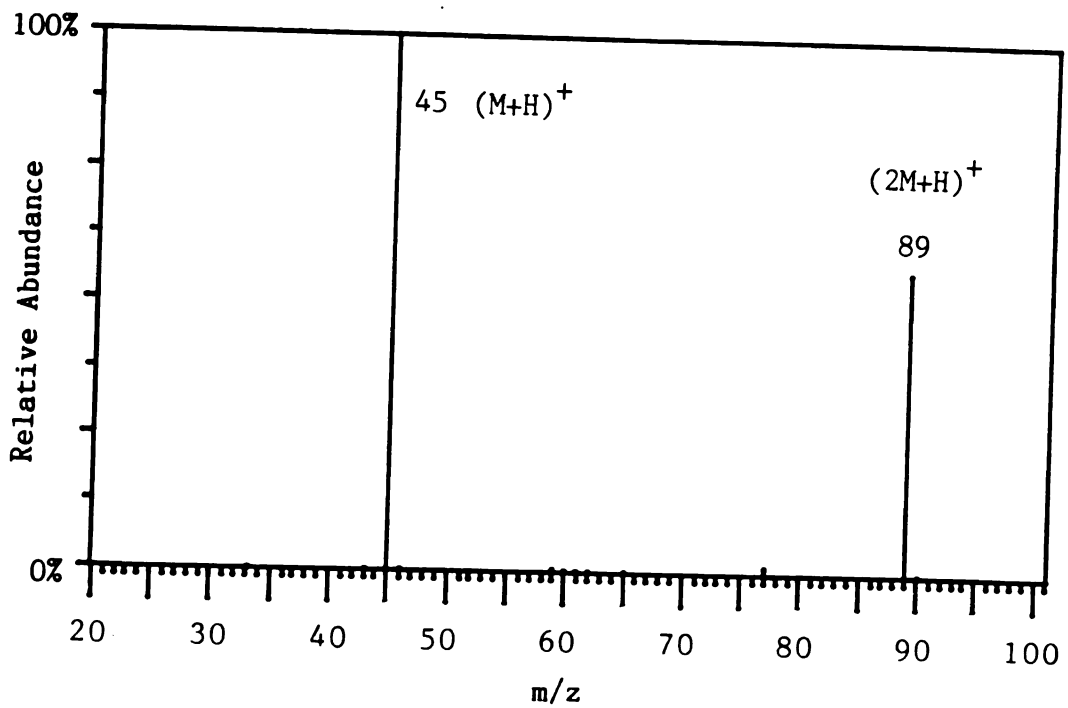

Figure 106. Argon CID Daughter Spectrum of the m/z 89 Peak from Acetaldehyde Self-CI

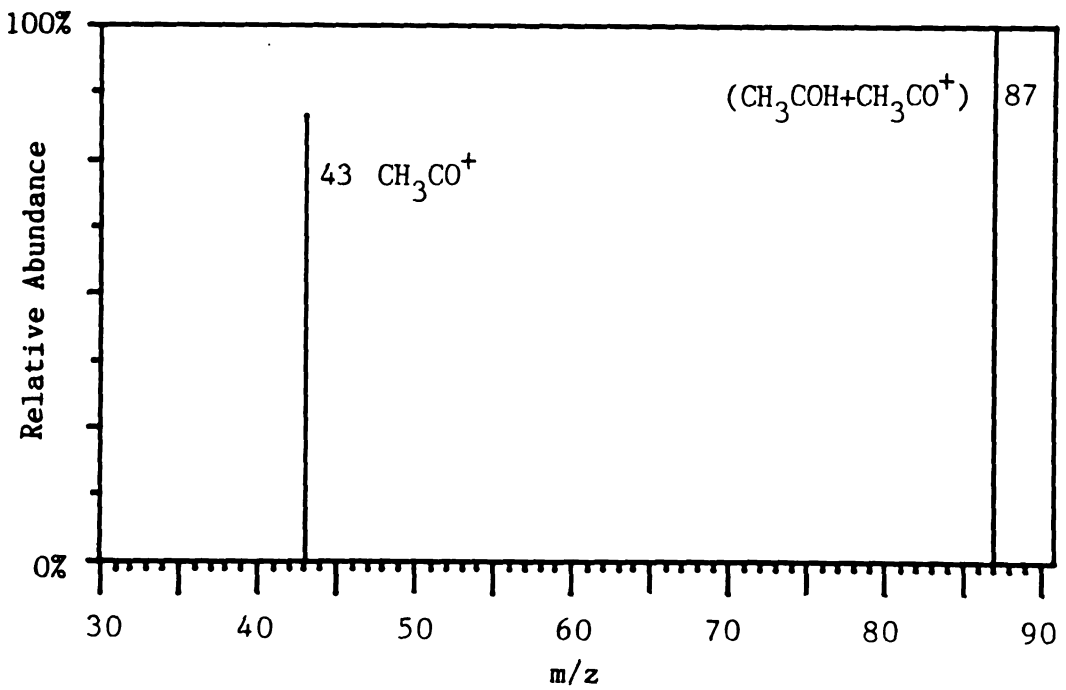

Figure 107. Argon CID Daughter Spectrum of the m/z 87 Peak from Acetaldehyde Self-CI

Scheme 16

Ion/Molecule Reactions in Acetaldehyde

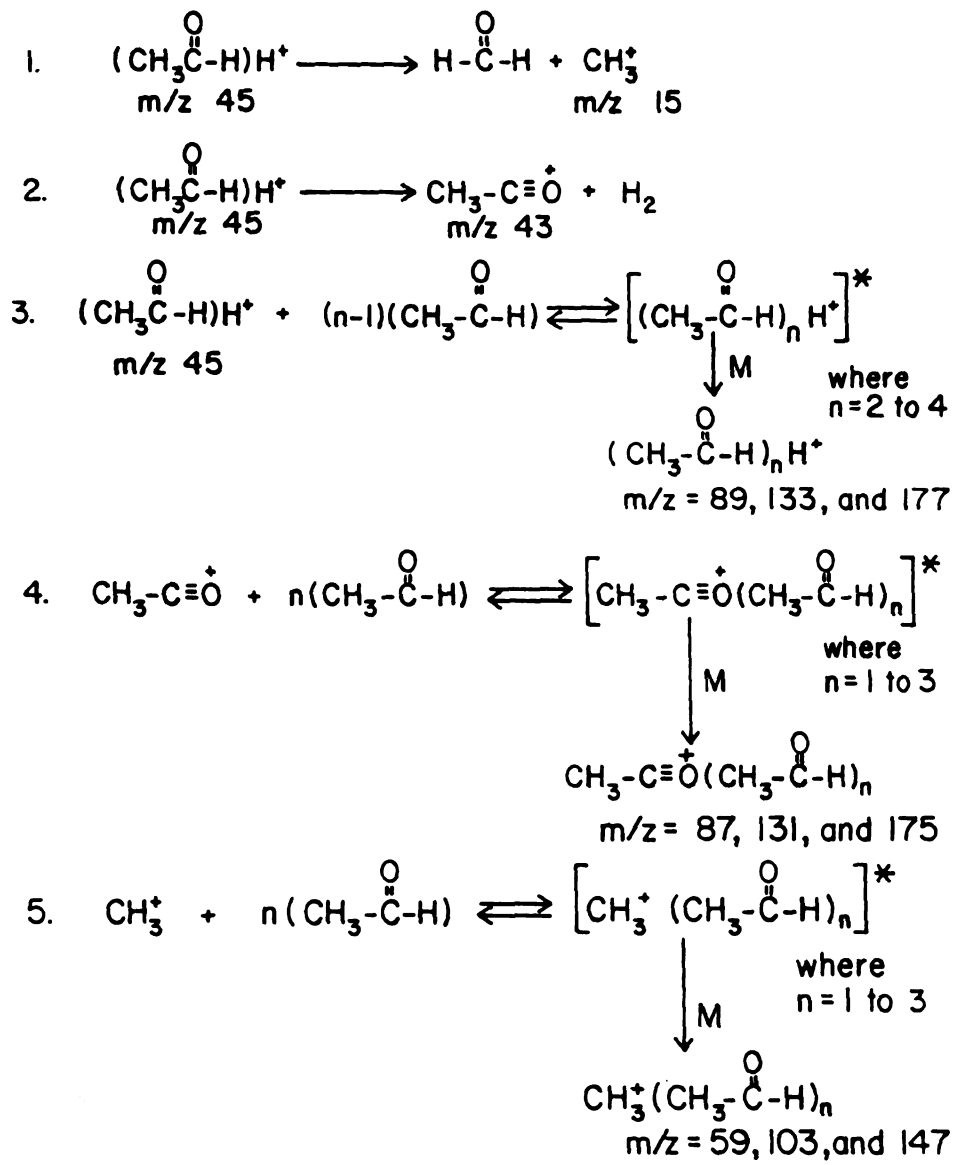

5. Ion/Molecule Reactions in Methanol/Acetone and Methanol/Acetaldehyde Mixtures

It is clear from the previous sections that carbonyl compounds of various types interact with themselves and each other in the gas phase to form a variety of weakly bound cluster ions. From the discussion in Chapter V. of this dissertation, it is apparent that the reactions of alcohols with acetic acid (which contains a carbonyl group) produce covalently bound species as well as cluster ions. With the hope of discovering more reactions of this type, the author explored the reactions of protonated acetone and protonated acetaldehyde with methanol.

Figure 108 shows the product spectrum of the reaction in the central quadrupole between the protonated molecule of acetone and neutral methanol. The predominant process is CID to form the acetyl ion. There is a low intensity peak at m/z 33 which indicates proton transfer to methanol. The peak at m/z 91 is representative of the proton-bound adduct of acetone and methanol. The peak at m/z 76 is probably the adduct of water and acetone.

Figure 109 shows the CI spectrum of a mixture of acetone and methanol. The CI spectrum shows all of the peaks associated with the ion/molecule reactions in methanol (m/z 15, 33, 47, 65, 79, and 97; see Chapter V.), and all of the peaks associated with ion/molecule reactions in acetone. When these peaks are taken into account, the remaining peaks are m/z 76, 91, 123, and 149. The m/z 76 and 91 peaks are familiar from Figure 108, and at the higher pressures in CI, the reaction produces the $(M+2A+H)^+$ ion (M=methanol, A=acetone) (m/z 149), and the $(A+2M+H)^+$ ion (m/z 123).

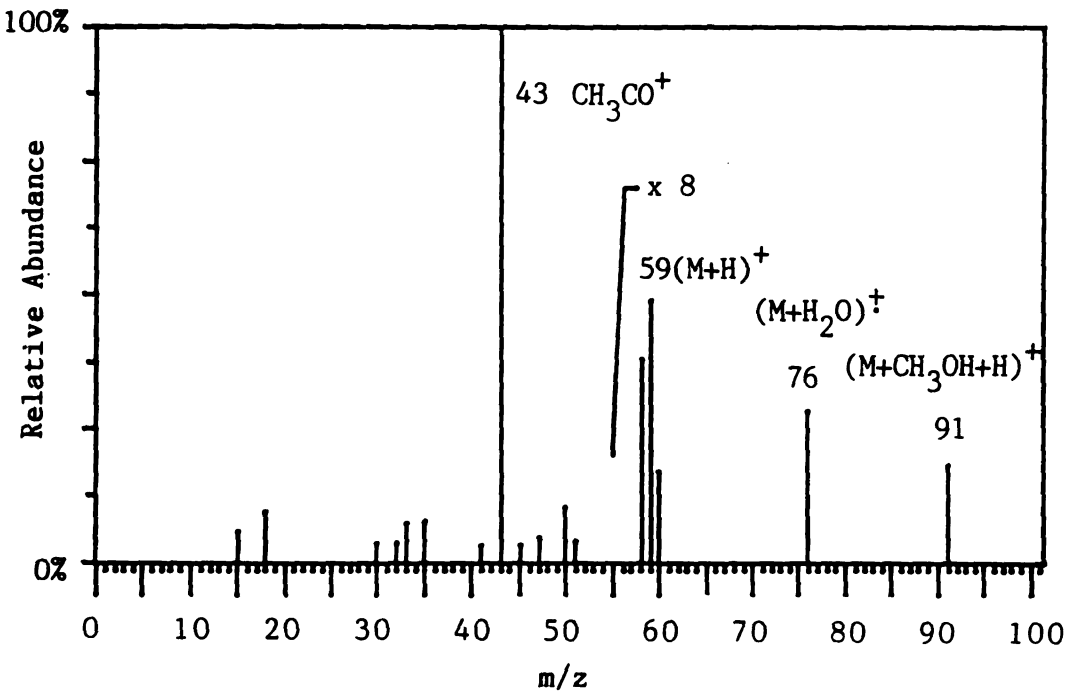

Figure 108. The Product Spectrum of the Reaction Between the M^+ of Acetone and Methanol in the Central Quadrupole

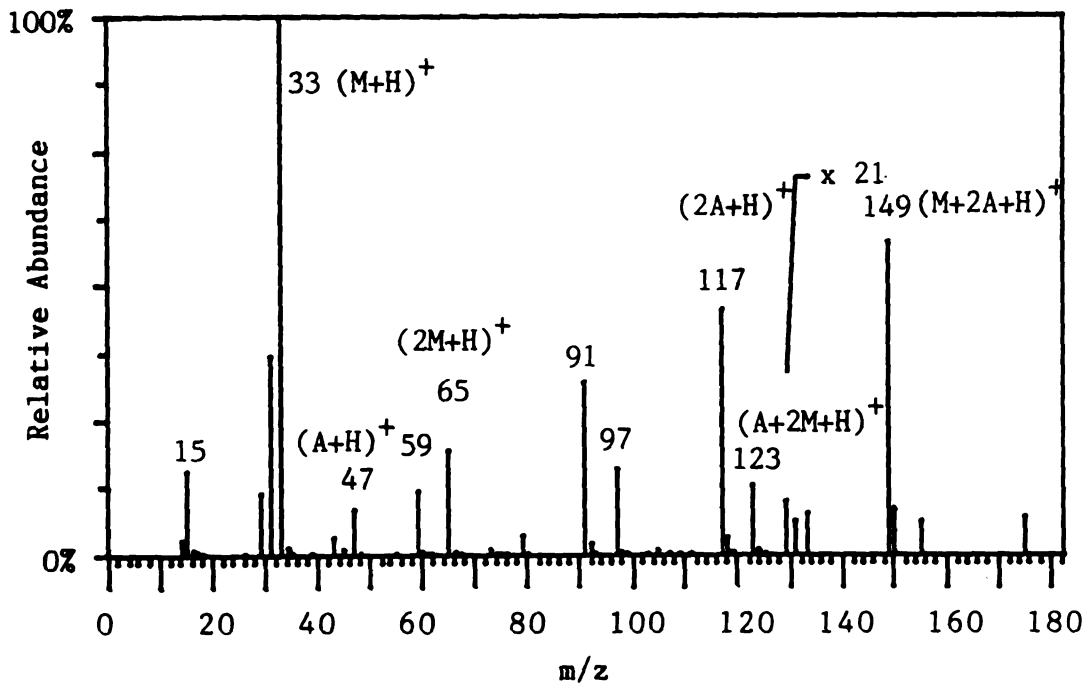

Figure 109. CI Mass Spectrum of a Mixture of Acetone and Methanol in the CI Volume

The reactions between the protonated molecule of acetaldehyde and methanol are altogether different. Figure 110 shows the product spectrum of that reaction as it occurs in the central quadrupole. One observes, of course, the parent ion peak at m/z 45 and the peak for protonated methanol at m/z 33, but the base peak of the spectrum is at m/z 59. The author checked the purity of the methanol being leaked into the central quadrupole, since the m/z 59 peak could easily be due to acetone dissolved in the methanol. Both the acetaldehyde and the methanol used for this experiment were HPLC grade, and under EI conditions showed no peak at m/z 58. Therefore, since the m/z 59 peak was not due to an impurity, it must have been generated by the reaction of protonated acetaldehyde and methanol. In addition to the m/z 59 ion, there are a large number of peaks with low intensity, indicating that there are numerous other products being formed that subsequently decompose during the ion-trapping phase of the experiment. In fact, the m/z 77 peak which represents the proton-bound adduct of acetaldehyde and methanol is a very minor peak which decreases in relative abundance with ion trapping.

The ions which decomposed in the central quadrupole were collisionally stabilized by the higher pressures in CI, as is shown in Figure 111. In addition to producing m/z 59, mixing acetaldehyde and methanol in the CI volume yields product ions at m/z 77, 91, 103, and 117. The peak at m/z 117 is the proton-bound dimer of m/z 59 as is shown by its argon CID spectrum in Figure 112. The peak at m/z 103 represents the proton-bound adduct of m/z 59 and acetaldehyde as is shown by its CID spectrum in Figure 113. The peak at m/z 91 is the proton-bound adduct of m/z 59 and methanol as is shown by its CID

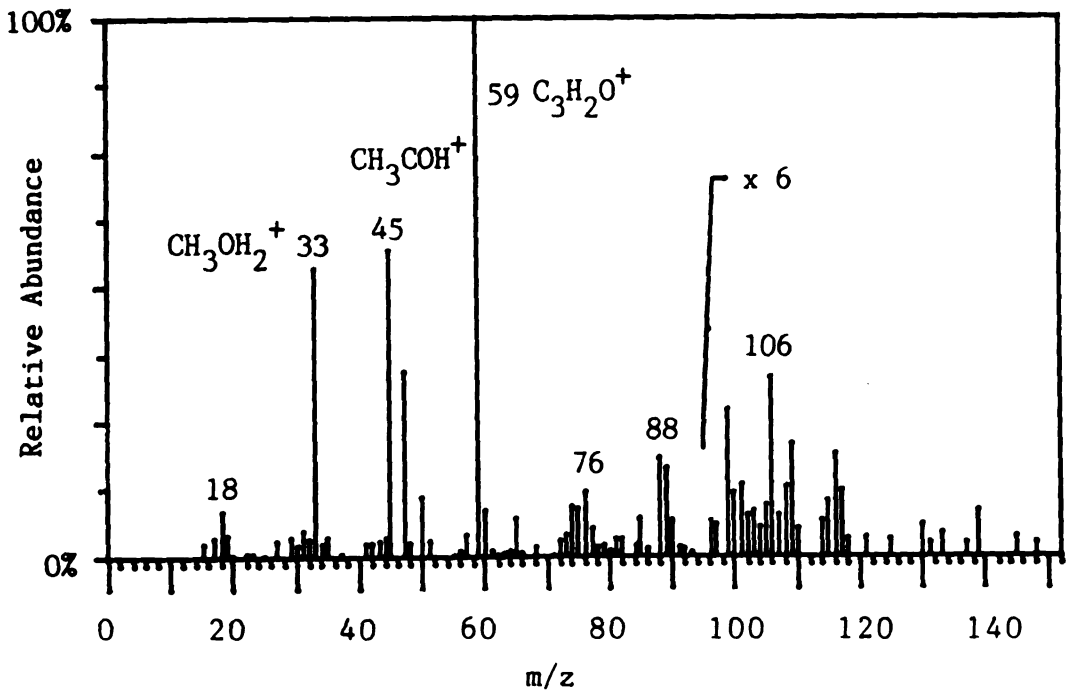

Figure 110. The Product Spectrum of the Reaction Between the Protonated Molecule of Acetaldehyde and Methanol in the Central Quadrupole

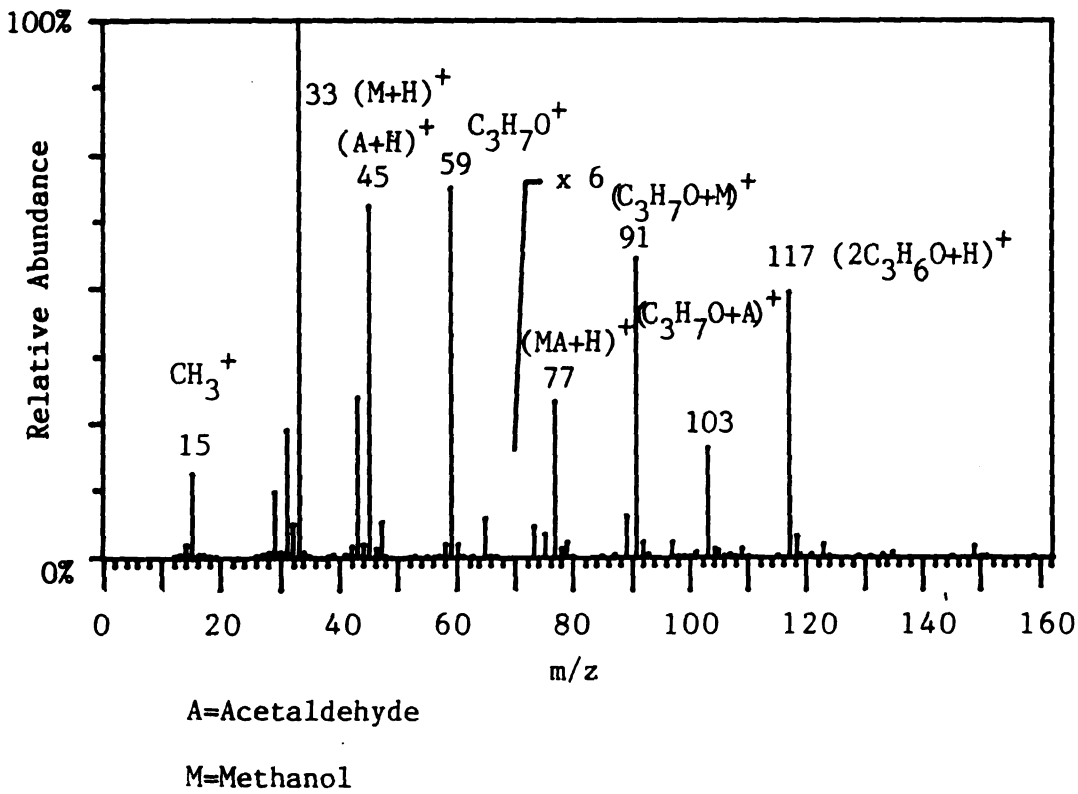

A=Acetaldehyde

M=Methanol

Figure 111. CI Mass Spectrum of a Mixture of Acetaldehyde and Methanol in the CI Volume

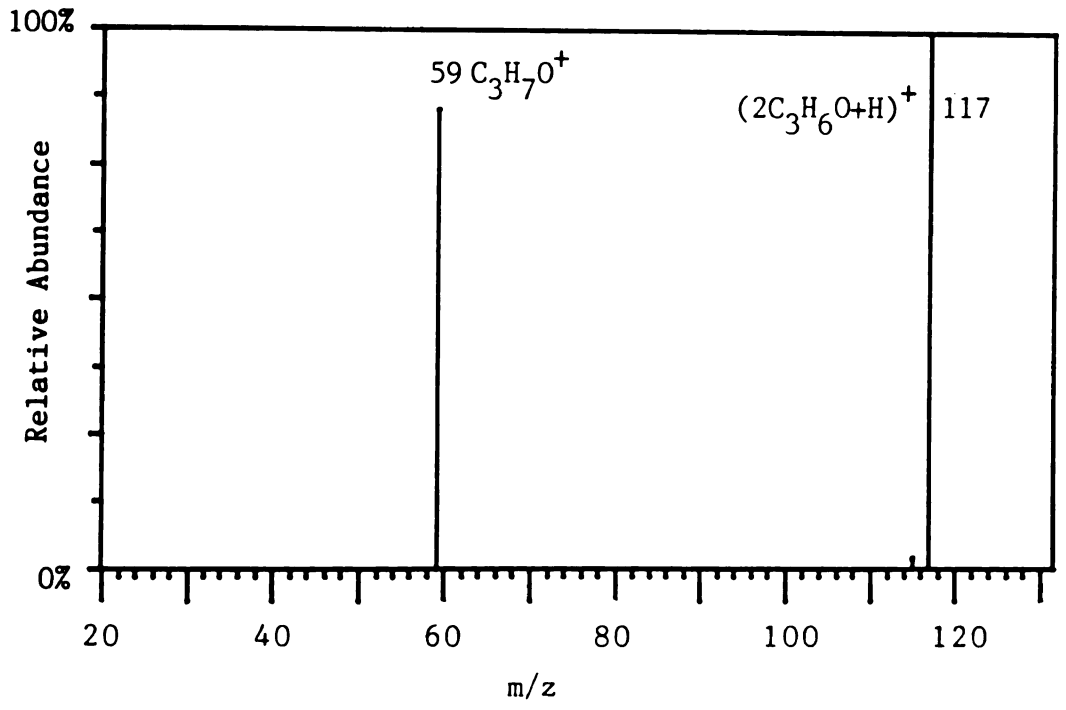

Figure 112. Argon CID Daughter Spectrum of the m/z 117 Peak from Acetaldehyde/Methanol CI

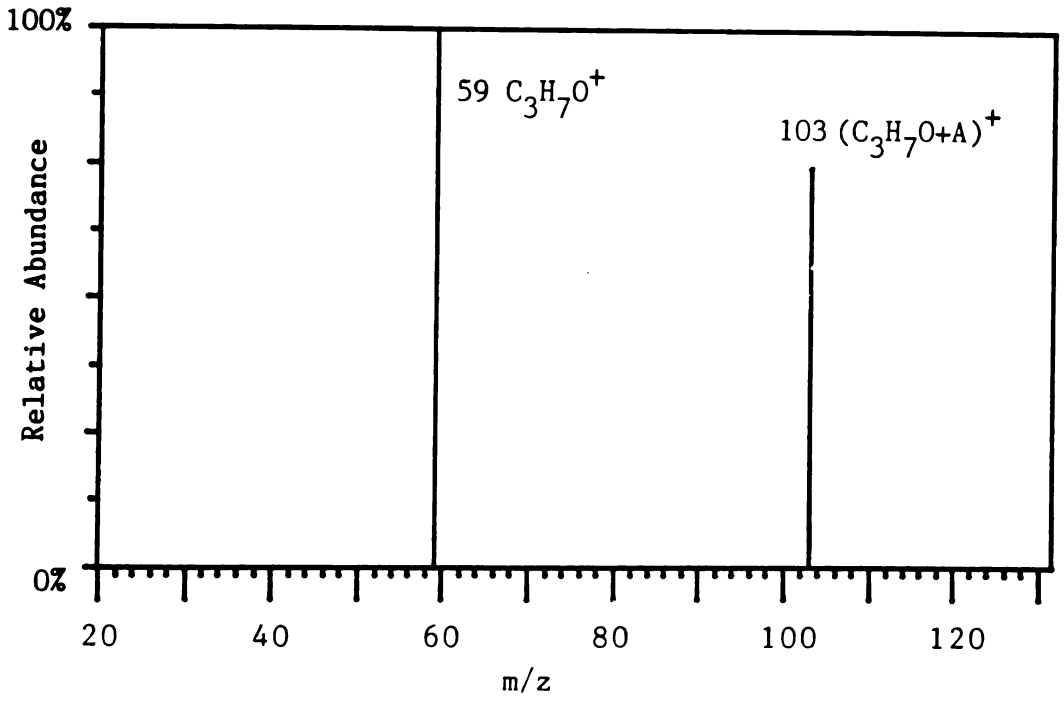

Figure 113. Argon CID Daughter Spectrum of the m/z 103 Peak from Acetaldehyde/Methanol CI

spectrum in Figure 114. These products indicate that the m/z 59 ion may be protonated acetone since the clustering reactions of the m/z 59 ion are identical to those shown in schemes 1 through 8.

The argon CAD daughter spectrum of m/z 77 in Figure 115 suggests that it is the proton-bound adduct of acetaldehyde and methanol (due to daughter ions at m/z 45 and 33), but there is also a daughter ion peak at m/z 59 which indicates that the activated m/z 77 ion is the intermediate in the reaction of protonated acetaldehyde and methanol that forms the m/z 59 ion. A possible mechanism for the formation of the protonated acetone ion is shown in Scheme 17.

The mechanism shown in Scheme 17 is strongly reminiscent of the reactions of protonated acetic acid with alcohols to form protonated esters (see Chapter V.). In this case we have instead, a protonated aldehyde reacting with an alcohol to form a protonated ketone. The author described a similar reaction of nonanal reacting with protonated methanol to form the protonated ketone in Chapter II. These two examples are, to the best of the author's knowledge, the first mention of this ion/molecule reaction in the chemical literature. Another possibility is that the m/z 59 ion is an isomer of protonated acetone and has a hemi-acetal structure. The structure of the m/z 59 ion produced by the reaction of protonated methanol and acetaldehyde is discussed further in Chapter X. of this dissertation.

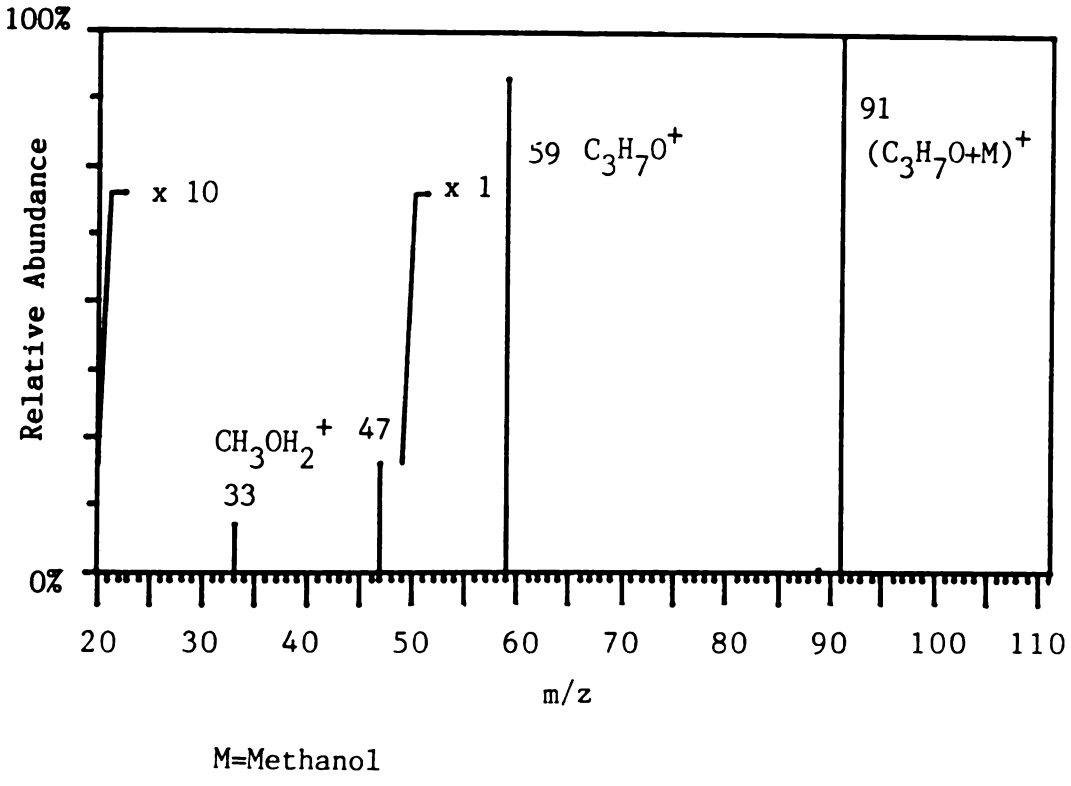

Figure 114. Argon CID Daughter Spectrum of the m/z 91 Peak from Acetaldehyde/Methanol CI

Scheme 17

Reaction of Protonated Acetaldehyde with Methanol to form Protonated Acetone

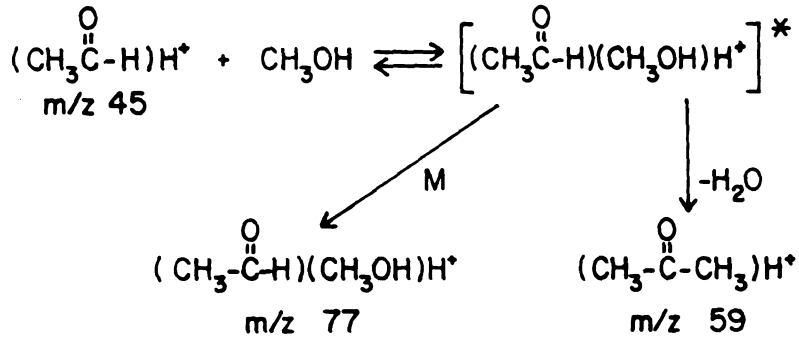

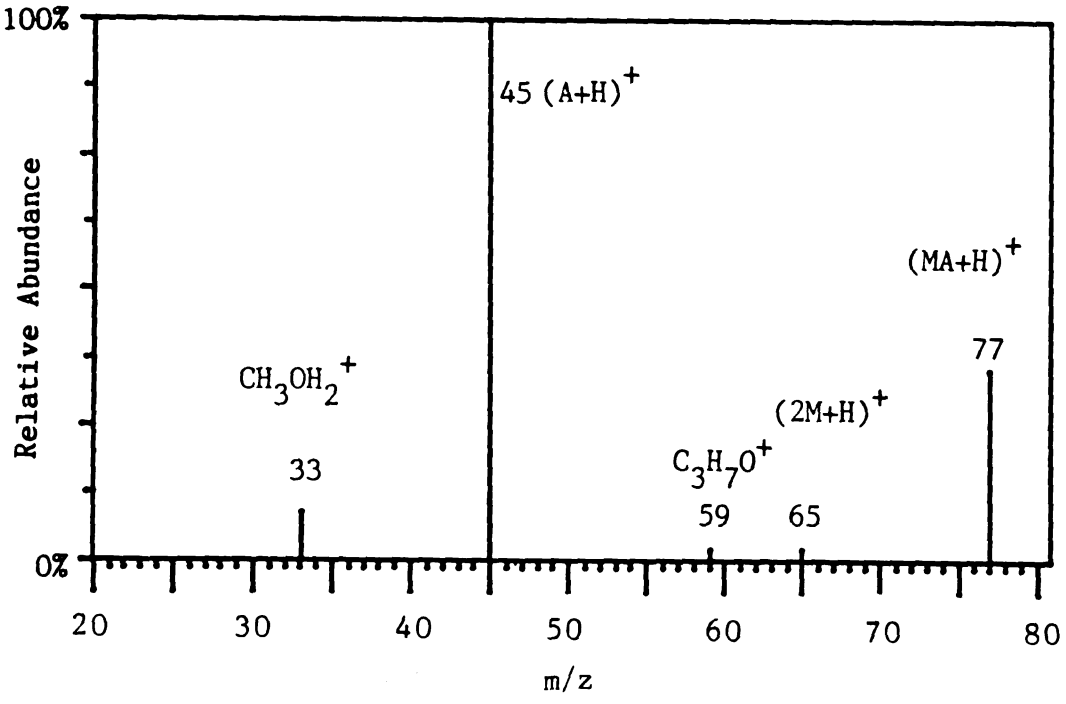

M=Methanol

A=Acetadehyde

Figure 115. Argon CID Daughter Spectrum of the m/z 77 Peak from Acetaldehyde/Methanol CI

6. Ion/Molecule Reactions Between Protonated Ethylacetate and Propanol

Tiedemann and Riveros (90) reported a reaction between protonated esters and alcohols. The product is the result of a condensation reaction between the two species followed by loss of water to form an ion with only covalent bonds that could have either an oxonium ion or acetal structure. Since the reaction was performed using ICR instrumentation, it was not possible at the time to determine which structure the ion possessed. This section describes how the same reaction was performed in the TQMS using protonated ethylacetate and propanol as the reactants, with the intent of determining the product ion's structure. The expected product for the reaction has an mass-to-charge ratio of 131, and the two possible structures according to Riveros and Tiedemann are shown in Table 13.

The product spectrum of the reaction between protonated ethylacetate and propanol in the central quadrupole of the TQMS is shown in Figure 116. Figure 116A shows that without ion trapping the only peaks observed represent the parent ion (m/z 89) and the protonated molecule of propanol (m/z 61). Figure 116B shows that with ion trapping the product spectrum becomes much more interesting and complicated. Unlike in the ICR experiments in which the product peak of interest is a major product, the m/z 131 peak is of low intensity in the central quadrupole. Of much greater abundance is the proton-bound adduct of ethylacetate and propanol at m/z 149. The reason for this change in abundance is that the pressure in the ICR experiments was considerably lower than in the central quadrupole. In the center quadrupole, the collisional stabilization that allows one to observe the intermediate of

Table 13

Possible Structures of the $C_7H_{15}O_2^+$ Ion

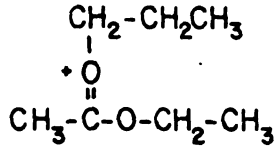

acetal ion

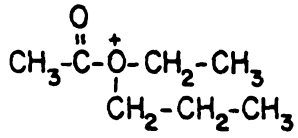

oxonium ion

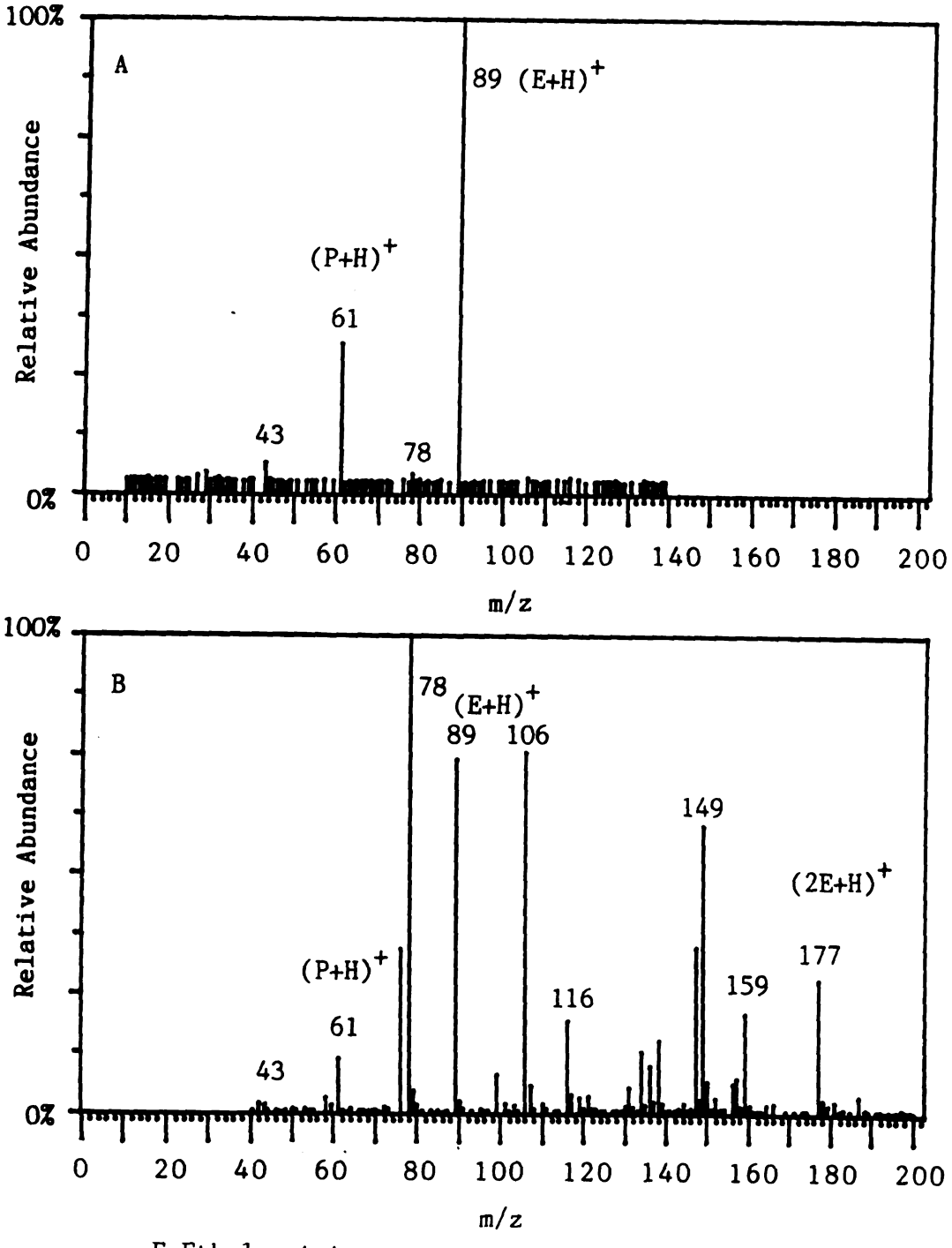

E=Ethylacetate

P=Propanol

Figure 116. The Product Spectrum of the Reaction Between Protonated Ethylacetate and Propanol (A) Without Ion Trapping, and (B) With Ion Trapping in the Central Quadrupole

the reaction (m/z 149) reduces the yield of the final product (m/z 131). In the ICR, the lack of collisional stabilization increases the yield of the final product but does not allow one to observe the intermediate. All of the other peaks in the spectrum are products of ion/molecule reactions in propanol or in ethylacetate.

Figure 117 shows the CI spectrum of propanol. One observes the sets of cluster ions that appear in Table 14. The self-CI spectrum of propanol is quite similar to that of methanol discussed in Chapter V. If one combines propanol and ethylacetate in the CI volume, one obtains the spectrum shown in Figure 118. All of the peaks in Figure 118 can be explained as arising from either or both of the self-CI spectra of ethylacetate and propanol shown in this chapter. In particular, the m/z 131 peak arises from both the pure ethylacetate CI spectrum and the mixed ethylacetate-propanol spectrum. In both cases the m/z 131 peak is a very minor product. The argon CID daughter spectrum of the m/z 131 ion arising from ethylacetate self-CI has already been shown in Figure 102 and shows peaks at m/z 43, 61, and 89. The argon CID spectrum of the m/z 131 ion arising from the mixture of ethylacetate and propanol is shown in Figure 119. One still observes the m/z 43, 61, and 89 peaks in approximately the same ratios as in Figure 102, but there is an additional peak at m/z 71. It would seem that part of the ion current of the m/z 131 ion is generated by self-CI of ethylacetate and the rest by the reaction between protonated ethylacetate and propanol.

The m/z 71 daughter ion peak gives a clue as to the structure of the m/z 131 product ion. Of the possible formulas ($C_5H_{11}^+$, $C_4H_7O^+$, and $C_3H_3O_2^+$) for the m/z 71 ion, the $C_4H_7O^+$ formula is by far the most likely, considering the proposed structures for the m/z 131 parent ion.

Table 14

Products from the Ion/Molecule Reactions in Propanol

$(CH_3CH_2CH_2OH)_n H^+$ where n = 2 to 5

m/z = 121, 181, 241, and 301

$CH_3CH_2CH_2^+ (CH_3CH_2CH_2OH)_n$ where n = 1 to 3

m/z = 105, 163, and 223

$CH_3CH_2^+ (CH_3CH_2CH_2OH)_n$ where n = 1 to 3

m/z = 89, 149, and 209

$H_2O^+ (CH_3CH_2CH_2OH)_n$ where n = 1 to 3

m/z 78, 138, and 198

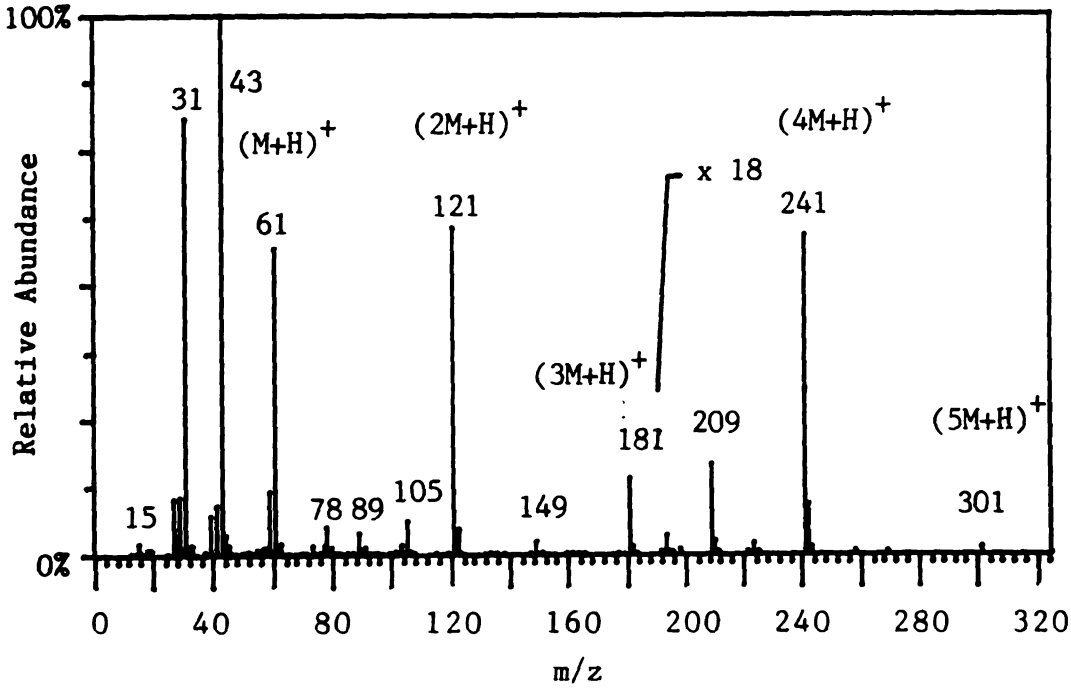

Figure 117. Self-CI Mass Spectrum of Propanol

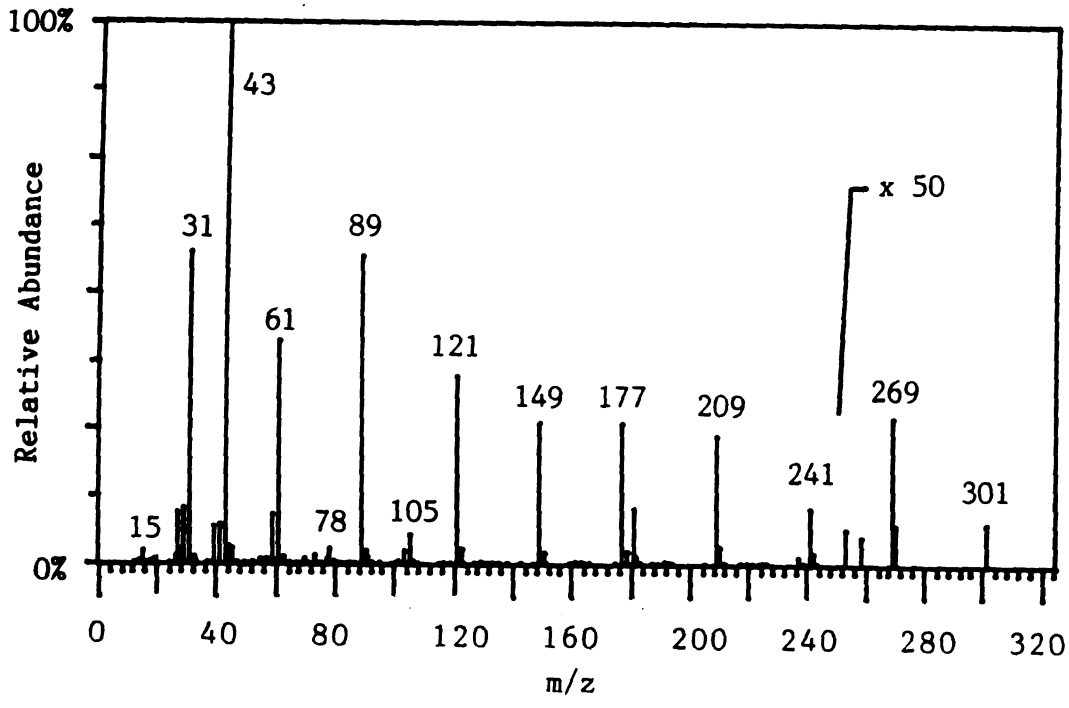

Figure 118. Mass Spectrum of a Mixture of Ethylacetate and Propanol in the CI Volume

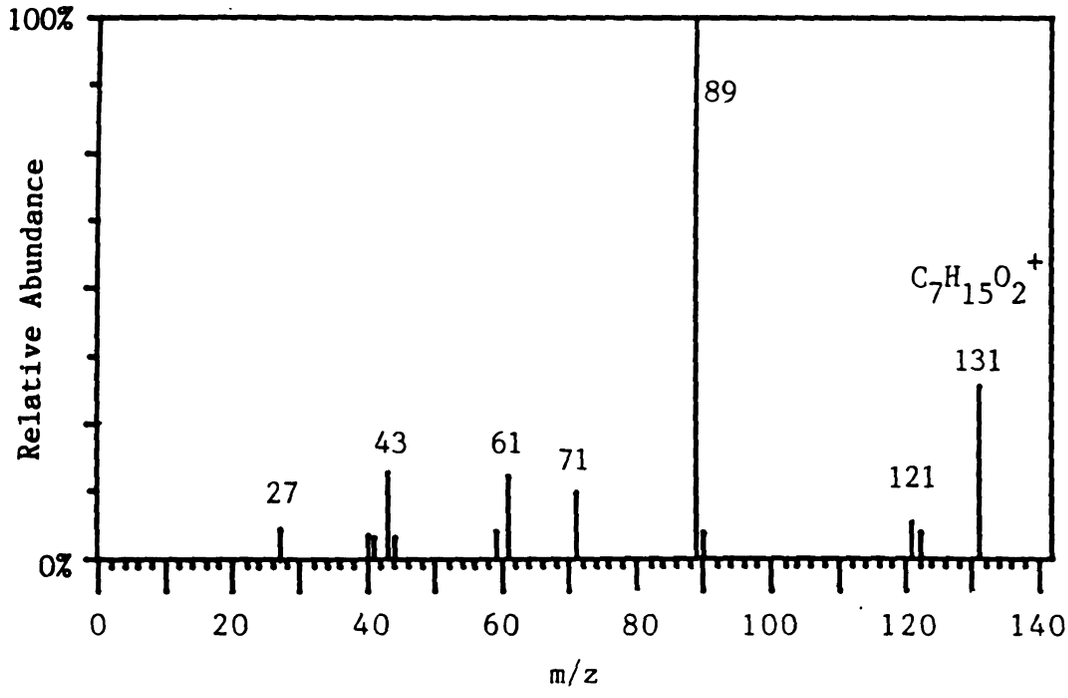

Figure 119. Argon CID Daughter Spectrum of the m/z 131 Peak from Ethylacetate/Propanol CI

The neutral loss from the parent to the m/z 71 daughter is 60 u. The possible neutral losses of 60 u are: $CH_3CH_2CH_2OH$, CH_3COOH, $CO + CH_3OH$, $CH_4 + CO_2$, and $CH_2O + H_2O$. The second, third, fourth, and fifth neutral losses, however, cannot result in an intact m/z 71 ion being produced from either of the proposed structures utilizing simple fragmentation schemes minimizing the number of bonds cleaved. The loss of propanol, however, can be envisioned in the acetal structure (but not from the oxonium ion structure) by means of the McLafferty-type double hydrogen rearrangement shown in Scheme 18. Since the m/z 71 daughter ion can be produced in theory from the acetal structure, the CID evidence lends credence to the formation of an acetal ion from the reaction between the protonated ester and the alcohol.

D. Conclusion

The reactions of carbonyl ions with carbonyl compounds in this chapter, and in Chapters II. and V., indicate that carbonyl compounds readily form numerous types of cluster ions in either the CI volume or in the central quadrupole of the TQMS. The mechanisms of these reactions that form the cluster ions are interesting and complex. Carbonyl ions whether protonated or not, readily form clusters with most polar compounds, and are therefore not generally of analytical interest as selective reagent ions in CI or in reactive collision gas MS/MS. The exception to this rule appears to be the reactions of carbonyl compounds with alcohols. A wide variety of carbonyl compounds including carboxylic acids, esters, and aldehydes react specifically with protonated alcohols to form condensation products which eliminate water to form covalently bound compounds. These products form most

Scheme 18

Mechanism for Loss of Propanol From $C_7H_{15}O_2^+$ by CID

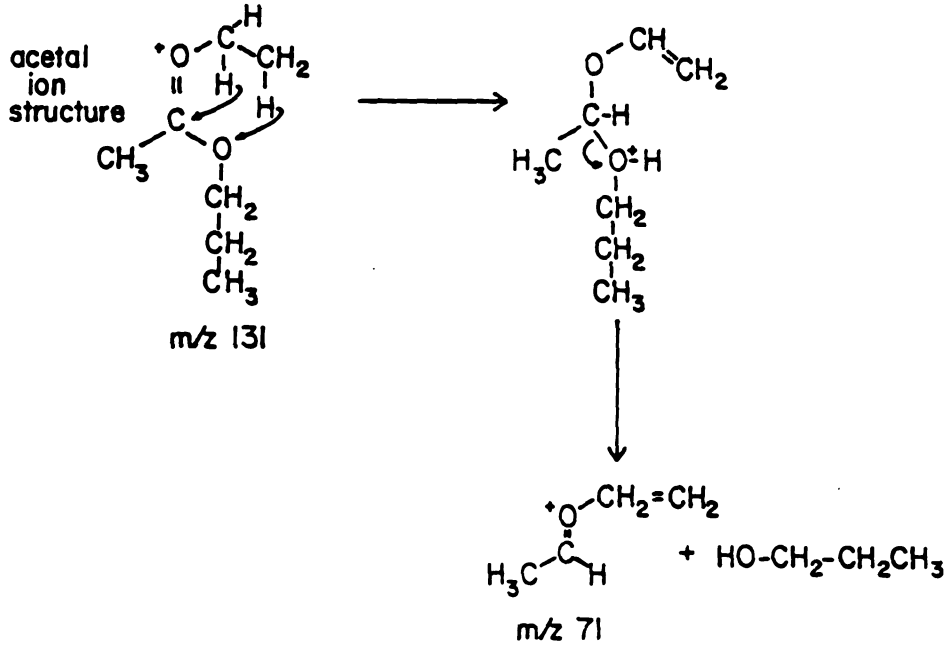

efficiently at low pressures in which the intermediates of the reactions cannot be stabilized collisionally. Low pressures of methanol in the central quadrupole combined with relatively long periods of ion trapping may be very effective for selected reaction monitoring of certain acids, esters, and aldehydes.

CHAPTER IX.

ION/MOLECULE REACTIONS OF THE 2-CHLORO-5-NITROPYRIDINE MOLECULAR ANION WITH METHANOL: A GAS-PHASE ANALOG OF THE S_N(ANRORC) PROCESS?

A. Introduction

The previous chapters of this dissertation have established that there is a strong relationship between the ion/molecule reactions that occur in positive ion chemical ionization and in the positive ion trap and pulse technique using the central quadrupole of the TQMS. The first goal of this chapter is to explore the relationship between negative ion chemical ionization (NCI) and negative ion trap and pulse. A secondary goal is to use NCI and negative ion trap and pulse to investigate in the gas phase a particular nucleophilic aromatic substitution reaction which has been determined to proceed via an anionic intermediate in solution (147).

In solution, the electron deficient nature of aromatic rings containing heterocyclic nitrogens makes the electrophilic aromatic substitution reactions that are typical of aromatic systems, very difficult, but instead facilitates nucleophilic substitution reactions (147). Nucleophilic aromatic substitution is generally thought to occur in solution by three separate mechanisms (148), the addition-elimination mechanism (S_N(AE)), the benzyne mechanism that is also called the elimination-addition mechanism (S_N(EA)), and the aromatic nucleophilic substitution by means of ring opening and ring closing mechanism (S_N(ANRORC)).

The S_N(AE) mechanism is illustrated in Scheme 19 in which a pyridine ring is attacked by a powerful nucleophile forming a negative ion sigma complex followed by elimination of a leaving group as an anion.

The S_N(EA) mechanism is illustrated in Scheme 20 in which a pyridine ring is attacked by a strong base which abstracts a proton to form a 2,3-pyridyne intermediate with elimination of a leaving group. The intermediate is then attacked by the stong base, now acting as a nucleophile, to form a mixture of products.

The S_N(ANRORC) mechanism is illustrated in Scheme 21 in which a pyrimidine ring is attacked by a stong nucleophile to form an unstable sigma complex which undergoes ring opening. Elimination of a leaving group with ring closure forms the end product.

Aromatic nucleophilic substitution in general is typical of the solution reactions of nitrogen-containing aromatic heterocycles. The S_N(ANRORC) reaction, however, is an interesting and fairly unusual reaction that occurs only with very strong bases such as OH^- and NH_2^- reacting with substituted pyridines, pyrimidines, triazines, and purines. The reaction is most common when the compounds are substituted with a very good leaving group located ortho to a ring nitrogen.

S_N(ANRORC) reactions, because of their unusual mechanism, have received considerable attention in the organic chemistry literature in recent years (147, 149, 160, 161). The author was involved in one particular investigation of this sort at the College of Wooster (147). The reaction investigated in that research involved the attack of the hydroxide ion on the 2-chloro-5-nitropyridine (2CL5NP) in a mixed solvent of water and dimethylsulfoxide.

Scheme 19

The $S_N(AE)$ Mechanism in Solution

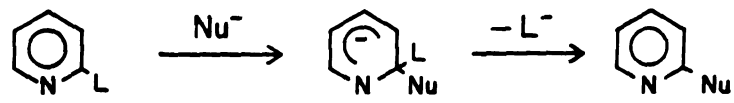

L^- = leaving group

Nu^- = nucleophile

Scheme 20

The $S_N(EA)$ Mechanism in Solution

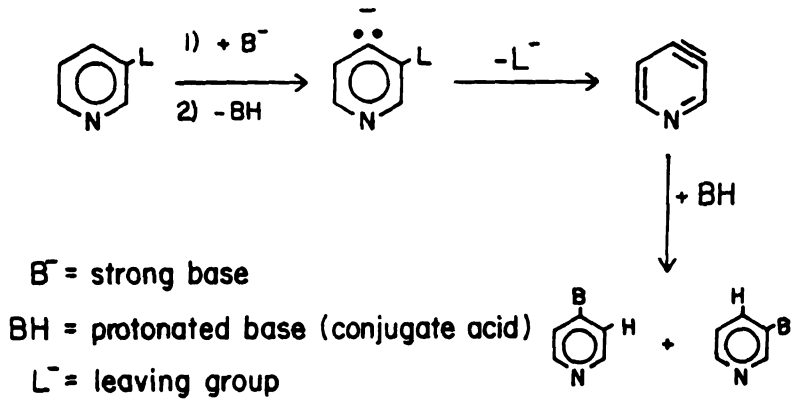

Scheme 21

The S_N(ANRORC) Mechanism in Solution

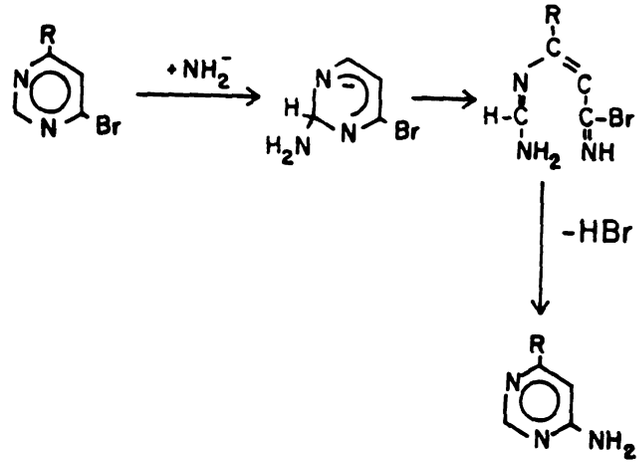

Scheme 22 shows the attack of the hydroxide ion on the 2CL5NP to form an unstable sigma complex which undergoes ring opening. The ring-opened species, however, is immediately attacked by another OH^- ion with loss of water and Cl^- to form an extremely stable intermediate with an unusual structure. It is, in fact, possible to isolate the intermediate by lyophilizing the solution at this point in the reaction. Addition of excess hydroxide ion closes the ring again and leads to the expected nucleophilic addition product. Structures of species 1, 4, and 5 in Scheme 22 were determined by NMR and IR techniques.

This S_N(ANRORC) reaction of 2CL5NP and the hydroxide ion is particularly amenable to mass spectrometric investigation by NCI and negative ion trap and pulse since all of the species of interest in the reaction are negatively charged and are sufficiently volatile to enter the gas phase following a moderate amount of heating. Furthermore, the intermediate of the reaction can be isolated by solution chemistry to serve as a reference compound whose CID spectrum can be compared to the CID spectra of any ions generated by ion/molecule reactions in the gas phase.

Gas-phase negative ion chemistry in the ICR and FT-ICR (150) instruments has recently been reviewed. Most of the ion/molecule reaction of negative ions have been involved with aliphatic carbonyl compounds and with high electron affinity ions such as F^- and OCH_3^-. Many of these reactions have been shown to have nucleophilic substitution mechanisms of the S_N2 type. There are a few examples of aromatic nucleophilic substitution reactions in the literature, the mechanisms of which are given in Scheme 23 (151,152), but there have

Scheme 22

The Solution Reaction of 2CL5NP with OH^-

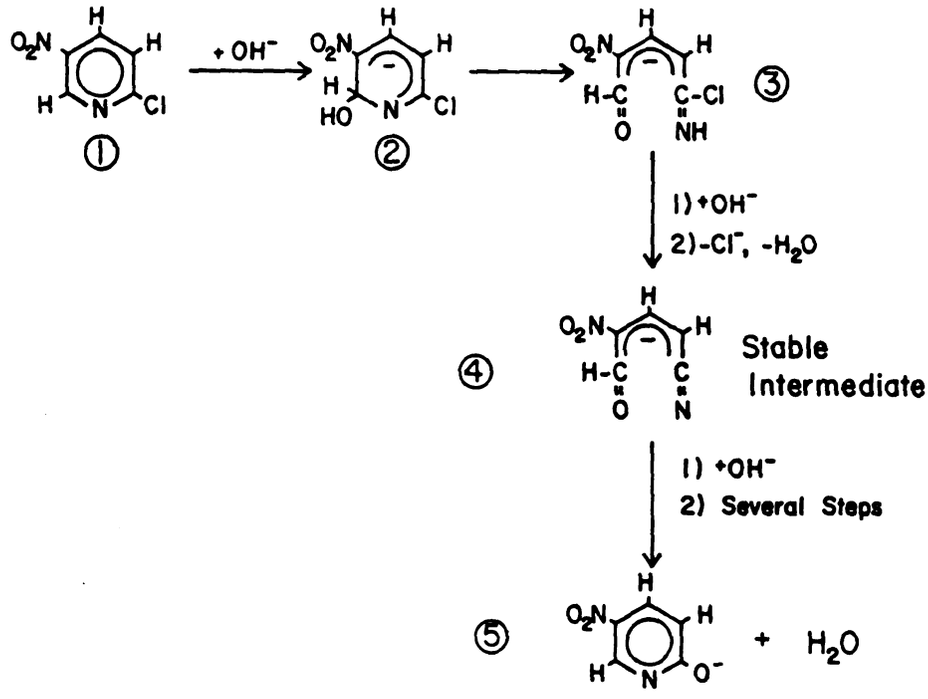

Scheme 23

Nucleophilic Aromatic Substitution Reaction in the Gas Phase (151,152)

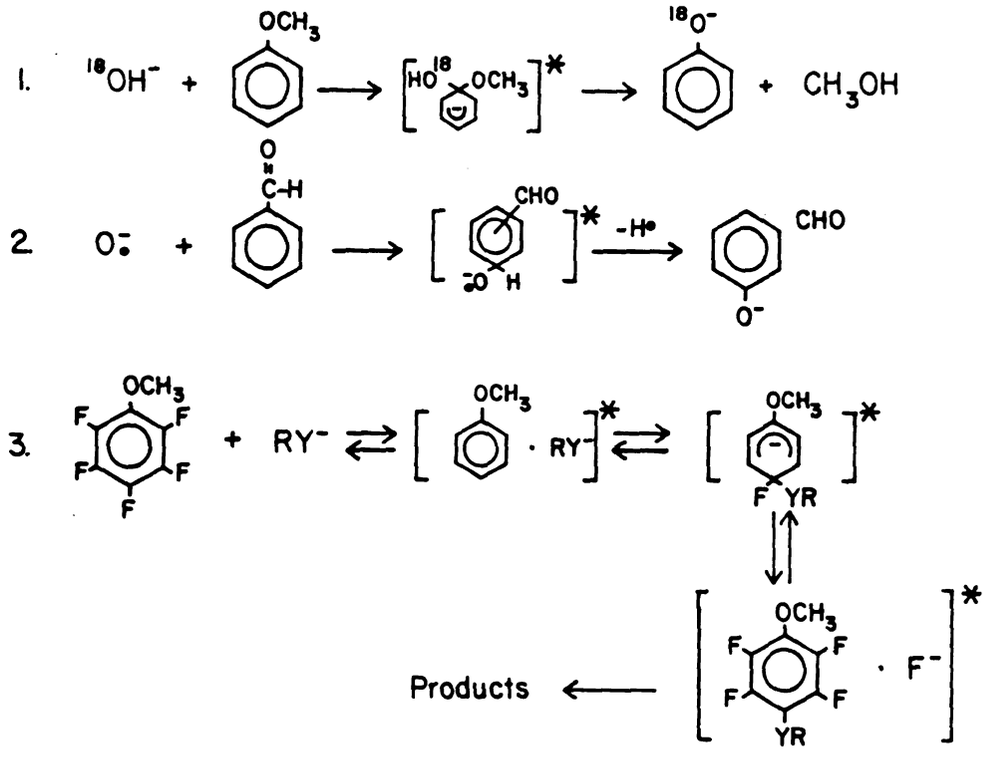

been no S_N(ANRORC) type nucleophilic substitution reactions investigated in the gas phase by any technique.

B. Experimental

1. Preparation of Standards

2-chloro-5-nitropyridine (2CL5NP) was obtained from Aldrich Chemical Company as a gold label chemical in the form of crystals. The stable intermediate was formed as in Reinheimer et. al. (147) by addition of 2 mmoles of NaOH dissolved in water to 1 mmole of 2CL5NP dissolved in dimethylsulfoxide (DMSO). This reaction is almost immediate and the solution changes color from almost colorless to dark yellow. The dark yellow solution was lyophilized for 24 hours yielding a dark viscous oil. The end product of the reaction, 2-hydroxy-5-nitropyridine (2OH5NP), was obtained by adding 3 mmoles of NaOH dissolved in water to 1 mmole of 2CL5NP dissolved in DMSO. This solution was heated in a water bath for 3 hours and then neutralized to precipitate out crystals of 2OH5NP.

2. Isobutane CI Conditions

In order to obtain the negative ion mass spectra of the standards and to generate the parent ions for argon CID, the author used isobutane as the buffer gas. The pressure of isobutane was measured to be $4X10^{-4}$torr at the throat of the ion source turbomolecular pump. The ion source and the direct probe were heated to 50°C for the 2CL5NP. The direct probe was heated to 100°C to observe the M^- ion of the 2CL5NP, and to 200°C to observe the M^- ion of the 2OH5NP. The temperature of

the ion source rose to 75°C due to indirect heating from the direct probe and the CI filament.

3. Methanol NCI Conditions

The author considered methanol to be the NCI gas which was most likely to produce the desired nucleophilic aromatic substitution reaction. The ion/molecule products that did result were analyzed by argon CID and by methanol trap and pulse in the central quadrupole of the TQMS.

Methanol NCI was accomplished with nearly the same conditions as isobutane NCI. The measured pressure of methanol was $4X10^{-4}$ torr in the throat of the ion source turbomolecular pump. The ion source and direct probe were both heated to 50°C to volatilize the 2CL5NP into the CI volume.

4. Conditions in the Central Quadrupole

The parameters shown in Table 14 are the voltages used in the TQMS for negative ion CID and trap and pulse. the pressure of argon in the central quadrupole for CID experiments was $2X10^{-3}$, and the pressure of methanol in the central quadrupole for trap and pulse experiments was $4X10^{-3}$ torr. The average trapping time for all ions in the central quadrupole was 100 msec.

C. Results and Discussion

1. Negative Ions in the TQMS

The mechanisms for the production of negative ions in chemical ionization can be very different from the mechanism that produces

positive ions. In CI, the major method of producing positively charged analyte ions involves ion/molecule reactions of abundant reagent ions, such as $CH_3OH_2^+$, with the neutral analyte molecules. If one chooses an appropriate CI gas, one can also produce negatively charged reagent ions that undergo ion/molecule reactions with neutral analyte molecules to produce negative ions from the analyte. However, the most common gases used for NCI, methane and isobutane, produce virtually no reagent ions, but, nevertheless, manage to produce abundant molecular anions of certain compounds with high electron affinities, such as polychlorinated biphenyls. The mechanism for this process appears to be that the high energy (70-100 eV) electrons produced by the CI filament ionize gas molecules which release slow secondary electrons. These slow electrons can then be captured by compounds with high electron affinities yielding abundant quantities of negatively charged analyte ions. This process is usually called electron-capture negative ionization (ECNI) and has been compared to the electron capture detector (153) used in gas chromatography for detecting trace quantities of compounds with high electron affinities.

With the trap and pulse methodology it is possible to simulate the conditions for both negative reagent ion NCI and ECNI. One can trap a negative parent ion in the central quadrupole, and react it in the gas phase with a particular neutral analyte as in negative reagent ion CI, or one can trap a negative parent ion with a low electron affinity in the central quadrupole where it can transfer its electron to a molecule with a high electron affinity in an analogous fashion to ECNI.

Neither isobutane nor methanol produces a significant abundance of reagent ions under NCI conditions in the TQMS. Since reagent ions are

absent, one can assume that the major mode of ionization in isobutane and methanol is ECNI. The assumption of ECNI as the dominant ionization mechanism does not rule out the possibility of ion/molecule reactions because there are copious quantities of the neutral buffer gas that can interact subsequently with the negatively charged analyte ion. As we will see, however, methanol is much more reactive with the negative ions produced in this study than is isobutane. This means that isobutane can be used as a "blank" for the ion/molecule reactions of negative ions with methanol.

2. Isobutane NCI/MS and Argon CID of 2CL5NP

The starting material, 2CL5NP, produces the isobutane NCI mass spectrum shown in Figure 120. The spectrum has two major peaks at m/z 158 and m/z 160. The m/z 158 peak corresponds to the molecular anion of 2CL5NP and the m/z 160 peak corresponds to its ^{37}Cl isotope. There are also a number of fragment ions of low abundance. Figure 121 shows the argon CID daughter spectrum of the parent ion at m/z 158. The base peak represents the parent ion and there are four peaks representing daughter ions. The peak at m/z 35 is the chloride ion, the peak at m/z 46 is the NO_2^- ion, and the peak at m/z 128 is probably the $(M-NO)^-$ ion. These daughter ions correspond to the major fragment ion peaks in the isobutane NCI spectrum in Figure 120.

3. Ion/Molecule Reaction of $(2CL5NP)^-$ with Methanol

If one substitutes methanol for argon in the collision chamber, and does a trap and pulse product scan of the reaction products between the molecular anion of 2CL5NP and methanol, the spectrum, as shown in

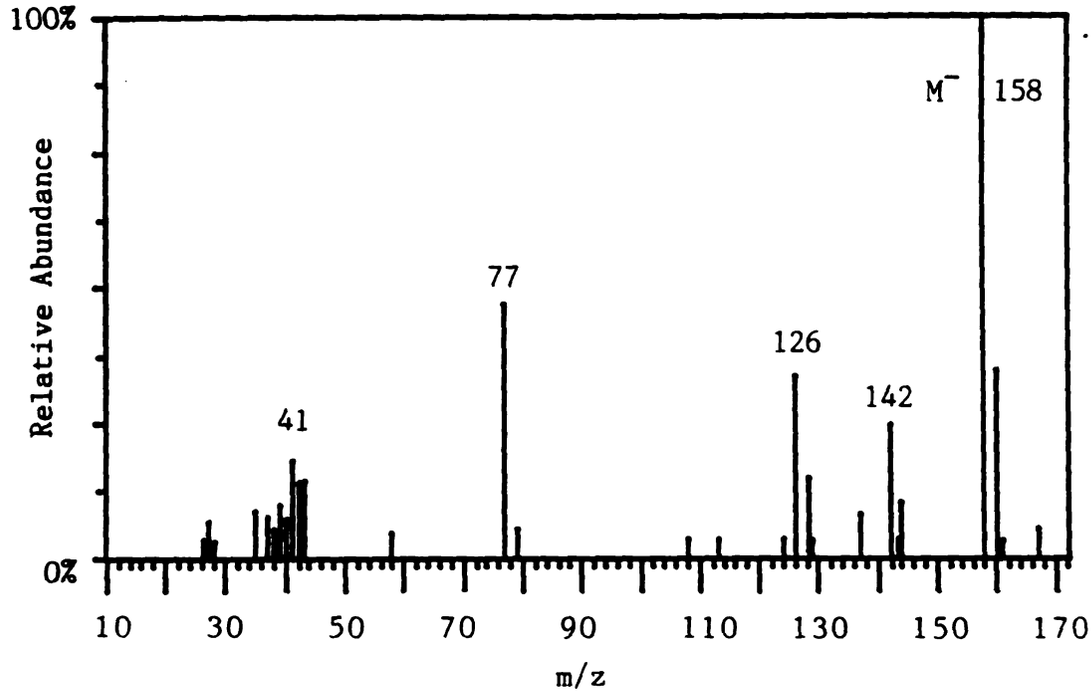

Figure 120. Isobutane NCI Mass Spectrum of 2-Chloro-5-Nitropyridine (2CL5NP)

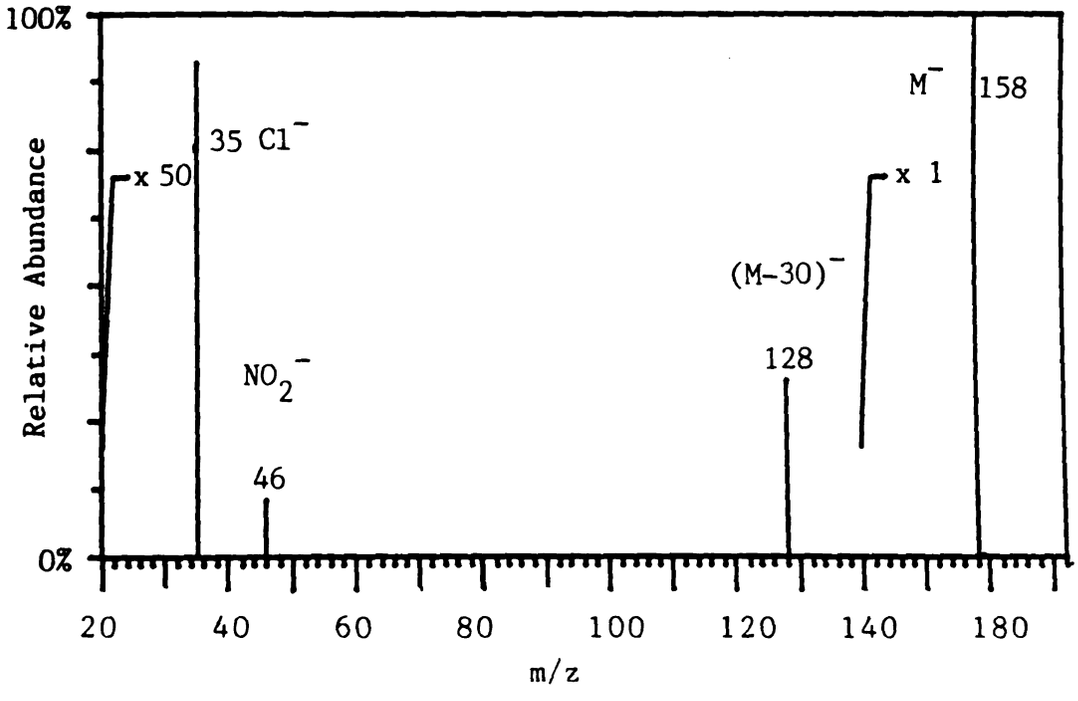

Figure 121. Argon CID Daughter Spectrum of the M^- Ion of 2CL5NP

Figure 122, reveals the CID peaks and additional peaks at m/z 139 and m/z 190. The m/z 190 peak is almost certainly the negative ion adduct of methanol and 2CL5NP, but the identity of the m/z 139 peak is uncertain. If one chooses the m/z 160 peak of 2CL5NP that contains the ^{37}Cl isotope for the parent ion, one obtains the same product spectrum as in Figure 122, except that the peak at m/z 190 shifts to m/z 192. This indicates that the m/z 190 ion contains chlorine but that the m/z 139 ion does not. The m/z 139 peak, therefore, could be either the ring-opened stable intermediate ion from Scheme 22 or the final product ion from Scheme 22.

The same reaction observed in the collision chamber can be made to occur in the chemical ionization source by methanol NCI of 2CL5NP. The reaction is highly sensitive to methanol pressure and the ion source temperature, but the NCI spectrum shown in Figure 123 is typical, with numerous peaks of low intensity at low m/z values and three peaks of major intensity: m/z 139, 158, and 160.

The argon CID daughter spectrum of the m/z 139 peak produced by methanol NCI is shown in Figure 124A. The argon CID spectrum of the S_N(ANRORC) intermediate ion isolated from solution is shown in Figure 124B. Isobutane NCI of 2OH5NP does not produce an $(M-H)^-$ ion at m/z 139 but does produce an M^- ion at m/z 140. Only two daughter ions arise from the m/z 140 peak, and they are m/z 46 $(NO_2)^-$, and m/z 93 $(M-HNO_2)^-$. It is apparent from the spectra in Figure 124 that the daughter ions produced by the ion/molecule product ion at m/z 139 are the same as those ions generated from the stable intermediate ion at m/z 139. A mechanism which is consistent with all of the data presented in this chapter for the production of the m/z 139 peak is shown in Scheme 24.

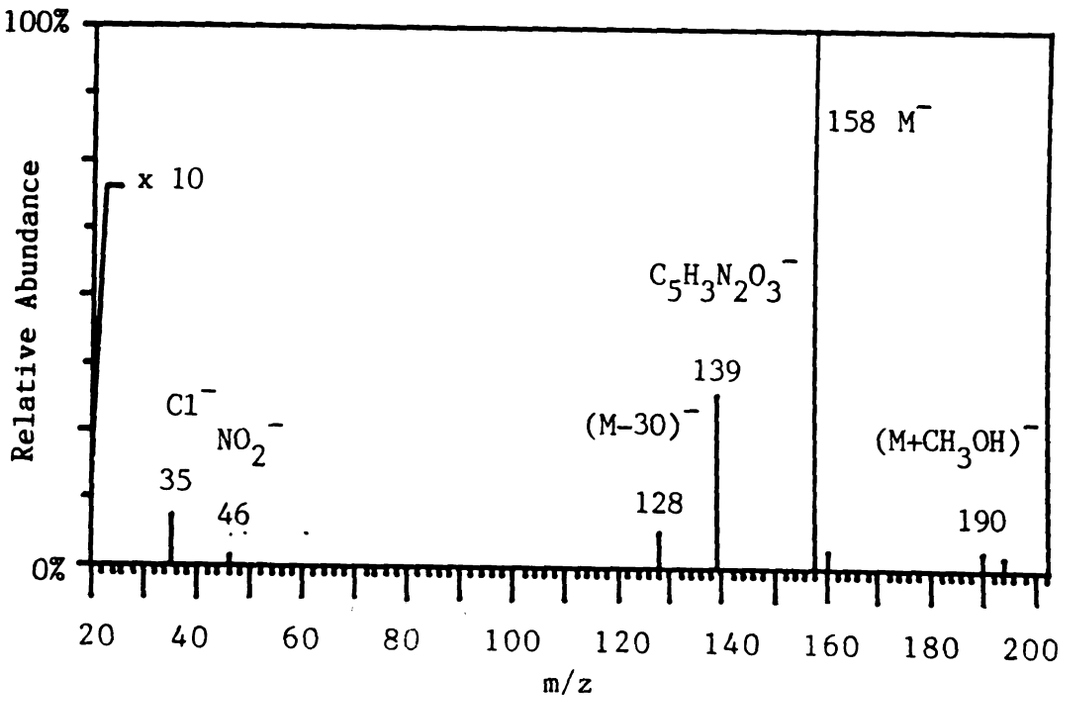

Figure 122. The Product Spectrum of the Reaction Between the M^- of 2CL5NP and Methanol in the Central Quadrupole

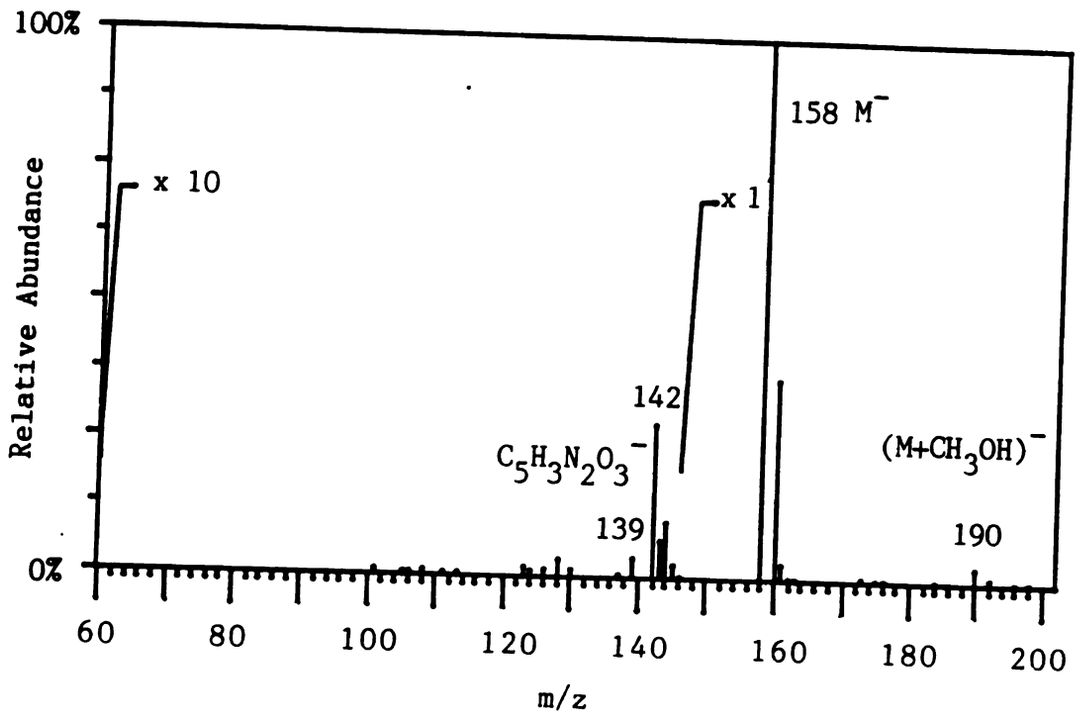

Figure 123. Methanol NCI Mass Spectrum of 2CL5NP

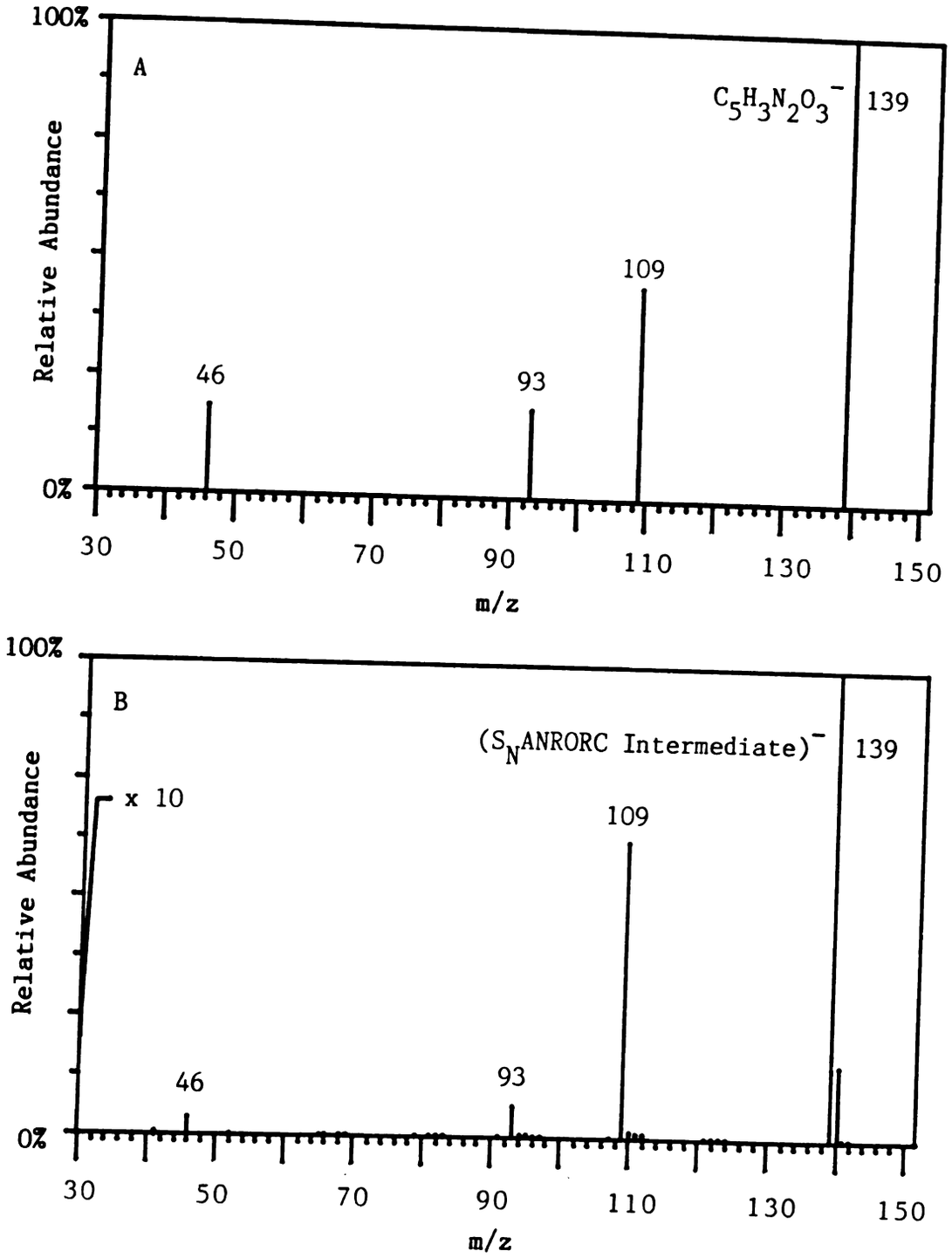

Figure 124. Argon CID Daughter Spectra of (A) the m/z 139 Peak From Methanol CI of 2CL5NP and the (B) M^- of the S_N(ANRORC) Intermediate From Solution

Scheme 24

The Gas-Phase Reaction of 2CL5NP$^-$ with CH_3OH

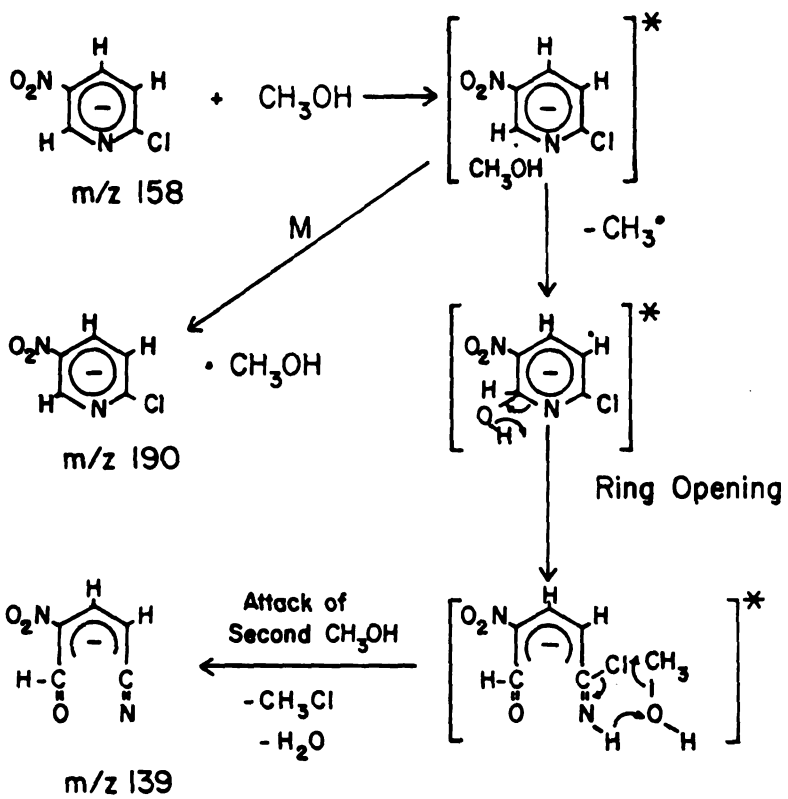

Scheme 26 suggests that the methanol molecule reacts with the 2CL5NP molecular anion to form an activated intermediate which can be collisionally stabilized in the central quadrupole to form a peak at m/z 190. The activated intermediate could readily lose a methyl radical and then undergo a ring opening step identical to that observed in solution. The ring-opened ion could react with a second molecule of methanol to form the relatively stable product ion ion at m/z 139.

This chapter presents the first evidence that an analog of the S_N(ANRORC) reaction may occur in the gas phase. This reaction occurs under methanol NCI or methanol trap and pulse conditions. The particular mechanism proposed for the reaction of 2CL5NP is probably unique to this compound, but nucleophilic aromatic substitution is a general reaction for aromatic nitrogen heterocycles and could be developed as an analytical technique in negative ion mass spectrometry for selective detection of this class of compounds.

CHAPTER X.

THERMOCHEMISTRY OF ION/MOLECULE REACTIONS

A. Introduction

To the extent that it is possible, this chapter explores the energetics of the ion/molecule reactions that have been investigated in the preceding nine chapters of this dissertation. The goal of this chapter is to use tabulated heats of formation, proton affinities, and ionization potentials to calculate heats of reaction for the various reactions in this study with the hope of providing a theoretical basis for the experimental observations presented in this dissertation.

Table 15 is a list of compounds used in this chapter arranged by functional group with their respective proton affinities, heats of formation of the neutral molecules, heats of formation of the $(M+H)^+$ ions, and heats of formation of the $M^{+\cdot}$ ions. The proton affinities, and heats of formation of the neutral and protonated molecules were taken primarily from Lias et. al. (164), except for the proton affinity of glycerol which was taken from Sunner et. al. (165). The heats of formation of the molecular ions were calculated from the heats of formation of the neutral molecules and the ionization potentials taken from McLafferty (136). The heat of formation of the phenyl cation was contributed by J. Allison (166). All of the thermodynamic quantities in Table 15 are given in kilocalories per mole.

Table 15

Thermochemical Properties of Selected Compounds

Name	Formula	P.A.	ΔH_f (M)	ΔHf ($M+H^+$)	ΔH_f ($M^{+\cdot}$)
Hydroxy Compounds					
Water	H_2O	166.5	-58	141	233
Methanol	CH_4O	181.9	-48	135.5	201
Ethanol	C_2H_6O	188.3	-56	121	186
Propanol	$n\text{-}C_3H_8O$	190.8	-61	114	---
Butanol	$n\text{-}C_4H_{10}O$	191.1	-66	109	167
Phenol	C_6H_6O	196.3	-23	146	173
Glycerol	$C_3H_8O_3$	209.0	---	---	---
Aldehydes					
Formal-	CH_2O	171.7	-26	168	225
Acetal-	C_2H_4O	186.6	-40	139	195
Propional -	C_3H_6O	189.6	-45	133	---
Butanal	C_4H_8O	191.5	-50	124	178
Pentanal	$C_5H_{10}O$	192.6	-55	118	---
Ethers					
Diethyl-	$C_4H_{10}O$	200.2	-60	105.5	161
Methylvinyl-	C_3H_6O	207.4	-24	134	---
Aliphatic Hydrocarbons					
Hydrogen	H_2	101.2	0	264.5	355
Methane	CH_4	132	-18	216	270
Ethane	C_2H_6	143.6	-20	202	245
Propane	C_3H_8	150	-25	191	229
Butane	$i\text{-}C_4H_{10}$	163.3	-32	170	212
Amines					
Ammonia	NH_3	204.0	-11	151	224
Methylamine	CH_5N	214.1	-5	146	---
Ethylamine	C_2H_7N	217.0	-11	137	194
Propylamine	$n\text{-}C_3H_9N$	217.9	-17	131	---
Butylamine	$n\text{-}C_4H_{11}N$	218.4	-22	125	179
Pentylamine	$n\text{-}C_5H_{13}N$	218.9	-26	120.6	---
Hexylamine	$n\text{-}C_6H_{15}N$	218.9	-31	116	---
Heptylamine	$n\text{-}C_7H_{17}N$	219.0	-36	111	---
Dimethyl-	C_2H_7N	220.6	-4.5	140.5	---
Tributyl-	$n\text{-}C_{12}H_{27}N$	234.8	-53	78	---
Aniline	C_6H_7N	209.5	21	177	199
Pyridine	C_5H_5N	220.8	33	178	247

Table 15 (cont.)

Name	Formula	P.A.	ΔH_f (M)	ΔHf ($M+H^+$)	ΔH_f ($M^{+\cdot}$)
Aromatic Hydrocarbons					
Benzene	C_6H_6	181.3	20	204	232
Phenyl	$C_6H_5^+$	---	285	---	---
Benzyne	C_6H_4	213	119	271	338
Toluene	C_7H_8	189.8	12	188	215
p-Xylene	C_8H_{10}	192.0	4	178	---
Naphthalene	$C_{10}H_8$	194.7	36	207	223
Biphenyl	$C_{12}H_{10}$	196.1	43	213	232
Anthracene	$C_{14}H_{10}$	207	55	214	228
Carboxylic Acids					
Formic Acid	CH_2O_2	178.8	-90.5	96	171
Acetic Acid	$C_2H_4O_2$	190.2	-103	72	137
Propionic -	$C_3H_6O_2$	191.8	-107	67	---
Ketones					
Acetone	C_3H_6O	196.7	-52	117	172
Methylethyl-	C_4H_8O	199.8	-57	109	162
Esters					
Methylformate	$C_2H_4O_2$	188.9	-85	92	---
Ethylformate	$C_3H_6O_2$	193.1	-92	80	---
Methylacetate	$C_3H_6O_2$	197.8	-99	69	---
Ethylacetate	$C_4H_8O_2$	200.7	-106	59	---
Methylpropan.	$C_4H_8O_2$	200.2	-103	62	133
Methylbutan.	$C_5H_{10}O_2$	200.1	-108	57	---
Methylpentan.	$t\text{-}C_6H_{12}O_2$	202.8	-117	45.5	---
Radicals					
H radical	$H\cdot$	63	52	355	366
Cl radical	Cl	123.6	29.1	271.8	329
NH_2 radical	$NH_2\cdot$	187	44	223	302
Methyl rad.	$CH_3\cdot$	131.1	35.1	270	261
Anilinyl rad.	$C_6H_7N\cdot$	219	57	198	---

Proton affinity (P.A.) is defined as the $-\Delta H$ of the reaction: $M + H^+ = MH^+$. The gas-phase basicity is defined as the $-\Delta G$ of the same reaction. Most proton affinities, however, are determined by the following reaction: $MH^+ + N = NH^+ + M$. One determines the proton affinity experimentally by measuring the equilibrium constant (K_{eq}) of the second reaction where $K_{eq} = [NH^+]/[MH^+] \cdot [M]/[N]$.

Since $-RT\ln K_{eq} = \Delta G$, one can determine the Gibb's free energy of the reaction, and from $\Delta G = \Delta H - T\Delta S$, one can determine the enthalpy of the reaction, if one has an estimate of the entropy. The entropy change in a simple proton exchange reaction is usually small, so the Gibb's free energy and the enthalpy of reaction are approximately equal (165). (This is not true for multifunctional molecules like glycerol.) Thus by reacting MH^+ with a series of bases, and by observing whether or not proton transfer occurs, one can calculate relative gas-phase basicities and relative proton affinities from a "bracketing technique" (164).

For the purposes of Table 15 and for this chapter the heat of formation of the proton is 366 kcal/mol (164), the heat of formation of the hydrogen radical is 52 kcal/mol (167), and the bond strength of the hydrogen molecule is 104 kcal/mol (167) The gas-phase heats of formation of the $(M+H)^+$ ions in Table 15 are calculated using the following equation: $-(P.A.) + \Delta H_f(M) + \Delta H_f(H^+) = \Delta H_f(MH^+)$. The gas-phase heats of formation of the $M^{+\cdot}$ ions in Table 15 are calculated from: $\Delta H_f(M) + I.P. = \Delta H_f(M^{+\cdot})$, where I.P. is the ionization potential of the compound M.

B. Thermochemistry of the PTM Compounds

The isobutane, methanol, acetone, and benzene CI mass spectra of the PTM compounds are shown in Chapter II. At the end of that experiment the author was curious whether certain aspects of the data could be explained using thermochemistry. Occasionally the protonated molecules of certain PTM compounds were not detected. If the proton affinity of the protonated reagent ion is lower than that of the compound being analyzed, then the protonated molecule of the compound should have been formed according to thermodynamics. Table 16 shows a matrix of the PTM compounds versus the four reagent gases used. If the proton transfer reaction should occur (based on thermodynamics) for a particular protonated reagent ion / PTM compound pair then a Y is indicated in Table 15, if not, an N is indicated. In parenthesis next to the each entry is a Y if the protonated molecule was indeed detected, or an N if it was not.

Table 16

Proton Transfer to the PTM Compounds in CI

PTM Compounds and their P.A.'s	Isobutane 163.3	Methanol 181.4	Acetone 196.7	Benzene 181.3
Butanediol 200	Y(Y)	Y(Y)	Y(Y)	Y(Y)
Decane 160	N(N)	N(N)	N(N)	N(N)
1-Octanol 195	Y(N)	Y(Y)	N(N)	Y(N)
2,6-Dimethylphenol 197	Y(Y)	Y(Y)	Y(Y)	Y(Y)
Nonanal 193	Y(Y)	Y(Y)	N(N)	Y(N)
Undecane 160	N(N)	N(N)	N(N)	N(N)
2-Ethylhexanoic Acid 192	Y(Y)	Y(Y)	N(N)	Y(N)
2,6-Dimethylaniline 210	Y(Y)	Y(Y)	Y(Y)	Y(Y)
C_{10}-Acid Methyl Ester 200	Y(Y)	Y(Y)	Y(Y)	Y(Y)
Dicyclohexylamine 230	Y(Y)	Y(Y)	Y(Y)	Y(Y)
C_{11}-Acid Methyl Ester 200	Y(Y)	Y(Y)	Y(Y)	Y(Y)
C_{12}-Acid Methyl Ester 200	Y(Y)	Y(Y)	Y(Y)	Y(Y)

The proton affinity values in Table 16 are all given in kcal/mol. The proton affinities of the reagent gas protonated molecules are from Table 15, but the proton affinities of the PTM compounds have been estimated from trends in compounds with the same functional group.

In nearly all the cases shown in Table 16, the thermodynamic prediction concerning the presence or absence of a protonated molecule agrees with the observed data. In isobutane CI of 1-octanol the protonated molecule is not observed even though it is predicted, but upon inspection of the spectrum, one notices that the $(MH-H_2O)^+$ peak is the base peak. This leads the author to believe that in this case the protonated molecule does form as predicted, but is so unstable that it immediately loses water and, therefore, is not detected. In benzene CI of 1-octanol, nonanal, and 2-ethylhexanoic acid protonated molecules are predicted to occur but are not observed. The amount of protonated benzene in benzene CI is relatively small compared the protonated molecules in the other CI techniques. This makes the overall sensitivity of benzene CI lower than either of the other three CI methods studied. Since sensitivity is low, and since 1-octanol, nonanal, and 2-ethylhexanoic acid are the smallest peaks in all of the chromatograms, it seems reasonable that the protonated molecules of these compounds were not detected due to signal-to-noise considerations not due to unusual thermodynamics. In any event, none of the PTM protonated molecules are detected when thermodynamics predicts their absence.

C. Thermochemistry of the Protonated Alcohol Reactions

A number of reactions involving protonated alcohols have been reported in Chapters V. and VIII. The first set of reactions is that of protonated alcohols with carboxylic acids to form protonated esters. Reactions 1, 2, and 3 are typical of this process.

1) $CH_3COOH + CH_3OH_2^+ \longrightarrow (CH_3COOCH_3)H^+ + H_2O$

$\Delta H_{rn} = -21.5$ kcal/mol

2) $CH_3COOH + CH_3CH_2OH_2^+ \longrightarrow (CH_3CH_2COOCH_3)H^+ + H_2O$

$\Delta H_{rn} = -17$ kcal/mol

3) $CH_3COOH + CH_3CH_2CH_2OH_2^+ \longrightarrow (CH_3CH_2CH_2COOCH_3)H^+ + H_2O$

$\Delta H_{rn} = -12$ kcal/mol

All of these reactions are exothermic, but with increasing chain length, the reaction becomes less exothermic, and one would predict that at chain lengths greater than five carbons the reaction would be endothermic. Reaction 4 is an example of the esterification reaction that does not occur in the gas phase either in an ICR (90) or in the TQMS even though it is exothermic, because the proton affinity of the formic acid (178.8 kcal/mol) is less than the proton affinity of methanol (181.9 kcal/mol).

4) $HCOOH + CH_3OH_2^+ \longrightarrow (HCOOCH_3)H^+ + H_2O$

$\Delta H_{rn} = -11$ kcal/mol

Protonated methanol also reacts with acetaldehyde in the gas phase to produce an ionic product at m/z 59. Reactions 5 and 6 show two possibilities for the structure of the reaction products.

5) $CH_3COH + CH_3OH_2^+ \longrightarrow CH_3-\overset{H}{\overset{|}{C}}=OCH_3^+ + H_2O$

ΔH_{rn} = -19.5 kcal/mol

6) $CH_3COH + CH_3OH_2^+ \longrightarrow (CH_3COCH_3)H^+ + H_2O$

ΔH_{rn} = -36.5 kcal/mol

In reaction 5, the product is in the form of a hemi-acetal, and in reaction 6, the product is in the form of protonated acetone. Even though reaction 5 is analogous to the solution reaction, both reactions are exothermic, so it is not possible to determine from the thermodynamics which product is formed in the gas phase.

D. Thermochemistry of the Aryl Cation Reactions

Aryl cations undergo numerous reactions in the gas phase, and since they have been studied more extensively than many other organic ion/molecule reactions, there are many tabulated values for heats of formation of aromatic ions. The result of this fact is that the author was able to calculate enthalpies of reaction for more of the aryl cation reactions than for any other type discussed in this dissertation. Reactions 7 and 8 demonstrate why aromatic hydrocarbon ions react differently than aliphatic hydrocarbon ions with methanol in the gas phase.

7) $C_6H_5^+ + CH_3OH \longrightarrow C_6H_5OH^{+\cdot} + CH_3\cdot$

ΔH_{rn} = -28.9 kcal/mol

8) $C_6H_{13}^+ + CH_3OH \longrightarrow C_6H_{13}OH^{+\cdot} + CH_3^+$

ΔH_{rn} = +74 kcal/mol

The heat of formation of the hexanol molecular ion in reaction 8 was estimated from trends in alcohols (see table 15) to be 143 kcal/mol. The reaction of the phenyl cation with methanol in reaction 7 to form phenol happens in the TQMS whereas the reaction of the hexyl ion with methanol in reaction 8 to form hexanol does not, because the formation phenol is exothermic and the formation of hexanol is strongly endothermic. These two reactions are the basis for the selectivity of the methanol reaction for aryl cations.

Reactions 9 and 10 compare the reactions that form the $C_7H_7^+$ ion from the reactions of the phenyl cation with methanol or with methane. Both reactions 9 and 10 occur in the TQMS and both are exothermic. It is not known whether the structure of $C_7H_7^+$ product is in the form of a tropylium ion or a benzyl ion, but both are possible based on the thermodynamics.

9) $C_6H_5^+ + CH_3OH \longrightarrow C_7H_7^+ + H_2O$

ΔH_{rn} = -78 kcal/mol (if benzyl)

ΔH_{rn} = -62 kcal/mol (if tropylium)

10) $C_6H_5^+ + CH_4 \longrightarrow C_7H_7^+ + H_2$

ΔH_{rn} = -50 kcal/mol (if benzyl)

ΔH_{rn} = -34 kcal/mol (if tropylium)

The phenyl cation also reacts with benzene to form two ions which may or may not have structures associated with neutral biphenyl. CID evidence in Chapter VI suggests that they may not have the biphenyl structure, in contradiction to other evidence in the literature. Reactions 11 and 12 show these two processes.

11) $C_6H_5^+ + C_6H_6^+ \longrightarrow C_{12}H_{10}^{+\cdot} + H\cdot$

$\Delta H_{rn} = -21$ kcal/mol

12) $C_6H_5^+ + C_6H_6^+ \longrightarrow C_{12}H_{11}^{+\cdot}$

$\Delta H_{rn} = -92$ kcal/mol

Both reactions 11 and 12 occur in the TQMS, and both are exothermic. It is clear though, that the product in reaction 12 must be collisionally stabilized or the excess thermal energy generated by the reaction will cause the product ion to fragment.

Reactions 13, 14, 15, and 16 are concerned with the interactions between the phenyl cation and ammonia. All four reactions were observed in the central quadrupole of the TQMS, whereas only the first two were observed by another researcher (137) in an ICR.

13) $C_6H_5^+ + NH_3 \longrightarrow C_6H_5NH_3^+$

$\Delta H_{rn} = -97$ kcal/mol

14) $C_6H_5^+ + NH_3 \longrightarrow C_6H_5NH_2^+ + H\cdot$

$\Delta H_{rn} = -23$ kcal/mol

15) $C_6H_5^+ + NH_3 \longrightarrow C_6H_4 + NH_4^+$

$\Delta H_{rn} = 0$ kcal/mol

16) $C_6H_5^+ + NH_3 \longrightarrow C_6H_6^{+\cdot} + NH_2^+$

$\Delta H_{rn} = +2$ kcal/mol

Both reactions 13 and 14 are exothermic and were observed in both the TQMS and ICR. Normally one would not expect to observe the protonated aniline product from reaction 13 in an ICR, since the reaction is extremely exothermic and the product probably would have to

be collisionally stabilized. It is also unusual that reaction 15 was not observed in the ICR since it is isothermic and requires no collisional stabilization. However, it is not surprising that reaction 16 was not observed in the ICR since it is endothermic. The fact that the benzene molecular ion is observed in the reaction of the phenyl cation and ammonia in the central quadrupole of the TQMS indicates that this endothermic reaction may be driven by some of the parent ion's kinetic energy being converted to thermal energy through collision with an ammonia molecule. Before one can make this conclusion for certain, however, one would have to do the reaction again in the TQMS, to make sure that the m/z 78 peak was not due to poor parent ion resolution since the phenyl cation was generated by EI of benzene.

CHAPTER XI.

SUMMARY

Ion/molecule reactions that occur in the gas phase are frequently analogous to reactions that occur in organic solution chemistry. Studying organic reactions in the gas phase has the advantage that both the intermediates and the final products of a reaction can be observed directly.

Ion/molecule reactions also may be useful for analytical purposes. It is possible that ion/molecule reactions can be used as chemical probes for specific structural features of compounds with unknown structures. In addition, ion/molecule reactions might be used as a selective technique for detecting and quantifying target compounds in complex mixtures. Accomplishing these analytical tasks by means of ion/molecule reactions requires both an in-depth understanding of ion/molecule chemistry and appropriate instrumentation.

Ion/molecule chemistry is a small but expanding field that is beginning to make advances in the understanding of gas-phase chemistry. Further progress in this field requires both more time and better instrumentation. Most of the instruments currently used for studying these reactions are hardly what one would call "analytical instrumentation": they either require vast quantities of sample, as in flowing afterglow, or their effectiveness is restricted to volatile samples, as in cyclotron resonance spectrometry.

The triple quadrupole mass spectrometer (TQMS) is a relatively new instrument which has the unique qualification of being an analytical

instrument with the capability for studying ion/molecule reactions. In fact, the TQMS has two arenas for such analyses: the ion source and the central quadrupole. One can employ the central quadrupole as a reaction chamber and select both the reagent ions and the product ions with unit mass resolution. The ion source is also effective as a reaction chamber, and has the advantage that it allows the structure of product ions to be investigated by CID in the central quadrupole. However, one cannot select the reagent ion when performing reactions in the ion source. Therefore, both the central quadrupole and the collision chamber are necessary for a complete study of an ion/molecule reaction because each provides different and complementary information.

This study has confirmed the reports of other researchers that the yields of ion/molecule reactions in the central quadrupole are quite low relative to those in the chemical ionization source. The low yields are due to insufficient interaction time in the central quadrupole between ions and molecules. A pulsed ion-trapping technique has therefore been devised which greatly increases the interaction time of ions and molecules in the central quadrupole. This "trap and pulse" technique is similar to the double resonance technique in ICR in that one can select a reagent ion, store that ion for a given period of time in the presence of reactive molecules, and detect the product ion with unit mass resolution. The ion-trapping technique in the TQMS is more versatile than the ICR technique because it can be operated over a greater range of pressures without degrading the mass resolution of the instrument, and because a much greater variety of ionization methods and sample introduction methods are available on the TQMS. The ion-trapping technique in the TQMS enhances the observed yield of product ions,

increases the signal-to-noise ratio of stable product ions, yields product ions that would otherwise not be observed, and decreases the need for high pressures of reactive gases. The development of ion-trapping in the TQMS has led also to a computerized ion-trapped multiple reaction monitoring technique that can detect selectively microgram quantities of gas chromatographic eluents by means of ion/molecule reactions.

In addition, the ionization technique fast atom bombardment (FAB) was implemented on the TQMS in the MSU-NIH-MSF in order to expand the number of compounds whose ion/molecule reactions could be investigated. This had the immediate benefit that the author was able to substantiate that ion/molecule reactions play an important role in the FAB process.

The ion/molecule reactions studied in this research with the TQMS include those of alcohols, carbonyl compounds, and aromatic compounds. These three functional groups were chosen because methanol, benzene, and acetone chemical ionization techniques all exhibited numerous ion/molecule reactions with a commercial mixture of polar compounds called programmed test mixture (PTM). This experiment showed that GC-CI/MS can be an excellent method for performing a survey of ion/molecule reactions.

Methanol has been determined in this study to be a remarkably reactive species in the gas phase. It reacts with aromatic $(M-H)^+$ ions to form phenolic ions, with protonated alcohols to form protonated ethers, with protonated aldehydes to form products that may be protonated ketones or acetals, with protonated acids to form protonated esters, with protonated esters to form acetals, and with substituted pyridine anions to form a variety of unusual products. All of these

reactions can be observed in both the collision cell and the CI volume of the TQMS, and all of them are analogous to reactions that occur in solution. The methanol CI spectra of the compounds in the PTM illustrate this point. Nearly all of the compounds in the mixture reacted with protonated methanol to form ion/molecule products. In general, the higher molecular weight alcohols produce lower yields of all the covalently bound product ions mentioned above, and higher yields of proton-bound adducts.

Whereas protonated alcohols react with alcohols and other species to form protonated products which subsequently lose water to form covalently bound species, protonated carbonyl compounds tend to react with other carbonyls to form proton-bound adducts which do not lose a neutral to form covalently bound species. Therefore, except with alcohols, the protonated carbonyls react to form a variety of loosely bound adduct ions. These adduct ions exhibit simple CID spectra which show only dissociation to the starting materials. These clustering reactions of positively charged carbonyls produce abundant product ions with most polar compounds.

Aromatic ions react with aromatic molecules to form a variety of hydrocarbon products whose structures are uncertain. It is possible to generate polycyclic aromatic hydrocarbons such as indene and naphthalene from ion/molecule reactions in benzene, but whether or not the biphenyl and protonated biphenyl ions are generated by ion/molecule reaction in benzene is uncertain, since different instrumental methods yield conflicting data.

Research into a possible gas-phase analog of the S_N(ANRORC) reaction has demonstrated that the TQMS is fully capable of studying

negative ion/molecule reaction both by NCI and by ion trapping in the central quadrupole. Research into negative ion/molecule reactions has received some attention in the chemical literature recently, but the topic is very new and is as yet largely uninvestigated.

A study of the thermodynamics of the reactions investigated in this dissertation indicated that nearly all of the observed ion/molecule reaction product ions were generated by exothermic reactions. Although endothermic ion/molecule reaction have been reported as occuring in the TQMS, no unambiguous cases of this phenomenon were encountered in this research. Thermodynamic values have been tabulated in this dissertation for all of the compounds used according to functional group, except for the compounds in the PTM mixture. Proton affinities for the PTM compounds were estimated from trends in the respective functional groups, and these estimated proton affinities have helped to explain the presence or absence of particular $(M+H)^+$ ions in isobutane, methanol, benzene, and acetone CI.

Simple ion/molecule reactions such as protonation (as in CI) have been used for years as analytical techniques. Chemically more complex reactions such as those investigated in this research might prove to be ideal for solving particular analytical problems which other methods have failed to solve. Negative ion/molecule reactions may in fact be the most analytically useful, since negative ion mass spectrometry has recently been used to detect extremely small quantities of halogenated compounds.

The data presented in this dissertation show that the TQMS is a useful tool for studying ion/molecule reactions of all kinds, and that ion/molecule reactions in the TQMS have the potential to be used for

analytical purposes. Ion/molecule research on the TQMS deserves to be continued because much of organic gas-phase chemistry remains virtually unexplored, and because ion/molecule reactions may provide a breakthrough in analytical chemistry either for structural elucidation or for selective detection of trace compounds.

LIST OF REFERENCES

LIST OF REFERENCES

1. R. G. Cooks, G. Glish, Chem. Eng. News, 1981, 59, 40-52.
2. R. Dromey, M. Stefik, T. Rindfleisch, A. Butterfield, Anal. Chem., 1976, 48, 1368-1375.
3. J. F. Holland, C. G. Enke, J. Allison, J. T. Stults, J. D. Pinkston, B. Newcome, J. T. Watson, Anal. Chem., 1983, 55, 997A.
4. R. Voyksner, J. Hass, M. Bursey, Anal. Lett., 1982, 15, 1-12.
5. R. Smith, J. Burger, A. Johnson, Anal. Chem., 1981, 53, 1603-1611.
6. R. A. Yost, C. G. Enke, Anal. Chem., 1979, 51, 1251A-1264A.
7. L. Wright, S. McLuckey, R. G. Cooks, K. Wood, Int. J. Mass Spectrom. Ion Phys., 1982, 42, 115-124.
8. D. Davis, R. G. Cooks, B. Meyer, J. McLaughlin, Anal. Chem., 1983, 55, 1302-1305.
9. R. Perchalski, R. A. Yost, B. Wilder, Anal. Chem., 1983, 55, 2002-2005.
10. M. Barber, R. Bordoli, R. Sedgwick, L. Tetler, Org. Mass Spectrom., 1981, 16, 256-260.
11. P. Todd, G. Glish, W. Christie, Int. J. Mass Spectrom. Ion Proc., 1984, 61, 215-230.
12. K. Tomer, F. Crow, H. Knoche, M. L. Gross, Anal. Chem., 1983, 55, 1033-1036.
13. S. Unger, Anal. Chem., 1984, 56, 363-368.
14. P. Lyon, W. Stebbings, F. Crow, K. Tomer, D. Lippsten, M. L. Gross, Anal. Chem., 1984, 56, 8-13.

15. I. Amster, M. Baldwin, M. Cheng, C. Proctor, F. T. McLafferty, J. Am. Chem. Soc., 1983, 105, 1654-1655.

16. G. Glish, P. Todd, K. Busch, R. Cooks, Int. J. Mass Spectrom. Ion Proc., 1984, 56, 177-192.

17. K. Busch, B. Hsu, K. Wood, R. G. Cooks, C. Schwarz, A. Katritzky, J. Org. Chem., 1984, 49, 764-769.

18. K. Tomer, F. Crow, M. L. Gross, K. Kopple, Anal. Chem., 1984, 56, 880-886.

19. F. Crow, K. Tomer, M. L. Gross, Mass Spectrom. Rev., 1983, 2, 47-76.

20. R. A. Yost, C. G. Enke, D. C. McGilvery, D. Smith, J. D. Morrison, Int. J. Mass Spectrom. Ion Phys., 1979, 30, 127-136.

21. D. C. McGilvery, J. D. Morrison, Int. J. Mass Spectrom. Ion Phys., 1978, 28, 81-92.

22. R. G. Cooks, Purdue University MS/MS Short Course, Unpublished Research, 1984.

23. J. Benyon, R. G. Cooks, J. Amy, W. Baitinger, T. Ridley, Anal. Chem., 1973, 45, 1023A.

24. A. Bruins, K. R. Jennings, S. Evans, Int. J. Mass Spectrom. Ion Phys., 1978, 26, 395-404.

25. D. Hunt, J. Shabanowitz, T. Harvey, M. Coates, Anal. Chem., 1985, 57, 525-537.

26. C. Myerholtz, B. Newcome, C. G. Enke, 31st Ann. Conf. Mass Spectrom. All. Top., 1983, 171-172.

27. T. Yu, M. Cheng, V. Kempter, F. Lampe, J. Phys. Chem., 1972, 76, 3321-3330.

28. S. Verma, J. Ciupek, R. G. Cooks, A. Schoen, P. Dobberstein, Int. J. Mass Spectrom. Ion Proc., 1983, 52, 311.

29. J. D. Pinkston, M. Rabb, J. T. Watson, and J. Allison, Rev. Sci. Instrum., 1986, 57, 583-592.

30. F. T. McLafferty, Science, 1981, 214, 280-287.

31. J. T. Stults, C. G. Enke, J. F. Holland, Anal. Chem., 1983, 55, 1323-1330.

32. R. Cody, R. Burnier, B. Freiser, Anal. Chem., 1982, 54, 96-101.

33. H. Brotherton, R. A. Yost, Anal. Chem., 1983, 55, 549-553.

34. R. O'Brien, D. Dumdei, S. Hummel, R. Yost, Anal. Chem., 1984, 56, 1329-1335.

35. K. Wood, C. Schmidt, R. G. Cooks, B. Batts, Anal. Chem., 1984, 56, 1335-1338.

36. D. Hunt, W. Bone, J. Shabanowitz, J. Rhodes, J. Ballard, Anal. Chem., 1981, 53, 1706-1708.

37. K. Tomer, F. Crow, M. L. Gross, J. Am. Chem. Soc., 1983, 105, 5487-5488.

38. I. Isern-Flecha, R. G. Cooks, K. Wood, Int. J. Mass Spectrom. Ion Proc., 1984, 62, 73-87.

39. D. Burinsky, R. G. Cooks, J. Org. Chem., 1982, 47, 4864-4869.

40. D. Burinsky, J. Campana, R. G. Cooks, Int. J. Mass Spectrom. Ion Phys., 1984, 62, 303-315.

41. K. Wood, D. Burinsky, D. Cameron, R. Cooks, J. Org. Chem., 1983, 48, 5236-5242.

42. H. Budizkiewicz, G. Laufenberg, A. Brauner, Org. Mass Spectrom., 1985, 20, 65-69.

43. D. Peake, M. L. Gross, Anal. Chem., 1985, 57, 115-120.

44. J. Stone, N. Moote, Org. Mass Spectrom., 1985, 20, 41-45.

45. D. Fetterolf, R. A. Yost, Int. J. Mass Spectrom. Ion Proc., 1984, 62, 33-49.

46. F. Cacace, G. Ciranni, C. Sparapani, M. Speranza, J. Am. Chem. Soc., 1984, 106, 8046-8050.

47. M. Speranza, Y. Keheyan, G. Angelini, J. Am. Chem. Soc., 1983, 105, 6377-6380.

48. G. Angelini, S. Fornarini, M. Speranza, J. Am. Chem. Soc., 1982, 104, 4773-4780.

49. G. Angelini, C. Sparapani, M. Speranza, J. Am. Chem. Soc., 1982, 104, 7084-7091.

50. N. Pepe, M. Speranza, J. Chem. Soc. Perkin Trans. II, 1981, 1430-1436.

51. M. Speranza, J. Chem. Soc. Chem. Commun., 1981, 1177-1178.

52. M. Speranza, C. Sparapani, J. Am Chem. Soc., 1980, 102, 3120-3124.

53. G. Klass, J. Sheldon, J. Bowie, J. Chem. Soc. Perkin Trans. II, 1983, 1337-1341.

54. I. Blair, V. Trenerry, J. Bowie, Org. Mass Spectrom., 1980, 15, 15-17.

55. V. Trenerry, J. Bowie, J. Chem. Soc. Perkin Trans. II, 1979, 1640-1643.

56. M. Jones, S. Kass, J. Filley, R. Barkley, G. Ellison, J. Am. Chem. Soc., 1985, 107, 109-115.

57. J. Chakel, C. G. Enke, 30th Ann. Conf. Mass Spectrom. All. Top., 1982, 758.

58. J. D. Morrison, K. Stanney, J. Tedder, J. Chem. Soc. Perkin Trans. II, 1981, 967-969.

59. J. D. Morrison, K. Stanney, J. Tedder, J. Chem. Soc. Perkin Trans. II, 1981, 838-841.

60. J. Schmit, P. Dawson, 30th Ann. Conf. Mass Spectrom. All. Top., 1982, 487-488.

61. D. Carroll, J. Norlin, R. Stillwell, E. Horning, 30th Ann. Conf. Mass Spectrom. All. Top., 1982, 522.

62. R. A. Yost, D. Fetterolf, Mass Spectrom. Rev., 1983, 2, 1-45.

63. S. Martin, C. Costello, K. Biemann, Anal. Chem., 1982, 54, 2362-2368.

64. G. Puzo, J. Prome, Org. Mass Spectrom., 1984, 19, 448-451.

65. G. Dube, Org. Mass Spectrom., 1984, 19, 242-243.

66. A. Dell, G. Taylor, Mass Spectrom. Rev., 1984, 3, 357-394.

67. M. Barber, R. Bordoli, G. Elliot, A. Tyler, J. Bill, B. Green, Biomed. Mass Spectrom., 1984, 11, 182-186.

68. B. L. Ackermann, J. T. Watson, J. Newton Jr., J. Hook, W. Braselton Jr., Biomed. Mass Spectrom., 1984, 11, 502-511.

69. S. Seki, H. Kambara, H. Naoki, Org. Mass Spectrom., 1985, 20, 18-24.

70. K. Faull, A. Tyler, H. Sim, J. Barchas, I. Massey, C. Kenyon, P. Goodley, J. Mahoney, J. Perel, Anal. Chem., 1984, 56, 308-311.

71. R. Stoll, D. Harran, J. Hass, Int. J. Mass Spectrom. Ion Proc., 1984, 61, 71-79.

72. T. Murata, J. Lipid Res., 1978, 19, 166-171.

73. J. Lankelma, E. Ayanoglu, C. Djerassi, Lipids, 1983, 18, 853-858.

74. T. Murata, T. Ariga, E. Araki, J. Lipid Res., 1978, 19, 172-176.

75. Y. Lin, L. Smith, Mass Spectrom. Rev., 1984, 3, 313-355.

76. D. Miller, M. L. Gross, J. Am. Chem. Soc., 1983, 105, 3783-3788.

77. Md. A. Mabud, M. J. Dekrey, R. G. Cooks, Int. J. Mass Spectrom. Ion Phys., 1985, 67, 285.

78. A. J. T. Jull, Int. J. Mass Spectrom. Ion Phys., 1982, 41, 135-141.

79. K. Wittmaack, Int. J Mass Spectrom. Ion Proc., 1986, 69, 197-209.

80. D. C. McGilvery, J. D. Morrison, Int. J. Mass Spectrom. Ion Phys., 1978, 28, .81-92.

81. M. L. Vestal, J. H. Futrell, Chem. Phys. Lett., 1974, 28, 559-560.

82. J. N. Louris, L. G. Wright, R. G. Cooks, A. E. Schoen, Anal. Chem., 1985, 57, 2918.

83. R. R. Corderman, J.L. Beauchamp, J. Am. Chem. Soc., 1976, 98, 5700; M. Lombarski, J. Allison, Int. J. Mass Spectrom. Ion Phys., 1985, 65, 31.

84. J. D. Cox, G. Pilcher, Thermochemistry of Organic and Organometallic Compounds, Academic Press, London, 1970.

85. H. M. Rosenstock, K. Draxl, B. W. Steiner, J. T. Herron, J. Phys. Chem Ref. Data 6, Suppl. 1, 1977, p. 738.

86. D. J. Burinsky, J. E. Campana, R. G. Cooks, Int. J. Mass Spectrom. Ion Proc., 1984, 62, 303-315.

87. D. J. Burinsky, R. Cooks, J. Org. Chem., 1982, 47, 4864-4869.

88. G. Klass, J. C. Sheldon, J. H. Bowie, J. Chem. Soc. Perkin Trans. II, 1983, 1337-1341.

89. W. D. Reents, Jr., B. S. Freiser, J. Am. Chem Soc., 1980, 102, 271-276.

90. P. W. Tiedemann, J. M. Riveros, J. Am. Chem. Soc., 1974, 96, 179-183.

91. J. E. Bartmess, R. L. Hays, G. Caldwell, J. Am Chem. Soc., 1981, 103, 1338-1344.

92. J. P. Schmit, P. H. Dawson, N. Beaulieu, Org. Mass Spectrom., 1985, 20, 269-275.

93. H. Suming, C. Yaozu, J. Longfei, X. Shuman, Org. Mass Spectrom., 1985, 20, 719-723.

94. G. B. Anderson, R. G. Gillis, Q. N. Porter, Org. Mass Spectrom., ,383-384.

95. J. Jalonen, J. Chem. Soc. Chem. Commun., 1985, 872-874.

96. M. T. Kuter, M. M. Bursey, J. Am. Chem. Soc., 1986, 108, 1797-1801.

97. D. D. Fetterolf, R. A. Kost, J. R. Eyler, Org. Mass Spectrom., 1984, 105, 104-105.

98. J. A. Chakel, C. G. Enke, Anal. Chem., in press.

99. B. Ackermann, J. T. Watson, J. F. Holland, Anal. Chem., 1985, 57, 2656-2663.

100. G.-R. Her, G. G. Dolnikowski, J. T. Watson, Org. Mass Spectrom., 1986, 21, 329-334.

101. D. C. McGilvery, J. D. Morrison, Int. J. Mass Spectrom. Ion Phys., 1978, 28, 81-92.

102. M. L. Vestal, J. H. Futrell, Chem. Phys. Lett., 1974, 28, 559-560.

103. R. A. Yost, C. G. Enke, D. C. McGilvery, J. D. Morrison, Int. J. Mass Spectrom. Ion Phys., 1979, 30, 127-136.

104. J. D. Morrison, K. Stanney, J. M. Tedder, J. Chem. Soc. Perkin Trans. II, 1981, 838-841.

105. J. D. Morrison, K. Stanney, J. M. Tedder, J. Chem. Soc. Perkin Trans. II, 1981, 967-969.

106. J. A. Chakel, C. G. Enke, Anal. Chem., in press.

107. D. D. Fetterolf, R. A. Yost, J. R. Eyler, Org. Mass Spectrom., 1984, 19, 104-105.

108. R. A. Yost, D. D. Fetterolf, Mass Spectrom. Rev., 1983, 2, 1-45.

109. D. D. Fetterolf, R. A. Yost, Int. J. Mass Spectrom. Ion Proc., 1984, 62, 33-49.

110. J. P. Schmidt, and P. H. Dawson, N. Beaulieu, Org. Mass Spectrom., 1985, 20, 269-275.

111. J. Jalonen, J. Chem. Soc., Chem. Commun., 1985, 872-874.

112. J. P. Schmit, S. Beaudet, A. Brisson Org. Mass Spectrom., 1986, 21, 493-498.

113. C. A. Myerholtz, Ph. D. Dissertation, Michigan State University, 1983.

114. R. D. Smith, D. A. Herold, T. A. Elwood, J. H. Futrell J. Am. Chem. Soc., 1977, 99, 6042-6045.

115. P. W. Tiedemann, J. M. Riveros, J. Am. Chem. Soc., 1974, 96, 185-189.

116. R. G. Cooks, Private Communication, 1986.

117. A. E. Schoen, J.W. Amy, J.D. Ciupek, R.G. Cooks, P. Dobberstein, G. Jung, Int. J. Mass Spectrom. Ion Proc., 1985, 65, 125-140.

118. A. Streitweiser, Jr. C. H. Heathcock, "Introduction to Organic Chemistry," Macmillan Publishing Co,, Inc., New York, 1981, pp. 516-518.

119. T. Murata, T. Ariga, E. Araki, J. Lipid Res., 1978, 19, 172-176.

120. A. Streitweiser, Jr. C. H. Heathcock, "Introduction to Organic Chemistry," Macmillan Publishing Co,, Inc., New York, 1981, pp 949-950.

121. F. Cacace, J. Chem. Soc. Perkin Trans. II, 1982, 1129-1132.

122. R. Sievert, I. Cadeiz, J. VanDoren, A. W. Castleman, Jr., J. Phys. Chem., 1984, 88, 4502-4505.

123. V. A. Sunner. R. Kulatunga, P. Kebarle, Anal. Chem., 1986, 58, 2009-2014.

124. S. F. Smith, J. Chandrasekhar, W. L. Jorgensen, J. Phys. Chem., 1982, 86, 3308-3318.

125. R. D. Smith, J. J. Decorpo, J. H. Furtrell, Int. J. Mass Spectrom. Ion Phys., 1978, 26, 279-288.

126. C. Lifshitz, M. Weiss, Int. J. Mass Spectrom. Ion Phys., 1980, 34, 311-315.

127. R. Wolfschutz, H. Schwarz, Int. J. Mass Spectrom. Ion Phys., 1980, 33, 285-290.

128. G. Smolinsky, M. J. Vasile, Int. J. Mass Spectrom. Ion Phys.,1977, 24, 311-322.

129. G. Occhiucci, F. Cacace, M. Speranza, J. Am. Chem. Soc., 1986, 108, 872-876.

130. R. T. McLafferty, Jr., R. L. Hunter, W. D. Bowers, Int. J. Mass Spectrom. Ion Proc., 1985, 64, 67-77.

131. J. O. Lay, Jr., M. L. Gross, Lect. Notes Chem., 1982, 31, 237-257.

132. C. Lifshitz, D. Gibson, K. Levsen, Int. J. Mass Spectrom. Ion Phys., 1980, 35, 365-370.

133. J. R. Eyler, J. E. Campana, Int. J. Mass Spectrom. Ion Proc., 1984, 55, 171-188.

134. J. A. Harris, R. P. Morgan, J. H. Benyon, Org. Mass Spectrom., 1975, 10, 584.

135. M. Colosimo, M. Speranza, F. Cacace, G. Ciranni, Tetrahedron, 1984, 40, 4873-4883.

136. F. W. McLafferty, "Mass Spectrometry of Organic Ions," Academic Press, New York, 1963.

137. J. B. Dunbar, Jr., Ph.D. Dissertation, Washington University, 1983.

138. N. H. Mahle, R. G. Cooks, R. W. Korzeniowski, Anal. Chem., 1983, 55, 2272-2275.

139. M. S. B. Munson, J. Am. Chem. Soc., 1965, 87, 5313.

140. P. W. Tiedemann, J. M. Riveros, J. Am. Chem. Soc., 1973, 95, 3140-3144.

141. W. J. van der Hart, H. A. van Sprang, J. Am. Chem. Soc., 1977, 99, 32-35.

142. M. Kumakura, T. Sugiura, J. Phys. Chem., 1978, 82, 639-643.

143. Z. Luczynski, H. Wincel, Int. J. Mass Spectrom. Ion Phys., 1977, 23, 37-44.

144. J. -P. Schmitt, S. Beandet, A. Brisson, Org. Mass Spectrom., 1986, 21, 493-498.

145. G. Podda, A. Maccioni, S. Daolio, P. Traldi, J. Heterocyclic Chem., 1984, 21, 557-560.

146. O. I. Asubiojo, J. I. Brauman, J. Am. Chem. Soc., 1979, 101, 3715-3724.

147. J. D. Reinheimer, L. L. Mayle, G. G. Dolnikowski, J. T. Gerig, J. Org. Chem., 1980, 45, 3097-3100.

148. H. C. Van der Plas, Acc. Chem. Res., 1978, 11, 462.

149. H. B. Bell, D. R. Carver, J. S. Hubbard, Y. P. Sachdeva, J. F. Wolfe, J. Org. Chem., 1985, 50, 3442-3444.

150. D. A. Laude, Jr., C. L. Johlman, R. S. Brown, D. A. Weil, C. L. Wilkins, Mass Spectrom. Rev., 1986, 5, 107-166.

151. E. P. Grimsrud, S. Chowdhury, P. Kebarle, Int. J. Mass Spectrom. Ion Proc., 1986, 68, 57-70.

152. J. C. Kleingeld, N. M. M. Nibbering, Lect. Notes Chem., 1982, 31, 209-238.

153. D. Bombick, J. D. Pinkston, J. Allison, Anal. Chem., 1984, 56, 392-402.

154. B. D. Musselman, J. T. Watson, C. K. Chang, Biomed. Mass Spectrom., 1985, 215-219.

155. K. Grob, Jr., et al., J. Chromatogr., 1987, 156, 1-20.

156. M. E. Rose, C. Longstaff, P. D. C. Dean, Biomed. Mass Spectrom., 1983, 10, 512-527.

157. R. B. Freas, M. M. Ross, J. E. Campana, J. Am. Chem. Soc., 1985, 107, 6195-6201.

158. Private Communications, 34th Ann. Conf. Mass Spectrom. All. Top., 1986.

159. J. C. Kleingeld, N. M. M. Nibbering, Tetrahedron, 1984, 40, 2789-2794.

160. M. P. Moon, A. P. Komin, J. F. Wolfe, G. F. Morris, J. Org Chem., 1983, 48, 2392-2399.

161. A Counotte-Potman, H. C. van der Plas, B. van Veldhuizen, C. A. Landheer, J. Org. Chem., 1981, 46, 5102-5109.

162. M. M. Bursey, T. A. Elwood, M. K. Hoiffman, T. A. Lehman, J. M. Tesarek, Anal. Chem., 1970, 42, 1370-1374.

163. D. L. Smith, J. H. Futrell, Int. J. Mass Spectrom. Ion Phys., 1974, 14, 171-181.

164. S. G. Lias, J. F. Liebman, R. D. Levin, J. Phys. Chem. Ref. Data, 1984, 13(3), 695-808.

165. J. A. Sunner, R. Kulatunga, P. Kebarle, Anal. Chem., 1986, 58, 1312-1316.

166. J. Allison, Michigan State University, Private Communication, July 1987.

167. CRC Handbook of Chemistry and Physics, 1986.